HIGH-TEMPERATURE RADICAL POLYMERIZATION OF METHYL METHACRYLATE IN A CONTINUOUS PILOT SCALE PROCESS

THÈSE N^O 3460 (2006)

PRÉSENTÉE LE 10 MARS 2006

À LA FACULTÉ SCIENCES DE BASE
GROUPE DES PROCÉDÉS MACROMOLÉCULAIRES

SECTION DE CHIMIE ET GÉNIE CHIMIQUE

ÉCOLE POLYTECHNIQUE FÉDÉRALE DE LAUSANNE

POUR L'OBTENTION DU GRADE DE DOCTEUR ÈS SCIENCES

PAR

Philip NISING

Dipl.-Ing. Univ., Friedrich-Alexander-Universität, Erlangen-Nürnberg, Allemagne
et de nationalité allemande

acceptée sur proposition du jury:

Prof. P. Vogel, président du jury
Dr Th. Meyer, directeur de thèse
Dr R. Carloff, rapporteur
Prof. H.-A. Klok, rapporteur
Prof. F. Pla, rapporteur

EPFL
ÉCOLE POLYTECHNIQUE
FÉDÉRALE DE LAUSANNE

Lausanne, EPFL
2006

Abstract

The present PhD thesis deals with the high temperature polymerization of methyl methacrylate in a continuous pilot scale process. The major aim is to investigate the feasibility of a polymerization process for the production of PMMA molding compound at temperatures in the range from 140 °C to 170 °C. Increasing the process temperature has the advantage of decreasing molecular weight and viscosity of the reaction mixture, thus allowing to reduce the addition of chain transfer agent and to increase the polymer content in the reactor. At the same time, the reaction rates are higher and the devolatilization is facilitated compared to low conversion polymerizations. Altogether, it leads to an improved space time yield of the process. However, increasing the process temperature also has an important impact on both, polymerization kinetics and polymer properties.

The first two parts of this work are, therefore, dedicated to the self-initiation respectively the high temperature gel effect observed for the polymerization of MMA at the given temperature range. The self-initiation of MMA is mostly caused by polymeric peroxides that form from physically dissolved oxygen and the monomer, itself. The formation, decomposition and constitution of these peroxides are intensively studied and a formal kinetic is proposed for the formation and decomposition reaction.

The polymerization of MMA is subject to a rather strong auto-acceleration, called gel effect, the intensity of which depends on process conditions and solvent content. There are several models proposed in the specialized literature to describe this phenomenon by modifying the termination rate constant as a function of conversion and temperature. The second part of this study contains the evaluation of these models with regards to their applicability to high

temperature MMA polymerization as well as the development of a new variant of an existing model, which correctly describes the gel effect in the temperature range of interest as a function of polymer content, temperature and molecular weight. The advantage of this new variant is that it includes all other factors influencing the gel effect, i.e. chain transfer agent, initiator load, comonomer and solvent content, and that it is suitable for the description of batch and continuous processes. A complete kinetic model for the description of the high temperature copolymerization of MMA and MA, containing the results from the first two parts of this work, is established within the software package PREDICI® and validated by means of several series of batch polymerizations.

In the third part of this work, a complete pilot plant installation for the continuous polymerization of MMA is designed and constructed in order to study the impact of increasing the reaction temperature on process properties and product quality under conditions similar to those of an industrial-scale polymerization. The pilot plant is based on a combination of recycle loop and consecutive tube reactor, equipped with SULZER SMXL® / SMX® static mixing technology. Furthermore, it is equipped with a static one-step flash devolatilization and a pelletizer for polymer granulation. At the same time, a refined method for inline conversion monitoring by speed of sound measurement is developed and tested in the pilot plant. By means of this technique it is possible to follow the dynamic behavior of the reactor and to measure directly the monomer conversion without taking a sample. The results of several pilot plant polymerizations carried out under different conditions are presented and the impact of temperature, comonomer and chain transfer agent on the thermal stability of the product is analyzed. From these results, the r-parameters for the copolymerization of MMA and MA at 160 °C as well as the chain transfer constant for n-dodecanethiol at 140 °C are determined. Finally, the pilot plant experiments are used to validate the kinetic model established beforehand in PREDICI® for the continuous copolymerization.

Keywords: *High Temperature Polymerization, Methyl methacrylate, Copolymerization, Reactivity ratio, Chain Transfer, Ultrasound conversion monitoring, Gel effect, Thermal stability, Kinetic Modeling, Pilot Plant Technology, Static mixing*

Version abrégée

Cette thèse traite de la polymérisation à haute température du méthacrylate de méthyle dans un procédé à l'échelle d'un système pilote. Le but principal est l'étude de faisabilité d'un procédé de polymérisation pour la production de PMMA fondu à des températures entre 140 °C et 170 °C. Dans ce procédé l'augmentation de la température a pour avantage la diminution de la masse moléculaire et de la viscosité du mélange réactionnel, ce qui permet de réduire l'ajout d'agent de transfert de chaîne et d'augmenter la quantité de polymère dans le réacteur. En même temps, les vitesses de réaction sont plus élevées et la dévolatilisation est facilitée par rapport à des polymérisations à basse conversion. Pris ensemble, ces éléments permettent d'améliorer le rendement en espace et en temps du procédé. Toutefois, augmenter la température du procédé a aussi un effet important sur la cinétique de polymérisation, ainsi que sur les propriétés des polymères.

Les deux premières parties de ce travail sont, par conséquent, dédiées à l'auto-initiation et à l'effet de gel à haute température, observés dans l'intervalle de température considéré. L'auto-initiation du MMA est principalement causée par des peroxydes polymères formés par réactions des monomères avec de l'oxygène dissous dans les derniers. La formation, la décomposition et la constitution de ces peroxydes sont étudiées de manière intensive et une cinétique formelle est proposée pour les réactions de formation et de décomposition.

La polymérisation du MMA est sujette à une auto-accélération conséquente appelée "effet de gel", dont l'intensité dépend des conditions du procédé et de la quantité de solvant. Plusieurs modèles proposés dans la littérature spécialisée décrivent ce phénomène en modifiant la constante de vitesse de terminaison en fonction de la conversion et de la température. La seconde partie de cette étude comprend l'évaluation de ces modèles au regard de leur applica-

bilité à la polymérisation à haute température du MMA, ainsi que le développement d'une nouvelle variante d'un modèle existant, décrivant correctement l'effet gel dans l'intervalle de température considéré en fonction de la quantité de polymère, de la température et de la masse moléculaire. Les avantages de cette nouvelle variante sont le fait qu'elle inclut tous les autres facteurs influençant l'effet gel, à savoir l'agent de transfert de chaîne, la charge d'initiateur, les quantités de comonomère et de solvant, et sa capacité à décrire les procédés en batch et en continu. Un modèle cinétique complet pour la description de la copolymérisation à haute température du MMA et du MA, contenant les résultats des deux premières parties de ce travail, est établi à l'aide du logiciel PREDICI® et validé par plusieurs séries de polymérisations en batch.

Dans la troisième partie de ce travail, une installation pilote complète pour la polymérisation du MMA est conçue et construite, de façon à pouvoir étudier l'effet de l'augmentation de la température de réaction sur les propriétés du processus et la qualité du produit dans des conditions similaires à celles d'une polymérisation à l'échelle industrielle. L'installation pilote est formée à la base de la succession d'un réacteur avec recyclage en boucle et d'un réacteur tubulaire, équipés de mélangeurs statiques Sulzer SMXL® / SMX®. Elle est en outre équipée d'un dévaporisateur flash à une étape et d'une granuleuse. De plus, une méthode affinée pour la surveillance de la conversion en ligne par mesure de la vitesse du son est développée et testée sur l'installation pilote. Il est possible au moyen de cette technique de suivre le comportement dynamique du réacteur et de mesurer directement la conversion de monomère sans prendre d'échantillon. Les résultats de plusieurs polymérisations en installation pilote effectuées dans différentes conditions sont présentés, et les influences de la température, du comonomère et de l'agent de transfert de chaîne sur la stabilité thermique du produit sont analysées. Ces résultats permettent en outre la détermination des paramètres r pour la copolymérisation du MMA et du MA à 160 °C, et de la constante de transfert de chaîne pour le n-dodécanethiol à 140 °C. Finalement, les expériences en installation pilote sont utilisées pour valider le modèle cinétique établi auparavant avec PREDICI® pour la copolymérisation en continu.

Mots-clés: Polymérisation radicalaire, Haute température, Méthacrylate de méthyle, Copolymérisation, Surveillance en ligne par ultrason, Effect de gel, Stabilité thermique, Modélisation cinetique, Pilot Plant Technologie, Mélangeurs statiques.

Table of contents

Preface

The research on pilot scale polymerization reactions in the polymer reaction engineering group at EPFL began more than 20 years ago. The first PhD thesis of 1982 [1] dealt with a newly developed tubular reactor concept that was based on tubes equipped with Sulzer mixing elements. Up to that moment, industrial polymerization reactors consisted mainly of stirred tank reactors, whereas tubular reactors played only an unimportant role due to their bad heat exchange properties and small capacities. The aim of that first thesis was to describe the fluid- and thermodynamical behavior of this new type of reactor, which generally consists of a recycle loop and a consecutive tube, as well as to prove its superiority to classical stirred tank reactors. In the following years, this concept was continuously further-developed in various different projects [2-4] and although first researches concentrated on the polymerization of styrene as a model reaction, the same kind of reactor setup has lately been employed with great success for methyl methacrylate (MMA) polymerizations:

The work of P.-A. Fleury [5] in the 90's dealt for the first time with the high-temperature polymerization of MMA in the Sulzer pilot plant.

Between 1998 and 2001, the plant was used in the frame of a European research project that aimed for the reduction of residual volatiles' concentration (LOWRESCO) in industrial polymerization and degassing. From the side of EPFL it was the thesis of Thomas Zeilmann [6] that contributed to this project. The pilot plant setup designed for that project was the basis

1

for the one used in the present work: recycle loop, consecutive plug flow tube and devolatilization chamber with continuous polymer discharge. Also the ultrasound conversion measurement, which had been developed by Renken and Cavin shortly beforehand [7, 8], was applied for the first time in an installation of this size.

When I came to EPFL in January 2001 for my diploma work [9], which was a part of the before-mentioned project, Thomas Zeilmann was in the last year of his thesis. During the following time, various interesting features concerning PMMA, itself, and the continuous polymerization of MMA were investigated. These were in particular the thermal stability and thermal stabilization of PMMA during devolatilization, the two-phase devolatilization strategy and the addition of a stripping agent to the reaction mixture for improved devolatilization.

At the end of 2001, a first contact with the Degussa Röhm GmbH&Co KG in Darmstadt, one of the most important producers of acrylics in the world, was established with the aim of a joint research project between Röhm and EPFL. This was also the moment when I took the decision to stay in Lausanne for my PhD thesis. Luckily, we received a very positive feedback from Degussa Röhm concerning the cooperation and in the beginning of 2003, after one year of preparations and defining the general frame for this quest, the project officially started.

This cooperation with Degussa brought a new, rather industrially orientated drive into the research on pilot scale polymerization at EPFL, with a major focus on the high temperature polymerization process and the kinetic particularities connected to it. Also, for the first time, the produced polymer had actually to compete with the commercial grade product and, although the "real" production conditions remained a well-kept secret, the process conditions for the pilot plant experiments came much closer to reality than they had been in earlier projects.

During the three years of this PhD project, I had the opportunity not only to present my results at various international conferences but also in various meetings with the industrial partner, from where I received constant feedback concerning the progress of my work, which, looking back, I would not have liked to miss.

In the following chapters and appendixes, the results of this joint research project, which unfortunately has to end with the present report, are presented and I already want to express my deep gratitude to all persons that have been involved in it, no matter to what extent.

CHAPTER 1

Introduction

1.1   General

Since its discovery in the late nineteenth century, poly (methyl methacrylate) or *PMMA* has been continuously developed and gained an important role in our daily life. Better known as PLEXIGLAS®[1], they can be found not only as a more robust alternative to glass in the building and construction industry but also in automobiles, in many electronic devices, and increasingly also in the medical sector. An application that underlines the mechanical and optical properties of PMMA is its use for aircraft windows and canopies.

With a worldwide capacity of around 840'000 tons per year [10], poly (methyl methacrylates) have become an important product for the manufacturers of thermoplastics. Their aim to increase the number of applications and thus the demand for PMMA on the market at the same time requires better and more specific product properties. Furthermore, with the intensifying

---

1. *PLEXIGLAS* is a registered trademark of the DEGUSSA Röhm GmbH, Germany

competition on the world market, the need to optimize processes and process yields has become even more evident.

For a long time, PMMA was only manufactured by casting. A few applications, i.e. aircraft windows and thick polymer sheets, where very high molecular weights are mandatory in order to guarantee a maximum mechanical strength, still require this discontinuous process. However, with the increasing demand for lower molecular weight types, especially for extrusion and injection moulding, continuous polymerization processes are needed to meet production capacity and product quality requirements.

The continuous technical and product development has produced a huge amount of different polymer and copolymer types, the composition of which strongly depends on their application. There are highly specialized mixtures for applications in the optical and coating industry on the one hand, and on the other hand large-scale copolymer commodities for the automobile and construction industry. Most of them have in common to be polymerized in solution or bulk polymerization processes. The by far mostly spread process variant is the CSTR - tube reactor combination with process temperatures up to 140 °C. In order to improve the thermal and mechanical strength of the polymer, comonomers and other additives (e.g. transfer agents) are added in small amounts. At the end of the polymerization process, the polymer melt is degassed in several steps and the devolatilized polymer is pelletized for transport and storage.

For the production of work pieces with the desired shape (e.g. car lights), the polymer pellets are molten up in an extruder and injected into part-specific molds. During this last production step, the thermal stress on the polymer is the highest and thermal stability of the polymer becomes a very important issue.

1.2   Historical background

When Polymethylmethacrylate was synthesized for the first time in the year 1877 [11], the general understanding of polymerization and its products was still in its infancy. Polymers were regarded as useless side products and discarded. The person who started the research and further development of PMMA was Otto Röhm by his thesis in 1901. Yet, it took him another 30 years to build up the first production of cast PMMA sheets. This was the basis for his company, the German Röhm GmbH, today subsidiary of the Degussa AG, which introduced in 1934 Polymethyl-

methacrylate under the registered trademark Plexiglas®, still the most common name for this polymer. At the same time, the British Imperial Chemical Industries (ICI), started the production of PMMA.

During the Second World War, the polymer gained importance in the production of military aircraft canopies because of its, compared to glass, smaller specific weight and its strong mechanical properties. It was considered as war-important and thus, the production capacity was increased considerably in the United States, Britain and Germany. After the war, the demand for PMMA drastically decreased until other, civil applications were found, among which the use for streetlamps, neon tubes, safety glass and optical lenses. Also, first copolymers with acrylonitrile were applied for their better impact strength. With the ability to injection mould poly (methacrylates), the continuous production of molding compound pellets catched up quickly with the casting and, nowadays, more than two thirds of monomer are converted to moulding compound.

Four European manufacturers - Atoglas (Atofina), Degussa-Röhm, Barlo PLC and Ineos - and four Asian manufacturers dominate the present PMMA market. Together, they have a production capacity of about 840'000 tons / year. Yet, compared to other thermoplastics, PMMA holds only a small share of all thermoplastics on the world market, as figure 1.1 shows. In order to increase this share, manufacturers of acrylics make every effort to develop new product qualities for highly sophisticated applications. These include the use of acrylic polymers for optical discs, for example new generations of the DVD, where the concurrence with polycarbonates is the driving force for new product developments.
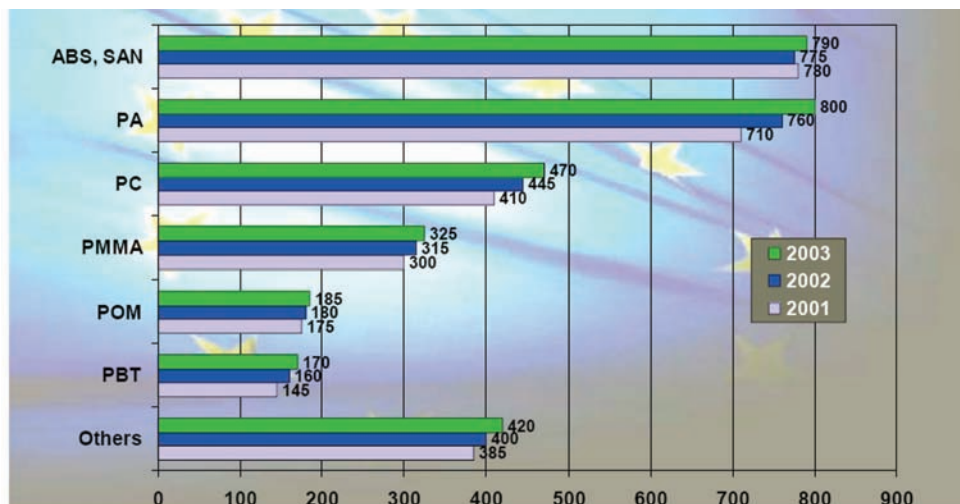
Figure 1.1: Thermoplastic consumption in Western Europe 2001-2003 [12]

1.3   Aim of this work

The aim of this work, which has been carried out in close cooperation with industry, is to kinetically describe the high temperature polymerization of methyl (methacrylate), to investigate the feasibility of a polymerization process at 140 °C < T < 170 °C and to study the impact of temperature on the product quality in a continuous pilot-scale process.

The polymerization of methyl methacrylate is probably the best described polymerization reaction in polymer science. However, most research that has been published in the specialized literature deals with the polymerization at a rather low temperature range (< 100 °C). Unfortunately, increasing the reaction temperature above this value changes significantly the underlying polymerization kinetics. In particular, the following three phenomena have to be reevaluated:

- the self-initiation reactions
- the gel effect
- and the depolymerization

It was, therefore, necessary to start with the determination of kinetic parameters and the development of a gel effect model for the given temperature range and to validate both with the help of experimental data. These features could then be included in a general kinetic model for the description of the whole polymerization process. Several series of experiments were carried out at bench-scale and various analytical methods had to be established in order to accomplish this important part of this work.

The second step was the design and setup of a continuous pilot plant in order to investigate the polymerization under conditions similar to the industrial process. For the present work, a setup based on the combination of a recycle loop and tube reactor was chosen, as it had been already successfully employed in earlier research studies of this workgroup. The frame of the continuous polymerization process also allowed a development study of a relatively new process monitoring technique based on the speed of sound measurement and the determination of copolymerization and chain transfer related parameters from steady-state polymerizations.

The various goals of this PhD project are itemized once again in the following list containing each individual part of this work together with a brief description of the work carried out to achieve them.

Self-Initiation at high temperatures

- Determination of the **formation kinetics** of **MMA peroxides** in batch experiments:

  Development of an **analytical method** for the determination of **organic peroxides**

- Determination of the **decomposition kinetics** of **MMA peroxides** by DSC:

  Synthesis and **Isolation** of MMA peroxides

  Method for the determination of reaction kinetics by DSC

- **Characterization** of MMA peroxides by GPC, TGA and NMR

- Investigation and characterization of **other mechanisms** influencing the self-initiation of MMA (thermal initiation, initiation by CTA, dimerization)

- **Verification** of the entire self-initiation kinetics in **batch polymerization experiments**

Gel effect at high temperatures

- **Evaluation** of **existing gel effect models** toward their application at high temperatures

- Derivation of an **adapted model** for the correct description of the high temperature gel effect

- Determination of the **parameters influencing the gel effect**

- **Model verification** by means of batch polymerization experiments

Continuous High Temperature Polymerization

- **Design** and **construction** of a **pilot plant** with a capacity of 1-5 kg PMMA per hour

- Development of a method for the **direct** and **inline monomer conversion monitoring** by **speed of sound measurement**

- Determination of r-parameters for the copolymerization MMA / MA

- Determination of the chain transfer constant for n-dodecanethiol

- **Evaluation** of the obtained **product** at high temperatures concerning **molecular weight, residual monomer** and **thermal stability**

- Production of several batches of polymer pellets for the evaluation of the product quality in injection molding experiments (carried out by the industrial partner)

- Establishing a **kinetic model** in **PREDICI®** for the description of the continuous copolymerization process and validation with experimental data

CHAPTER 2

Self-Initiation at high temperatures

Monomers used in radical polymerization are unsaturated compounds that can undergo various reactions and therefore exhibit only a limited stability. Many of them polymerize already at room temperature when not sufficiently stabilized by radical scavengers. Styrene, for example, has a very distinctive self-initiation potential, which is caused by intermolecular interactions due to its molecular structure, i.e. the formation of an unstable dimer [13]. Therefore, it usually needs to be stored under cooling or with rather large amounts of stabilizer. Since this self-initiation gets more important with increasing temperature, it is usually referred to also as "spontaneous thermal initiation".

For MMA, the thermal initiation also exists but, due to the different molecular structure compared to styrene, the mechanism is much slower. Depending on the temperature, it usually takes days if not months for a sample of purified MMA to polymerize to noticeable extents. However, if technical MMA as supplied by the producers is heated to above 100°C, quickly a considerable polymerization with monomer conversions of more than 20% can be observed. This motivates the question of which nature the initiation that is the cause for this polymerization might be and, if there are radicals involved in the mechanism, what their origin is.

In literature, several reasons for thermal polymerization of MMA can be found. Stickler, Lingnau and Meyerhoff, for example, have carried out extensive research on this topic. In their series of publications "The Spontaneous Thermal Polymerization of Methyl Methacrylate 1-6" [14-19], they determine the rate constants for the reproducible spontaneous thermal initiation, which is not overlaid by initiation reactions of impurities, and discuss furthermore the forma-

tion of di- and trimers as well as the initiation potential of chain transfer agents. Even the initiation by cosmic and environmental radiation is taken into account and evaluated by them. As concerns initiation reactions caused by impurities, the attention is quickly drawn to peroxides in the relevant literature. The possibility that MMA and other unsaturated compounds react with oxygen traces to form peroxides has already been described in the 50's by Mayo and Miller [20] and Barnes et al. [21]. These peroxides have been proven to decompose at higher temperatures and to form radicals that can initiate polymerization. This mechanism is even supposed to be the dominant reason for "thermal initiation" of MMA at temperatures above 100°C [22].

In this chapter, the different initiation mechanisms[1] are discussed, first of all the MMA peroxide initiation, and experimental results that were obtained in this work are presented. The characterization of MMA peroxides, their formation and decomposition has been one of the key interests of this project. Especially in industrial processes, where impurities and atmospheric gases are always present, it is of great importance to carefully characterize these reactions since they may have a significant influence on process safety and are able to falsify results in pilot plant experiments, which can then lead to misinterpretation of data.

2.1 MMA peroxides

2.1.1 Introduction

Methyl methacrylate is in most cases stabilized for transportation and storage with stabilizers of the hydroquinone type, e.g. hydroquinone and 4-methoxyphenol. The active principle of this class of stabilizers is based on an interaction with oxygen, since they are not capable of capturing radicals themselves [23, 24]. However, they readily react with peroxy radicals. In the following, the stabilization mechanism is presented and the role of oxygen in the stabilization becomes evident.

The primary radical R⋅ is generated by not further defined, arbitrary processes as for example radiation, molecular interactions or decomposition of other impurities in the system. The oxy-

---

1. The dimerization does not represent an initiation mechanism for the radical polymerization of MMA but is discussed nevertheless in this chapter as it can have significant effects on the monomer conversion at high temperatures.

gen molecule O_2 is a biradical with a very high affinity to other radicals. Therefore, the radical R·
rather reacts with oxygen than with another radical [23]. As long as there is enough stabilizer and
oxygen present in the system, radical initiation of the polymerization is inhibited:

$$\text{OH}-\text{C}_6\text{H}_4-\text{OCH}_3 \;+\; \text{R·} \;\;\xcancel{\longrightarrow} \qquad\qquad (EQ\ 2.1)$$

$$\text{R·} + \text{O}_2 \longrightarrow \text{ROO·} \qquad\qquad (EQ\ 2.2)$$

$$\text{ROO·} + \text{OH}-\text{C}_6\text{H}_4-\text{OCH}_3 \longrightarrow \text{ROOH} + \text{·O}-\text{C}_6\text{H}_4-\text{OCH}_3 \qquad (EQ\ 2.3)$$

$$\text{ROO·} + \text{·O}-\text{C}_6\text{H}_4-\text{OCH}_3 \longrightarrow \text{O}=\text{C}_6\text{H}_4(\text{OCH}_3)(\text{OOR}) \qquad (EQ\ 2.4)$$
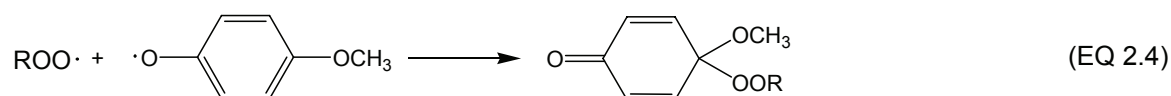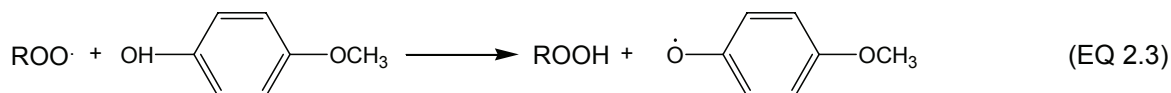
Hence, it is important to store the monomer under oxygen containing atmosphere so that the
inhibition is guaranteed.

In the absence of stabilizer, either in purified monomer or due to its consumption by reac-
tions as in equation 2.3 and equation 2.4, the radical ROO· from equation 2.2 is no longer trapped
by the methoxyphenol, but can react freely with other molecules. Thus, if there's enough oxygen
present, it creates an alternating, copolymeric chain of oxygen and monomer, as it was proven by
NMR, FTIR and pyrolysis studies [25, 26]:

$$\text{ROO·} + \text{M} \longrightarrow \text{ROOM·} \xdashrightarrow{\;O_2\;} \text{ROO(MOO)}_n\text{·} \quad \text{(qualitative mechanism)} \qquad (EQ\ 2.5)$$
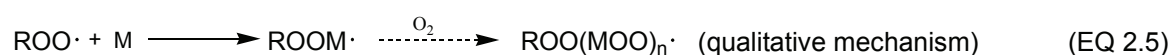
The peroxide obtained is also referred to as *PMMA peroxide, MMA polyperoxide, MMA-OO*
or simply *PMMAP*. Since these chains are stable at medium temperatures (i.e. in general below
100 °C), also oxygen indirectly has a stabilizing effect on the monomer (by scavenging radicals
and forming peroxides), which means that storage under oxygen containing atmosphere is already
enough in order to prevent polymerization. The principle of this stabilization with oxygen was
first investigated in 1955 by Schulz and Henrici [27]. However, with time the peroxide chains
accumulate in the monomer, a fact that becomes an issue at higher temperatures. As reported by
several authors, the thermal decomposition of PMMAP starts between 130 °C [28] and 150 °C
[25]. In the latter article also a decomposition mechanism via radical chain scission is proposed:

(EQ 2.6)
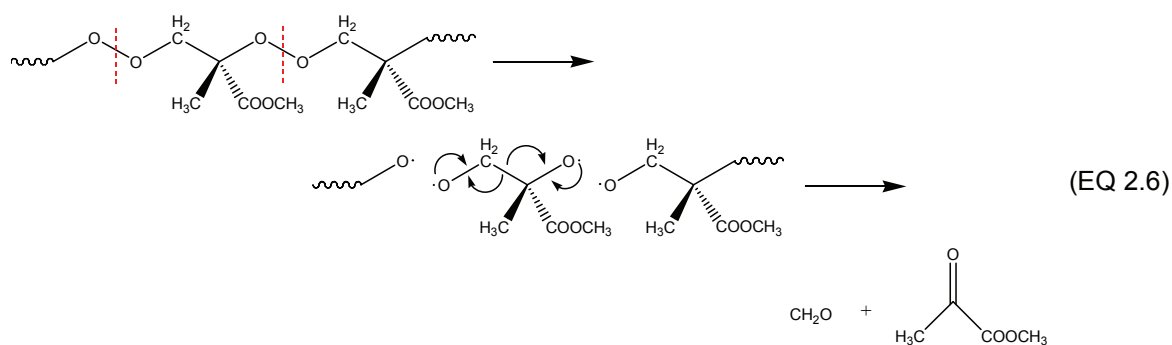
The produced radicals have a high initiation potential [29] and, therefore, PMMAP can be also considered as a high-temperature initiator for radical polymerizations.

An alternative to equation 2.5 is the formation of hydroperoxides [30]. These are supposed to consist of one or more monomer units with a hydroperoxide -OOH group at the alpha methyl group and, therefore, to be more volatile than polyperoxides. However, it is difficult to distinguish with the available analytical methods between poly- and hydroperoxide. One possibility could be the use of MALDI mass spectroscopy but, unfortunately, the time frame of this work did not allow further investigations. Only the presence of polyperoxide could be proven by NMR, whereas hydroperoxides were not detected in any sample (see also "Isolation and Characterization of PMMAP" on page 21).

In the following, the formation, decomposition and structure of poly (methyl methacrylate) peroxide is once again discussed on the basis of various experiments carried out during this project, and the results are compared to the above mentioned literature data. Due to their initiation ability at high temperature, it is very important for modeling the high temperature polymerization to carefully describe the properties of PMMAP and the results of the following subchapters will be found again in the modeling section of this work.

2.1.2   Formation of poly (methyl methacrylate) peroxide (PMMAP)

For the determination of the PMMAP formation kinetics, several approaches are possible. One is to measure the oxygen absorption or consumption rate in MMA at different temperatures [23, 31, 32]. With the above mentioned formation mechanism, the kinetics can then be estimated. Another way, which was chosen in this work, is to determine directly the peroxide concentration in the monomer. However, this proved to be a non-trivial problem, since most methods for peroxide determination work in aqueous media only. Few titration methods for organic peroxides were found, working with sodium iodide (NaI) and thiosulfate (NaS_2O_3) and glacial acetic acid as reagents in solvents like isopropanol [33] or chloroform / methanol mixtures or even two-phase systems with water. The problem is already to dissolve the inorganic salts in the organic solvents. A second weak point of these methods is that iodide is readily oxidized by atmospheric oxygen in these solvents, so the measurement error is relatively high. Additionally, within the expected rather low concentration range (< 100 ppm O_2), the precision of titration methods was considered to be not sufficient for kinetic investigations.

Finally, a method found in [34] from 1946, which is described by the authors to be not influenced by air in the same extent than other methods, was modified to work in combination with UV-Vis spectrophotometry. The only difference between this procedure and the previously mentioned one is that it uses acetic anhydride as a solvent, which acts as solvent and proton donor for the oxidation of I^- at the same time and exhibits excellent solubility for NaI.

For the peroxide analysis according to the modified method presented in appendix 1, "Organic Peroxide Determination by UV", samples of 5 ml MMA were mixed with 10 ml of acetic anhydride containing ca. 0.1 g of dissolved NaI. After 15 minutes of stirring, the mixture has turned yellow depending to its peroxide content. The coloration is caused by the iodine formed according to equation 2.7 [30] or equation 2.8, which shows the reduction of a commercial peroxide (e.g. benzoyl peroxide) used for calibration of the UV.

$$ROOR \ + \ 2\,H^+ \ + \ 2\,I^- \ \longrightarrow \ I_2 \ + \ 2\,ROH \qquad\qquad \text{(EQ 2.7)}$$

$$\text{(EQ 2.8)}$$
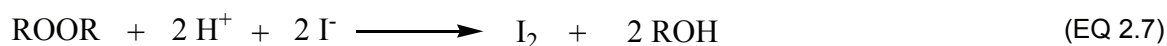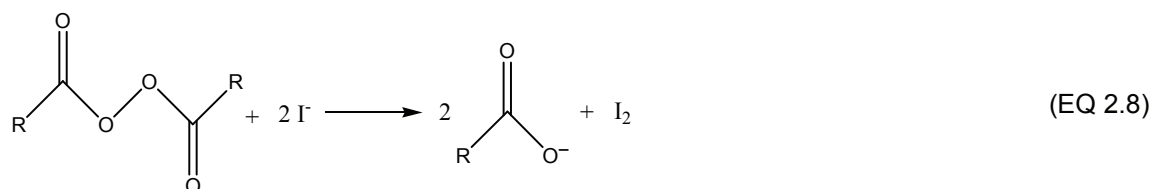
This iodine can then be either determined by titration with NaS_2O_3, or directly by UV-Vis Spectrophotometry, since it absorbs light with a maximum at 360nm. UV-Spectrophotometry has the advantage that it is fast and very precise in given calibration intervals, and the problematic of finding a calibrated NaS_2O_3 solution that dissolves in acetic anhydride does not present itself. Detailed information on the employed UV method can be found in appendix 1 together with the other analytical methods.

One important point concerning the investigation of the PMMAP formation is the quality of the monomer. As mentioned before, the monomer is usually stabilized for transport and storage with 4-methoxyphenol, which consumes oxygen and prevents the formation of PMMAP until it is completely consumed. Therefore, to obtain reproducible measurements, it is necessary to purify the monomer prior to the experiments. The purification method is described in the appendix.

MMA-peroxide formation experiments

In the beginning, the monomer was only washed with 2N NaOH, neutralized with $H_2O_{demin.}$, dried over $CaCl_2$ and used without further distillation. During subsequent storage, the contact with atmosphere was guaranteed by closing the flask with a drying tube containing $CaCl_2$ instead of a stopper. Proceeding like this was necessary to ensure oxygen saturation. For the experiments, the MMA was filled into 7.4 ml screw cap vials (Fluka 27149), which were filled to the top in order to avoid air in the vial and subsequently completely submerged into temperature-controlled oil-baths (see figure 2.1 a). Due to the complete submersion, it can be excluded that atmospheric oxygen could penetrate the vials through their sealings.

(a)   (b)
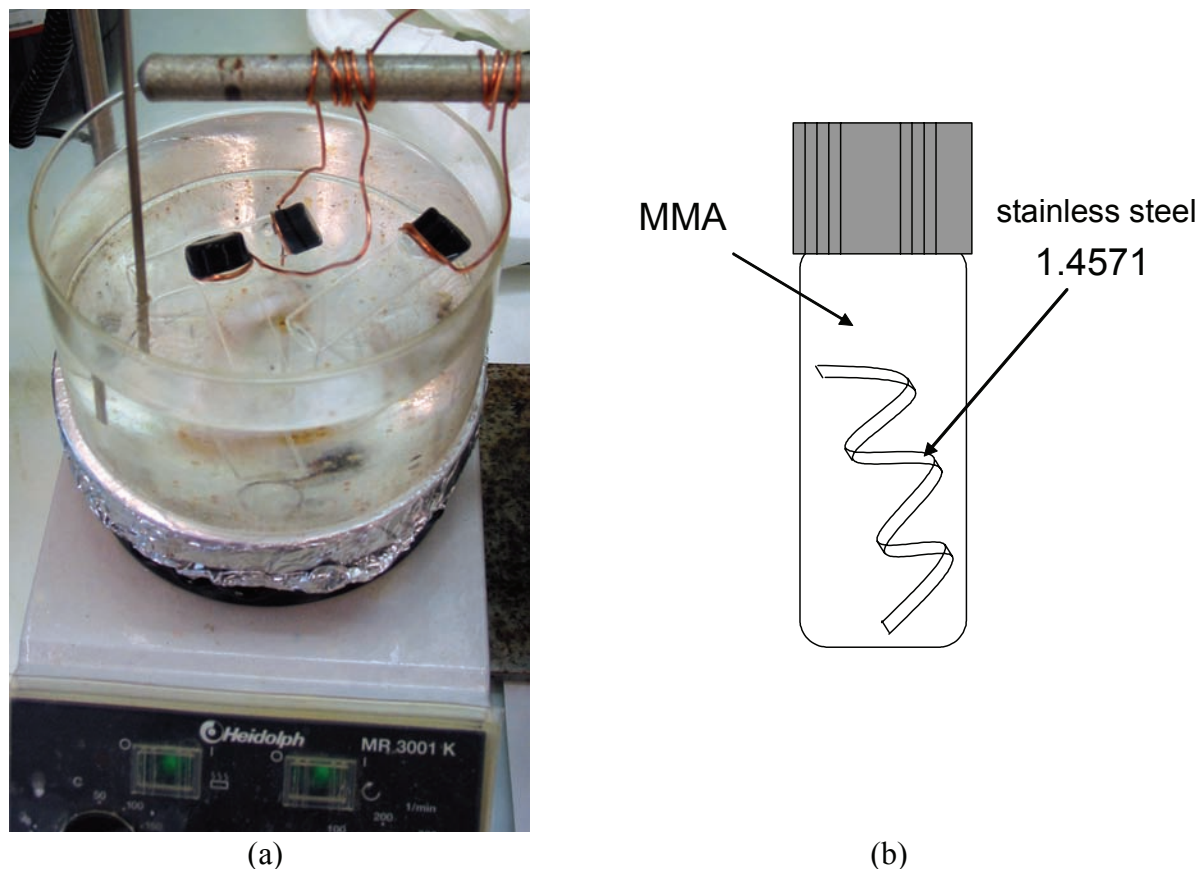
*Figure 2.1: (a) Oil bath with monomer-filled screw cap vials for peroxide formation experiments
(b) Testing of the influence of stainless steel on the formation of MMA-OO*

After given periods of time, one vial at a time was removed from the oil bath, quenched in iced water and directly analyzed as described above.

The following graphic, figure 2.2, shows the measured peroxide concentrations in this non-distilled monomer over time for different temperatures. After 50 hours at 40 °C, still no significant peroxide concentration was measured. Also the time scale for higher temperatures is remarkably large, i.e. it takes hours for a noticeable peroxide content to appear in the sample. Only at 80 °C, respectively 90 °C, the peroxide concentration increases significantly within the first two hours.
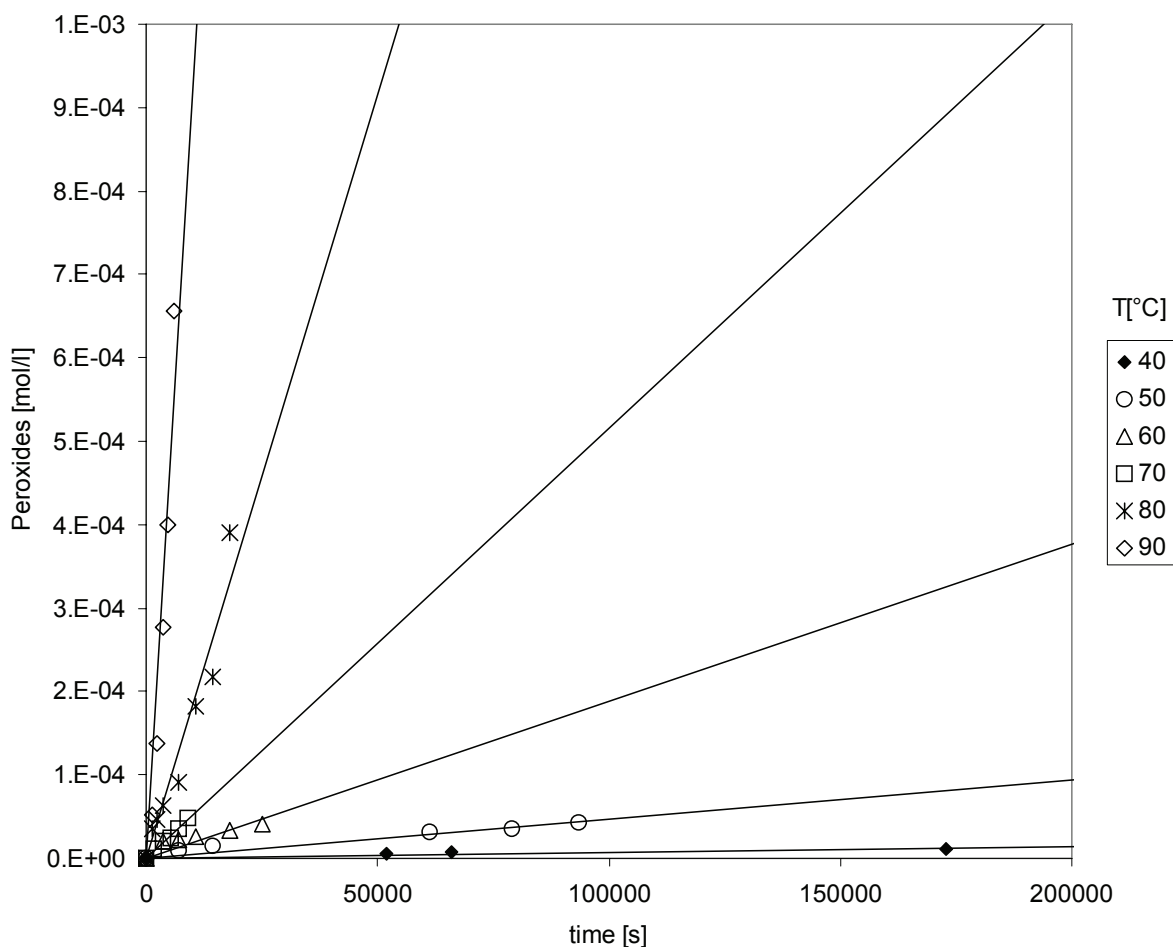
*Figure 2.2: Peroxide formation in NaOH-washed, dried and air-saturated monomer
(non-distilled, filled in gas-tight vial)*

Since it cannot be said for sure that all inhibitor is removed from the monomer by the washing, as well as all water removed by drying, it might be due to these factors that the peroxide formation appears rather slow in the above experiments. Therefore, the complete series was repeated with distilled monomer (see appendix for distillation procedure). However, the distilled monomer, too, was stored in an open flask afterwards, in order to ensure oxygen saturation.

For the distilled monomer the peroxide formation rate was found to be much higher. Also the reproducibility between several series of measurements was high, contrary to the non-distilled monomer where this was not the case. The results of one series of experiments are presented in figure 2.3, which has the same y-scale than figure 2.2 but a much shorter time scale. This proves

that in distilled monomer, the rate of peroxide formation is by a factor of approximately 10 higher than in the non-distilled one.

A possible explanation for this observation is, as mentioned before, the presence of water in the monomer. At least it was found that the time the monomer was dried over $CaCl_2$ after washing with NaOH had a major influence on the obtained monomer conversion in blind experiments: the longer the monomer was dried the higher were the conversions. Inversely, when water was added to dried monomer, the conversion decreased. This might be evidence for an inhibiting effect of water. However, due to the strongly irreproducible character of these results, they are not presented at this point. Future experiments should concentrate on this effect and especially investigate the influence of water on the formation of MMA peroxide.
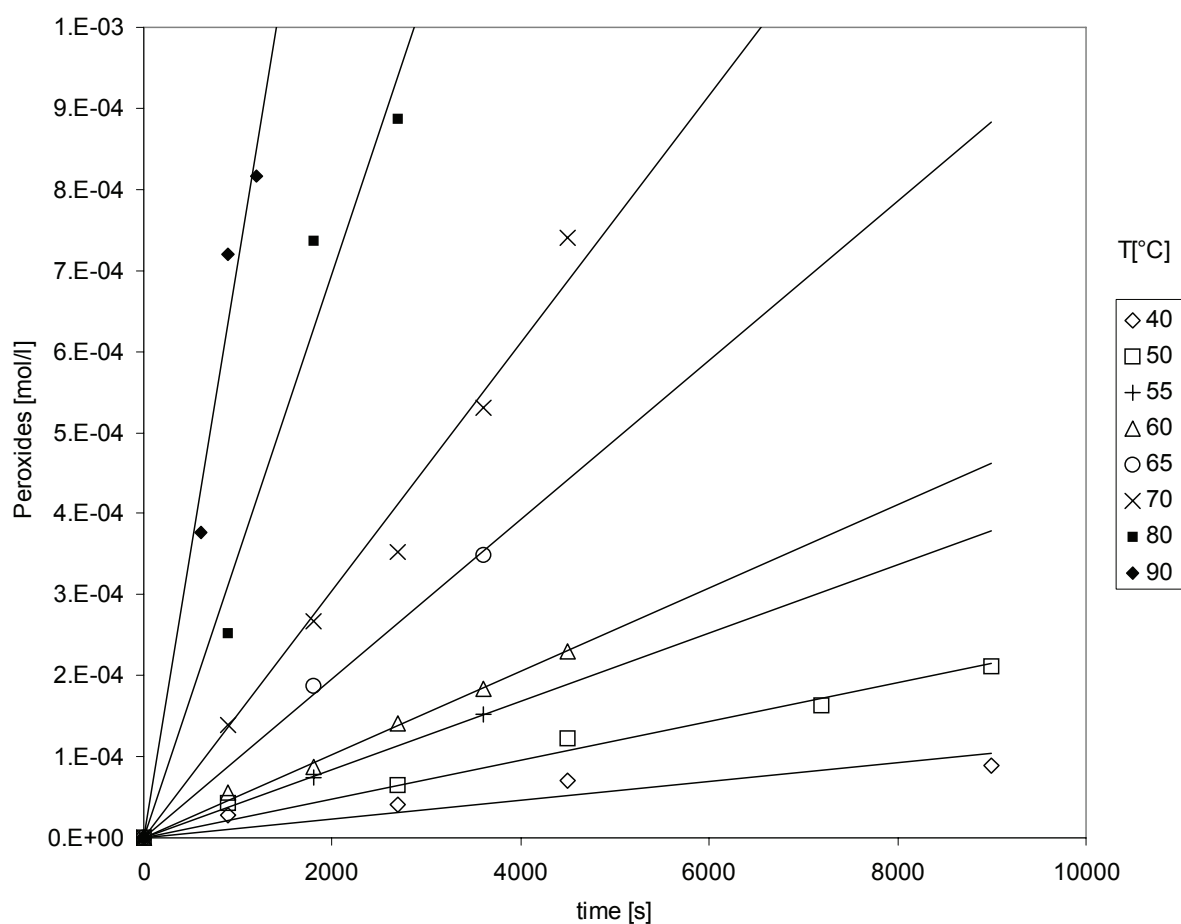
Figure 2.3: Peroxide formation in distilled, air-saturated monomer (filled in gas-tight vials)

In order to use this data in a way to obtain formation kinetics for PMMAP, some mechanistic considerations and simplifications had to be made. Since PMMAP is a polymeric peroxide with only ideally an alternating copolymeric structure, the correct mathematical description of its formation would be quite complicated. Therefore, an idealized unimolecular approach was chosen to determine the kinetic constants according to Arrhenius, which will be explained in the following. One unknown in this approach is the oxygen concentration in the monomer at the beginning of the experiment, i.e. the temperature-dependant saturation concentration of O_2 in MMA. This oxygen concentration has been determined experimentally for acrylic acid / methacrylic acid [23] and for tripropylene glycol diacrylate (TPGDA) [35]. In both cases, the results were in the order of 60 ppm or 10^{-3} mol/l, so it seems justified to assume this value also for MMA in this work.

The simplified mechanism for the peroxide formation is:

$$\text{MMA} + \text{O}_2 \ \rightarrow \ \text{ROOR'} \tag{EQ 2.9}$$

The rate of peroxide formation is therefore:

$$\frac{d[\text{ROOR'}]}{dt} = k[\text{MMA}]^m[\text{O}_2]^n \tag{EQ 2.10}$$

Due to its great excess with regards to oxygen, the MMA concentration can be considered constant:

$$[\text{MMA}] \ \triangleq \ \text{constant} \ \Rightarrow \ k[\text{MMA}]^m = k_{obs} \tag{EQ 2.11}$$

Since not the oxygen concentration but the peroxide concentration at time t is measured, it is necessary to express $[O_2]$ by $[ROOR']$ and the initial oxygen concentration $[O_2]_0$:

$$[\text{O}_2] = [\text{O}_2]_0 - [\text{ROOR'}] \tag{EQ 2.12}$$

Hence, the rate of peroxide formation becomes:

$$\Rightarrow \ \frac{d[\text{ROOR'}]}{dt} = k_{obs}\left([\text{O}_2]_0 - [\text{ROOR'}]\right)^n \tag{EQ 2.13}$$

$$\frac{d[ROOR']}{\left([O_2]_0 - [ROOR']\right)^n} = k_{obs}dt \qquad \text{(EQ 2.14)}$$

Integration of equation 2.14 yields equation 2.15 and equation 2.16 for $n = 1$, respectively, $n \neq 1$. However, with equation 2.15, a straight line is obtained in the Arrhenius diagram, which legitimates the assumption of first order kinetics with regards to oxygen and of zero-th order kinetics with regards to monomer.

$$n = 1 \Rightarrow \ln\left(\frac{\left([O_2]_0 - [ROOR']_0\right)}{\left([O_2]_0 - [ROOR']\right)}\right) = k_{obs}t \qquad \text{(EQ 2.15)}$$

$$n \neq 1 \Rightarrow \frac{1}{n-1}\left[\frac{1}{\left([O_2]_0 - [ROOR']\right)^{n-1}} - \frac{1}{\left([O_2]_0 - [ROOR']_0\right)^{n-1}}\right] = k_{obs}t \qquad \text{(EQ 2.16)}$$

The Arrhenius diagram for this simplified formation kinetics is shown in figure 2.4. From its slope and y-axis interception, the parameters k_0 and E_A were determined. Their values are reported in table 1. In comparison to the data previously published [36], they have slightly changed due to the addition of two more measurement series.

Table 1: Arrhenius parameters of the PMMAP formation in distilled monomer

	Value	Error
$\ln k_0 \ [s^{-1}]$	14.386	$\pm\,3\%$
$E_A \ [kJ\ mol^{-1}]$	70.3	$\pm\,2\%$

For higher temperatures, i.e. above 70 °C, the data becomes less reliable since PMMAP already starts decomposing and the measured concentration might already have been reduced by this decomposition. In addition, with a boiling point of $T_b=100$ °C for MMA, the monomer can partly evaporate from the vials due to its increasing vapor pressure. This might explain why the upper data points in figure 2.4 seem to break out of the line.

On the other hand, the precision of the measurement gets worse for low temperatures, where very small concentrations in the region of the measurement uncertainty have to be determined.

In order to investigate whether there is an influence of stainless steel on the MMA-OO formation reaction, several runs were carried out with HNO_3-treated swarfs of 1.4571/316Ti steel (compare figure 2.1 b), by which it could be shown that the formation is not at all influenced by the metallic surface in a reactor.
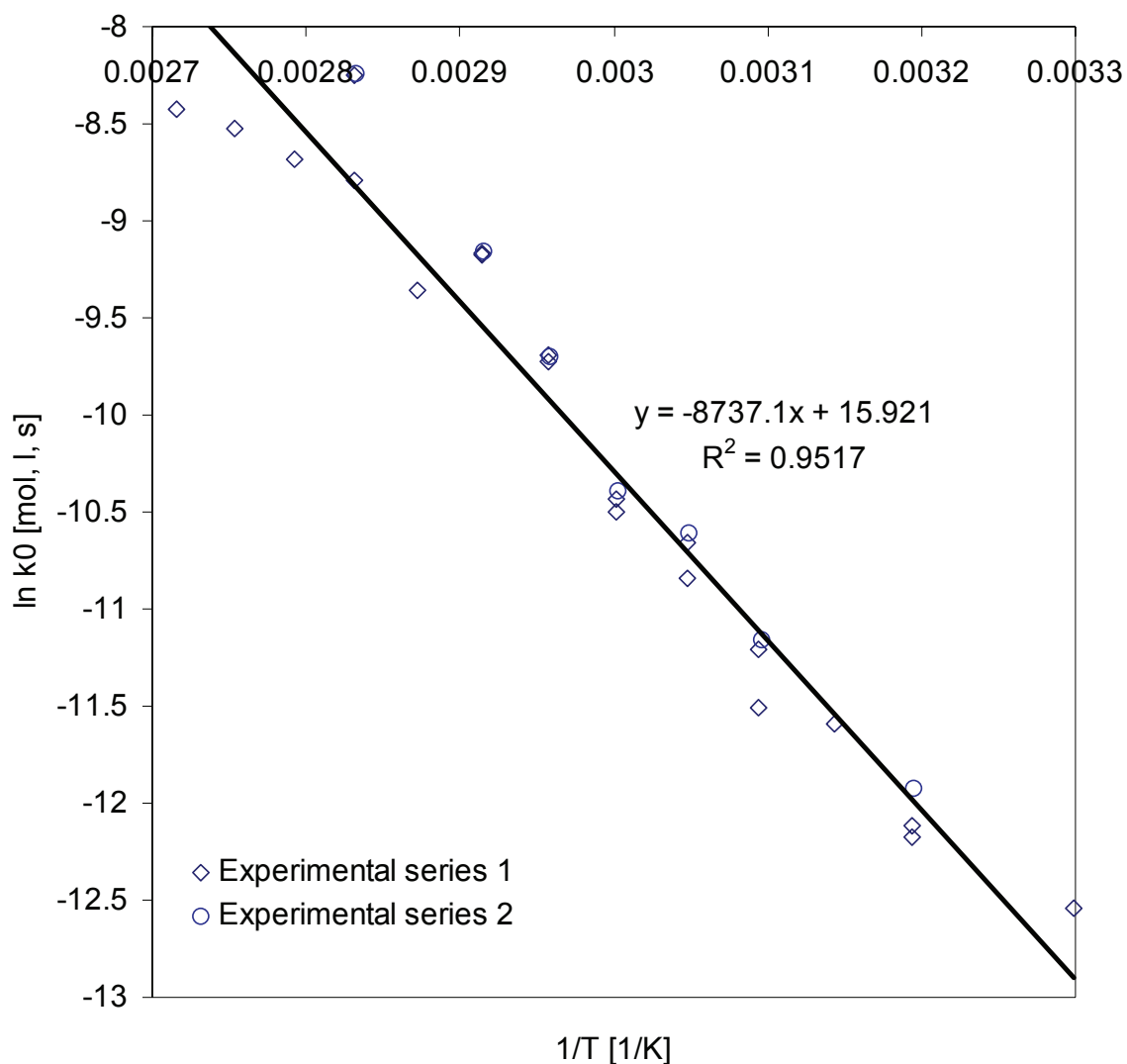
Figure 2.4: Arrhenius diagram for the formation of PMMAP (several series of experiments) according to equation 2.15

2.1.3   Isolation and Characterization of PMMAP

The amounts of PMMAP produced in the formation experiments of chapter 2.1.2 are certainly not sufficient for further analysis and characterization of the peroxide. In order to carry out GPC and NMR experiments for conformational analysis, sample weights in the order of some milligrams are needed. Thus, the aim was to synthesize and isolate the polymeric peroxide.

Since the oxygen, which is physically dissolved in the monomer at equilibrium state (20 °C, <100 ppm, compare appendix 1, "Oxygen determination in organic solvents"), is not present in sufficiently large amounts to produce enough peroxide for the different analyses, it was necessary to bubble pure oxygen directly from a gas cylinder through the monomer at elevated temperature. Therefore, distilled MMA was heated to 70 °C under reflux for several hours (see figure 2.5). After this, the content of the round flask was reduced in a rotary evaporator at reduced pressure (from 150 mbar to 2 mbar) until a viscous, clear liquid was obtained. The condensed volatile phase was checked for peroxides but the concentration was below the detection limit of 2 ppm. Hence, it can be excluded that any volatile peroxides were formed. The viscous residue was precipitated in fridge-cold petroleum ether (bp. 40-60 °C) at a volume ratio of 1:20 (volume of the liquid : volume of petrol ether), centrifuged and redissolved in 2 ml chloroform ($CHCl_3$). This procedure was repeated several times until a white, sticky substance was obtained.
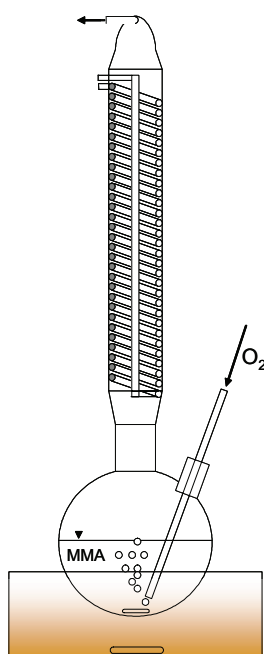
Figure 2.5: Experimental setup for the synthesis of PMMAP

The obtained sticky polymer was supposed to be or at least to contain the PMMAP. However, it could not be excluded that also ordinary PMMA had been formed during the oxygen bubbling due to radicals produced by the various reactions described above. Thus, in order to clarify the composition of the substance, at a first instance GPC analysis was done (details about the used GPC method in appendix 1).

Size Exclusion Chromatography (SEC/GPC)

Figure 2.6 shows the result of a GPC injection of three different solutions of the same polymer in THF (c = 1.8, 2.4 and 3.7 mg/ml). It can be seen that there are two peaks that change with concentration, corresponding to molecular weights of $M_w \sim 2.5 \; 10^6$ g/mol and of $M_w \sim 8'200$ g/mol, respectively. These average molecular weights were obtained by conventional calibration with PMMA standards (PSS, Mainz, Germany, M_w values can be found in appendix 1).

The smaller one is attributed to the PMMAP, which is in good agreement with literature data: Sivalingam et. al. [37] found a molecular weight of $M_n \sim 2'750$ g/mol for their PMMAP, which was polymerized at 50 °C with 0.01mol/l azoisobutyronitril (AIBN). Subramanian [28] reports a molecular weight of 1'800 g/mol for PMMAP that was polymerized at 40 °C with AIBN as radical source. However, in the latter case it is not clear if the reported molecular weight is M_n or M_w. The rather low molecular weight of PMMAP is explained by a high transfer activity and mutual termination of peroxy radicals [38].

The higher molecular weight peak is assumed to correspond to a high molecular PMMA that is formed in parallel to the peroxide by radical initiation at 70 °C. The high molecular weight is caused by the small amount of radicals following thermal breakdown of peroxides in the system and the rather low polymerization temperature.

This hypothesis of two separate polymers formed during the experiment also corresponds to the conclusion that Bamford and Morris come to in their work [38]. Looking at the surface under each peaks, which corresponds to the concentration of each component, reveals a ratio PMMA : PMMAP of 75% : 25%. However, the concentration is only comparable for identical dn/dc[1] val-

---

1. dn/dc stands for the change in refractive index n of a solution with increasing solute concentration c. This value is characteristic for various polymers and other substances.

ues of each polymer. In this case, it can, therefore, only be an approximation, as the dn/dc value for PMMAP is not known but likely to differ from the one for PMMA. Anyway, the peroxide content of the sample will be discussed later together with the results from the TGA measurements.
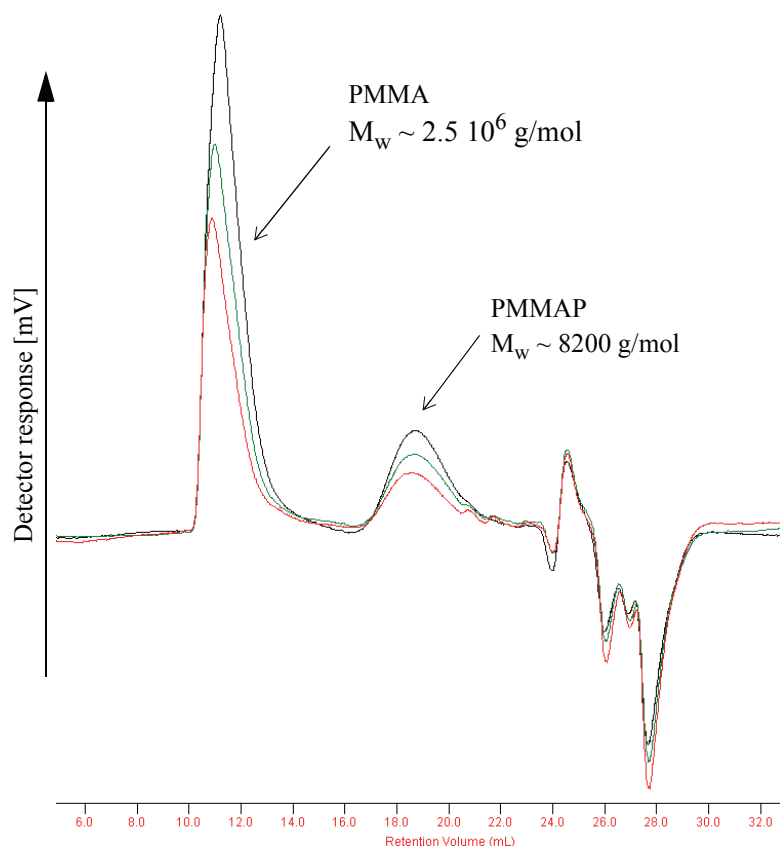
Figure 2.6: GPC analysis of the substance obtained in the PMMAP synthesis experiment

Table 2: Molecular weights of different PMMAP syntheses (GPC analysis)

	Mn [g/mol]	Mw [g/mol]	PD
1	1'961	7'451	3.8
2	2'893	6'921	2.4
3	3'654	8'172	2.2

NMR

For conformational analysis as well as for identification of PMMAP in the polymeric residue, ^{1}H- and ^{13}C-NMR spectra were taken. Due to the strong deshielding effect of the oxygen [30], peroxide groups in the polymer can be identified by several chemical shifts as explained in the following.

The ^{1}H-NMR spectrum, taken on a Bruker NMR at 400MHz, is depicted in figure 2.7. Corresponding to literature data [25] and information provided by an NMR specialist from the industrial partner [39], the spectrum shows the expected signals for PMMAP:

- 1.44 ppm $\quad\quad\quad\quad$ $-CCH_3-$
- 3.76 ppm $\quad\quad\quad\quad$ $-OCH_3$
- 4.34 ppm $\quad\quad\quad\quad$ $-OCH_2-$

The same applies for the ^{13}C-NMR spectrum, shown in figure 2.8, despite a small shift towards lower values with respect to the following literature data:

- 18.47 ppm $\quad\quad\quad\quad$ CH_3-C-
- 52.33 ppm $\quad\quad\quad\quad$ $CH_3-C=O$
- 75.79 ppm, 75.41 ppm $\quad\quad$ $-CH_2-O-$
- 84.78 ppm $\quad\quad\quad\quad$ $-C-O-$
- 171.03 ppm $\quad\quad\quad\quad$ $-C=O$

The decomposition product of PMMAP, *methyl pyruvate* or *propanoic acid-2-oxo-methyl-ester*, could be identified ([1]H: 2.46, and 3.86 ppm). On the other hand, no evidence of hydroperoxides was found ([1]H: 6.4, 5.9 and 4.7ppm, [13]C: 165.8, 128.7, 135.1 and 72.8 ppm).
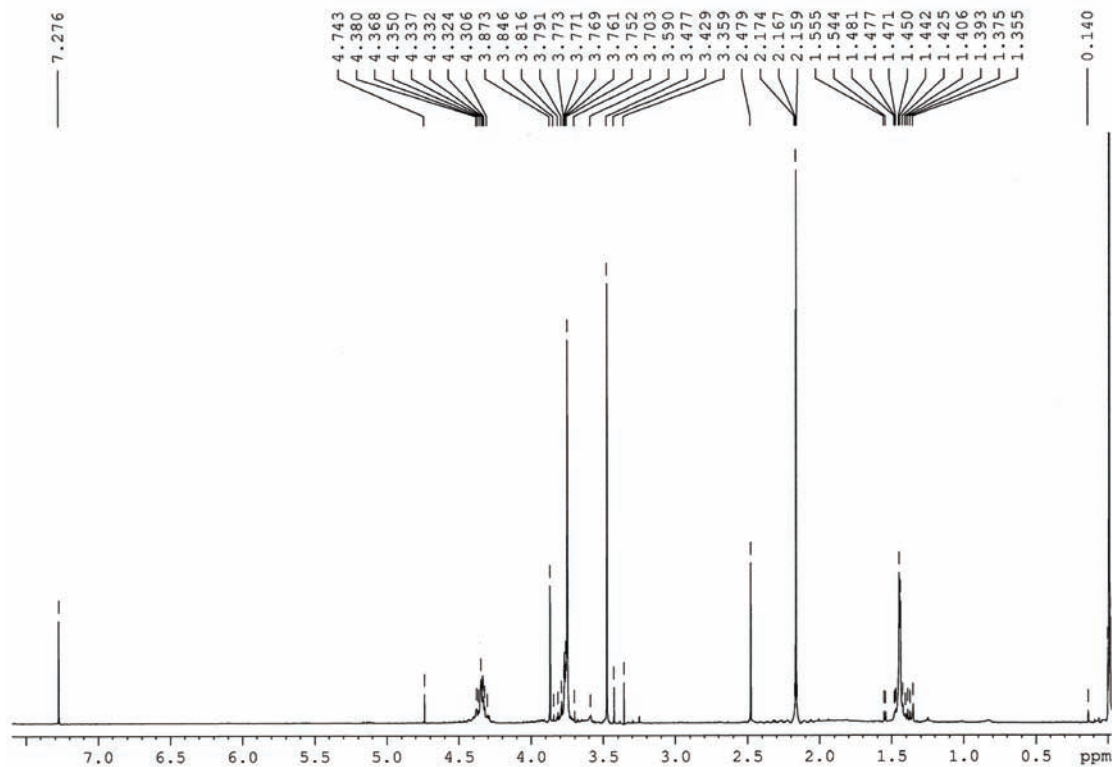
Figure 2.7: ^{1}H-NMR spectrum of the polymeric residue
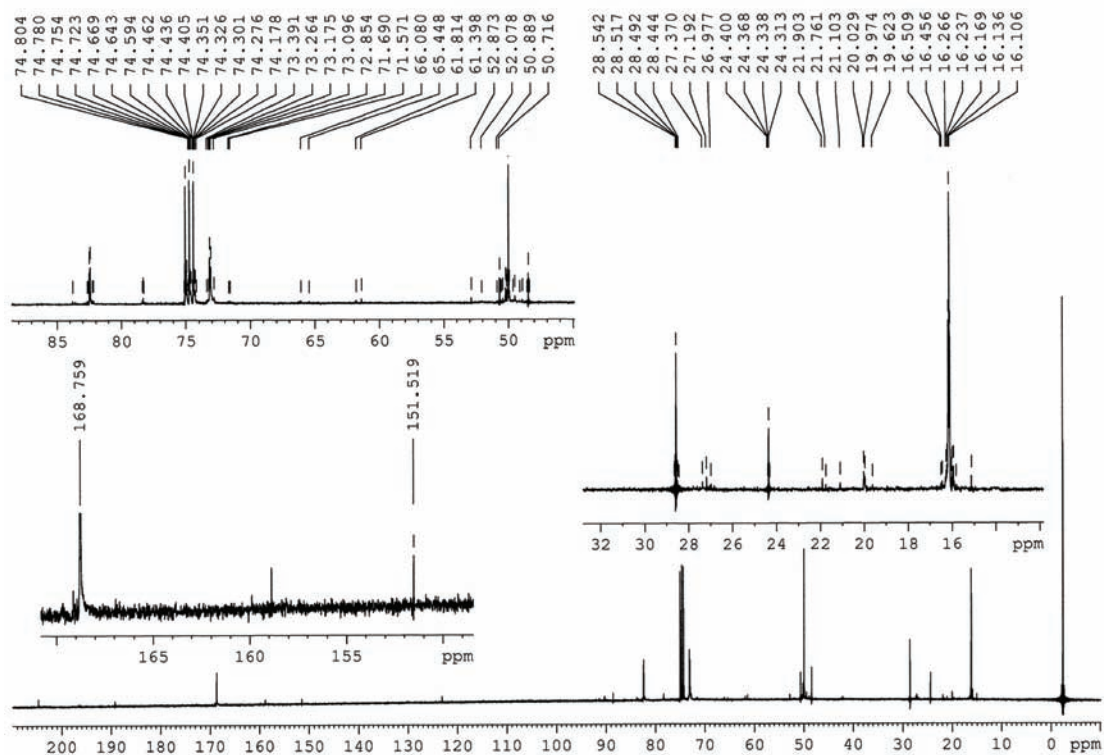
Figure 2.8: ^{13}C-NMR spectrum of the polymeric residue

2.1.4   Decomposition of PMMAP

The decomposition mechanism for PMMAP has already been mentioned before (see equation 2.6) and was proven by the identification of the pyrolysis products *formaldehyde* and *methyl pyruvate*. However, when it comes to the determination of the decomposition rate, respectively the decomposition kinetics, the data found in literature are quite inconsistent. Mukundan and Kishore [25] report a starting point of 100 °C with a maximum rate at 150 °C for the decomposition measured by DSC and TGA. Subramanian [28] mentions a thermal degradation temperature determined by TGA of 132 °C - 134 °C, respectively of 145 °C in case of DSC measurement. It seems that both, the method of measurement, and possible differences in the molecular structure of the peroxide itself influence the results. At least it seems plausible that polymerization temperature and the fact that initiator was added or not can have an effect on the thermal stability of the produced peroxide.

In this work, different approaches have been undertaken to determine the decomposition kinetics for PMMAP. First of all, DSC scanning experiments were carried out in combination with a software-integrated calculation method for the kinetics (see below). Secondly, TGA-MS experiments were used to verify the degradation mechanism by its products. Finally, the decomposition kinetics were determined in batch polymerizations by means of the Odian method [40] (dead-end polymerization).

Differential Scanning Calorimetry (DSC)

A very comfortable way to determine kinetics in general is by DSC scanning experiments (compare "Differential Scanning Calorimetry"in appendix 1). Since due to the linear heating ramp the reaction virtually runs through an infinite number of infinitesimal isothermal temperature steps, the Arrhenius parameters k_0 and E_A can be determined from only one experiment. For the mathematical treatment of the measured data, there are several methods available (e.g. Friedman method, Chang method, Kissinger method [37]). The software of the DSC device uses a multilinear regression for the determination of k_0, E_A and reaction order n as explained in the following [41].

The time-dependent degree of conversion X for a reaction of n-th order can be expressed by equation 2.17.

$$\frac{dX}{dt} = k_0 \cdot e^{-\frac{E_A}{RT}} \cdot (1-X)^n \qquad\qquad \text{(EQ 2.17)}$$

In order to solve this equation, either one variable needs to be held constant (this is the case in isothermal experiments: $d\frac{X}{dt}\Big|_{T\,=\,const}$) or related with another one. The latter can be achieved for constant heating rates by relating the temperature with time, since it is

$$\beta = \frac{dT}{dt} \qquad\qquad \text{(EQ 2.18)}$$

the definition of the heating rate. Now, combining equation 2.17 with equation 2.18 leads to the following expression, which is used in its linearized form (equation 2.20) to determine the kinetic parameters.

$$\beta \cdot \frac{dX}{dT} = k_0 \cdot e^{-\frac{E_A}{RT}} \cdot (1-X)^n \qquad\qquad \text{(EQ 2.19)}$$

$$\ln\left(\beta \cdot \frac{dX}{dT}\right) = \ln(k_0) - \frac{E_A}{RT} + n \cdot \ln(1-X) \qquad\qquad \text{(EQ 2.20)}$$

From the DSC curve, values for ΔH and $\Delta H_{partial}(t)$ are derived, which, in the case that the reaction terminates with full conversion, can be related with the conversion by the following expression:

$$X = \frac{\Delta H_{partial}}{\Delta H} \qquad\qquad \text{(EQ 2.21)}$$

In this equation, ΔH corresponds to the total energy dissipated by the reaction and $\Delta H_{partial}(t)$ to the dissipated energy from t=0 to t (area under the DSC curve). With this information, the software can now determine k_0, E_A and n by multilinear regression.

Figure 2.9 shows the heat flux diagram for the decomposition of the bulk PMMAP containing residue (i.e. not in solution). The strong exothermal character of the reaction is clearly visible. At a heating rate of 3 °C/min, the decomposition starts at approximately 100 °C with a maximum rate at 145 °C. This corresponds very well to the above mentioned literature data.

The specific heat of reaction of this sample was determined to be ΔH_R = 190 J/g. However, the total amount of sample contained probably both, PMMAP and regular PMMA. Therefore, this heat of reaction needs to be normalized to the weight of the peroxide only. To obtain this information, i.e. how much peroxide, respectively, polymer there is in the residue, experiments with a thermobalance were carried out as described later in this chapter (see "Mass-spectrometer coupled Thermogravimetry (TGA-MS)" on page 33). Assuming a peroxide content of 36.5% (compare figure 2.14), the corrected value becomes ΔH_R = 520 J/g (for comparison: the heat of decomposition of tert.butyl peroxide (DTBP was determined to be ΔH_R = 1113 J/g as shown in appendix 4).

DSC Scanning Kinetics
Limit1 = 118.98°C (5.00%)
Limit2 = 155.12°C (90.01%)
Delta H = -189.78 J/g
Delta Cp = 0.00 J/g*°C
ln Z = 30.532 ± 0.192 1/sec
Ea = 125.12 ± 0.653 KJ/mole
n = 1.000 ± 0.000
Baseline: Standard
X1 = 105.43 °C
X2 = 165.85 °C
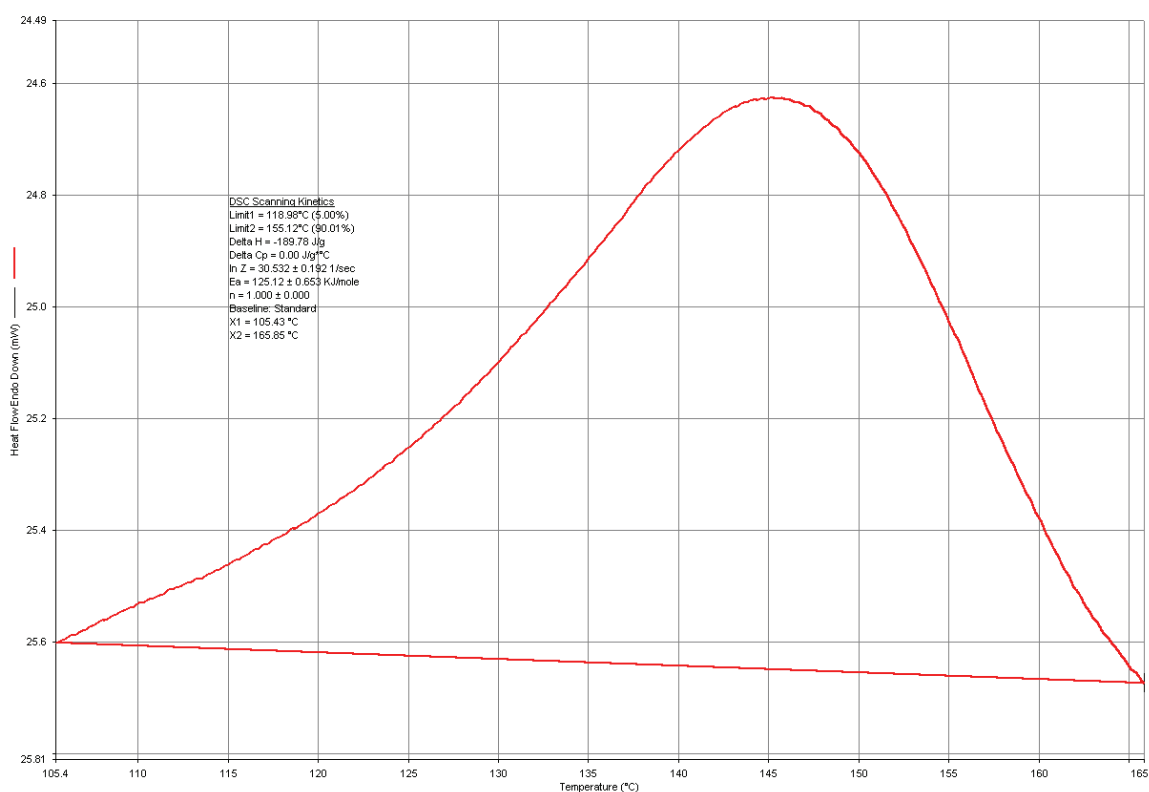
Figure 2.9: DSC diagram (heat flux over time) for the PMMAP decomposition with integration for kinetic analysis (heating rate 3°C/min)

For the determination of the kinetics by means of the above equations this effect has no influence, though, since for the calculation of X in equation 2.21 a relative heat of reaction is used. The result of the scanning kinetics analysis is depicted in figure 2.10 in the form of an Arrhenius diagram. Although the software allows to fit also the reaction order n, it was preferred

to fix it to n=1. Trials with the fitting of all three parameters always lead to results for n close to 1, which is confirmed by literature (Sivalingam et al. [37] determined reaction orders between n = 0.8 and n = 1.3 depending on the method). Yet, since an irrational reaction order is not justified by the mechanism (unimolecular degradation), the fitting was reduced to 2 parameters by fixing the reaction order to n = 1.
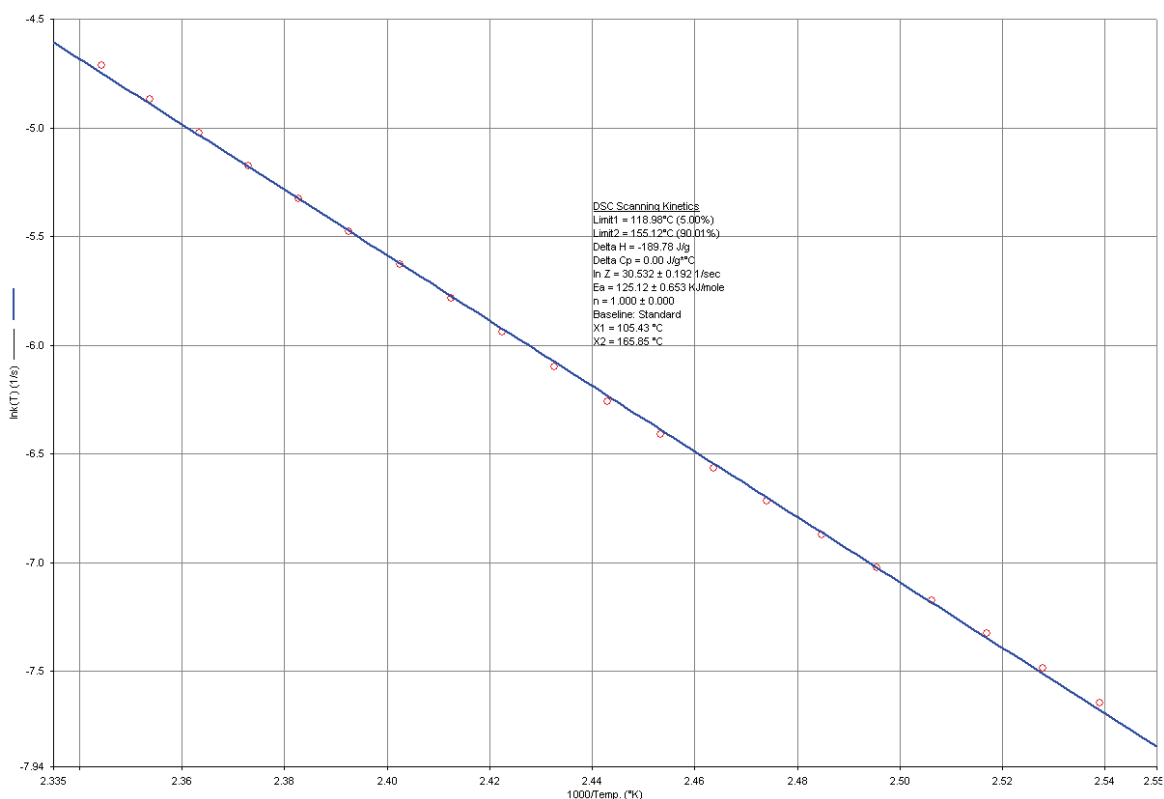
Figure 2.10: Example of an Arrhenius diagram (ln k over 1/T) from DSC scanning kinetics

An important aspect in the kinetic investigations of the degradation of PMMAP is the possibility of autocatalysis, i.e. the phenomenon that the reaction is accelerated in the bulk substance, while it appears slower in solution. The DSC decomposition experiment was therefore repeated in several dilutions and solvents. It was observed that, indeed, there seems to be a difference between the diluted and the bulk reaction. In table 3, the Arrhenius constants for different peroxide samples in different solvents are listed. It is evident that, for the undiluted peroxide, these constants are significantly higher. Furthermore, there also seems to be a difference between the solvents, themselves. 1,2-Dichlorobenzene and biphenyl exhibit the lowest decomposition values, whereas in butyl acetate, as quite polar solvent, both, prefactor and activation energy, are higher. This allows the assumption, that the decomposition is influenced by interactions with polar

groups, therefore also with other peroxidic groups, which might be a reason for the, what it seems, faster decomposition of the undiluted samples. The consequences of these differences are demonstrated by the halflife-time values for each sample, which are traced in figure 2.11.

Also given in table 3 is a literature value for the decomposition taken from Fenouillot et al. [42], who describe an "impurity" that decomposes quickly as reason for the fast increase in conversion in their blind experiments. It is reckoned by the author of the present work that this impurity is, indeed, PMMAP, which seems justified considering the agreement of the kinetic data (compare also figure 2.17).

Table 3: Kinetic values for the decomposition of PMMAP under different conditions (each sample comes from a different PMMAP synthesis)

		Peroxide Concentration	k_0 [s^{-1}]	E_A [kJ mol^{-1}]
Sample 1	Undiluted	-	$2.79 \cdot 10^{14}$	134.60
	Butyl Acetate	~ 10 %	$3.41 \cdot 10^6$	73.84
	1,2-DCB	~ 10 %	$9.81 \cdot 10^5$	68.64
Sample 2	Undiluted	-	$1.56 \cdot 10^{13}$	123.43
	Butyl Acetate	~ 30 %	$9.44 \cdot 10^7$	82.78
Sample 3	Butyl Acetate	~ 10 %	$4.72 \cdot 10^5$	65.76
	1,2-DCB	~ 10 %	$1.18 \cdot 10^5$	60.87
	Biphenyl	~ 3 %	$5.68 \cdot 10^5$	66.33
Sample 4	Undiluted	-	$2.72 \cdot 10^{14}$	132.9
Literature	[42]	-	$1.93 \cdot 10^{10}$	104.4
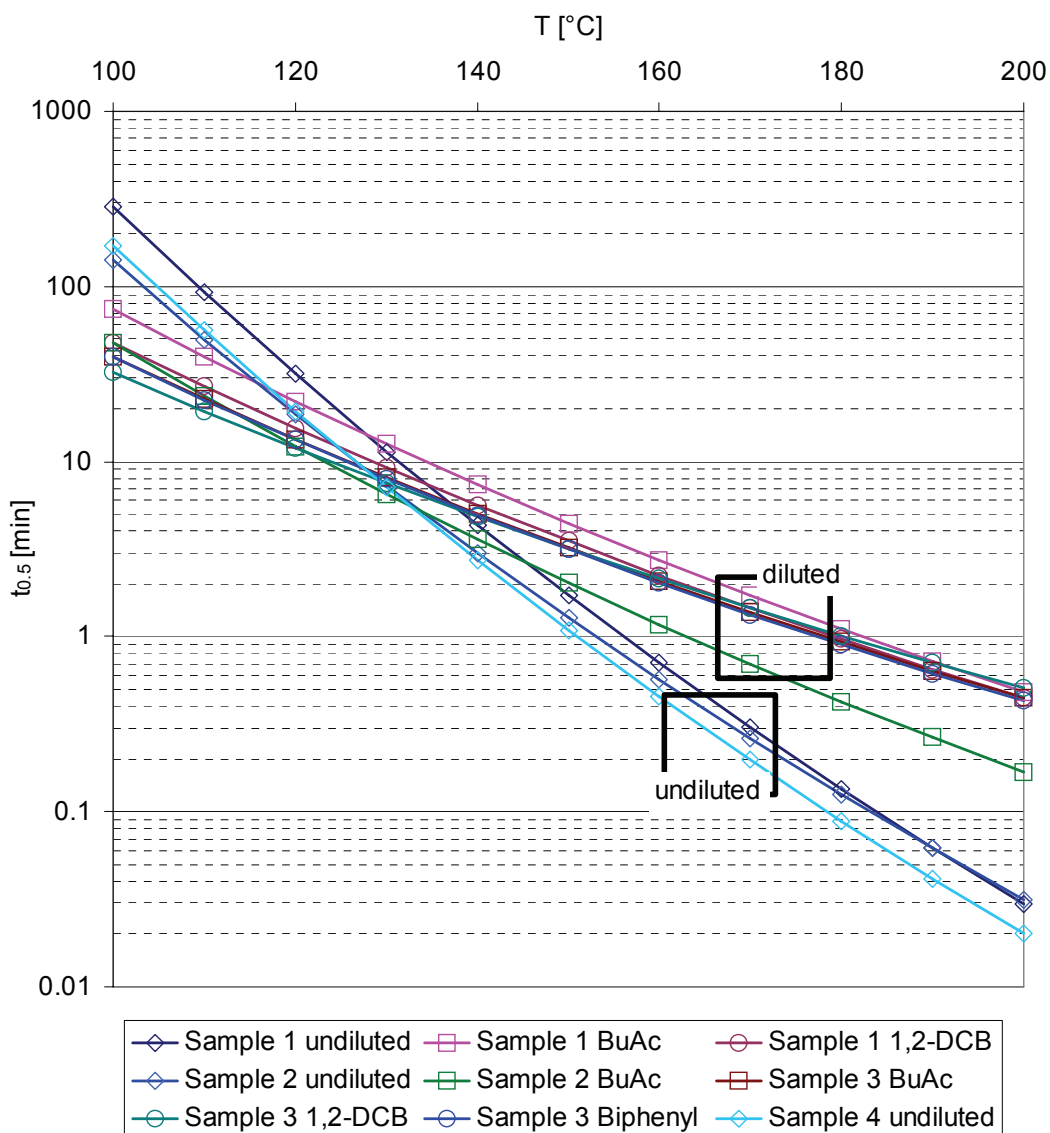
Figure 2.11: Half-life time - temperature plot for different peroxide samples and dilutions

In order to obtain kinetic values for $k_{po,d}$ to use in PREDICI® for the modeling of the initiation by MMA peroxides, the averages of the above described values for the undiluted and the diluted case were calculated by linear regression of the *ln k* over *1/T* curves for the different samples kinetics. The result is depicted in figure 2.12. From the average *ln k* over *1/T* curves, the following kinetics constants were calculated:

Table 4: Average values for the kinetic constants of the PMMAP decomposition

	k_0 [s^{-1}]	E_A [kJ mol^{-1}]
diluted[a]	$1.775 \cdot 10^6$	70.38
undiluted	$1.058 \cdot 10^{14}$	130.31

a. This value was used in the kinetic model

For the modeling of the decomposition kinetics it was found that the average value for the diluted peroxide sample describes best the experimental data obtained in batch polymerizations (compare "Verification of the Kinetics in Batch Experiments" later on). This is reasonable considering that in a batch polymerization, the peroxide is present only in very small concentrations and the interactions between the peroxide molecules influencing the decay as in the undiluted sample will be negligible.
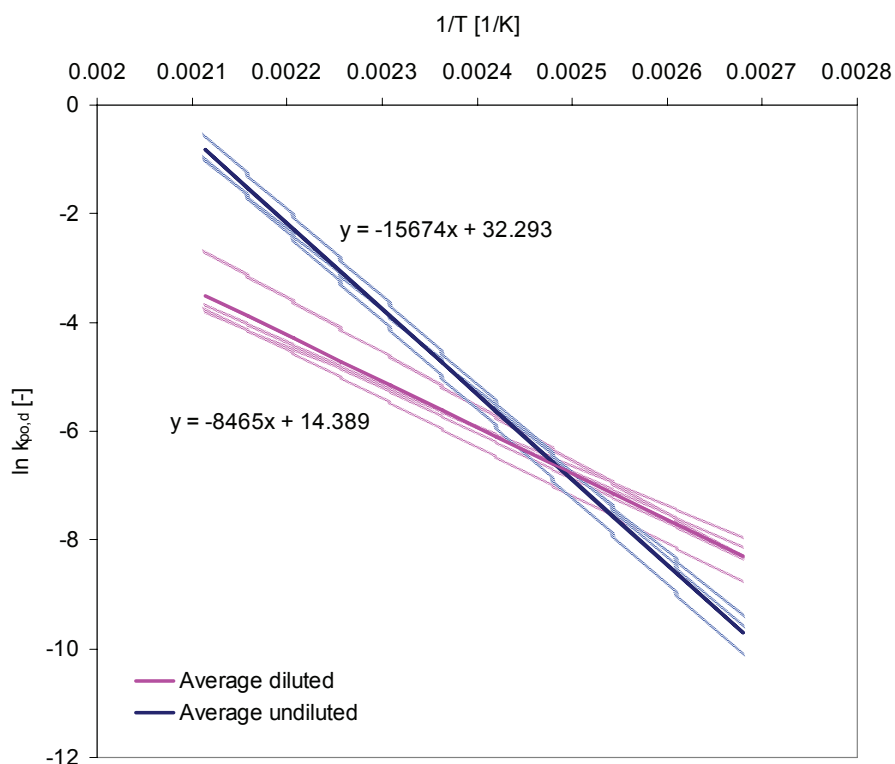
Figure 2.12: Calculation of average values for the decomposition kinetics of PMMAP for the diluted and undiluted samples by linear regression of the different lnk against 1/T curves

Mass-spectrometer coupled Thermogravimetry (TGA-MS)

In order to determine the composition of the polymeric residue, i.e. how much peroxide, respectively normal polymer was formed during the oxygenation reaction, TGA-MS runs were carried out with different samples. Thermogravimetry allows the determination of weight losses as a function of temperature. Furthermore, often a calorimetric signal is produced, which can help to describe the nature of the weight loss (i.e. exothermic, endothermic).

In this part of the project, TGA was employed to investigate and understand the composition of the peroxide samples obtained from the above oxygenation experiments. It has been already conjectured that the samples do not consist of polymeric peroxide only but that there is also "ordinary" PMMA present. If this is the case, then in the thermogravimetry there should be different weight loss steps, according to the amount of peroxide and polymer present. In fact, the samples decompose in two steps, as can be seen from figure 2.13, which shows the weight loss curve with increasing temperature (heating rate 5°C/min) under inert conditions. Here, the sample weight over temperature is depicted together with the SDTA® (single differential thermal analysis, trademark of Mettler Toledo, Switzerland) signal. The SDTA signal represents the temperature difference between the temperature near the sample and a reference program temperature. Analogous to the differential scanning calorimeter (DSC), the SDTA signal indicates whether a weight loss measured by the thermobalance is an exothermic or endothermic process. The SDTA signal can also measure heat flow of transitions that do not involve a weight change, i.e. melting of the sample.

The first weight loss corresponds to the decomposition of PMMAP. Firstly, it starts at approximately 100 °C and has its maximum rate between 140-150 °C, which is in perfect agreement with data from DSC experiments. Secondly, it is an exothermic weight loss, as can be seen from the SDTA curve, a fact, which underlines that this weight loss is due to the peroxide. The second weight loss, on the other hand, is endothermic. This is typical for a scission mechanism of a polymeric chain like PMMA. Also the temperature range of this step between 300 °C and 400 °C is typical for PMMA main chain scission [43].

In figure 2.14, the integration of the weight loss curve from figure 2.13 is shown. By step integration, it is calculated that of the total sample mass, 36% decompose during the first step and 50% during the second. The remaining 14% of the sample weight decompose in the transition

period between the two steps, probably due to weak linkages in the PMMA chains. The amount of residue in the crucible due to unreacted tar is negligible. Therefore, the amount of PMMA decomposed during the experiment can be estimated to be of 64% in total.

Still, this ratio is a little more in favor of the peroxide, compared to the results obtained by GPC before (see figure 2.6), where only 25% of the sample were assigned to PMMAP and 75% to PMMA. The reason for this difference might be that PMMA starts decomposing at temperatures as low as 150°C due to head-to-head bonds in the polymeric chains. Having a closer look at the TGA curve in figure 2.14 reveals that the weight loss between 150 °C and 200 °C is of approximately 10%. It might, therefore, be that within the 36% weight loss of the first decomposition step, there is already a significant part of "normal" decomposing PMMA included. Another important reason for the lower value found by GPC might be, as mentioned above, a difference in the dn/dc ratio for homogeneous PMMA and PMMAP. Each species has a different increment of the refractive index with concentration. The peak areas are - being strict on it - only comparable if this value is identical for both polymers. Otherwise the direct comparison of the peak areas in the GPC spectrum does not make sense. For PMMA and PMMAP a difference in dn/dc is possible since due to the peroxide groups the conformation of the polymer chains is no longer the same as for linear PMMA. The TGA result is, therefore, the more reliable as concerns the peroxide content of the sample.

Last but not least, the amount of peroxide in the sample also depends to a large extent on the synthesis conditions (temperature, duration). It is, thus, not necessarily a reproducible parameter.
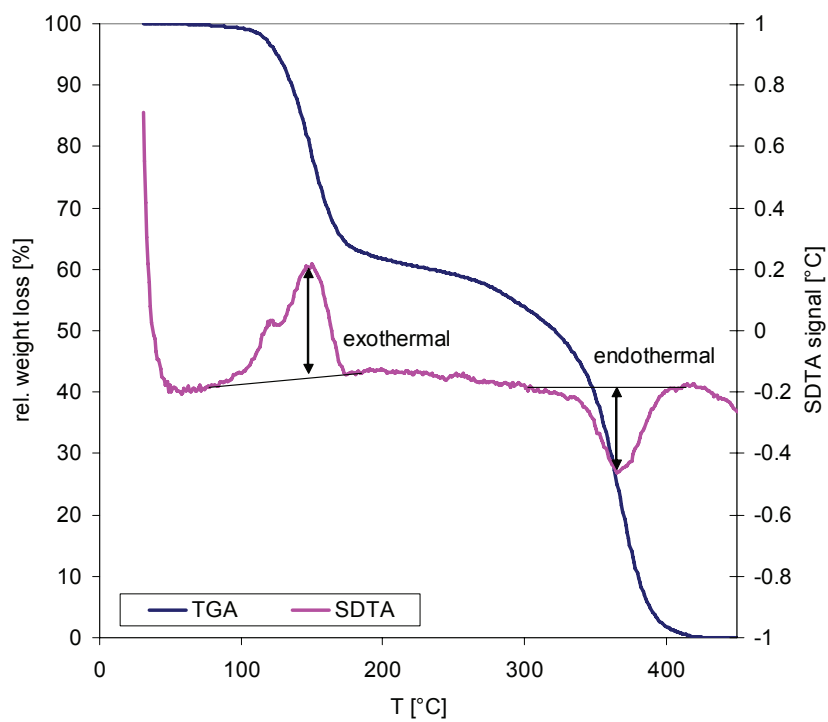
Figure 2.13: TGA curve (5°C/min) with SDTA signal for the decomposition of PMMAP in inert atmosphere
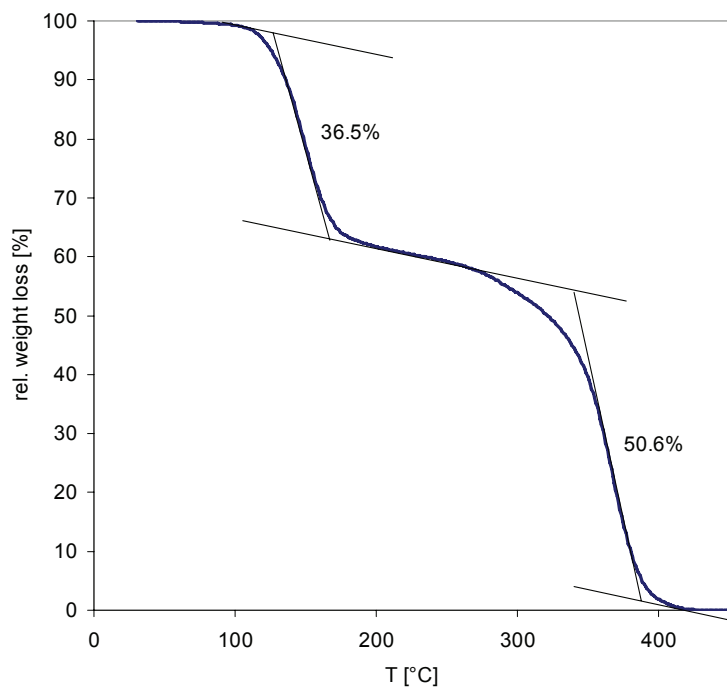
Figure 2.14: TGA curve with step integration for quantification of weight loss

An even more powerful tool for the analysis of solids is the coupling of TGA with mass spectrometry (TGA-MS). The principle of this kind of measurement is the identification of the pyrolysis products, which are transfered from the sample crucible through a capillary directly into the MS, by their molecular mass. Like this, it becomes possible to say something about the mechanism of the decomposition or to prove that a certain expected mechanism takes place.

The major decomposition product of PMMAP is methyl pyruvate (see equation 2.6), whereas linear PMMA decomposes by unzipping mostly back to MMA. The mass spectrum of methyl pyruvate and methyl methacrylate have their most important peaks at 43 amu, respectively 41 amu [44]. These masses represent the following fragments that are produced by alpha-scission of the respective molecules:

$$H_3C \diagdown \qquad \qquad H_3C \diagdown$$

41 amu   43 amu   (EQ 2.22)

Thus, as presented in figure 2.15, these masses were tracked simultaneously by the MS for the time of measurement. The above made assumption that the first decomposition step corresponds to PMMAP and the second to PMMA is well supported by the result of this experiment, which shows that during the first step, mostly methyl pyruvate is produced, while during the second step MMA is the dominant product. The presence of the mass 43u also during the second step might be due to the fact that it appears in the mass spectrum of MMA, too.
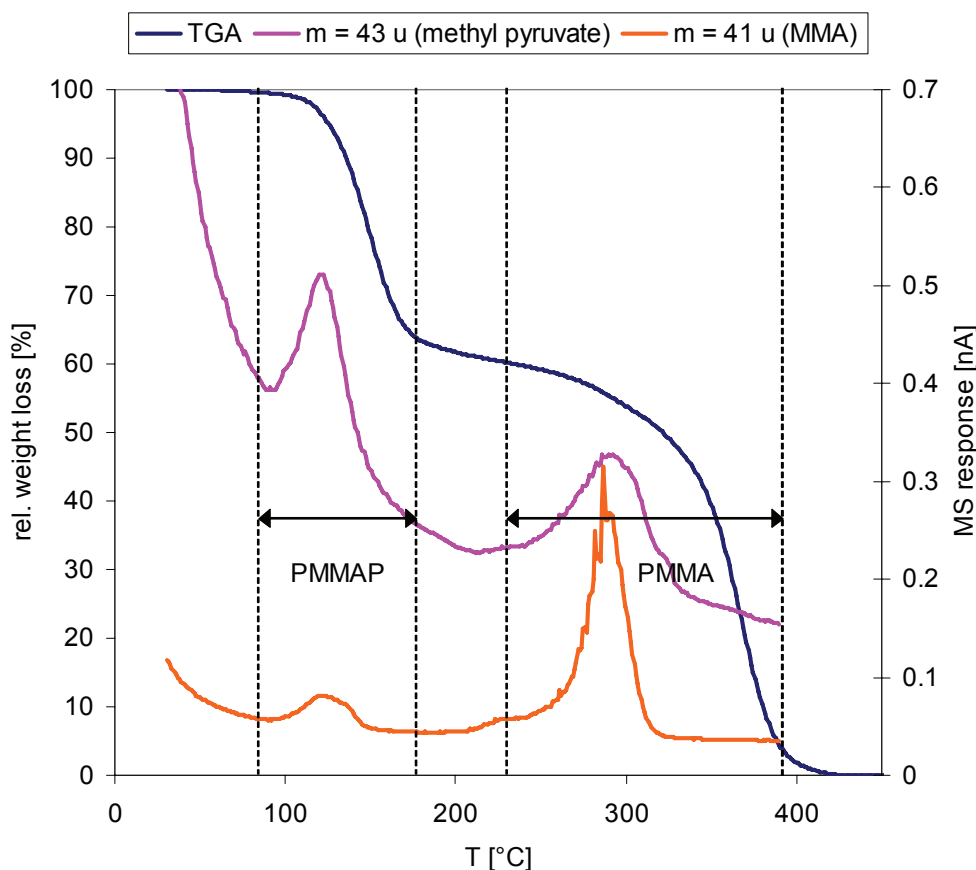
Figure 2.15: TGA-MS curves for the decomposition of PMMAP / PMMA

Odian method

It is generally preferable to determine decomposition kinetics of a species under the same conditions under which the decomposition takes place in the real process, rather than in isolated experiments where concentrations and interactions with other molecules are different. This means that rather than determining the decomposition in a DSC with the undiluted peroxide, it should be determined from a polymerization experiment in a stirred reactor. The Odian method [40] allows the estimation of both, initiator decomposition rate and efficiency, from dead-end batch polymerizations. A dead-end polymerization is a polymerization that stops short of its final conversion due to insufficient initiator (so-called "initiator burn-out").

Based on the expression

$$-\ln\left[1 - \frac{\ln(1-X)}{\ln(1-X_\infty)}\right] = \frac{-k_d \cdot t}{2} \qquad \text{(EQ 2.23)}$$

37

where X_∞ is the dead-end conversion (obtained by extrapolation of the measured conversion to $t \to \infty$), the parameter k_d can be determined from the slope of the graph $-ln[...]$ against t. The initiator effiency at zero conversion f_0 is then calculated in a second step by the following equation:

$$f_0 = \left(\frac{\ln(1-X_\infty)}{2 \cdot k_p}\right)^2 \cdot \frac{k_d \cdot k_t}{[I]_0}$$

(EQ 2.24)

However, for the calculation to be precise, it is necessary to have isothermal reaction conditions. This is not the case for the decomposition of PMMAP in a batch reaction, since it starts decomposing already during the heating phase. The resulting kinetics will, therefore, be much slower than the ones determined by DSC, since the effective temperature is significantly below the set temperature for each experiment. Only the efficiency value can be considered as reliable, when it is estimated according to equation 2.24 with the temperature dependent values for k_d, k_t and k_p, determined previously by other methods.

Yet, for initiators added later to the reaction, i.e. under isothermal conditions, the method is suitable. Results for the thermal initiators TBPEH and DTBP are presented in the section "Verification of the Kinetics in Batch Experiments" of this chapter.

For PMMAP, three curves were measured in a bench-scale batch reactor ($V_R = 1$ L) at different temperatures (130 °C, 150 °C, 170 °C). The graphs are presented in figure 2.16. For each curve, a k_d value can be determined with help of equation 2.23 and the following Arrhenius decomposition kinetics were calculated:

Table 5: Kinetic parameters for the PMMAP decomposition as calculated by the Odian method

	k_0 [l mol^{-1}s^{-1}]	E_A [kJ mol^{-1}]	f [-]
PMMAP	$4.72 \cdot 10^7$ [a]	85.6[a]	0.21[b]

a. These values are too small due to non-isothermal conditions (compare text). For modeling purposes use values provided in table 4.
b. Value estimated according to equation 2.24 considering the heating ramp and using literature k_t, k_p as well as the k_d determined by DSC.
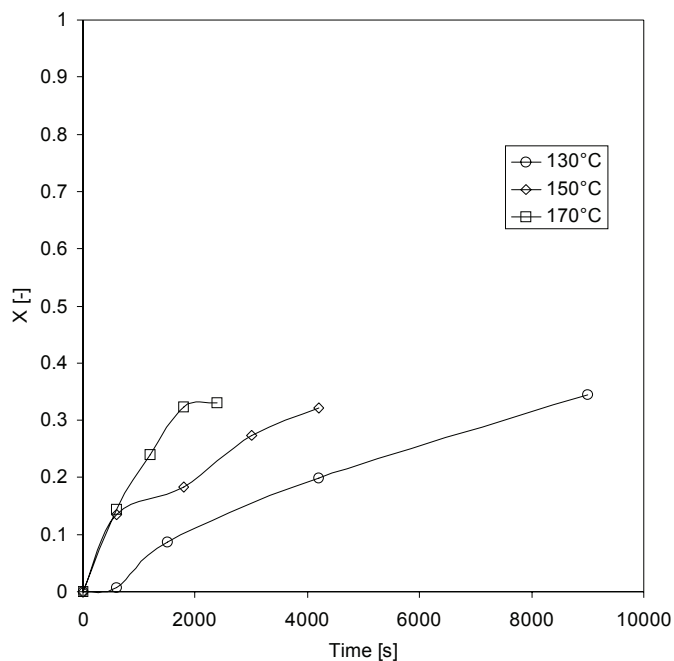
Figure 2.16: Batch blind polymerizations (without additional initiator) for Odian calculations of the PMMAP decomposition
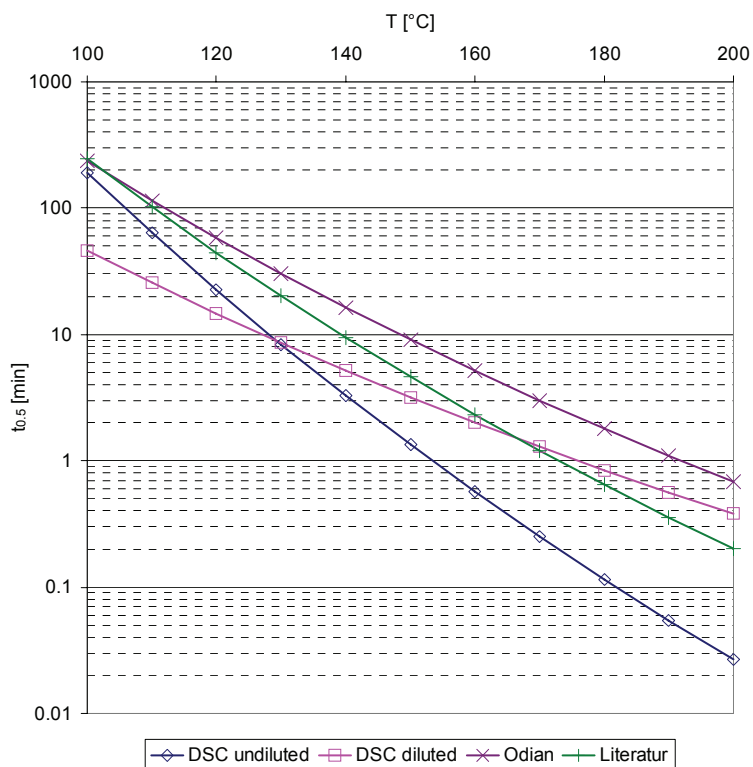
Figure 2.17: Comparison of the Odian kinetics with DSC and literature [42] values

From figure 2.17 it becomes evident that there is a rather large discrepancy between the different kinetics for the decompositon of PMMAP. The kinetic constants determined by the Odian method deliver, as expected, the slowest decomposition rate while the undiluted DSC sample yields the fastest one. The true values can be found somewhere inbetween and comparison to experimental data from batch polymerizations (conversion over time curves, see chapter 2.5) have shown that the kinetics determined by DSC for the diluted sample lead to the best matching results. Therefore, in all further modeling, the constants from table 4 were used for the PMMAP decomposition rate.

2.2   Thermal initiation

By the term "thermal initiation", polymer chemists understand the spontaneous initiation of polymerization without interaction of any other compound than the monomer itself. For MMA, this mechanism is, as explained in the following, bimolecular (unlike, for example, for styrene, where it is unimolecular):

$$M + M \rightarrow 2P_1*$$

(EQ 2.25)

This definition needs to be underlined here, since the simple fact of observing an important monomer conversion without addition of initiator does not necessarily reflect a thermal initiation. As seen before, many different reactions can take place in the reaction system, which cause initation. Thus, for the correct determination of "true" thermal initiation rate coefficients, the monomer must be carefully purified in order to exclude as much as possible impurities and foreign substances.

Stickler and Meyerhoff [14] undertook a whole series of experiments in the late 70's, where they purified the monomer in a specially developped high-vacuum distillation device, from which the monomer was immediately isolated in hermetic, silane treated glass ampoules. These ampoules were closed by melting under high vacuum (10^{-4} Pa). Accordingly, the authors obtained data for the thermal initiation that was significantly lower than what had been published before. In fact, the rate of polymerization was so low that even the radical production by natural ionising radiation (cosmic radiation) had to be taken into account. At 100 °C, the obtained polymer weight

fraction after 5 days was less than 4%. At 0 °C, it took almost 2 months to obtain 1% polymer. This is in clear contrast to the results obtained with monomer that has been purified with less sophisticated distillation techniques: Lehrle and Shortland [22] measured conversions of more than 20% within less than two days at 40 °C and Fenouillot et al. report values around 30% after 12 hours at 160-180 °C. In these cases, it may be that traces of MMA peroxides, chain transfer agents or residual amounts of initiator used for prepolymerization are the reasons for this elevated conversions.

As to the mechanism of the thermal initiation of MMA, Lingnau and Meyerhoff [17, 19] propose an initiation mechanism via a dimeric biradical $^.M_2^.$, which is formed by a tail-to-tail monomer addition, in combination with a transfer reaction to monomer, solvent or chain transfer agent. According to the authors, the biradical cannot grow into two directions to yield high polymers and, therefore, has to be terminated first on one side by a transfer reaction (see figure 2.18). This assumption is supported in their publications by various experimental and theoretical data (side products and energetic considerations).
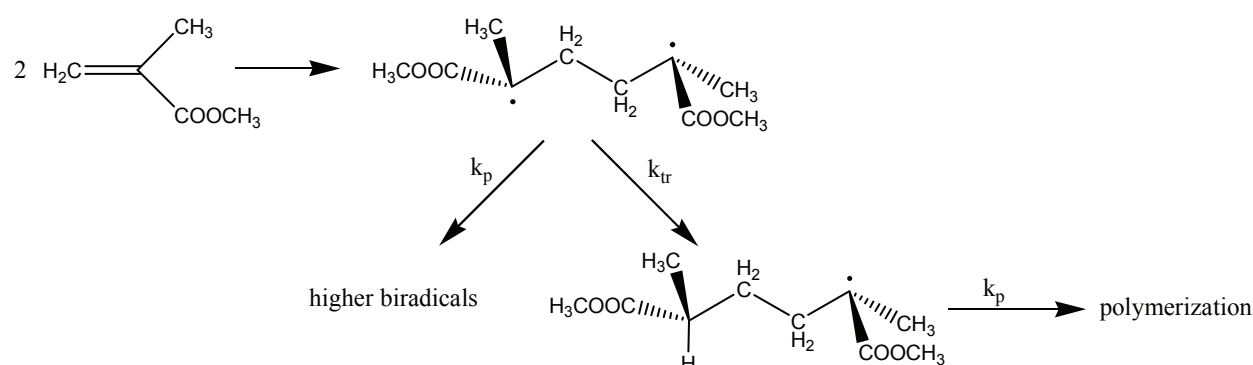
Figure 2.18: Mechanism for the thermal initiation of MMA via dimeric biradicals

Since, in this work, the initiation by MMA peroxides and other impurities is evaluated separately (i.e. no "global thermal initiation" rate, taking into account several mechanisms, is used), it seems close-at-hand to use the rate coefficients of Stickler and Meyerhoff for the "true" thermal initiation [1]:

---

1. The word *"true"* is set in quotation marks since, in spite of the advanced purification efforts made by Stickler, there is no final proof or certainty that the observed initiation reaction follows only this and no other mechanism. Therefore, it still remains a hypothesis - although the author of this work fiercely supports Stickler's explanation.

$$\log R_{th} = 0.73 - \frac{5670}{T} \qquad \text{(EQ 2.26)}$$

As mentioned above (equation 2.25), it is a second order reaction in monomer concentration, thus it is

$$\frac{d[M]}{dt} = -k_{th} \cdot [M]^2 \qquad \text{(EQ 2.27)}$$

Table 6: "True" thermal initiation rate coefficients from [14]

	k_0 [l mol^{-1}s^{-1}]	E_A [kJ mol^{-1}]
k_{th}	5.3703	108.5

2.3   Initiation by the Chain Transfer Agent

Apart from the thermal initiation reactions by peroxide and the monomer itself, also chain transfer agents can have a strong initiating potential. Common chain transfer agents in radical polymerization are thiols, substances with a more or less long carbon backbone and an -SH reactive end group. Most widely used are n-butanethiol, n-dodecanethiol and the aromatic species phenylthiol.

Concerning the initiation of radical polymerization, Xia et al. [45] have investigated this phenomenon for the MMA polymerization with different thiols at low temperatures and propose a hydrogen transfer from thiol to MMA as mechanism of initiation:

$$\text{RSH} + \text{MMA} \longrightarrow \text{RS} \cdot + \text{MMA} \cdot \qquad \text{(EQ 2.28)}$$

For the high temperature polymerization, the initiating behavior is even more pronounced than for low temperatures, as found by Fenouillot et al. [42], who determined the kinetic parameters for n-butanethiol and MMA in the temperature range 130 °C - 168 °C. Although in this work n-dodecanethiol (DDT) is used, these parameters were used for the modeling, assuming that they

are valid in good approximation also for longer chain thiols. In fact, as presented in the last part of this chapter, they lead to excellent results in batch polymerization experiments with DDT.

Table 7: Initiation by Chain Transfer Agent, rate coefficients from [42]

	k_0 [l mol^{-1}s^{-1}]	E_A [kJ mol^{-1}]
k_{dt}	$6.78 \cdot 10^7$	128.7

2.4 Formation of the Dimer

At elevated polymerization temperatures, an interesting phenomenon can be observed: values for the conversion measured by gas chromatography of the residual monomer differ significantly from gravimetric methods or methods determining the polymer (i.e. GPC). This means that monomer is consumed to important extents by a reaction other than the polymerization, which yields a product that is neither precipitating nor part of the polymer peak in the GPC.

Albisetti et al. [46] described in 1956 the preparation of dimers from unsaturated methacrylic compounds. For methyl methacrylate, the following mechanism based on a Diels-Alder-type reaction is proposed, leading to the unsaturated dimer, 2-methyl-5-methylene-hexanedioicacid-dimethylester, also referred to as H-1:
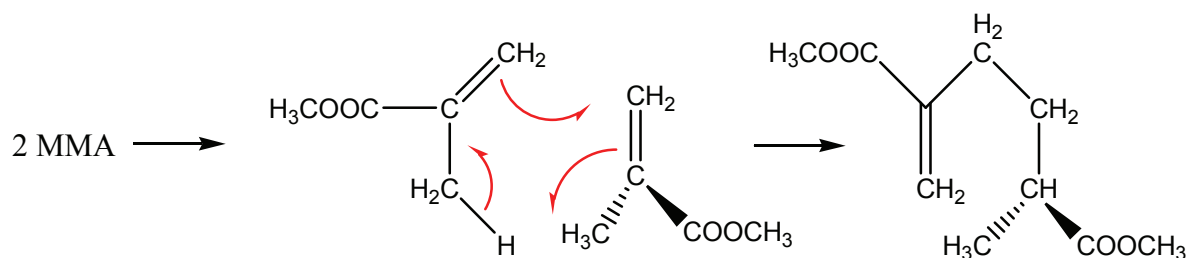
Figure 2.19: Pseudo Diels-Alder-Mechanism for the formation of MMA dimer [15]

It should be pointed out that the dimerization does not belong to the group of initiation reactions, but represents an additional effect influencing the conversion evolution at high temperatures.

Stickler and Meyerhoff [15] discuss the formation mechanism presented in figure 2.19 in comparison to a mechanism based on the formation of a biradical ·M-M· due to tail-to-tail addi-

tion of two monomer molecules analog to the one of the thermal MMA polymerization (see page 41), but in the end it appears that they favour the above presented enophilic mechanism.

In their publication, they also determine the formation rate for the MMA dimer over a wide temperature range (100 °C - 275 °C). In agreement with the mechanism in figure 2.19, they find second order reaction kinetics:

$$\frac{d[H-1]}{dt} = k_{H-1} \cdot [M]^2$$ (EQ 2.29)

The formed dimer can be incorporated in the growing PMMA chains by copolymerization as pointed out by Brand, Stickler and Meyerhoff [16], but this reaction as well as the homopolymerization of the dimer, itself, can be neglected in initiator-started polymerizations. The copolymerization might influence the thermal reaction of MMA, though.

Table 8: Formation rate coefficients for the dimerisation of MMA [15]

	k_0 [l mol^{-1} s^{-1}]	E_A [kJ mol^{-1}]
k_{H-1}	4.9386×10^5	107.2

2.5 Verification of the Kinetics in Batch Experiments

A series of batch experiments were carried out to verify the kinetics of the different thermal initiation mechanisms as discussed above. The reactor setup is presented in figure 2.20. It consists of a 1-l stainless steel reactor that is fixed into a double jacket and closed with a cover containing a mechanical stirrer. It is heated by a flow of heat transfer fluid (synthetic oil, Shell Aseol Trans SH) through the double jacket and an internal heating coil. For pressurization and sampling there is an immersion tube with a three-way valve. One end of the three-way valve is connected to a nitrogen gas cylinder, the other ends in a sampling vial. Samples are taken through the three-way valve directly into pre-cooled glass vials with screw caps (Schott Duran) and immediately frozen to -20°C. They are consecutively analyzed for conversion and molecular weight.

The addition of initiator or other additives under pressure is realized by a pressurized steel cylinder on top of the cover. The reactor content is mixed by a propeller and an anchor stirrer at the bottom, both fixed on the same axis.
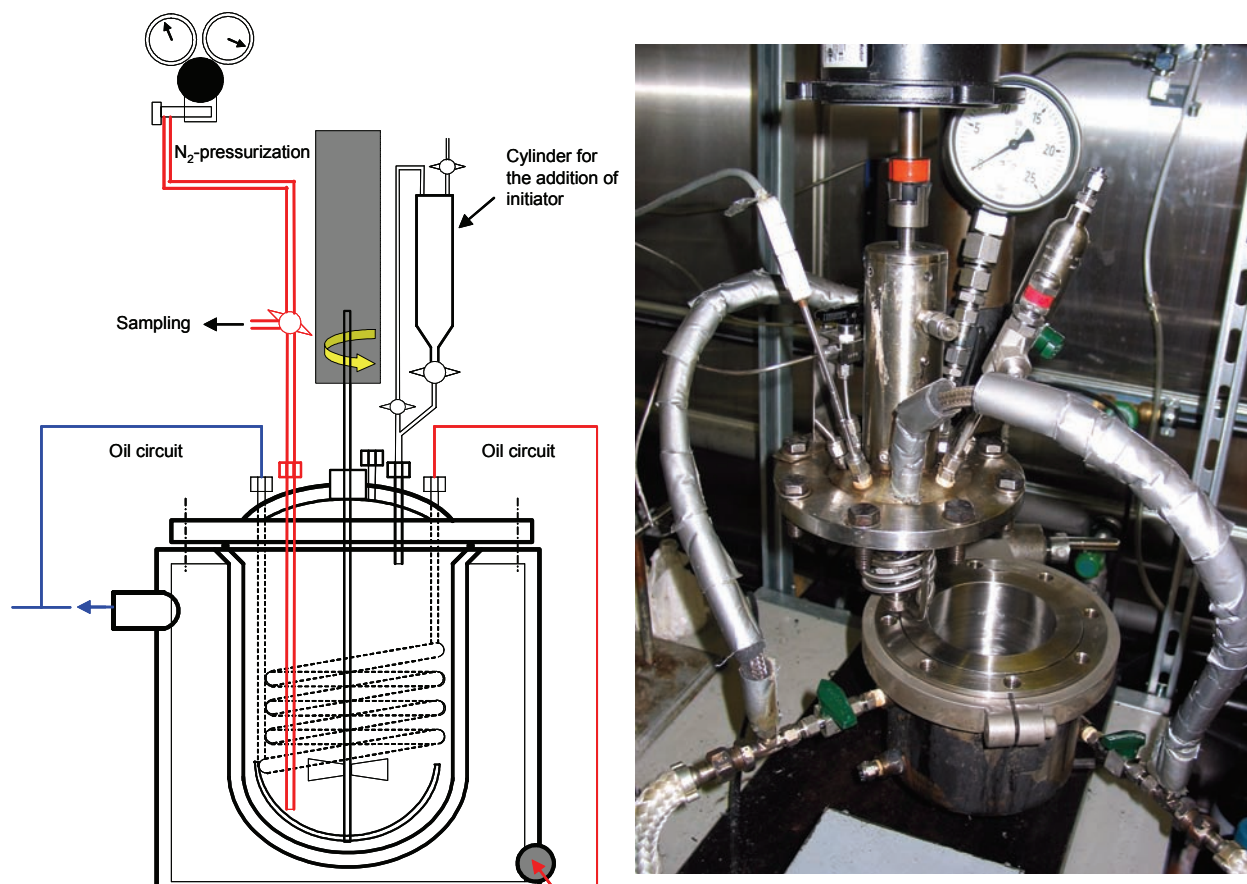
Figure 2.20: Schematic drawing and photograph of the 1-L batch reactor used in this work

The monomer / solvent mixture is filled into the open reactor, which is then closed tightly and pressurized with N_2 at 10 bar. With the help of an oil thermostat, the whole device is brought as quickly as possible to reaction temperature ($\Delta T/\Delta t \sim 3$ °C/min). Depending on the experiment, an initiator solution can be added at an arbitrary time t through the cylinder fixed on top of the reactor without opening or depressurizing the reactor.

In the beginning, blind experiments without any radical initiator were carried out to examine the auto-initiation of non-purified MMA (i.e. from the barrel) and to verify the model parameters determined in the preceding paragraphs. Figure 2.21 contains the results of these experiments

45

compared to the predicted data from the kinetic model established in PREDICI® (see appendix 3 for for a complete description of the model).

Graph (a) shows the conversion evolution for an assumed oxygen concentration of $[O_2]_0 = 60$ ppm. This value is considered throughout this work as the saturation concentration for physically dissolved oxygen in MMA at T = 20 °C and p = 1 bar (p_{O2}~0.2bar). However, this concentration is very susceptible to changes of the environment (T, p), which might be the explanation for the 170 °C curve to differ slightly from the experimental data points. The molecular weight distributions in graph (b) are well matched by the model prediction with the same discrepancy at 170 °C as for the conversion evolution. The fact that the molecular weights are quite low is due to the high amount of chain transfer agent, which was added in order to keep the viscosity low and not to risk entering the gel effect region.
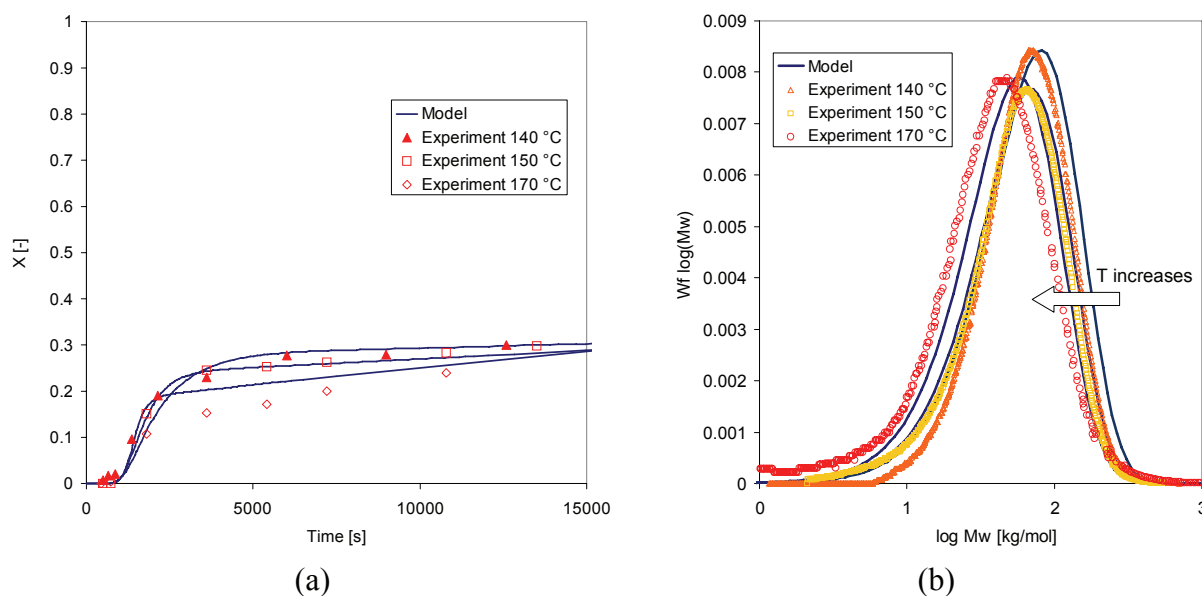
Figure 2.21: Batch blind experiment at different temperatures with model prediction (a) conversion evolution (b) molecular weight distribution [w_s = 30% butyl acetate, [CTA]$_0$ = 4000 ppm] (for kinetic constants used see appendix 3)

How big the influence of the oxygen concentration on the conversion evolution can be is demonstrated in figure 2.22 (a). It shows three times the same experiment, carried out under - presumedly - the same experimental conditions: monomer from the barrel, T = 140 °C, p = 10 bar. Yet, completely different conversions were measured, i.e. the reproducibility was very poor. This effect can be vividly explained: by changing the initial oxygen concentration of the system in the

model, the predicted curves perfectly match the different experimental ones. A loss of oxygen in the system easily occurs, for example when the reactor is accidentally opened after it had already been pressurized (in one particular case the operator had forgotten to add chain transfer agent and continued the experiment after having opened - *and depressurized!* - the reactor). Thus, the dissolved oxygen is so to speak driven out of the monomer together with the nitrogen. The same effect may be caused by a leak of the mechanical sealing of the stirrer's axis. Since the reactor is pressurized through an immersion tube, a small constant flow of nitrogen equals a degassing of the monomer by bubbling inert gas through it, which quickly diminishes the oxygen concentration. It is, therefore, not astonishing that different conversion evolutions are measured if one cannot be sure to have at 100% the same conditions for each experiment. At least with the given reactor setup, to achieve this absolute reproducibility was not possible.

Figure 2.22 (b) exhibits the influence of chain transfer agent on the initiation of the polymerization at T = 180 °C. The same experiment was carried out once with and once without the addition of 4000 ppm n-dodecanethiol (DDT). The strong initiating behaviour of a thiol at this temperature is clearly visible. For the experiment without CTA, on the other hand, the "true" thermal initiation can be noticed as a linear increase in conversion with time. However, its importance at this temperature is still much less pronounced than for the chain transfer agent.

(a)   (b)
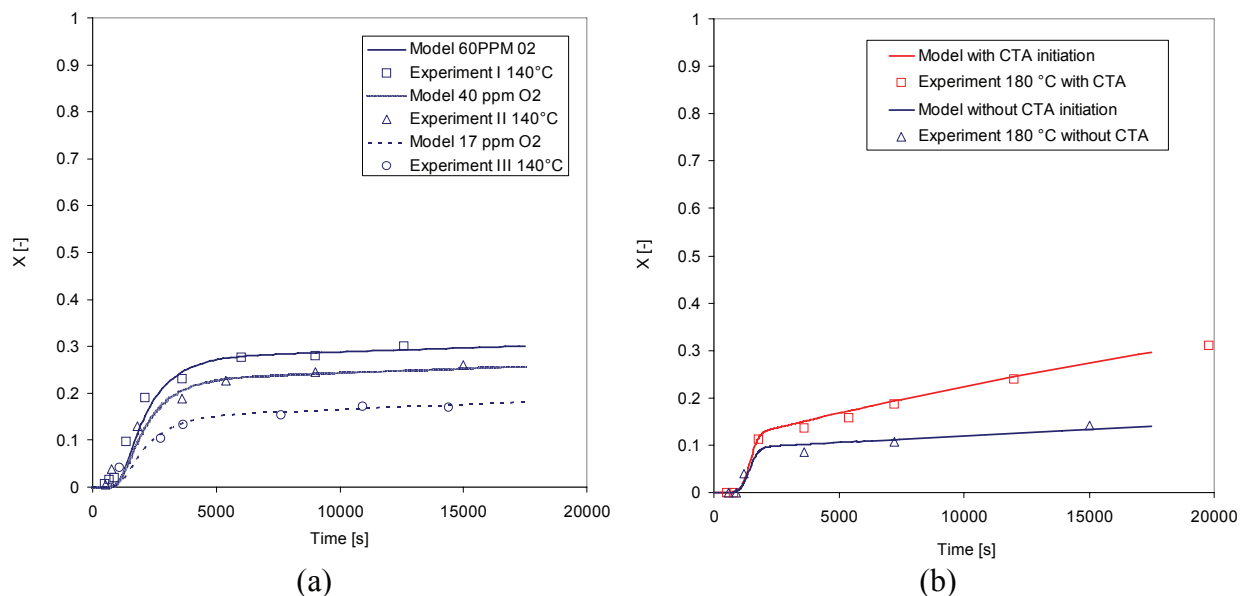
Figure 2.22: Influence of (a) the oxygen concentration and (b) the chain transfer agent on the conversion evolution [(a) 140 °C (b) 180 °C, both with w_s = 30% butyl acetate, $[CTA]_0$ = 4000 ppm]

For a final comparison of each species initiating potential, simulations were carried out with only one mechanism activated at a time, respectively all of them together, for a reaction temperature of T = 170 °C. The result is presented in figure 2.23. It is quite clear from this graph that mostly the chain transfer agent is responsible for the linear conversion increase after the burn-out of the MMA peroxide. The latter has with almost 20% monomer conversion the biggest share in the initiation of the polymerization. The conversion increase by dimerization can almost be neglected at this temperature, while the auto-initiation of MMA by intramolecular interactions, itself, plays quite a role for longer reactions times. With regards to a continuous process, where residence times of less than an hour are common, its influence is not too important, though.
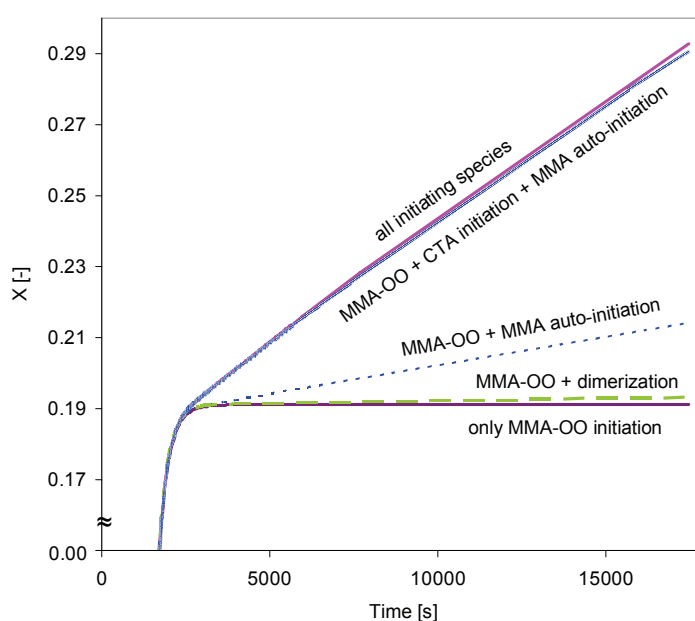
Figure 2.23: Comparison of all initiating species concerning their initiating potential (modeled conversion curves for T = 170 °C, [CTA] = 4000 ppm

In the same reactor setup, also experiments with initiator were carried out. For these experiments, an initiator-containing solution was added at a given time *t* through the pressurized steel funnel to the reaction mixture. This time *t* was ideally after the burn-out of PMMA peroxide in order to see the effect of both initiating species separately.

The figures on the following pages contain the results of two exemplary experiments, one at T = 127 °C with *TBPEH* (tert-Butyl-per-2-ethylhexanoat) as initiator and the other at T = 150 °C with *DTBP*.
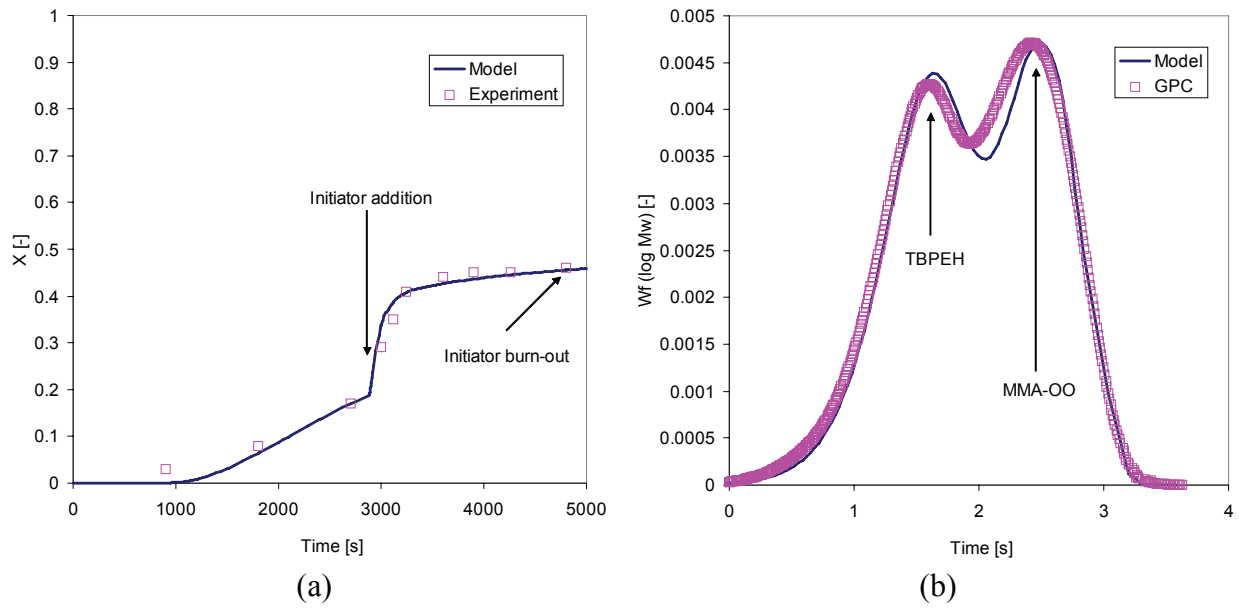
Figure 2.24: Results for the 127 °C batch experiment (50% BuAc, [TBPEH] = 1000 ppm, [CTA] = 100 ppm) (a) Conversion evolution (b) Molecular weight distribution (t = 5000 s)

Figure 2.25: Results for the 127 °C batch experiment (50% BuAc, [TBPEH] = 1000 ppm, [CTA] = 100 ppm) (a) Temperature and initiator concentrations (MMA-OO and TBPEH) over time (b) Molecular weight evolution (Mw, Mn)

The conversion evolution cleary shows the different initiating processes, i.e. first the initiation by MMA-peroxide and then by the added initiator. Each initiation process is responsible for a

different molecular weight distribution leading to a bimodal distribution at this temperature, which is shown in figure 2.24 (b). The attribution of each molecular weight distribution to one initiating species becomes especially clear in figure 2.26, where the evolution of the distribution with time is presented by means of a 3D-graph. Clearly visible is the "birth" of the lower molecular weight part at the moment of initiator addition.

The predicted extremely high molecular weight polymer in the beginning of the reaction (figure 2.25 (b)) has its origin in a misinterpretation of the model for very low radical concentrations. Its concentration can be neglected, though, as proven by the absence of very high molecular weights in the distribution graph (figure 2.24 (b)). In reality, inhibition reactions would prevent the formation of such high molecular weight chains. However, in the simulation these are not taken into account. For the rest of the results, the model shows excellent agreement with the measured data.
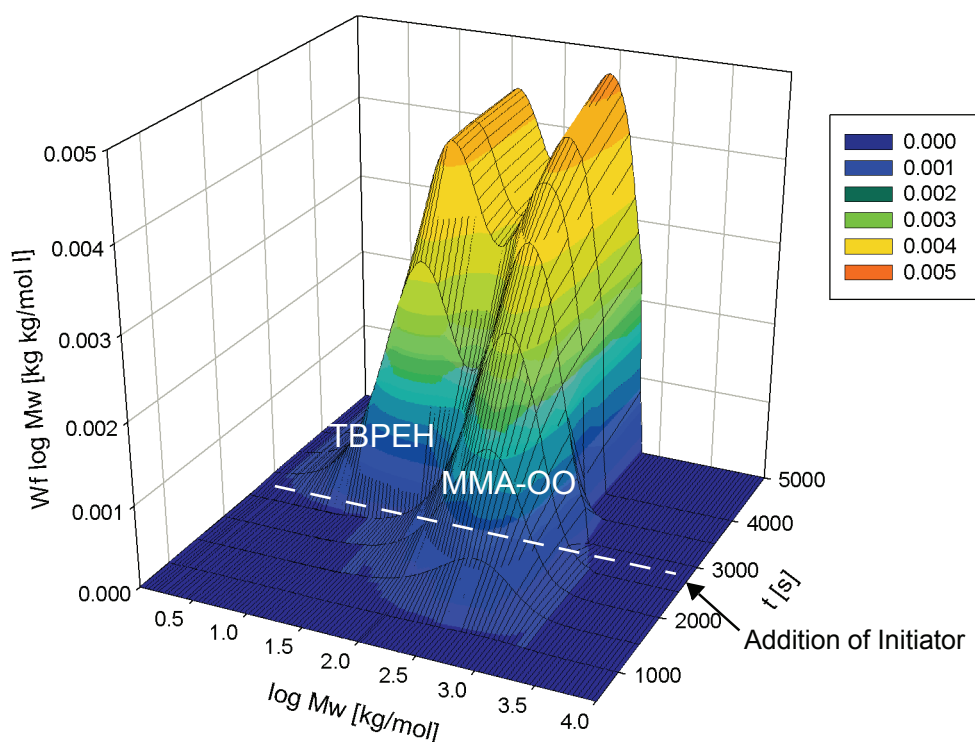
Figure 2.26: 3D-plot of the molecular weight distribution evolution with time at 127 °C

For T = 150 °C, the results look very similar. The only difference is that DTBP decomposes much slower than TBPEH. Therefore, the bimodality of the observed molecular weight distribu-

tion (figure 2.27 (b)) is less pronounced. At 120 °C, TBPEH decomposes rapidly producing a large radical flow, which leads to little polymer with significantly lower molecular weight than previously produced by the decomposing MMA-OO. Therefore, the distribution gets bimodal with two almost equally important peaks. For DTBP, the initiator concentration rises much higher (compare figure 2.25 (a) and figure 2.28 (a)) and rests much longer. The radical flow is, thus, much less intense, which leads to a larger amount of produced polymer with, at the same time, a higher molecular weight than during the earlier period. The polymer produced beforehand by the decomposing MMA-OO plays, therefore, only a minor role and appears in the final distribution only as shoulder (figure 2.27 (b)). This becomes evident once again in the molecular weight distribution evolution with time, as demonstrated illustratively by the 3D-graphic in figure 2.29.

Furthermore, it is important to remark that for this temperature range, the MMA peroxide is formed and decomposed already during the heating period. This leads to more than 20 % monomer conversion before the reactor has even reached its final temperature, which, once again, underlines the importance of MMA peroxide and oxygen in the polymerization of MMA.

From both experiments, k_d and the initiator efficiency at zero conversion f_0 could be determined following the Odian method (see "Odian method" on page 37). The values for k_d are in the same order of magnitude than the values determined by DSC in this work, although for TBPEH the decomposition is a little slower and for DTBP a little faster. Considering the rather low precision of the Odian method (double-logarithm, i.e. measurement errors are strongly amplified), this seems reasonable. The value for the efficiency of TBPEH and DTBP seem quite realistic, too. Unfortunately, there is no literature value available yet for the TBPEH efficiency.

Table 9: Kinetic parameters for the decomposition of thermal initiators TBPEH and DTBP determined from batch experiments according to the Odian method

	k_d [s^{-1}]	k_d [s^{-1}] (DSC)[a]	f_0 [-]	f_0 [-] [47]
TBPEH (127 °C)	$6.40 \cdot 10^{-3}$	$1.22 \cdot 10^{-2}$	0.51	-
DTBP (150 °C)	$9.35 \cdot 10^{-4}$	$5.07 \cdot 10^{-4}$	0.72	0.7

a. determined by DSC, compare appendix 4 for more details

(a)

(b)
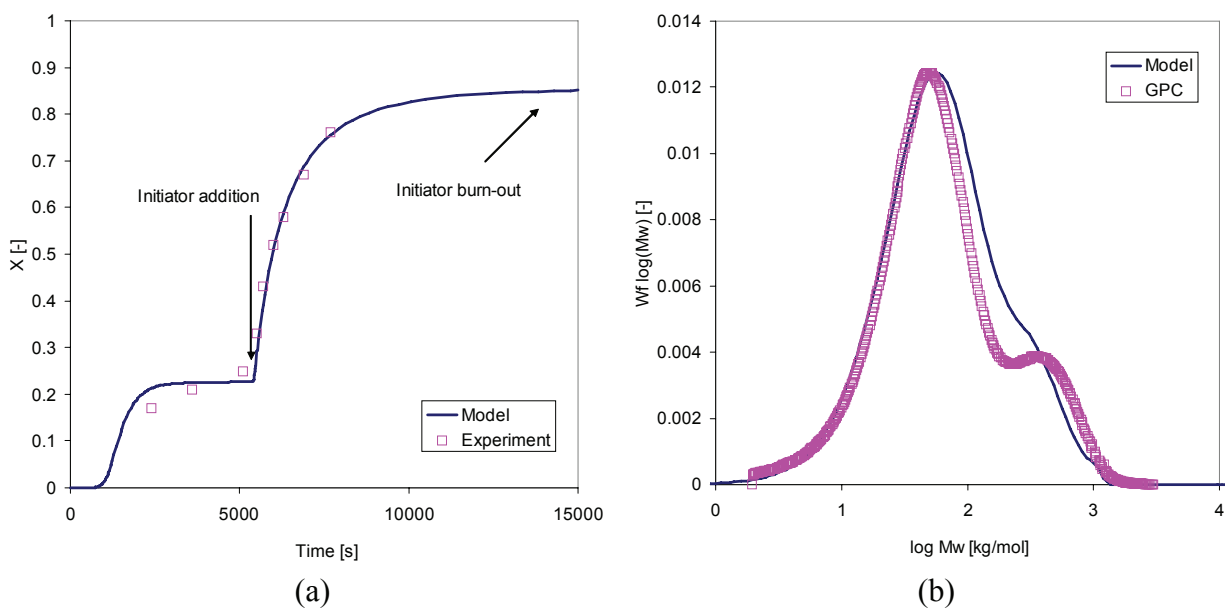
Figure 2.27: Results for the 150°C batch experiment (50% BuAc, [DTBP] = 1000 ppm, [CTA] = 100 ppm) (a) Conversion evolution (b) Molecular weight distribution (t = 15'000 s)

(a)

(b)

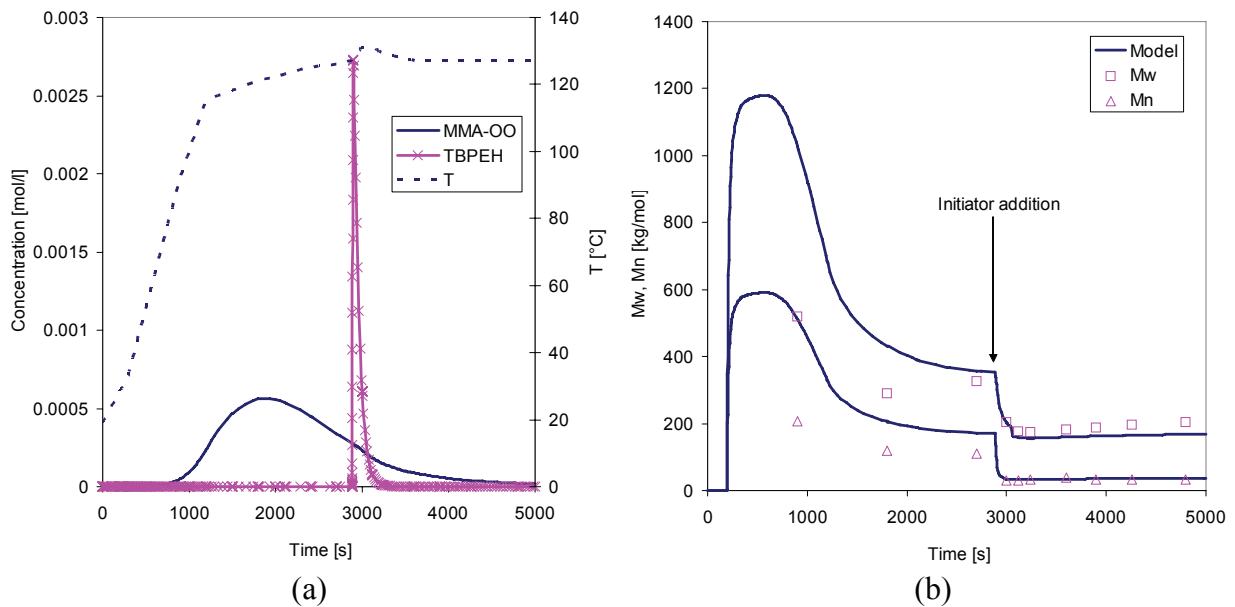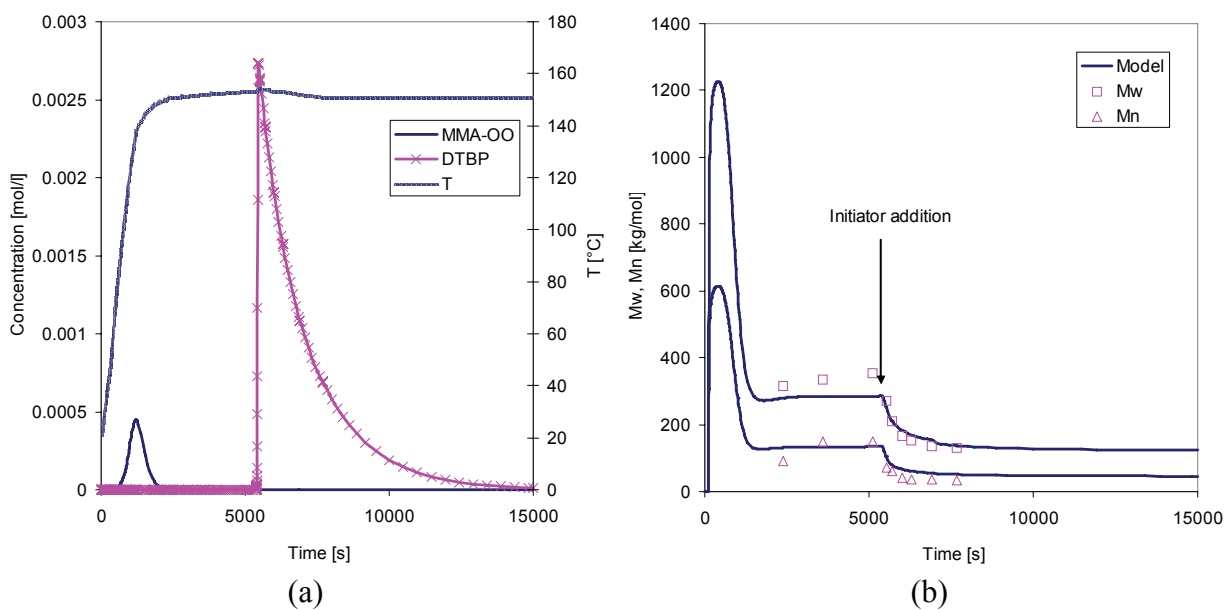*Figure 2.28: Results for the 150°C batch experiment (50% BuAc, [DTBP] = 1000 ppm, [CTA] = 100 ppm) (a) Temperature and initiator concentrations (MMA-OO and BTBP) over time (b) Molecular weight evolution (Mw, Mn)*
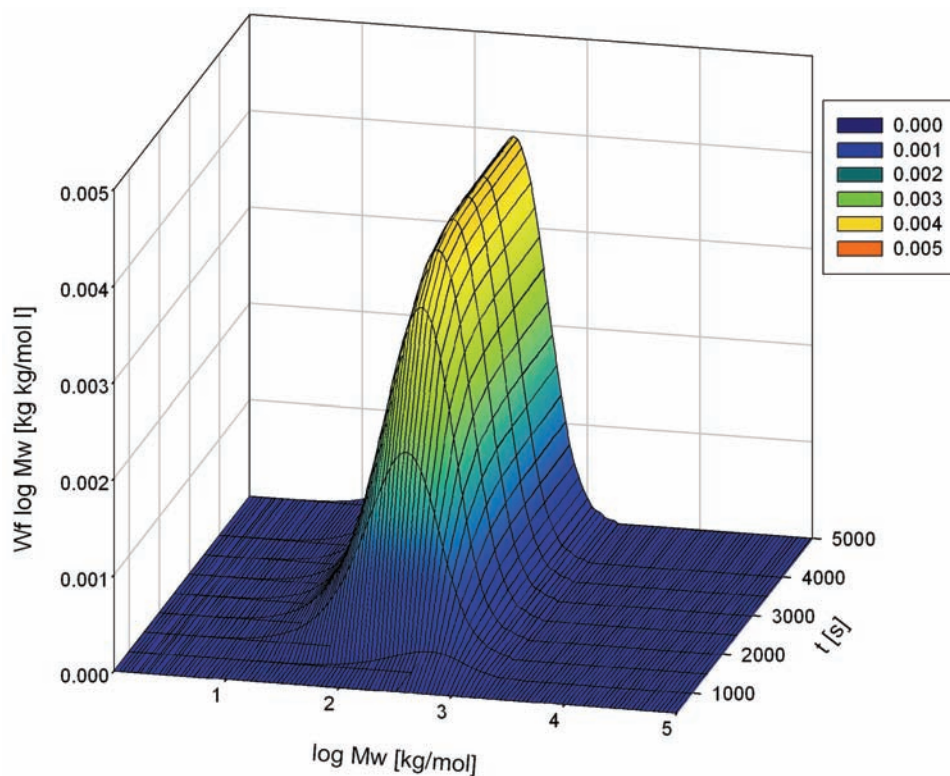
Figure 2.29: 3D-plot of the molecular weight distribution evolution with time at 150 °C

2.6 Discussion

The self-initiation of MMA and the behaviour of PMMA peroxides is one key topic of this work. For a long time underestimated in high-temperature MMA polymerizations, their full potential as thermal initiators and their influence on conversion and molecular weight evolution has been investigated in detail within this chapter. The results could mostly confirm the literature data on the formation and decomposition, as well as on the structure.

In particular, it was proven that physically dissolved oxygen ($[O_2]_{MMA}$ ~ 60 - 70 ppm saturation concentration at 20 °C) reacts with MMA (and probably other acrylic monomers) to form copolymeric peroxide chains with molecular weights between 2'000 and 10'000 g/mol, which

accumulate in the system until the monomer is heated. The presence of these peroxides was proven by several analytical techniques, among which NMR, GPC and TGA-MS.

At high temperatures (> 100 °C), these peroxides decompose exothermally and initiate the radical polymerization. It is, therefore, legitimate to speak of a *high-temperature decomposing initiator*. Depending on the reaction conditions, monomer conversions as high as 30 % can be observed.

The formation and decomposition kinetics were determined experimentally and the results included as reaction (formation-, decomposition- and initiation-) steps in a kinetic model (the complete model is presented in appendix 3). With this model, it is now possible to describe batch polymerizations with and without the addition of thermal initiator in a very precise way. A missing point is the possibility to determine reliably the oxygen content of MMA samples. The saturation concentration had to be estimated to 60-80 ppm, a value which corresponds to literature data for other acrylics and organic solvents [35, 48]. Especially in the batch reactor the reproducibility of experiments was sometimes rather poor, which is assumed to be due to changing oxygen concentrations. These are produced by the pressurization and depressurization of the reactor with nitrogen during the preparation phase. A determination of the O_2 amount in the organic phase could help improve the understanding of these effects.

Aside from the initiation by MMA peroxides, the initiation by chain transfer agent, the thermal initiation of MMA due to intramolecular interactions in the pure monomer, as well as the formation of dimers were also investigated. While the chain transfer agent has a significant influence on the initiation at 170 °C and above, the "true" thermal initiation of MMA plays no major role below 180 °C and is, therefore, negligible for most experiments carried out in this work. The same applies for the formation of dimers and higher oligomers, which only start having a measurable effect on the conversion even above 180 °C.

The observed phenomena will be included in the model for the description of the continuous pilot plant process and evaluated once again in this context.

Short Summary:

- The spontaneous polymerization of MMA is an important aspect in high temperature processes and cannot be neglected in the kinetic modeling
- Different mechanisms for the initiation and dimerization of MMA have been evaluated concerning their importance in terms of monomer conversion
- It was found that the major role in the thermal initiation of MMA play polymeric peroxides that form from physically dissolved oxygen
- The formation and decomposition kinetics of these peroxides were successfully determined in this work and the peroxides, themselves, were characterized by various analytical methods
- Finally, the determined kinetics for the various reaction mechanisms discussed in this chapter were discussed with respect to experimental data obtained from high temperature polymerization reactions carried out in this work.

CHAPTER 3

High Temperature Gel Effect

The term "gel effect" or "Trommsdorff effect" generally describes the phenomenon that, in homogeneous bulk polymerizations at higher polymer contents and in particular at low temperatures, the reaction rate and degree of polymerization increase significantly. This effect is especially intense in the methyl methacrylate polymerization, but occurs also for monomers like styrene, vinyl acetate and others. Trommsdorff [49] was among the first to explain his observations by the fact that, with increasing viscosity of the reaction medium, the diffusion of the macro radicals and, thus, the termination of the reactive chains is impeded whereas the diffusion of the smaller monomer molecules to the reactive centers at the chain ends continues undisturbed [50]. The reason of this apparent increase in reaction rate and degree of polymerization is, therefore, a strong drop of the termination rate with growing polymer fraction in the reaction medium.

In the modeling of MMA polymerizations, the gel effect is one of the most important factors to consider. It has a strong influence on both, the rate of monomer conversion and its final value (and, therefore, on the heat production that is to expect), as well as on the molecular weight distribution. Thus, it becomes inevitable for any kinetic model to correctly describe the changing of the termination rate k_t with increasing viscosity. The term *conversion* is avoided on purpose in this context, since the intensity of the gel effect does not only depend on the monomer conversion, but also on factors like solvent content, molecular weight and temperature. For example, as will be shown further on in this chapter, in a polymerization above 120°C with 30% solvent, the gel effect becomes almost negligible. The same applies to bulk polymer-

izations at temperatures above 170°C, where in the conversion-time curve no clear acceleration is visible anymore.

Since the beginnings of polymerization modeling, the gel effect has been extensively investigated and kinetically described by innumerable authors. In particular during the 80's, several important advances in its description were made. According to Tefera, Weickert and Westerterp [51], there exist 5 different model concepts, each of them describing the termination rate constant by another phenomenon:

- Viscosity based models
- Conversion or polymer weight fraction based models
- Reptation theory based models
- Entanglement concept based models
- Free volume theory based models,

Apart from the theory that lies behind each model, one major difference is the use of a break point in some of them, i.e. an artificial switch at a certain conversion, for example, from where on the calculation of k_t changes suddenly. This is, however, in contradiction to reality, since the gel effect does not start at a sudden time t, but is slowly increasing with the polymer fraction. Therefore, there is no sense in considering these models for this work. In the following, only models that offer a continuous correlation of k_t with other reaction parameters will be discussed, namely models based on the free volume theory.

Although these models are based on the same theory, i.e. the free volume theory of Vrentas and Duda [52-55], they differ fundamentally in their general concept. However, one thing they all have in common is the fact that they were derived for temperature ranges far below the glass transition temperature T_g, except for two models developed at EPFL in the 90's, one by Fleury and the other by Hoppe [5, 56]. The glass transition is the temperature, where the polymer changes from an amorphous glass state to a viscous melt, which comes along with drastic consequences on its physical properties, in particular the diffusion characteristics. The T_g for homogeneous PMMA is approximately 115°C [57], but varies depending on the method of determination and on the polymer characteristics (mostly the tacticity, which changes with polymerization temperature).

In this chapter, it will be tried to comprehensively explain the gel effect, the different gel effect models and their applicability to different types of processes. Finally, a refined model for the high temperature gel effect in batch and continuous processes is developed and presented.

3.1   Theory

Following a simplified model, the rate of polymerization for homogeneous radical polymer-izations is defined as:

$$R_p = -\frac{d[M]}{dt} = \frac{k_p}{\sqrt{k_t}} \cdot \sqrt{2 \cdot f \cdot k_d \cdot [I]} \cdot [M] \qquad \text{(EQ 3.1)}$$

and the kinetic chain length as:

$$\bar{P} = \frac{k_p^2}{k_t} \cdot \frac{[M]^2}{R_p} = \frac{k_p}{\sqrt{k_t}} \cdot \frac{1}{\sqrt{2 \cdot f \cdot k_d \cdot [I]}} \cdot [M] \qquad \text{(EQ 3.2)}$$

This "classical" kinetic description of the polymerization is only valid in first approxima-tion and for small monomer conversions, since it does not take into account any diffusion limita-tions. It assumes ideal homogeneous conditions, in which the rate determining steps are the reactions themselves. However, with increasing monomer conversion, the viscosity of the system can - *depending on the reaction conditions* - increase drastically, thus severely limiting the free-dom to move first only for the larger chain molecules, then also for the small monomer molecules. The first consequence of this limited mobility is that the active polymer chains are hindered from terminating each other by disproportionation or combination. According to the theory established by Chiu, Carratt and Soong [58] in 1983, the termination takes place in three steps:

1. The polymer radicals, initially separated by more than one molecular diameter, approach by translational diffusion

2. Once in direct proximity, the radical chain ends move toward each other (segmental diffusion)

3. After proper orientation of the chains to each other is reached, the termination reaction can take place

In figure 3.1 is illustrated schematically the surrounding of an active chain radical on the molecular level. Within the termination radius r_t around the active radical center, the termination rate is the intrinsic one $k_{t,0}$. This "true" termination rate reflects the speed of termination of two polymer radicals under ideal, i.e. not diffusion controlled, conditions. However, as soon as the dif-fusion of large chain molecules from $r \gg r_t$ to $r < r_t$ is limited, the apparent termination rate con-

stant k_t decreases, which according to equation 3.1 results in an increase of the rate of polymerization. This can be the case quite quickly, i.e. already at monomer conversions of less than 20% for MMA bulk polymerizations.
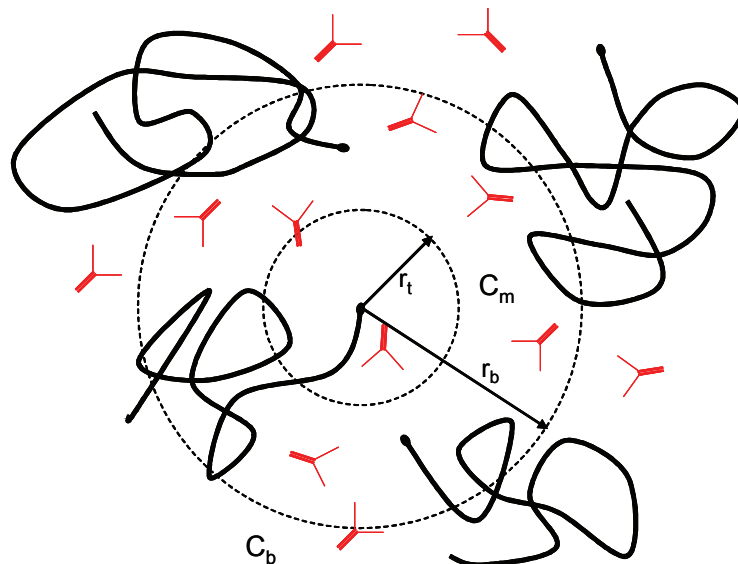
Figure 3.1: Schematic diagram for describing the radical termination process

The propagation rate k_p is not influenced so far, since the smaller monomer molecules (depicted schematically as =<) can still diffuse freely between the polymer chains. Only at very high conversions and below the glass transition temperature T_g, when, due to the growing amount of polymer chains the solution enters the so-called "glassy" state, also the monomer diffusion becomes limited. Consequently, with decreasing k_p, the rate of polymerization diminishes until the reaction "freezes". This phenomenon is called the "glass effect" and causes a significant conversion limitation for below-T_g polymerizations. However, since this work only deals with above-T_g polymerizations, the influence of viscosity on k_p is not taken into account.

An important point to keep in mind for further considerations is the significance of k_p <u>and</u> k_t for the rate of polymerization and the average degree of polymerization. In kinetic studies it is crucial to always have a look at the quotient shown in equation 3.3, since one constant alone is not meaningful for the kinetics. This is in particular the case for literature values, where generally the pair of kinetic constants must be adapted, never only one of them. Especially combining values for k_p and k_t from different sources is likely to result in wrong model characteristics.

$$R_p, \bar{P} \propto \frac{k_p}{\sqrt{k_t}} \qquad\qquad \text{(EQ 3.3)}$$

3.1.1 Model basics

So far, the theory behind the gel effect and the reasons leading to it have been discussed. As to its kinetic description in simulations, there are various possibilities to tackle this problem.

The classical "engineering" approach is to find an empirical equation and to fit it to experimental data. In the case of the gel effect, this can be achieved by exponential functions as presented in equation 3.4 [59]. This equation, which was fitted for a temperature range of 40 - 90 °C, expresses the dependence of the apparent termination rate constant k_t on the conversion without any physical background.

$$\frac{k_t}{k_{t,0}} = \left[\frac{1}{1-X} \cdot e^{(B \cdot X + C \cdot X^2)} \right]^2 \qquad\qquad \text{(EQ 3.4)}$$

However, although easy to obtain and to apply, these kinds of equation are usually very limited to specific conditions and applications and cannot claim any scientific legitimation.

The following steps for the development of a general kinetic model for the gel effect based on physical considerations were established by Chiu, Carratt and Soong [58] and represent the basis for models from many other authors.

The first assumption is the equilibrium within a sphere of the diameter r_t (see figure 3.1) between the radical transport from the bulk into the sphere and the consumption of radicals by the termination reaction (let us recall the fact that within the sphere, the termination is not diffusion limited, therefore has its true rate $k_{t,0}$). This equilibrium can be expressed by equation 3.5:

$$4\pi \cdot r_t \cdot D_{eff} \cdot (C_b - C_m) = \frac{4}{3}\pi \cdot r_t^3 \cdot k_{t,0} \cdot C_m \cdot C_b \qquad\qquad \text{(EQ 3.5)}$$

from where follows for the concentration within the sphere, C_m, which represents the probability for a center radical to find another radical within the distance r_t:

$$C_m = \frac{D \cdot C_b}{D + \dfrac{r_t^2}{3} \cdot k_{t,0} \cdot C_b}$$

(EQ 3.6)

The apparent reaction rate, which can be written as $k_t C_b{}^2$, is equal to $k_{t,0} C_b C_m$ (the intrinsic termination rate constant times the probability for two radicals to encounter each other), which gives:

$$k_t \cdot C_b^2 \equiv k_{t,0} \cdot C_b \cdot C_m$$

(EQ 3.7)

Therefore, from equation 3.6 and equation 3.7 follows the basic equation for the apparent termination rate, including reaction and mass-transfer limitation:

$$\frac{1}{k_t} = \frac{1}{k_{t,0}} + \frac{r_t^2 \cdot C_b}{3 D_{eff}}$$

(EQ 3.8)

$k_{t,0}$ is independent of conversion and molecular weight, yet strongly temperature dependent. The diffusion coefficient D_{eff}, on the other hand, is a function of temperature, conversion *and* molecular weight. The termination radius r_m can, for reasons of simplification, be considered constant.

Since r_m, C_b and D_{eff} are unknowns, the transformation of equation 3.8 into something more tangible is the basic work of the different authors that have developed their models on this basis. In the following, the most important ones will be presented.

3.2 Existing Model Evaluation

The following evaluation of existing models only represents a small part of all the different models that can be found in literature. Due to the limited time frame and the variety of different subjects dealt with in this work, only the most representative modeling approaches could be chosen for comparison. This should not imply that models not mentioned here are less suitable for the description of the gel effect under the conditions they were derived for. Namely the viscosity related model of Buback [60] and the free-volume gel effect model of Hamielec [61], which are well known in the polymer reaction engineering field, were not considered in the following evalu-

ation due to known issues at high temperatures [62]. A more exhaustive description of a large number of existing models can be found in [51].

3.2.1 Chiu, Carratt and Soong (CCS) [58]

Chiu, Carrat and Soong continued the development of their model by separating the diffusion coefficient D_{eff} into a temperature- and molecular-weight-dependent part $D(T, M_w)$ and a conversion dependent part $D(X)$:

$$\frac{1}{k_t} = \frac{1}{k_{t,0}} + \frac{r_t^2}{3D(T, M_w)} \cdot \frac{C_b}{D(X)} \equiv \frac{1}{k_{t,0}} + \theta_t \cdot \frac{\lambda_0}{D(X)} \qquad \text{(EQ 3.9)}$$

The term $\frac{r_t^2}{3D(T, M_w)}$ is expressed by a function $\theta_t(T, M_w)$; C_b is replaced by the zeroth moment of the polymer distribution. The temperature- and molecular-weight-dependence of θ_t can, according to the authors, not take any simple mathematical form and is, therefore, fitted to experimental data. Since the molecular weight, at least for non-chain-transfer-regulated batch polymerizations, is mainly governed by the initial initiator concentration $[I]_0$, it can also be written $\theta_t(T, [I]_0)$. The conversion dependence of D can be described by the free volume theory. The authors make use of the so-called Fujita-Doolittle equation:

$$\log\frac{D}{D_0} = \frac{\phi_m}{A(T) + B(T) \cdot \phi_m} \quad \text{with} \quad \phi_m = \frac{1-X}{1+\varepsilon X} \quad \text{(monomer volume fraction)} \qquad \text{(EQ 3.10)}$$

A and B are functions of temperature that have to be fitted to experimental data, too. D_0 is the diffusion coefficient at zero conversion. As result of the combination of above equations, the authors present the following:

$$\frac{1}{k_t} = \frac{1}{k_{t,0}(T)} + \theta_t(T, [I]_0) \cdot \frac{\lambda_0}{\exp\left[\dfrac{2.3\phi_m}{A(T) + B(T)\phi_m}\right]} \qquad \text{(EQ 3.11)}$$

D_0 was taken into the function $\theta_t(T, [I]_0)$ and transformation of the *log* into the natural logarithm *ln* leaves a factor $ln(10) = 2.3$. The necessary information about the fitting of the parameters $\theta_t(T, [I]_0)$, $A(T)$ and $B(T)$ to experimental data can, unfortunately, only be found in a consecutive article of the authors [63]: $\theta_t(T, [I]_0)$ is expressed by an Arrhenius law,

$$\theta_t(T, [I]_0) = \frac{1.1353 \times 10^{-22}}{[I]_0} \cdot e^{\frac{142\left[\frac{kJ}{mol}\right]}{R \cdot T[K]}} \qquad \text{(EQ 3.12)}$$

whereas A is a function of temperature (T_g is the glass transition temperature) and B was found to be constant:

$$A(T) = 0.168 - 8.21 \times 10^6 \cdot (T - T_g)^2 \qquad B = 0.03 \qquad \text{(EQ 3.13)}$$

These fittings, however, were carried out for a temperature range between 50°C and 90°C. Furthermore, the expression of the molecular weight dependence by the initiator load (equation 3.12) does not hold true for continuous or semi-batch polymerizations, where initiator is constantly added.

Figure 3.2 (a) and (b) show results obtained with the CSS model for 90°C and 150°C. While for 90°C the conversion evolution is modeled correctly, the model strongly underestimates the gel effect for higher temperatures, as can be seen also from the comparison of the termination rate constant with increasing conversion. This confirms that the model is not suitable as it is but needs to be refitted if used for high-temperature modeling.

(a)   (b)
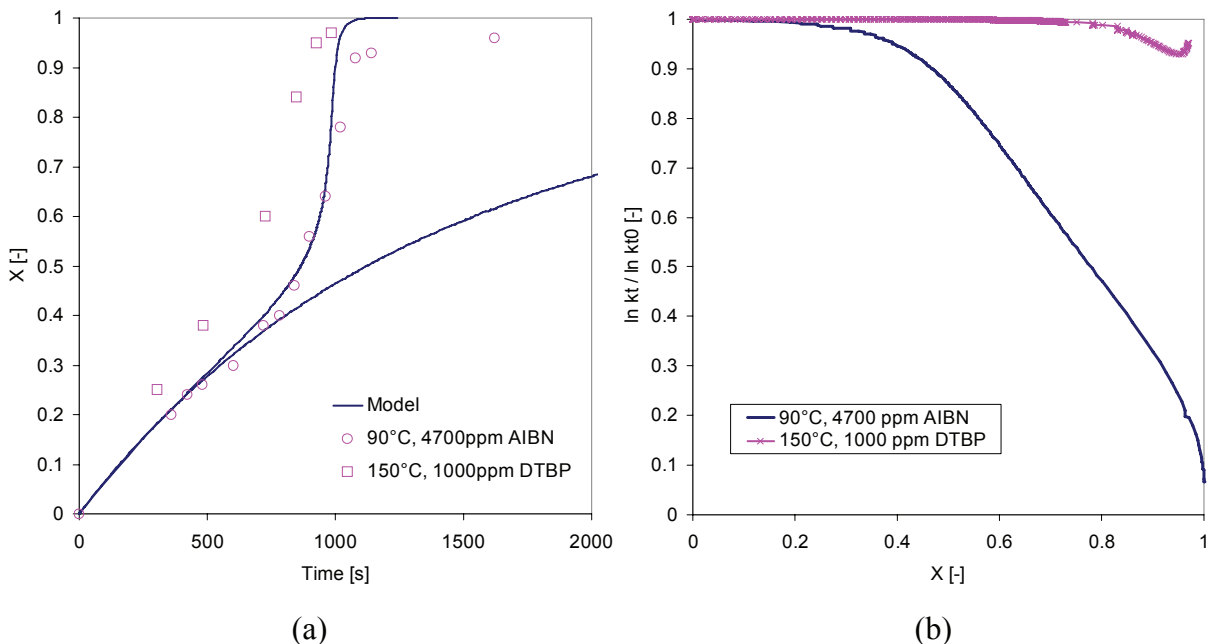
Figure 3.2: (a) Conversion over time curve according to the CSS model for 90°C and 150°C (b) modeled termination rate evolution with conversion for 90°C and 150°C (CSS model) (90°C conversion data taken from [58])

3.2.2 Achilias and Kiparissides [64]

The model of Achilias and Kiparissides uses the same basic considerations. Yet, the authors were motivated to derive a model that does not contain any adjustable parameters but only parameters that have a clear physical meaning and can be evaluated in terms of physical and transport properties of the reactive species. Thus, in spite of using the Fujita-Doolittle equation (see equation 3.10), they propose to calculate the diffusion coefficients of each species by physical means:

$$D_{eff} = N \cdot D_{p0} \cdot e^{-\frac{E_p}{RT}} \cdot e^{-\frac{\gamma(w_m \hat{V}_m' + w_p \hat{V}_p' \xi)}{\hat{V}_f \xi}} \quad \text{for the polymer} \qquad \text{(EQ 3.14)}$$

$$D'_{eff} = D_{m0} \cdot e^{-\frac{E_m}{RT}} \cdot e^{-\frac{\gamma(w_m \hat{V}_m' + w_p \hat{V}_p' \xi)}{\hat{V}_f}} \quad \text{for the monomer} \qquad \text{(EQ 3.15)}$$

with the following equations for the calculation of the specific volume of the solution:

$$\hat{V}_f = w_m[K_{11}(K_{21} + T - T_{gm})] + w_p[K_{12}(K_{22} + T - T_{gp})] \qquad \text{(EQ 3.16)}$$

$$w_m = \frac{\phi_m}{\left(\phi_m + \phi_p \cdot \frac{\hat{V}_m^{0}}{\hat{V}_p^{0}}\right)} \qquad w_m = \frac{\phi_p \cdot \frac{\hat{V}_m^{0}}{\hat{V}_p^{0}}}{\left(\phi_m + \phi_p \cdot \frac{\hat{V}_m^{0}}{\hat{V}_p^{0}}\right)} \qquad \text{(EQ 3.17)}$$

So, in order to calculate the effective diffusion coefficient D_{eff} in equation 3.8, already 15 nonadjustable physical parameters need to be calculated that will not be specified here any further: $\hat{V}_m^{0}$, $\hat{V}_p^{0}$, $\hat{V}_m'$, $\hat{V}_p'$, K_{11}, K_{12}, K_{21}, K_{22}, γ, ξ, N^*, D_{p0}, E_p, D_{m0}, E_m. And for these calculations, various further values are necessary, so that in the end more than 20 parameters are found only in the model for the gel effect. This becomes especially problematic when the reaction system becomes more complicated than the polymer-monomer binary system used in the work of Achilias and Kiparissides. In addition, most of the literature values for the needed parameters are only available for the classical temperature range 50-90°C. Considering the complexity of this model together with the fact that the achieved precision as regards the modeling of conversion and molecular weight is not significantly improved in comparison to semi-empirical approaches

[51], its adaptation for a continuous, high-temperature polymerization as in this work seems to be neither very promising nor justified.

3.2.3   Hoppe and Renken [56]

Nevertheless, this way was chosen by Hoppe and Renken in the 90's, who extended the Kiparissides model to a ternary mixture of monomer, polymer and solvent and added high-temperature characteristics from the work of Fleury [5], thus increasing its complexity once again. In the end, they manage to satisfactorily model the batch conversion evolution for different solvents over a large temperature range (45 - 165°C). The molecular weight modelling, however, is completely missed.

The problem with these non-empirical models is that they do not offer enough flexibility for industrial applications. The necessity to exactly know the physical and transport properties of each species in the system makes it impossible to apply them to large-scale polymerizations, let alone copolymerizations, where now and then quite exotic initiators and solvents are used. It is, therefore, of advantage to have a model that allows to be adapted to changing reaction conditions by fitting and that exhibits minimal calculation requirements. The approach of Chiu, Carrat and Soong was taken up again in the PhD work of Fleury on the high temperature polymerization of MMA.

3.2.4   Fleury [5]

In his model development, Fleury interprets the basic equation of the Chiu, Carrat and Soong model (equation 3.8) in a different way. His aim is to linearize the equation for the apparent termination rate constant:

$$\frac{k_{t,0}}{k_t} = 1 + \theta_t \cdot \frac{k_{t,0} \cdot \lambda_0}{\exp\left(\dfrac{2.3(1-\phi_p)}{A + B(1-\phi_p)}\right)} \qquad\qquad \text{(EQ 3.18)}$$

In order to simplify this expression, he reasons that while for small conversions the diffusion part of the equation is negligible

$$\frac{1}{k_t} = \frac{1}{k_{t,0}} + \frac{r_t^2 \cdot \cancel{C_b}}{\cancel{3D_{eff}}} \quad \text{so it is } k_t = k_{t,0} \qquad \text{(EQ 3.19)}$$

for higher conversions, this is the case for the intrinsic termination rate:

$$\frac{1}{k_t} = \cancel{\frac{1}{k_{t,0}}} + \frac{r_t^2 \cdot C_b}{3D_{eff}} \qquad \text{(EQ 3.20)}$$

With the Fujita-Doolittle theory, equation 3.20 can - for the diffusion regime - also be written as (compare equation 3.11):

$$k_t \cong \frac{\exp\left(\dfrac{2.3 \cdot (1 - \phi_p)}{A + B \cdot (1 - \phi_p)}\right)}{\theta_t \cdot \lambda_0} \qquad \text{(EQ 3.21)}$$

Now, for increasing polymer fractions ϕ_p, this means that the term $\theta_t(T, [I]_0)\, \lambda_0$ gets dominant:

$$\theta_t \cdot \lambda_0 \gg \exp\left(\frac{2.3 \cdot (1 - \phi_p)}{A + B \cdot (1 - \phi_p)}\right) \quad \text{and as well } A \gg B \cdot (1 - \phi_P) \qquad \text{(EQ 3.22)}$$

$$\phi_p = w_p \cdot \frac{\rho}{\rho_p} = (1 - w_s) \cdot X \cdot \frac{\rho}{\rho_p} \cong (1 - w_s) \cdot X \qquad \text{(EQ 3.23)}$$

Neglecting the two smaller terms in equation 3.22 and using equation 3.23 for the polymer fraction allows to write equation 3.18 in a logarithmic form:

$$\ln\left(\frac{k_t}{k_{t,0}}\right) = \frac{2.3}{A} - \ln(\theta_t \cdot \lambda_0 \cdot k_{t,0}) - \frac{2.3}{A}(1 - w_s) \cdot X \text{ with } \lambda_0 = 2 \cdot f \cdot k_d \cdot [I]_0 \qquad \text{(EQ 3.24)}$$

For a constant temperature, this equation represents a straight line, which can be parametrized as follows. First of all, the term $\ln(k_{t,0} \cdot \gamma)$ is added to both sides of the equation:

$$\ln\left(\frac{k_t}{k_{t,0}}\right) + \ln(k_{t,0} \cdot \gamma) = \frac{2.3}{A} - \ln(\theta_t \cdot \lambda_0 \cdot k_{t,0}) + \ln(k_{t,0} \cdot \gamma) - \frac{2.3}{A}(1 - w_s) \cdot X \qquad \text{(EQ 3.25)}$$

where γ has the value 1 and the inverse unit of the termination rate constant, so that in the end an adimensional expression is obtained within the logarithm. Further development of equation 3.25 leads to the following linear equation for the *diffusional* termination rate constant:

$$\ln(k_t) = \underbrace{\frac{2.3}{A} + \ln\left(\frac{\gamma}{\theta_t \cdot \lambda_0}\right)}_{\alpha} - \underbrace{\frac{2.3}{A}(1 - w_s)}_{\beta} \cdot X \qquad \text{(EQ 3.26)}$$

$$\ln(k_t) = \alpha - \beta \cdot X \qquad \text{(EQ 3.27)}$$

Combined with equation 3.18 this means that for the apparent termination rate constant can be written:

$$\frac{1}{k_t} = \frac{1}{k_{t,0}} + \frac{1}{\exp(\alpha - \beta \cdot X)} \qquad \text{(EQ 3.28)}$$

The parameters α and β are fittable to experimental data and determine the starting point of the gel effect (α and β) and its intensity (only β). Fleury fitted these parameters to his high-temperature (135°-165°C) batch experiments and found the following dependencies on temperature, solvent fraction and initiator concentration:

$$\alpha = \alpha_0 - 10.9 \cdot w_s + \ln\left(\frac{[I]_0}{[I]_{0,min}}\right)^{0.56} \qquad \text{(EQ 3.29)}$$

$$\beta = \beta_0 - \frac{T - T_g}{T_{ref} - T_g} - 38.3 \cdot w_s + 2.32 \cdot \left[1 - \exp\left(-\frac{[I]_0 / [I]_{0,min}}{3.34}\right)\right] \qquad \text{(EQ 3.30)}$$

with

$T_g = 114°C$

$T_{ref} = 123.3°C$

$[I]_{0,min} = 2 \text{ mol/m}^3$

$\alpha_0 = 14.14$

$\beta_0 = 14.34$

It is important not to forget that this fitting is only valid in the boundaries for which it was done ($135°C < T < 165°C$, $2 \text{ mol/m}^3 < [I]_0 < 200 \text{ mol/m}^3$, $0 < w_s < 0.2$).

The Fleury model is a good example for a semi-empirical model, where a basic theory was simplified and the adaptation to different experimental conditions enabled by introduction of adjustable parameters. However, its weak point is the use of the initiator concentration for molecular weight dependence modeling, which becomes obsolete for continuous process simulation, and the fact that the expressions for α and β lack any physico-chemical connection with regards to the theory of the gel effect.

In this work, the Fleury model was successfully applied to batch and DSC experiments. Yet, the parameters α_0 and β_0 needed to be refitted to experimental data. Taking a closer look at them revealed that they are not constant but temperature-dependant, which means that Fleury apparently did not correctly consider the changing of the gel effect with temperature in his model. Equations 3.31 and 3.32 contain the results of this fitting, which are valid for the temperature range 130 °C < T < 180 °C. The values are slightly different from those published earlier [65], which is due to the fact that several rate constants of the basic kinetic model were changed in the meanwhile in adaptation with the constants used by the industrial partner.

$$\alpha_0 = (0.0574 \pm 0.000758) \cdot T[°C] + (12.926 \pm 0.120267) \qquad \text{(EQ 3.31)}$$

$$\beta_0 = (0.0528 \pm 0.00128) \cdot T[°C] + (8.0716 \pm 0.203035) \qquad \text{(EQ 3.32)}$$

Figure 3.3 (a)-(f) shows the results from the modeling with the Fleury model obtained with the fitted values for α_0 and β_0. For conversion evolution (a) and heat flow signal (b) measured by the DSC, the model yields an excellent agreement with measured data as regards starting point and intensity of the gel effect. For the heat flow signal, the shape of the modeled curve is different in the beginning and in the end. This can be explained by how the modeled curve is calculated in the Predici$^{®}$ model, i.e. by determining the consumption rate of MMA (only) and multiplying it with the heat of polymerization ($\Delta^r H = 56$ kJ/mol) and the sample weight. It does not consider influences on the heat flow by other reactions (e.g. MMA peroxide, initiator decomposition etc.). An explanation for the slow drop of the modeled curve is the depolymerization step in the model, which continuously (i.e. also at almost full conversion) produces MMA from unterminated radical chains due to the absence of natural termination reactions (i.e. with the wall, intramolecular reactions etc.) in the model.

The average molecular weight (by number (c) and by weight (d)) shows some discrepancies at 130°C at the end of the reaction, i.e. for very high values of M_n resp. M_w. The shape of the molecular weight distribution (e) at this temperature, as well, does not perfectly match, although starting and ending point of the peak are the same for modeled and measured values. The difference in shape might be due to the fact that the columns of the GPC could not cope anymore with such high molecular weights (M_w at the right end of the distribution is > 2'000'000 g/mol!). At least, the uneven shape of the measured peak, in particular the steep drop-off on the right, reveals a problem of this kind.
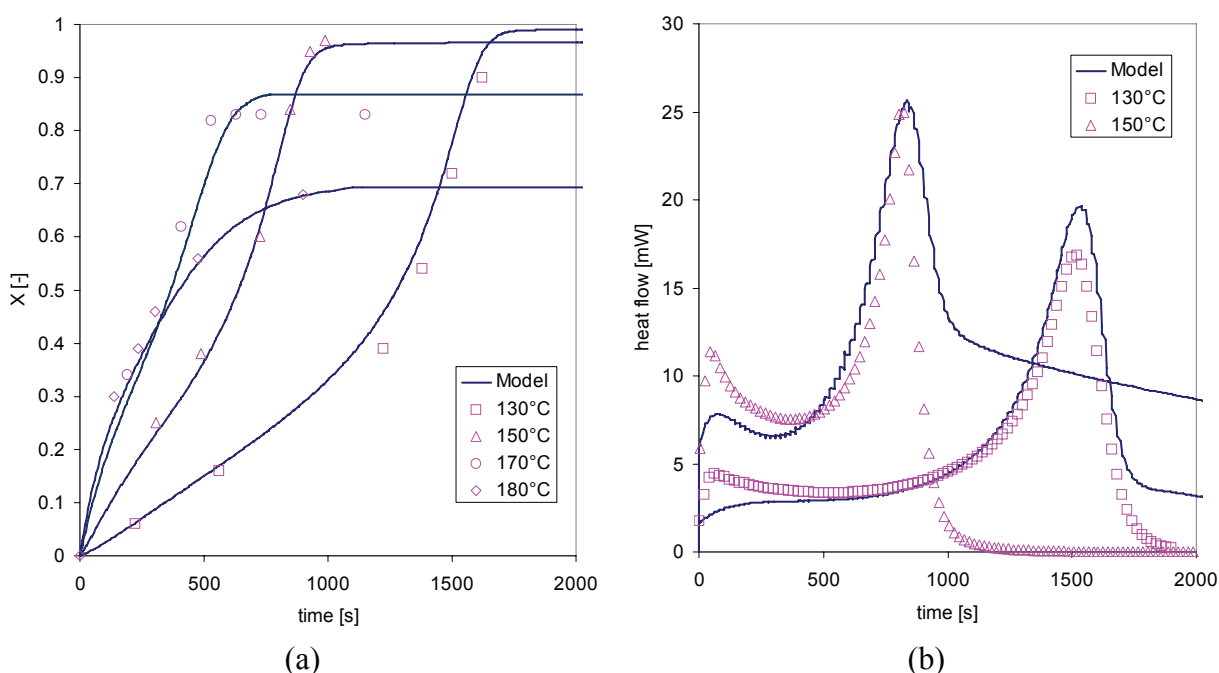
(a)

(b)

Figure 3.3: (a) Modeled and experimental conversion evolution for different temperatures
(b) Heat flow as modeled and measured by DSC for 130°C and 150°C
(c)+(d) Molecular weight (M_n resp. M_w) evolution as modeled and measured by GPC
(e) Molecular weight distribution prediction
(f) Termination rate constant evolution with conversion as predicted by the model
all: DSC MMA polymerization, $[I]_0$ = 1000 ppm DTBP, without CTA

Figure 3.3: (a) Modeled and experimental conversion evolution for different temperatures
(b) Heat flow as modeled and measured by DSC for 130°C and 150°C
(c)+(d) Molecular weight (M_n resp. M_w) evolution as modeled and measured by GPC
(e) Molecular weight distribution prediction
(f) Termination rate constant evolution with conversion as predicted by the model
all: DSC MMA polymerization, $[I]_0 = 1000$ ppm DTBP, without CTA

However, the weak point of the Fleury model is, as already mentioned above, that it does not take into account any chain transfer agent and its influence on the gel effect. Since CTAs

decrease the molecular weight without influencing the conversion, also the gel effect becomes less pronounced. This deficit is depicted in figure 3.4 (a), where it can be clearly seen that, for a CTA-containing polymerization, the model largely overestimates the gel effect. The influence of solvent, on the other hand, is considered in the model (compare eqs. 3.29 and 3.30). Therefore, the attenuation of the gel effect with increasing solvent content is more or less correctly mirrored (see figure 3.4 (b)).

(a)   (b)
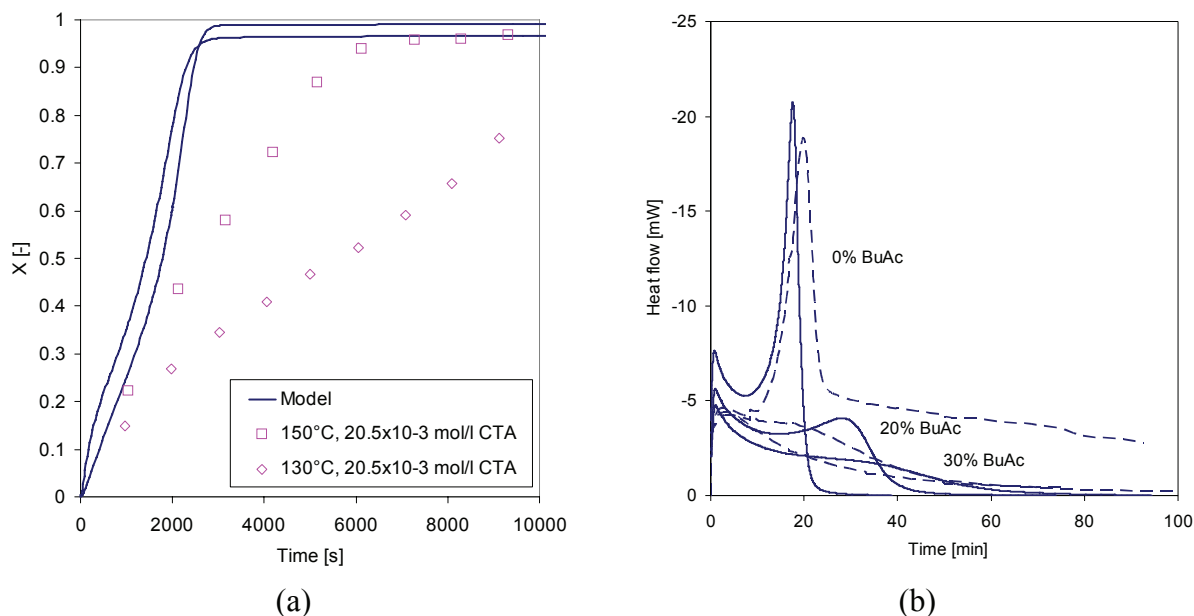
Figure 3.4: (a) Modeled and experimental conversion evolution for polymerization with CTA
(data points taken from [66])
(b) Modeled and experimental heat flow curve for solvent containing polymerization
(140°C, $[I]_0 = 1000$ ppm DTBP)

3.2.5   Fenouillot, Terrisse and Rimlinger [66]

The weakness of the Fleury model, i.e. the missing CTA influence, was improved by Fenouillot et al., who modified the Fleury equation in order to include the CTA concentration in the description of the gel effect. Unfortunately, they eliminated the solvent influence, which disqualifies the model again for industrial application. Additionally, this model as well needs an initial concentration (of CTA instead of initiator) as fixed parameter, which makes its use for continuous processes doubtful. The decisive equation for the gel effect is equation 3.33, which

was directly derived from the Fleury equation 3.28. Equation 3.33 also includes how the new parameter X_c is connected to the Fleury parameters.

$$\frac{1}{k_t} = \frac{1}{k_{t,0}} + \frac{1}{k_{t,0} \cdot \exp[\beta \cdot (X_c - X)]} \text{ with } X_c = \frac{\alpha - \ln k_{t,0}}{\beta} \qquad \text{(EQ 3.33)}$$

The Fenouillot parameters β and X_c were determined by fitting to be:

$$\beta = -17.85 + 0.5756 \cdot T - 0.002519 \cdot T^2 \qquad \text{(EQ 3.34)}$$

$$X_c = 4.289 - 0.05799 \cdot T + 0.00020422 \cdot T^2 + 0.11 \cdot \ln(1000 \cdot [CTA]_0 + 3) \qquad \text{(EQ 3.35)}$$

In figure 3.5 are depicted the conversion evolutions for three cases: one without chain transfer agent and solvent, one with chain transfer agent and one with solvent. As can be seen, the model correctly describes the attenuation of the gel effect in the presence of chain transfer agent. However, due to the above-mentioned lack of solvent consideration in the model, both modeled curves, with and without solvent, are equal.
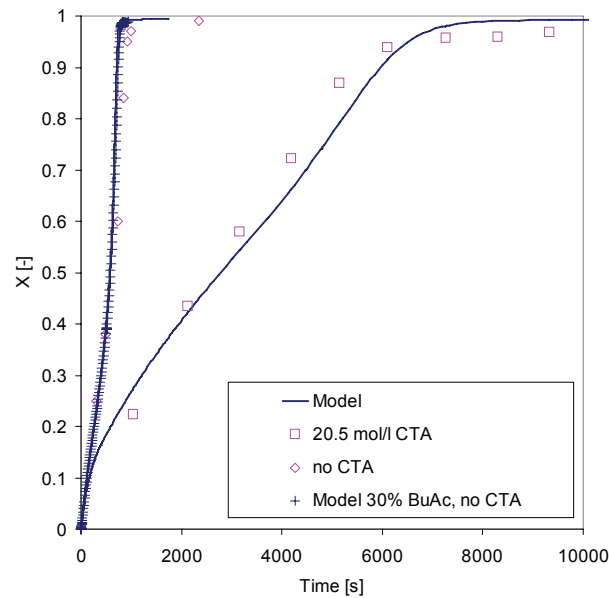
Figure 3.5: Modeled and experimental conversion evolution at 150°C for the Fenouillot model
□ [DTBP]$_0$ = 180 ppm, [CTA]$_0$ = 4400 ppm (data taken from [66])
◇ [DTBP]$_0$ = 1000 ppm, no CTA

73

3.2.6 Tefera, Weickert and Westerterp [51, 67]

Tefera, Weickert and Westerterp follow the same approach of a three-stage diffusion model for their description of the gel effect. Yet, they tackle the problem in a different way. For them, the apparent termination rate constant is governed by three mechanisms: the segmental diffusion at early polymerization stages, the translational diffusion at intermediate conversions and the reaction diffusion taking place throughout the whole reaction. In mathematical terms they express this by equation 3.36:

$$k_t = \frac{1}{\frac{1}{k_{tR}} + \frac{1}{k^*_{TD}}} + k_{RD} \qquad \text{(EQ 3.36)}$$

where k_{tR} is the intrinsic termination rate constant, k^*_{TD} the molecular weight dependent translational-diffusion termination rate coefficient and k_{RD} the reaction diffusion termination rate coefficient.

At very low conversions, the apparent termination rate constant k_t equals $k_{t,0}$, therefore it can be written for equation 3.36:

$$k_{t0} = \frac{1}{\frac{1}{k_{tR}} + \frac{1}{k^*_{TD,0}}} + k_{RD,0} \qquad \text{(EQ 3.37)}$$

So it follows for k_{tR}

$$\frac{1}{k_{tR}} = \frac{1}{(k_{t,0} - k_{RD,0})} - k^*_{TD,0} \qquad \text{(EQ 3.38)}$$

The molecular weight dependence of k^*_{TD} is expressed by the term

$$k^*_{TD} = \frac{k_{TD}}{M^n_w} \qquad \text{(EQ 3.39)}$$

where

$$k_{TD} = D \cdot \exp\left(-\frac{g_1}{V_f}\right) \qquad \text{(EQ 3.40)}$$

D is the diffusion coefficient, V_f the free volume and g_1 an adjustable parameter. Merging these equations into equation 3.36 gives for the apparent termination rate coefficient:

$$k_t = \cfrac{1}{\cfrac{1}{k_{t,0} - k_{RD,0}} + \cfrac{1}{k_{TD,0}}\left[M_w^n \cdot \exp\left(g_1\left(\frac{1}{V_f} - \frac{1}{V_{f,0}}\right)\right) - M_{w,0}^n\right]} + k_{RD} \qquad \text{(EQ 3.41)}$$

The free volume V_f is obtained assuming additivity of the free volume of the reaction components:

$$V_f = \sum_i V_{f,i} \cdot \phi_i \text{ with } V_{f,i} = V_{f,i,0} + \alpha \cdot (T - T_{g,i}) \qquad \text{(EQ 3.42)}$$

with $V_{f,i,0} = 0.025$ and $\alpha_m = 0.001 \text{ K}^{-1}$, respectively, $\alpha_p = 0.00048 \text{ K}^{-1}$. k_{RD} is determined by the frequency of monomer addition to the radical end and, therefore, it is

$$k_{RD} = k_p \cdot [M] \qquad \text{(EQ 3.43)}$$

$k_{TD,0}$ is unknown and needs to be fitted together with the parameter g_1 to experimental data. By introducing a third adjustable parameter, g_2, also the initiator efficiency becomes conversion dependent as a function of the free volume in this model:

$$f = \cfrac{2 \cdot f_0}{1 + \exp\left(g_2\left(\frac{1}{V_f} - \frac{1}{V_{f,0}}\right)\right)} \qquad \text{(EQ 3.44)}$$

The authors determined the four adjustable parameters for their experimental data in the temperature range of 50°C - 90°C to be

$g_1 = 1.8254$

$g_2 = 3.792 \text{ x } \exp(-746/T[K])$

$k_{TD,0} = 5.101 \text{ x } 10^9 \exp(3211/T[K])$

$n = 1$

The advantage of this model is its inclusion of the molecular weight dependence. In their article, the authors also claim that the model works for polymerizations with chain transfer agents. Unfortunately, it does not use a ternary monomer-polymer-solvent system. In any case, the three parameters need to be refitted to experimental data from high-temperature polymerizations in order to be valid for this temperature range.

Considering that the molecular weight dependence is, as proposed by Weickert et al., given by $n = 1$, there are still three parameters that have to be adjusted. Assuming further more that the initiator efficiency, given by equation 3.44 together with the value for g_2, is correct, the number of parameters is reduced to two: g_1 and $k_{TD,0}$. Suitable values at T = 130°C were found to be:

$$g_1 = 32 \qquad\qquad\qquad\qquad\qquad\qquad \text{(EQ 3.45)}$$

$$k_{TD,0} = 1.15 \cdot 10^{15} \qquad\qquad\qquad\qquad\qquad\qquad \text{(EQ 3.46)}$$

However, this refitting turns out to be tricky since the gel effect for high temperatures is much less pronounced than for temperatures below 100°C. Yet, the term $\left(\frac{1}{V_f} - \frac{1}{V_{f,0}}\right)$ in equation 3.41 and equation 3.44 causes a rather steep drop of the termination rate constant for high conversions, which is demonstrated in figure 3.6. Compared to the corresponding part of the Fleury equation 3.28, which is plotted in figure 3.6 (a) against the conversion as a straight line, the change in the region $0.5 < X < 1$ is much more important. Therefore, the decrease in k_t is also much more pronounced than for the Fleury model (see figure 3.6 (b)).
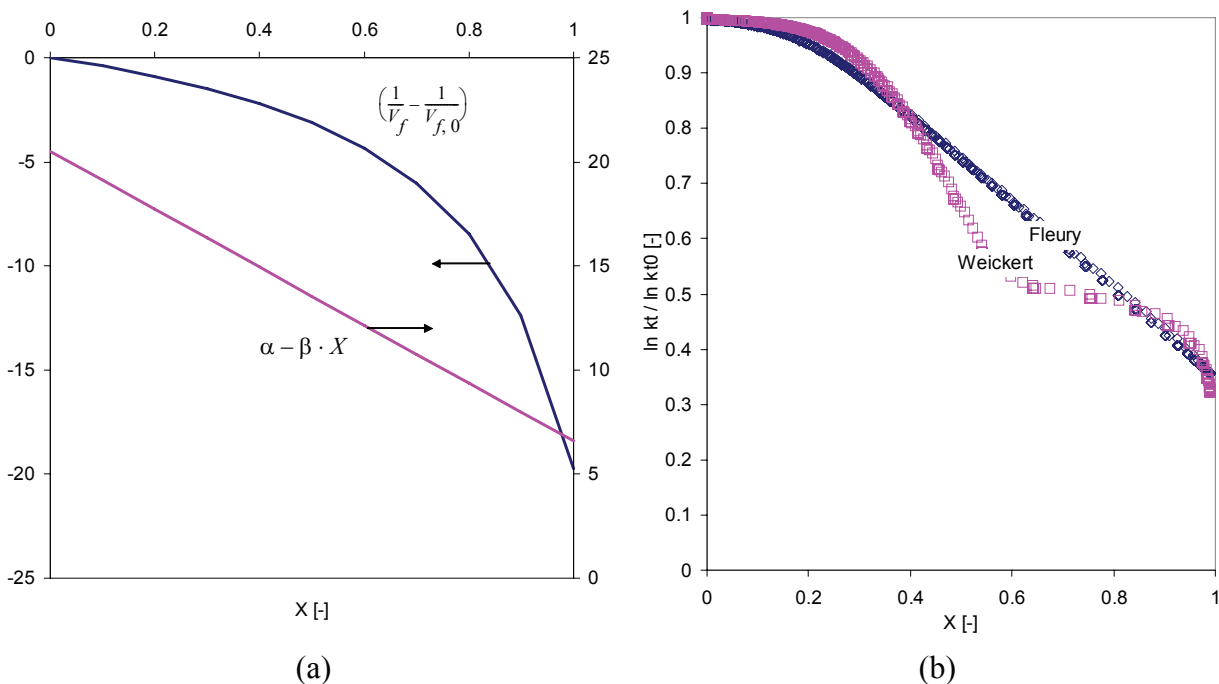
Figure 3.6: (a) Conversion dependent terms of the Weickert and the Fleury model
(b) Evolution of k_t with conversion for both models
T = 130°C, $[DTBP]_0 = 1000ppm$

The consequence for the modeling at high temperature is that it becomes extremely difficult, not to say impossible to find suitable parameters, with which the model correctly describes all different cases of reaction conditions, i.e. with or without CTA or solvent and at different temperatures. Already for one single experiment, the found values (see eqs. 3.45 and 3.46) do not lead to really satisfying results, as shown in figure 3.7 (a), where the conversion evolution is plotted for the model with the Weickert and with the newly fitted parameters. With the values from the original work, k_t already differs from $k_{t,0}$ since the very beginning of the reaction, leading to an overestimated raise of conversion. Afterwards, the gel effect, itself, is underestimated and occurs far too late. With the values determined in this work, the conversion evolution fits much better to experimental data.

Nevertheless, the steepness of the modeled conversion curve is too high compared to the measured one. This issue becomes even worse when chain transfer agent is added and the gel effect strongly attenuated. For this case, no suitable (and physically meaningful) combination of parameters could be found to correctly describe the polymerization. It appears that molecular weight dependence as well as the initiator efficiency are no longer valid either and would have to be refitted, too. The latter is represented in figure 3.7 (b) in comparison to the function used in this work (see appendix 3, "Modeling with Predici®").

Due to the poor perspectives to correctly model the high temperature gel effect (because of the shape of $\left(\frac{1}{V_f} - \frac{1}{V_{f,0}} \right)$), no more efforts were made in the further development of this model.

(a)	(b)
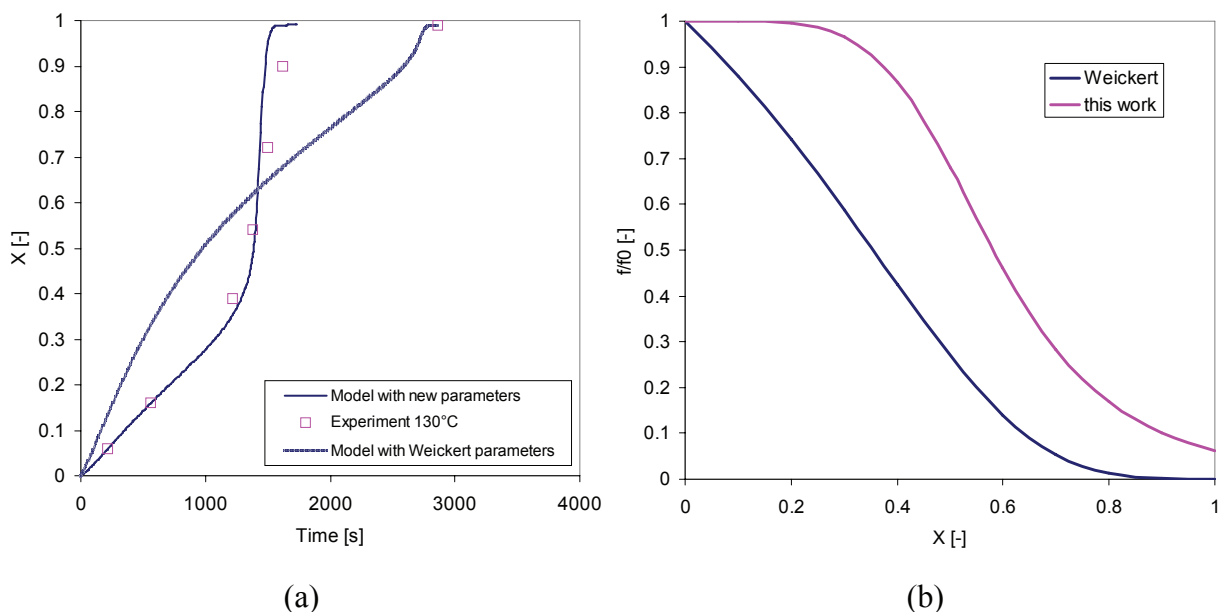
Figure 3.7: (a) Conversion evolution at T = 130°C, [DTBP]$_0$ = 1000ppm for the Weickert model with original and newly fitted parameters g$_1$ and k$_{TD,0}$
(b) Initiator efficiency as a function of conversion, Weickert model and model used in this work

3.3   A new approach for a gel effect model

All models presented so far in this chapter correctly describe the gel effect for their corresponding experimental conditions. It was even possible to refit some of them to other reaction conditions (in particular temperature). However, each of them has - somehow - a weak point, i.e. a dependency on the initiator-load, respectively a structure that is either too complicated for complex reaction systems or too simple in the sense that it does not include chain transfer or solvent effects. To put it in a nutshell: a new approach was needed to simulate the gel effect in the continuous high-temperature polymerization.

The ideal model should be built-up easily and comprise only few parameters, should correlate the gel effect to the molecular weight rather than to an initiator load and should be independent of any solvent content, i.e. of the fact that the system is binary or ternary.

The CCS model (subchapter 3.2.1) basically fulfils these demands, except for the molecular weight dependence. Hence, it was tried to modify its basic equation (see equation 3.9) in a way so that the diffusion limitation term is a function of M_w. The concept of the modification is presented in the following.

$$\frac{1}{k_t} = \frac{1}{k_{t,0}} + \frac{r_t^2 \lambda_0}{3D} \tag{EQ 3.47}$$

Combining $\frac{r_t^2}{3}$ in the function $\tau(T)$ and separating D again into a molecular-weight and a conversion-dependent part with the help of the Fujita-Doolittle equation leads to

$$\frac{1}{k_t} = \frac{1}{k_{t,0}} + \tau(T) \frac{\lambda_0}{D_0 \exp\left(\frac{2.3(1-\phi_p)}{A+B(1-\phi_p)}\right)} \tag{EQ 3.48}$$

The diffusion is inversely proportional to the molecular weight $D \sim \frac{1}{M_w^a}$. Hence, it will be introduced into equation 3.48 with a proportionality constant $\tilde{D}$.

$$\frac{1}{k_t} = \frac{1}{k_{t,0}} + \tau(T) \frac{\lambda_0 \cdot M_w^\alpha}{\tilde{D} \cdot \exp\left(\frac{2.3(1-\phi_p)}{A+B(1-\phi_p)}\right)} \tag{EQ 3.49}$$

Another consideration concerns the radical concentration λ_0, which substituted the bulk radical concentration C_b in equation 3.9 and which is mainly a function of the initiator load (see the simplified equation 3.50 for the example of a batch reaction) but, with increasing conversion, subject to an important increase due to the volume shrink:

$$\frac{d\lambda_0}{dt} = 2 \cdot f \cdot k_d \cdot [I] - k_t \cdot \lambda_0^2 - \frac{\lambda_0}{V} \cdot \frac{dV}{dt} \tag{EQ 3.50}$$

λ_0 has a strong influence on the obtained molecular weight (increasing the initiator load and, thus, the radical concentration, drastically decreases the molecular weight in an unregulated polymerization) and has, therefore, also an influence on the shape of the gel effect. Yet, since the molecular weight dependence is already accounted for in equation 3.49, the presence of λ_0 would constitute a repetition, i.e. an overestimation of the molecular weight influence and lead to a gel effect that is too steep with respect to reality. It shall be assumed in the course of this model development that λ_0 is included in the introduced term $\frac{M_w^\alpha}{\tilde{D}}$. Thus, equation 3.49 becomes:

$$\frac{1}{k_t} = \frac{1}{k_{t,0}} + \tau(T) \frac{M_w^\alpha}{\tilde{D} \cdot \exp\left(\frac{2.3(1-\phi_p)}{A+B(1-\phi_p)}\right)} \tag{EQ 3.51}$$

The parameters for A and B are taken from the CSS model (equation 3.13), whereas the parameters α, $\tilde{D}$ and $\tau(T)$ need to be refitted to experimental data in this work. For further simplification, the constant $\tilde{D}$ can be included in the temperature function $\tau(T)$, and therefore only one parameter is left for fitting.

$$A = 0.168 - 8.21 \times 10^{-6}(T - T_g)^2 \text{ and } B = 0.03 \tag{EQ 3.52}$$

Concerning the parameter α, different approaches are possible. Following the entanglement theory [68, 69], α would take the value of 3.4 above a certain critical molecular weight, whereas Panke found in his model [70] a value of 0.5 for the exponent of the molecular weight dependence. Finally, Marten and Hamielec give a value of $\alpha = 1.75$ for entangled solutions in their model of the styrene polymerization [71].

Comparison of the models with both, experimental and literature data, supported the latter assumption, since for $\alpha = 3.4$ the influence is by far too big and for $\alpha = 0.5$, respectively $\alpha = 0.7$, too small. Figure 3.8 shows a comparison between the three cases to illustrate the difference of their impact on the model.

However, the choice of the correct exponent is not unique. It is a matter of experimental conditions but also of interpretation to judge a chosen value as "best fit". Values of $1.3 < \alpha < 1.8$ lead to satisfying results and, because of the value found in literature, in the end $\alpha = 1.75$ was chosen as exponent for M_w. The difficulty in the determination of parameters of this kind is that there are always a variety of other influences on the result of the modeling. In this particular case, the chain transfer constant for the chain transfer to monomer and to chain transfer agent is the most important issue, since they directly influence the molecular weight, and thus also the gel effect, which in turn lets the molecular weight increase. There is a rather complex connection between these parameters and it is not astonishing that hardly any of them can be considered as generally valid for whatsoever model or experimental conditions.
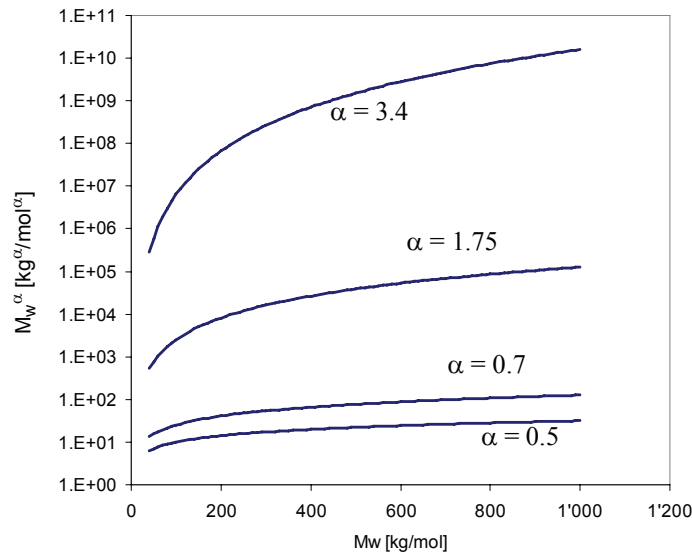
Figure 3.8: Comparison of different values for α

The fitting of α and $\tau(T)$ was done with data from literature [66] and DSC data obtained in this work. As mentioned above, the value for α was found to be α = 1.75 in accordance with the Marten-Hamielec literature value [71]. For the temperature-dependent parameter $\tau(T)$, an exponential dependence was found, which corresponds to $\theta_t(T)$ in the CSS model (see page 63). The Arrhenius diagram for the determination of $\tau(T)$ is depicted in figure 3.9, leading to the following equation:

$$\tau(T) \;=\; 7.69265 \cdot 10^{-9} \cdot e^{\dfrac{-4.0365 \cdot 10^4 [J/mol]}{RT[K]}} \quad [\text{-}] \tag{EQ 3.53}$$

It should be kept in mind that this equation is only valid for the model parameters used in this work and for the given set of kinetic constants (see appendix 3). Changing a rate constant, e.g. for the depolymerization or the chain transfer, can lead to significant changes in the values for $\tau(T)$.
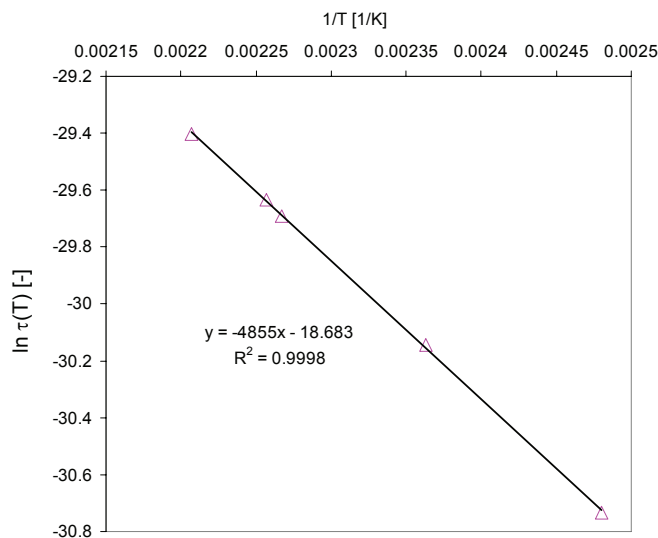
Figure 3.9: Arrhenius diagram for the calculation of the parameter $\tau(T)$ *in the gel effect model*

The results of the modeling with this equation for the gel effect are presented in the following. Figure 3.10 (a) and (b) shows the modeled and experimental conversion evolution for two cases: (a) for polymerizations at different temperatures without chain transfer agent, carried out as batch polymerizations in the DSC, and (b) for polymerizations with different chain transfer agent loads at constant temperature, carried out by Fenouillot et al. [66] as batch polymerizations in a dilatometric reactor setup. Note that for the second series of reactions, the initiator load is one order of magnitude smaller than for the DSC runs, leading to much longer reaction times.

For the DSC experiment without chain transfer agent, the model is in very good agreement with experimental data as regards conversion evolution (figure 3.10 (a)) and heat flow (figure 3.11 (a)), except that for T = 130 °C, the onset of the gel effect is a little too early. The source of this difference is the overestimation of the molecular weight in the beginning of the reaction, visible in figure 3.12 (a) + (b). The model predicts here a much higher molecular weight than measured, leading at the same time to an earlier onset of the gel effect. The reason for the overestimation of the molecular weight by the model might be that under experimental conditions inhibition reactions caused by impurities keep the molecular weight in the beginning of the reaction rather low, which the model does not account for. The difference in the beginning and the end of the heat flow curve has already been discussed earlier (see page 69).

For the variation of the chain transfer agent, which equals a variation of the molecular weight for the same conversion, the agreement between model and experiment for both, conversion and molecular weight, is rather good, too. Only for very small and very high CTA loads the modeled conversion evolution differs from the experimental points and seems to overestimate the influence on the gel effect (too low for small molecular weights, too big for high molecular weights). Yet, the question is how high the reliability of the experimental data taken from literature is. Unfortunately, it was not possible to use own experimental data obtained with chain transfer agent due to a problem with the molecular weight evolution for the DSC experiments. As will be explained later ("Influence of the chain transfer agent on the gel effect" on page 86), the molecular weight did not decrease as expected with increasing chain transfer agent concentration, which is explained by its consumption early during the reaction by another, not further explainable process. The model verification had, therefore, to be done by means of experimental data taken from literature.

With regards to this data, especially the similarity of the conversion points in the beginning of all experiments (up to 45% conversion) as well as for the two curves on the right hand side of the graph ([CTA] = 4400 ppm and [CTA] = 8500 ppm) is not comprehensible considering the large difference in CTA load. At the same time, considering a measured molecular weight of M_n = 260'000 g/mol (M_w = 642'000 g/mol, according to the polydispersity given in the article), a stronger gel effect than the one observed by the Fenouillot et al. should be expected for the curve with [CTA] = 214 ppm.

(a) (b)
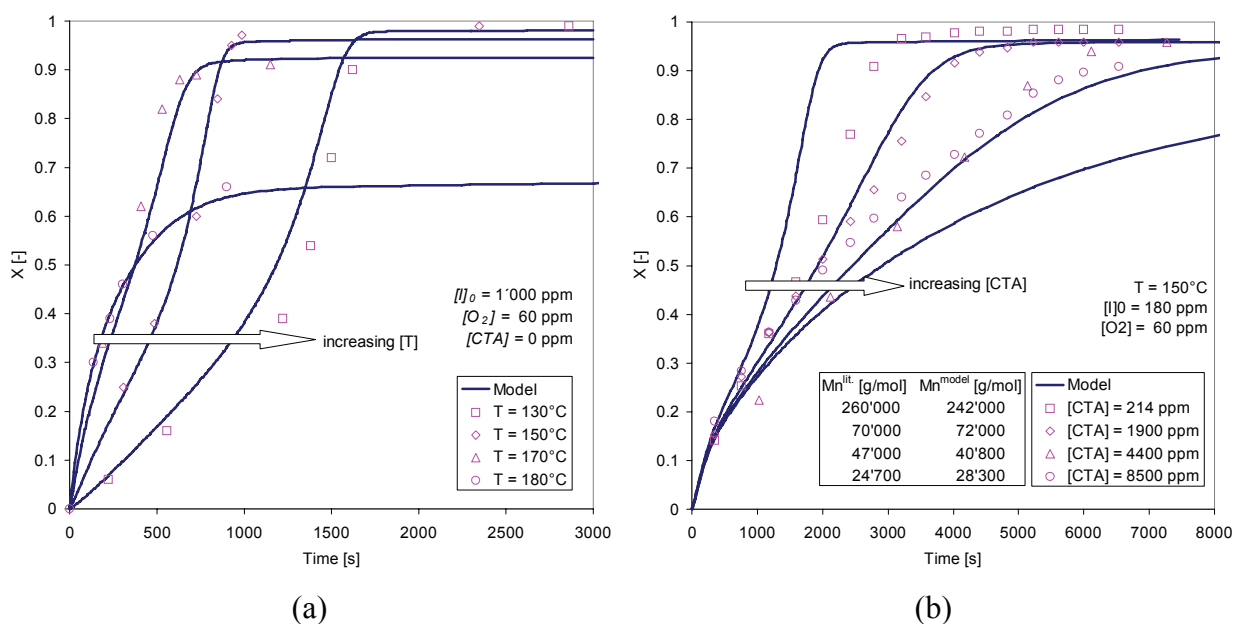
Figure 3.10: Description of the gel effect by the newly derived model for
(a) different temperatures (experimental data taken from DSC experiments)
(b) different initial chain transfer agent loads (experimental data taken from [66])

(a) (b)
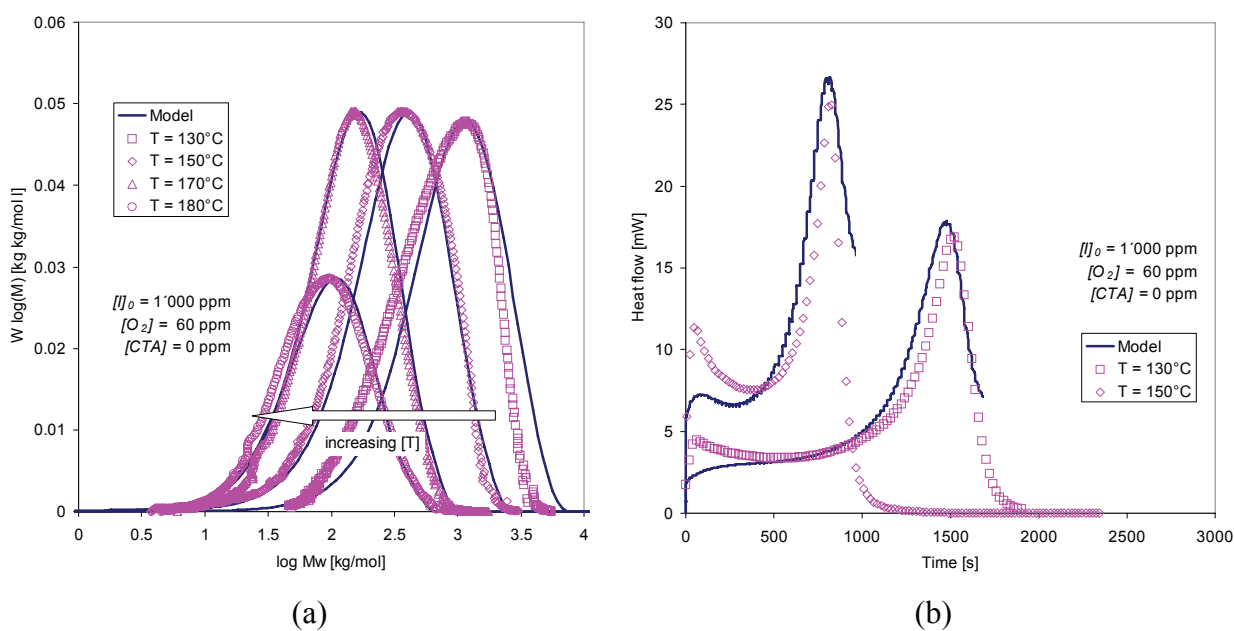
Figure 3.11: Modeling results for DSC batch polymerizations
(a) molecular weight distributions at different temperatures (without CTA)
(b) heat flow curves at different temperatures
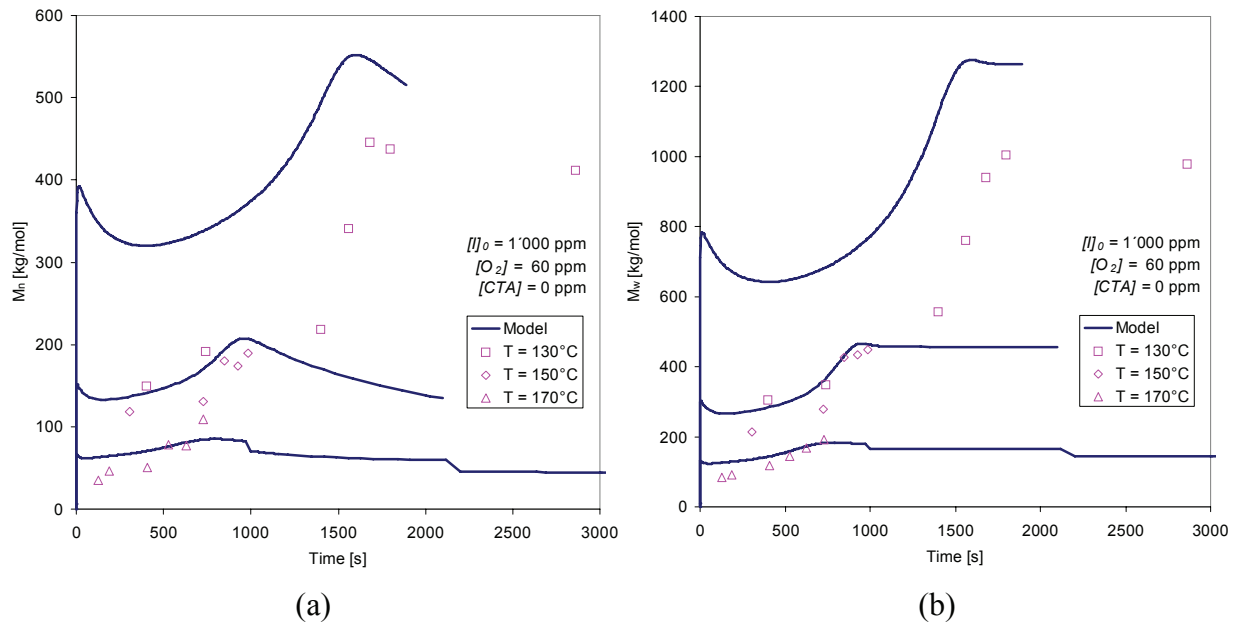
Figure 3.12: Molecular weight evolution for the DSC polymerizations at different temperature
(a) Number-average molecular weight
(b) Weight-average molecular weight

To conclude with the evaluation of this model, figure 3.13 shows the influence of conversion on the normalized termination rate constant. In comparison with the same graph for the Fleury model (figure 3.3 (f)), it should be remarked that the curves are not straight lines but becoming steeper with increasing conversion. This is due to the increasing molecular weight of the polymer, which intensifies the gel effect.

Altogether, the model that has been derived in this chapter, proved to satisfyingly describe the high temperature gel effect under various conditions. It relies, furthermore, only on the molecular weight of the polymer and does not need any initial concentration of CTA or initiator. In chapter 4, its suitability for the modeling of the continuous copolymerization will be tested and the results will be discussed with special regard to the influence of the gel effect on the reactor stability.
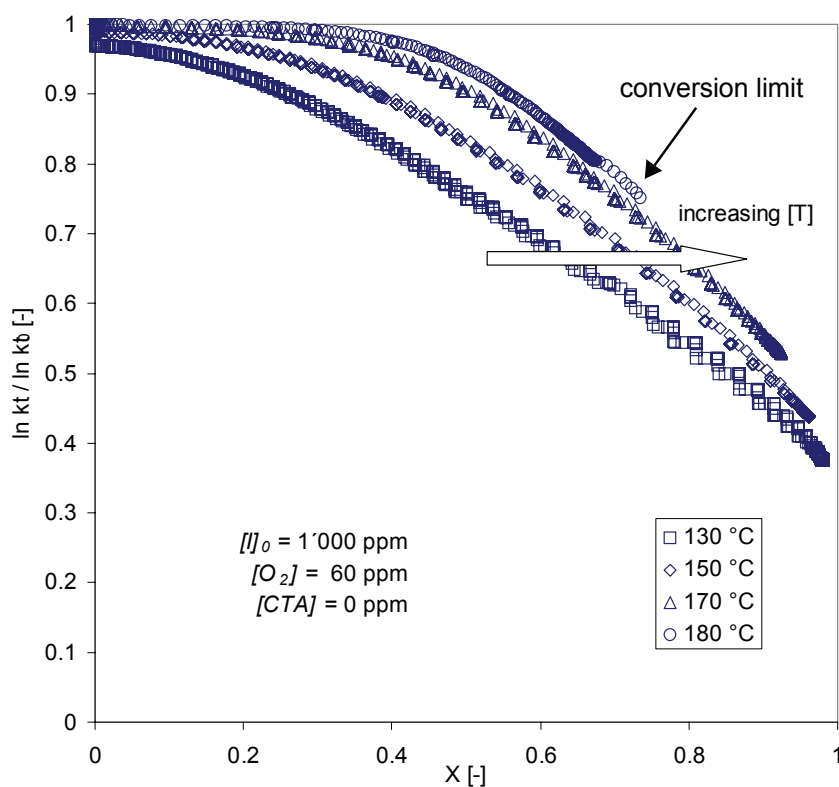
Figure 3.13: Logarithmic graph of the normalized termination rate constant over the whole range of conversion for the newly derived gel effect model

3.4   Influence of various parameters on the gel effect

In the following paragraphs, different influences on the shape and the intensity of the gel effect will be discussed, i.e. chain transfer agent, comonomer, temperature and solvent. The batch polymerizations in this subchapter have all been carried out by DSC.

3.4.1   Influence of the chain transfer agent on the gel effect

As already seen before, the gel effect is strongly attenuated in presence of chain transfer agents. This is due to the reduction of the molecular weight and, thus, of the viscosity of the reaction mixture. The following graphs (figure 3.14 (a) and (b)) show the heat flow curves of DSC polymerization at T = 140 °C for different initial CTA loads compared to model data. It can be seen that the modeled gel effect is attenuated stronger than the measured one. This becomes comprehensible when the molecular weight is compared for both cases. In figure 3.14 (b) are shown

the measured and expected M_w for each CTA concentration (assuming a transfer constant of $C_{CTA} = 0.68$ in the model). The molecular weight drops much less than predicted by the model, which indicates that either the chain transfer constant is wrong or that the CTA is less effective in the DSC experiment.

Figure 3.14: Attenuation of the gel effect with increasing CTA load and influence on the molecular weight (comparison model and DSC experiment carried out in bulk with $[DTBP]_0 = 1000 ppm$ at $T = 140 °C$)

It could be imagined that, due to the large surface to volume ratio in the DSC crucibles or to the lack of mixing, the chain transfer agent is not as efficient as one would expect in a larger scale bulk polymerization. But even a less important transfer constant C_{CTA} is not an explanation why the molecular weight would stagnate above $M_w = 300'000$ g/mol even with further increasing CTA concentration, which is in contradiction to the Mayo-equation:

$$\frac{1}{DP_n} = \frac{1}{DP_{n,0}} + C_{CTA} \cdot \frac{[CTA]}{[M]}$$

(EQ 3.54)

Therefore, the only plausible explanation for the measured molecular weight evolution is a side-reaction of the chain transfer agent. In fact, there is an effect that is clearly visible from the heat flow signal in figure 3.14 (a). Increasing with the chain transfer agent concentration, there is a heat flow peak in the beginning of the spectrum, which could indicate a consumption of CTA.

This could explain the high molecular weight, since the effective CTA concentration would be much lower than initially adjusted. The nature of this side-reaction is unknown but, in general, thioles can be easily oxidized, which - in this case - would be possible by the initiator or by oxygen from air.

3.4.2   Influence of temperature on the gel effect

Also the temperature has a rather strong effect on the gel effect, as seen already in the precedent subchapter. Up to approximately 150 °C, the gel effect intensifies as the reaction rate increases. Above 150 °C, the amplitude of the gel effect diminishes and both, depolymerization and low viscosity, reduce the acceleration of the reaction until it is hardly present, which is the case above 180 °C. In figure 3.15 (a) + (b) is presented this influence of the reaction temperature on gel effect and molecular weight for DSC batch polymerizations with $[DTBP]_0 = 1000$ ppm, compared to the model predictions for each case. For $T = 170$ °C, the model underestimates the heat flow curve a little and the precision is not as high as for the other cases. However, for the same experimental conditions, the conversion evolution, presented in figure 3.10 (a), is in perfect agreement with the model. It might, therefore, be that the measured heat flow curve for $T = 170$ °C presented in figure 3.15 (a) varies to a small extent from the other experiments carried out at this temperature.
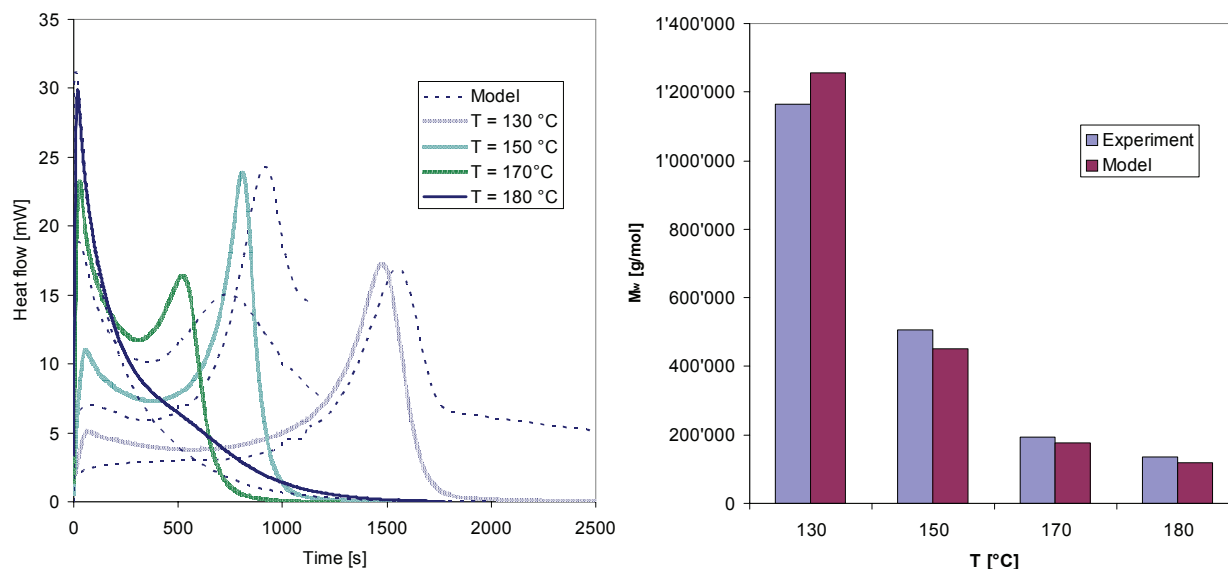
Figure 3.15: Changing of the gel effect with increasing reaction temperature and influence on the molecular weight (comparison model and DSC experiment carried out in bulk with $[DTBP]_0 = 1000$ ppm at $T = 140 °C$)

3.4.3   Influence of solvent on the gel effect

Since the gel effect is a viscosity related phenomenon, naturally also the presence of solvent has an important influence on its shape. Adding for example 30% solvent means reducing the polymer content w_p by 30%, too. As shown in figure 4.8 in chapter 4, a reduction of the polymer content of 30% reduces the viscosity of the solution by several orders of magnitude (for $T = 120°C$ and $Mw = 100'000$ g/mol the viscosity decreases by approximately a factor 10^4!). This is reflected also by the results from DSC experiments and the modeling. Figure 3.16 (a) + (b) contains the measured and simulated curves for three different solvent contents (0%, 20% and 30% of n-butyl acetate) as well as the molecular weights for each experiment. It is apparent that for 30% solvent, the gel effect is hardly remarkable anymore. The modeled molecular weight matches the GPC values very well, too. This is a confirmation that the transfer constant for the solvent, which had been assumed to be $C_S = 0.0001$, is more or less correct.
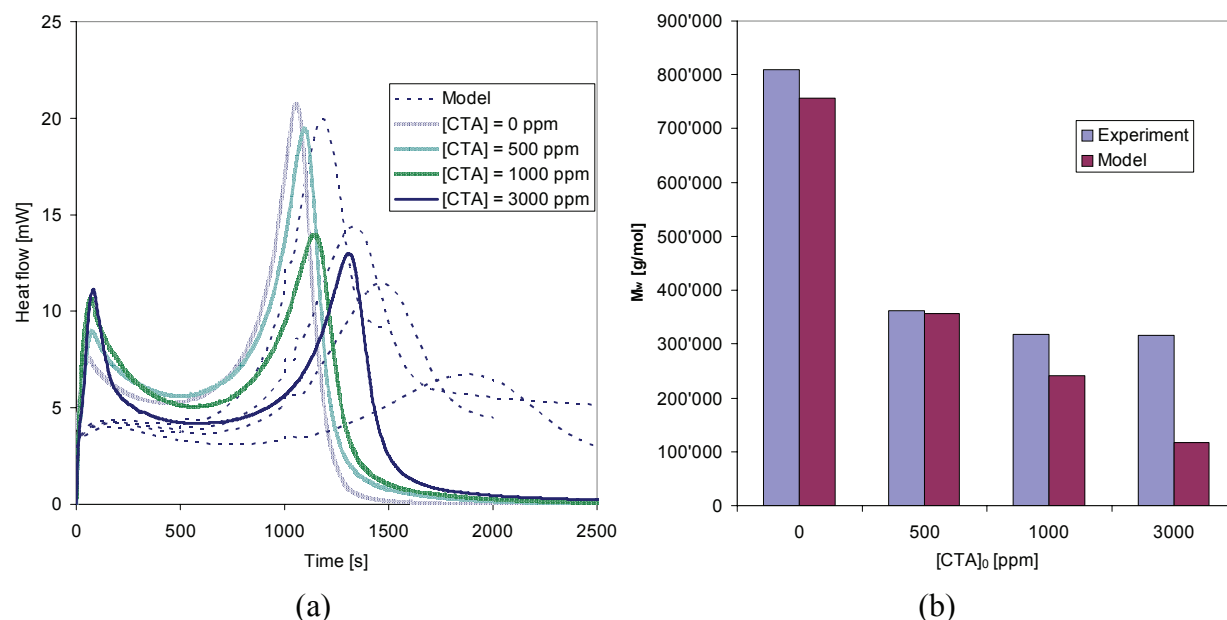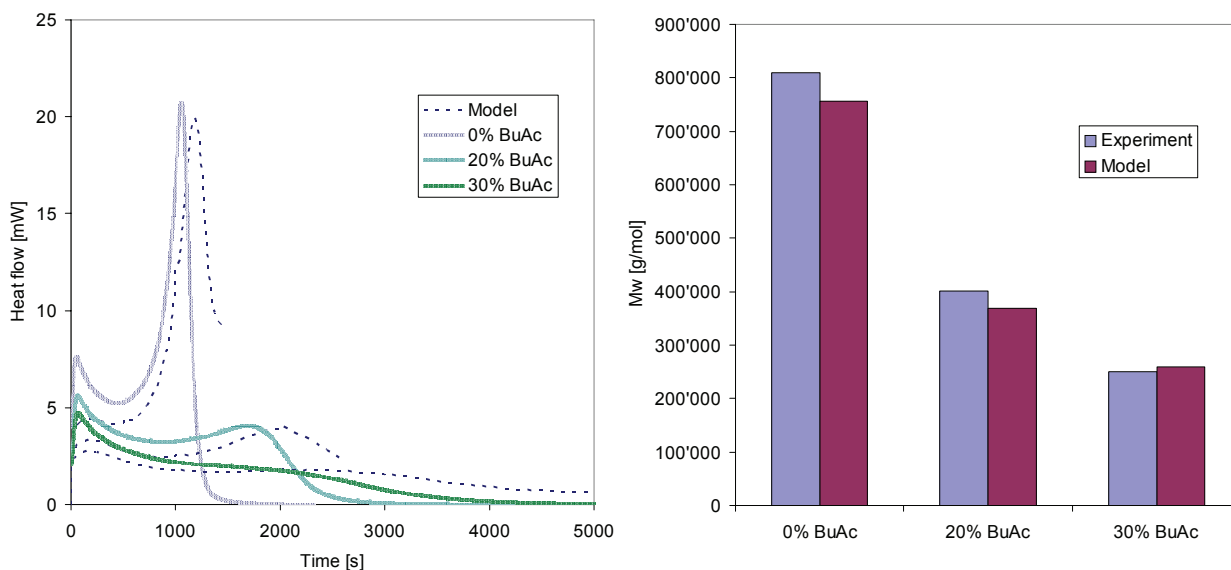
Figure 3.16: Attenuation of the gel effect with increasing solvent fraction and influence on the molecular weight (comparison model and DSC experiment carried out with [DTBP]$_0$ = 1000 ppm at T = 140 °C)

3.4.4   Influence of the comonomer

Although not having any direct influence on the viscosity of the reaction mixture like a solvent, also the presence of a comonomer can significantly alter the gel effect. This is the case when the reactivity ratios of the copolymerized monomers are rather different. For the system methyl methacrylate / methyl acrylate, which is investigated in this work, these values differ considerably as can be seen from table 1. A value of $r_1 > 1$ respectively $r_2 < 1$ means that the comonomer MA is incorporated slower into the growing polymer chain than the monomer MMA. For the overall polymerization rate this has the effect of slowing it down, therefore the gel effect is attenuated and much lower molecular weights are obtained (considering that with increasing comonomer concentration, the concentration of the monomer, itself, diminishes). The r-parameters also define how the polymer composition looks like and to which amount the different monomers are consumed instantaneously. The **Lewis-Mayo equation** (equation 3.55) gives access to the instantaneous, relative change of monomer concentrations and, thus, to the instantaneous polymer composition. It is valid only for small conversion ranges, otherwise it has to be integrated. More detailed explanations concerning the copolymerization are provided in chapter 4, "R-parameters" on page 138.

$$\frac{d[MMA]}{d[MA]} = \frac{1 + r_1 \cdot [MMA]/[MA]}{1 + r_2 \cdot [MA]/[MMA]}$$

(EQ 3.55)

Table 1: Reactivity ratios for the copolymerization system MMA/MA taken from literature

	Lit. values [72] (at T = 80 °C)
$r_1 = \dfrac{k_{p,1}}{k_{p,12}}$	2.36 ± 0.32
$r_2 = \dfrac{k_{p,2}}{k_{p,21}}$	0.42 ± 0.08

The attenuation of the gel effect with increasing comonomer fraction is demonstrated in figure 3.17 (a). The model correctly describes this weakening of the reaction acceleration compared to the homopolymerization of MMA. Yet, the measured curve for 15% MA differs from the modeled one as regards the peak position of the gel effect. This effect has already been observed for the chain transfer agent earlier in this chapter. And as for the chain transfer agent, also for the comonomer the beginning of the heat flow curve changes with increasing MA concentration. So there might be a secondary reaction during the start of the polymerization that influences the reaction path in the observed manner from the expected one. On the other hand, also the r-parameters might not be precise enough for this temperature range, since they were taken from literature for T = 80°C. They will, therefore, be re-evaluated later in this work. Nevertheless, the predicted molecular weights are in good agreement, as proven in figure 3.17 (b).

(a)   (b)
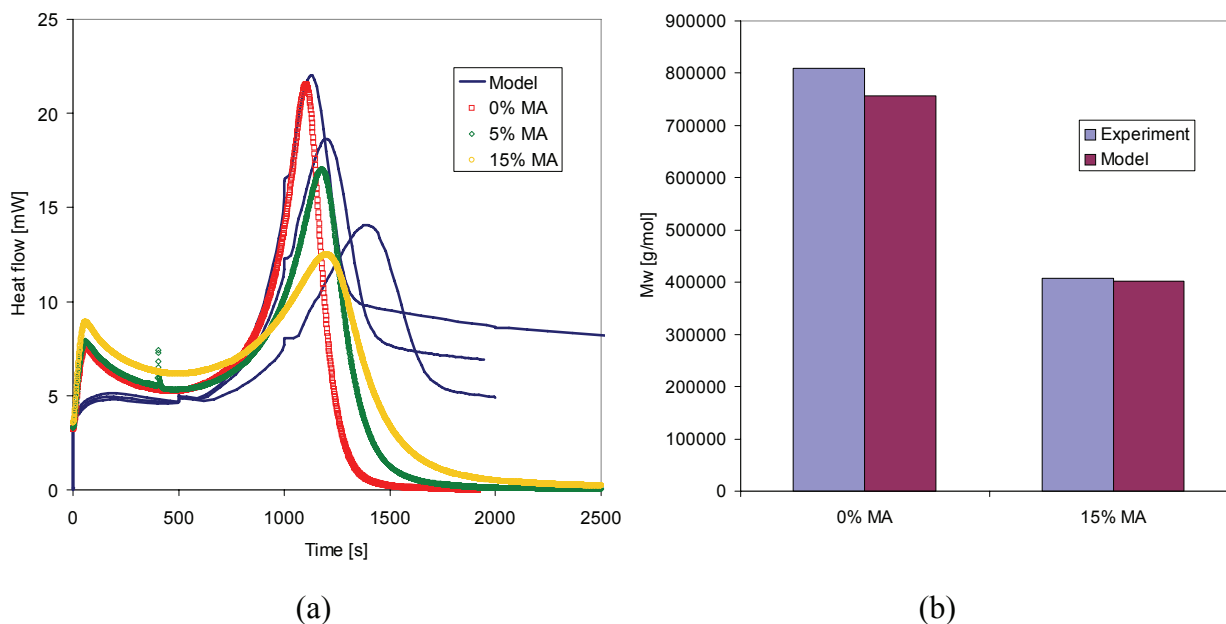
Figure 3.17: Influence of the comonomer on (a) the shape of the gel effect and (b) the molecular weight for DSC experiments (T = 140 °C, [DTBP]$_0$ = 1000 ppm)

3.5   Discussion

The present chapter discusses the problematic of the gel effect modeling at high temperature. Probably the most important conclusion to be drawn from the comparison of the different models available in literature is that there is no generally valid model. Each of the presented models describes sufficiently well the gel effect under the investigated conditions of each study. However, as soon as one leaves the "boundaries of validity", which are usually located not too far away from the conditions the authors of each study fitted their model to, the results differ in most cases unacceptably from reality. This is in particular the case for temperature. Most models available in literature describe a gel effect for below-T_g polymerizations, where it is much more pronounced than above T_g. The few that have been adapted to or developed for high temperature polymerizations, as the Hoppe & Renken, the Fleury or the Rimlinger one, are all ruled out as soon as it comes to continuous, *CTA*-regulated polymerizations as it has been demonstrated beforehand.

The newly developed gel effect model of the present work is surely not entitled to solve all of these problems. As much as the other models, it definitely has its boundaries of validity. Yet,

92

the innovation of this high-temperature model is that, based on the classic diffusion approach, it directly correlates the gel effect with molecular weight and polymer volume fraction, both deciding factors for solution viscosity. Thus, it takes into account the influence of chain transfer agent and changing initiator concentration without needing their concentrations. It does not matter, either, if the polymerization takes place in batch or in a continuous process.

At the same time, the rather simple model structure with few fitting parameters and practically no required material-related data, allows the comfortable adaptation of the model to different reaction conditions, if necessary. The two parameters fitted in this work, α and $\tau(T)$, might also leave room for some further optimization. They were determined with the help of DSC batch polymerizations, which surely exhibit some process-related limitations (no mixing, high surface-to-volume ratio, difficult sampling for GC and GPC etc.). The comparison to literature data, in this case the data of Rimlinger et al., illustrated the fact that the results of this fit should be carefully evaluated.

This will be done in the context of the pilot plant experiments, where the gel effect model derived in this chapter will be validated with the help of data from the continuous process. The results obtained for the batch polymerization and copolymerization of MMA are, however, very satisfactory. Apart from some minor inaccuracies, the model correctly predicts the influence of temperature, solvent, chain transfer agent and comonomer on monomer conversion and molecular weight. This flexibility is, to the knowledge of the author, not featured by any other gel effect model so far published in literature.

Short Summary:

- Different existing gel effect models for MMA have been examined towards their applicability to high temperature polymerizations
- By modifying a suitable existing gel effect model, a new one could be derived, which allows the correct description of the high temperature gel effect in batch and continuous polymerizations of MMA
- This new model was tested concerning the correct prediction of the gel effect under various conditions and validated by experimental data from this work and from literature.

Continuous High-Temperature Polymerization

Chapter 2 and chapter 3 dealt with some characteristic kinetic aspects of the high-temperature polymerization of MMA. More precisely, the thermal initiation reactions, caused among other by MMA peroxides, as well as the high-temperature gel effect were investigated by means of batch experiments. These points are extremely important, since they influence significantly the thermal behavior of the reaction.

The following chapter will now combine the results of the preceding ones with the concept of continuous polymerization at pilot-scale. For industrial considerations these pilot trials are inevitable for the evaluation of a high-temperature process as to its feasibility and final product qualities. It is important to conduct these experiments under conditions as similar as possible to those of a "real" production process to allow a direct comparison. The problem with most scientific research is that it is done under conditions that are far from the "production reality" and routines, for example the use of highly purified material, while in industrial-scale reactions rather technical grades are present, or of miniaturized reactors without mixing and heat transfer issues as they are present in large-scale industrial reactors. This part of the present work was, therefore, carried out using commercial grade raw materials as provided by the producers (see appendix 6), and a reactor setup similar to that of an industrial reactor.

In industry, a widely used setup for bulk polymerization processes is the combination of CSTR and plug flow tubular reactor (see figure 4.1). In the CSTR, the polymerization is usually conducted to medium polymer fractions below 50% (for high temperatures sometimes up

to 70% [73]), with or without solvent. At polymer fractions, respectively conversions, the viscosity would get too high for sufficient mixing and heat transfer out of the reactor and the discharge of the product from the vessel becomes impossible. The reaction is taken to higher conversions in a consecutive plug flow reactor, where conversions of 80 - 90% can be handled safely, depending on the design of the tube.
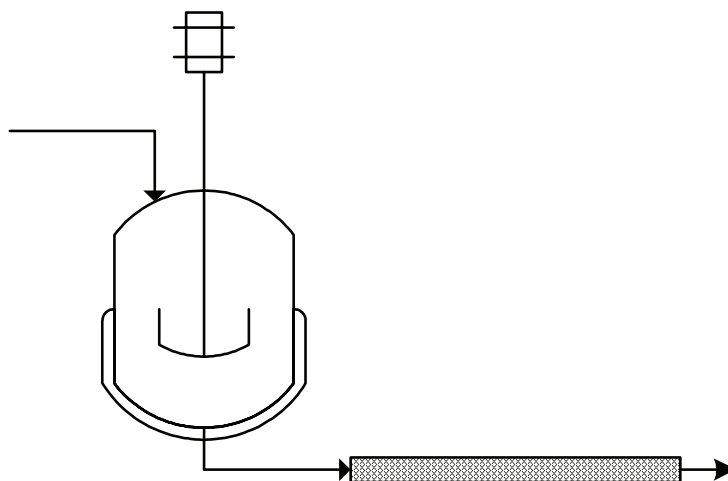
Figure 4.1: Commonly used setup for industrial bulk polymerization processes

The polymerization of MMA is a very fast and exothermal reaction ($-\Delta_r H = 56$ kJ/mol), which comes along with a strong increase in viscosity that can easily be of several orders of magnitude (10^{-3} to 200 Pa·s). The reaction kinetics is therefore strongly influenced by a gel effect, which means that, depending on the residence time and above a critical conversion, a reaction runaway by auto acceleration occurs. For the stability of a continuous process, these aspects have the following consequences:

- the process must be kinetically stable, i.e. with enough distance to runaway conditions, in order to obtain desired conversions / molecular weights
- the viscosity must not exceed a critical value in order to avoid a too high pressure drop over the length of the reactor and possible plugging
- mixing and heat removal capacity must be sufficient to avoid thermal runaway of the reaction and local hot spots in the reactor

As to the danger of a thermal runaway, an advantage of the MMA polymerization is that it exhibits a rather strong depolymerization at high temperatures. With a ceiling temperature of $T_c = 220°C$ [11], above which no propagation takes place anymore, a possible runaway of the reaction, at least in terms of the polymerization heat, would come automatically to halt. Nevertheless, a sufficient heat removal capacity is indispensible for safe control of the reaction conditions. Finally, the presence of local hot spots can lead to thermal degradation of the polymer and to a widening of the molecular weight distribution, both leading to a reduced product quality.

The runaway of the medium viscosity is a rather delicate matter concerning the reactor stability, as already small changes in reaction conditions (T, τ) may have drastic effects. These changes might be due to technical problems, i.e. failure of the feed pump or feed flow variations, temperature drop of the heating circuit, or may be caused by long-term phenomena as, for example, the obstruction of heat removal due to the formation of polymer residues on the reactor walls. An unforeseen increase in viscosity usually has severe consequences for the process: the reactor pressure increases until either sealings break or the reactor plugs completely, and the heat removal becomes more difficult leading to an increase in temperature and a consecutive reaction acceleration. It must, therefore, be taken care of the right choice of residence time with eventual security margins in case of feed flow variations.

One of the goals of the present work is to design a pilot plant for the continuous production of PMMA molding compound that takes into account the above-mentioned issues. The reactor concept chosen to achieve this goal is a combination of a tubular, high-recycle-ratio loop, replacing the common CSTR, followed by a plug flow tube reactor. These concepts have already been successfully applied in other research projects at EPFL (Recycle loop: [1, 5, 74], combination loop / tube: [6, 75]). The operating conditions are predetermined by constraints from the industrial partner of this project.

4.1   The Sulzer Pilot Plant

4.1.1   Viscous tubular flows

Since the environment of polymerization reactions is usually rather viscous, the flow profile in a tubular reactor exhibits laminar behavior. This means that the flow rate in the middle of the tube is high, whereas in close proximity to the reactor wall the flow stagnates. The consequence is

that the residence time at outer diametric zones are much higher than in the inner tube, for bulk polymerizations first leading to highly viscous films and finally to solid, high molecular weight polymer deposits on the tube wall. This effect is even enhanced when the heat transfer is limited by the viscosity of the medium and the temperature drops at the outer tube zones (let's recall that the reaction is highly exothermal and heat needs to be removed from the reactor). A heated tube wall can, therefore, increase significantly the heat transfer and lead to a more uniform flow profile. In figure 4.2 are shown schematically the flow profiles for laminar flows in an empty tube. It is easily understandable that an empty tube, even with wall heating, is not the ideal configuration for a polymerization reactor.
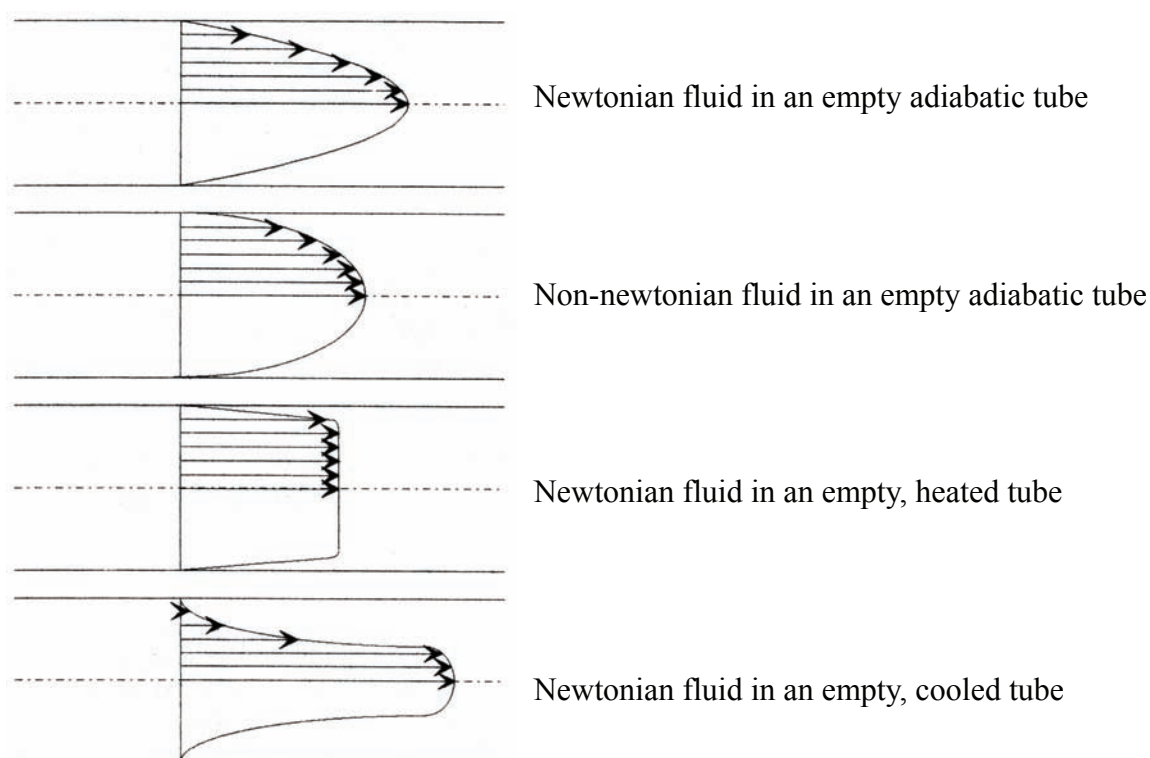
Figure 4.2: Different laminar flow profiles in an empty tube depending on fluid-type and conditions at the tube walls [5]

4.1.2   The concept of static mixing

The concept of static mixing elements - in contrast to active mixing in an extruder - is the use of the mechanical energy of the flow to ensure intense radial mixing and to achieve a homogenous flowrate and temperature profile over the entire tubes' section. Additionally, metallic static

mixers can help distribute the produced reaction enthalpy by heat conduction within the medium or to the reactor walls. The mixing principle is the division of the laminar flow into several dynamic layers and to recombine them in the following by choice of a suitable mixer geometry. As a result, the flowrate and temperature profile can be compared to the one of an ideal plug flow, as shown in figure 4.3. The radial flow velocity and concentration profile can, thus, be neglected (for the bulk polymerization of polystyrene this was already demonstrated by Tien [76]).
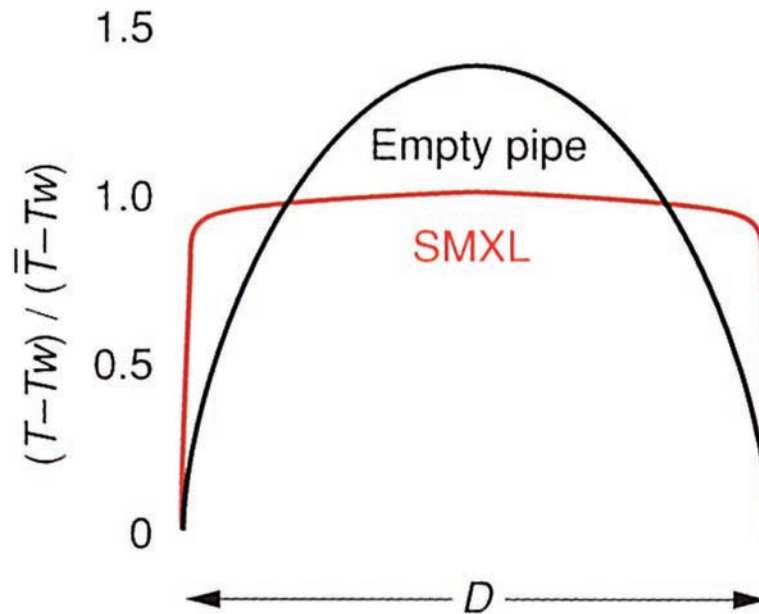
Figure 4.3: Normalized temperature profile for an empty and an SMXL-equipped tube over the tube diameter D (T medium temperature, T_w wall temperature) [77]

The axial dispersion, on the other side, is characterized by the dimensionless Bodenstein number $Bo = \frac{u \cdot L}{D_{ax}}$, which correlates the axial stuff transport by convection with the transport by (molecular) diffusion respectively (hydrodynamic) dispersion. For the ideal plug flow, it diverges to infinity (no dispersion, $D_{ax} \rightarrow 0$), whereas it tends zero for an ideally mixed CSTR (very high back mixing, $D_{ax} \rightarrow \infty$) - compare to figure 4.4.

Juvet [78] and Zeilmann [6] determined the axial dispersion coefficient for Sulzer SMXL mixing elements to be $D_{ax} = 6 \cdot 10^{-4}$ $[m^2\ s^{-1}]$. Considering a high recycle ratio (40:1) in the loop reactor and a throughput of 2 kg/h of a 50% polymer solution at T = 140°C ($\rho = 0.95 kg l^{-1}$) in a DN20 SMXL tube, the Bodenstein number per meter of reactor can be calculated to be $\frac{Bo}{L} = 134 m^{-1}$, which - according to the relation $N \cong \frac{Bo}{2}$ for small dispersion coefficients [5] - corre-

sponds to a cascade of 67 CSTR's per meter SMXL tube. This illustrates that the axial dispersion can be neglected as well for the recycle loop.
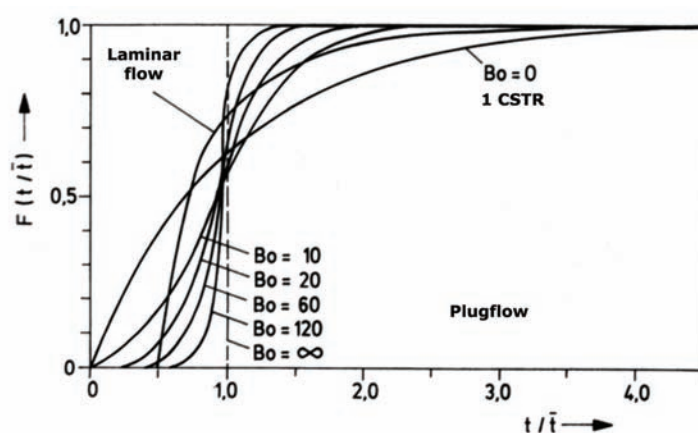
Figure 4.4: Normalized residence time distribution at different Bodenstein numbers [77]

4.1.3   Choice of mixing elements

Sulzer offers three different types of static mixers, depending on the geometry of the reactor:

The SMX and SMXL type are employed for tube diameters up to 10 cm. The L in SMXL stands for "large", which means that the geometry is more open than the one of the SMX (see figure 4.5). It is characterized by a higher porosity (less volume taken by the mixing elements) and lower shear of the product. On the other hand, the SMX mixer exhibits better mixing (higher Bodenstein number).

For larger tubes, the specific surface for the heat exchange, which decreases by the factor $\frac{4}{d_t}$ with the contact diameter of the heat exchanger, becomes too small to cope with the strong heat dissipation of exothermal reactions and local hot spots can occur [79]. Therefore, the SMR mixer type was designed with "active" mixing elements, i.e. contrary to the other two types where the mixing elements are metal shapes welded to the tube wall and therefore only heat conductors, the mixing elements of the SMR type are hollow and actively heated / cooled by flowing heat transfer medium. Thus, they exhibit a quasi constant volume specific heat exchange surface. Table 1 contains the main design parameters for the three different mixer types. The data was taken from a Sulzer sales brochure for given tube diameters [80].
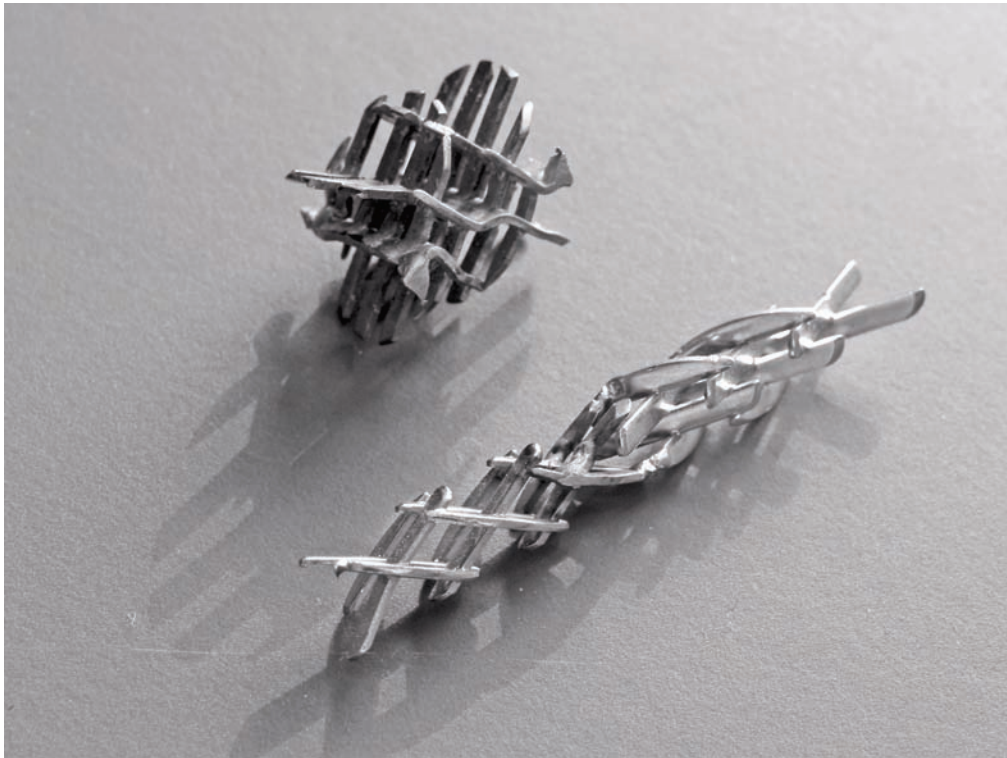
Figure 4.5: Picture of SMX (left, DN 20) and SMXL (right, DN 10) mixing elements

Table 1: Different static mixing element types offered by Sulzer Chemtech (CH) with the most important design parameters [80]

Parameter	Unit	SMXL DN20	SMX DN40	SMR87
contact diameter d_t	[mm]	20	40	8
specific heat exchange surface	[m^{-1}]	200	100	104.17
$\lambda_{\text{stainless steel}}$	[W m^{-1} K^{-1}]	16	16	16
porosity ε	[-]	0.91	0.88	0.792
hydrodynamic diameter d_h	[mm]	8.96	12.32	21.07
shear constant K_γ	[-]	27.79	54.5	5
NeRe	[-]	354	1310.5	10

The advantage of the different mixing elements is that their heat transfer coefficient compare to each other, which is an important factor in the scale-up of polymerization processes. A pilot-scale reactor can, therefore, directly be scaled-up to production-scale since the heat transfer is more or less the same. This is illustrated in figure 4.6, where the pilot-scale SMXL tube is compared to an industrial-scale SMR reactor.
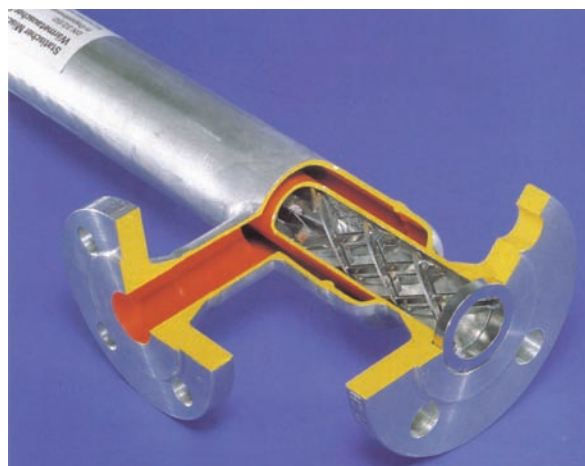
Pilot: SMXL DN 20

$U = 220$ W m^{-2} K^{-1}

$A = 130$ m^2 m^{-3}

Volume specific heat transfer coefficient:

$K = 28$ kW m^{-3} K^{-1}
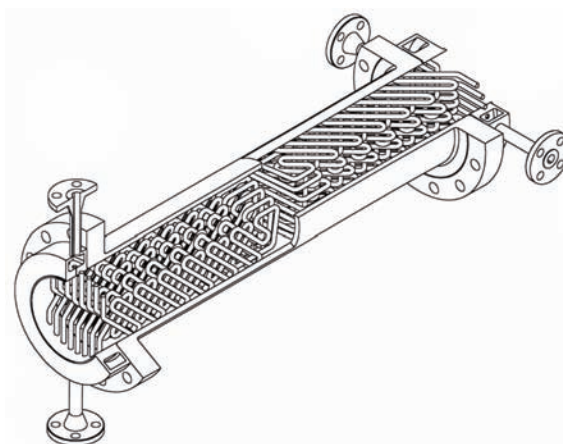
Industrial: SMR DN 100-1500

$U = 310$ W m^{-2} K^{-1}

$A = 85$ m^2 m^{-3}

$K = 26$ kW m^{-3} K^{-1}

Comparison CSTR: $A = 1\text{-}4$ m^2 m^{-3}

Figure 4.6: Comparison of SMXL and SMR mixer type as regards the scale-up of the process

The relatively constant heat exchange coefficient of the SMR type is once again illustrated in figure 4.7, where it is compared to other types of reactors used for the production of polymers. For high reactor volumes, the heat transfer coefficient drastically drops for the empty tube and the CSTR. As discussed above, also the conventional static mixers reach quite soon a certain limit due to the fact that they only conduct the heat to the reactor wall.
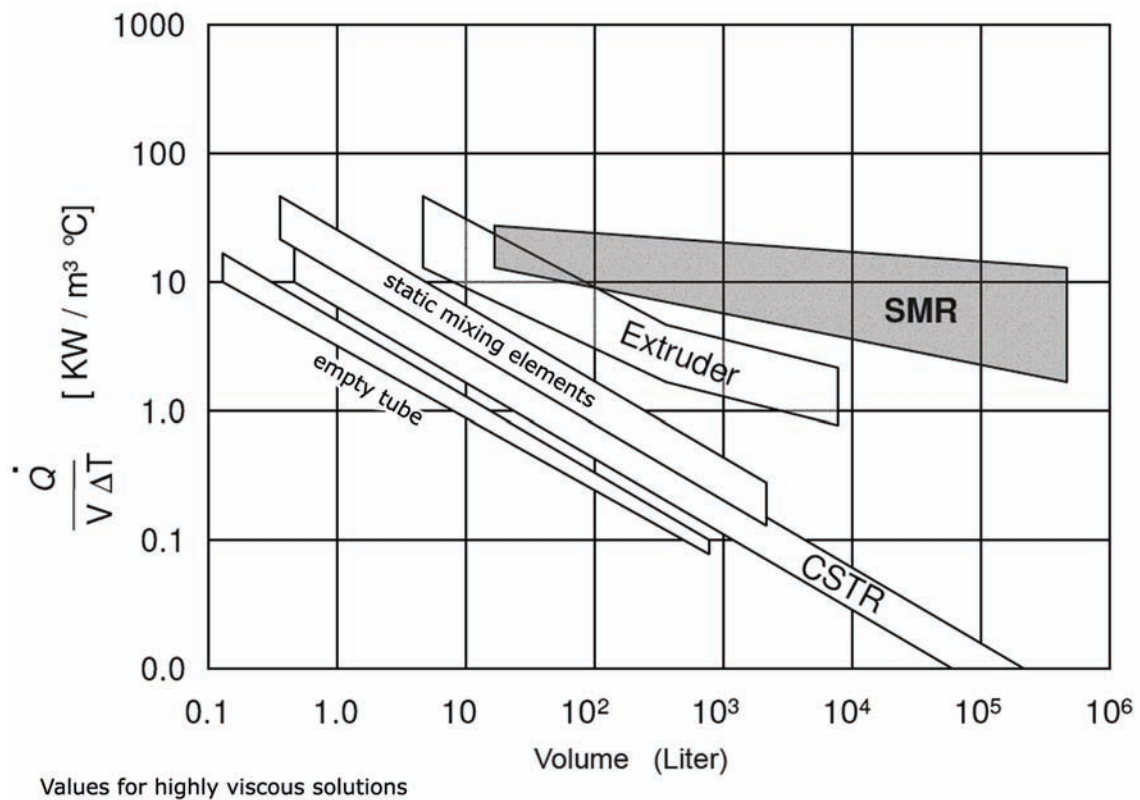
Figure 4.7: Comparison of the volume specific heat transfer coefficient for different reactor types [77]

4.1.4 Considerations concerning the viscosity

One crucial point in bulk polymerization reactions is the viscosity, as it influences kinetics, heat transfer and pressure drop in the reactor. The calculation or prediction of viscosities for polymeric systems is far from trivial. Mostly empirical equations based on measured data are used to estimate polymer viscosities. One model describing the dynamic viscosity of polymers is the one of Stuber [81, 82]:

According to the theory of Stuber, the dynamic viscosity is a function of the "zero-shear" viscosity and the shear rate itself:

$$\frac{\eta}{\eta_0} = \frac{1}{1 + m \cdot \dot{\gamma}^{1-n}} \tag{EQ 4.1}$$

The viscosity at zero shear, itself, can be expressed as a function of molecular weight (in kg/mol) and polymer fraction of the solution by the following equations:

$$\eta_0 = \lim_{\dot{\gamma} \to 0} \eta = F \cdot D \qquad \text{(EQ 4.2)}$$

$$F = k[1 + a_1 \cdot (100 \cdot w_p \cdot \overline{M}_w)^{0.5} + a_2 \cdot (100 \cdot w_p \cdot \overline{M}_w)^{3.4}] \qquad \text{(EQ 4.3)}$$

$$D = \exp\left([b_0 + b_1 \cdot (100 \cdot w_p) + b_2 \cdot (100 \cdot w_p)^2] \cdot \left[\frac{1}{T} - \frac{1}{T_{ref}} \right] + b_3 \cdot (100 \cdot w_p)^3 \right) \qquad \text{(EQ 4.4)}$$

$$n = \exp\left(\frac{n_0 \cdot w_p^4 \cdot \sqrt{\overline{M}_w}}{T - 273.15} \right) \qquad \text{(EQ 4.5)}$$

$$m = m_0 \cdot \left(\frac{1}{n} - 1 \right) \cdot \frac{(100 \cdot w_p)^4}{(T - 273.15)^3} \cdot \sqrt{\overline{M}_w} \qquad \text{(EQ 4.6)}$$

The parameters of this model were correlated to experimental data for the PMMA/MMA system by Fleury [5], who determined the values listed in table 2 based on the values found by Stuber, by viscosity measurement at different temperatures respectively with polymer of different molecular weights.

Table 2: Parameter for the viscosity model of Stuber (refitted by Fleury)

Parameter	Unit	Value
n_0	$mol^{0.5} \, kg^{-0.5} \, K$	-34.806
m_0	$s \, mol^{0.5} \, kg^{-0.5} \, K^3$	0.0014
k	Pa s	$3 \cdot 10^{-4}$
a_1	$mol^{0.5} \, kg^{-0.5}$	0.125
a_2	$mol^{0.75} \, kg^{-0.75}$	$3.75 \cdot 10^{-11}$
b_0	K	600
b_1	K	80
b_2	K	1
b_3	-	$1.2 \cdot 10^{-5}$
T_{ref}	K	465.15

With these values, statements can be made on how the viscosity develops during the course of the polymerization reaction. Figure 4.8 a shows the viscosity evolution from a polymer weight fraction of $w_p = 0$ to $w_p = 1$ for a polymer of the molecular weight $M_w = 100$ kg/mol. Between 120°C and 150°C, the zero-shear viscosity increases by one order of magnitude. When handling undiluted polymer melts, e.g. in the devolatilization, rather high temperatures are needed to be able to pump the melt through the installation. At 250°C for example, which is the devolatilization temperature in this work, the viscosity is sufficiently low so that the polymer still flows through the preheater and into the discharge gear pump. Figure 4.8 b shows the dependence of the viscosity on the molecular weight of the polymer. Here, too, the influence is quite significant as can be seen for an increase of M_w from 100 to 150 kg/mol, which causes a viscosity raise by factor 4. These two points are important to consider, since both parameters, temperature and molecular weight, can easily be subject to minor changes (e.g. due to failure of heating, false concentrations of CTA, etc.), which can have drastic effects on viscosity and, thus, on the pressure drop in the reactor.

(a) (b)
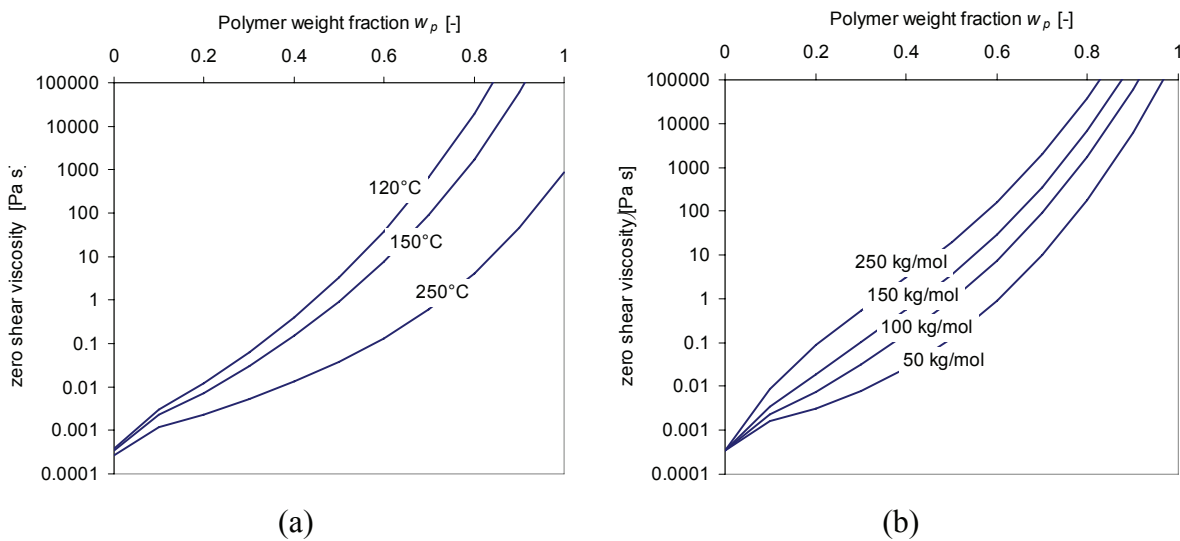
Figure 4.8: Zero shear viscosity for (a) Mw=100 kg/mol at different temperatures and (b) at 150°C for different molecular weights

With the data from table 1 and eqs. 4.7 and 4.8, shear rate, viscosity and pressure drop per meter can be calculated for Sulzer SMXL tubes used in this work (values for K_γ and d_t can be found in table 1).

$$\dot{\gamma} = \frac{K_\gamma \cdot u_z}{d_t}$$

(EQ 4.7)

$$\frac{\Delta p}{L} = \frac{NeRe \cdot \eta \cdot u_z}{d_t^2} \qquad \left[\frac{Pa}{m}\right]$$

(EQ 4.8)

Assuming a monomer conversion of $X = 50\%$ in the loop reactor ($u_z = 0.07$ m/s at a recycle ratio of 45:1) with a molecular weight of $M_w = 100$ kg/mol at 150°C results, according to this calculation, in a pressure drop of $\Delta p = 0.58$ bar/m, which is easy to handle. However, in the case of a feed pump failure, the reaction mixture would go straight into gel effect conditions and lead to conversions around 80 to 90%, which would result in a pressure drop of uncontrollable $\Delta p = 190$ bar/m, i.e. the sure plugging of the reactor.

A detailed discussion of the pressure drop in different zones of the pilot plant will follow together with the results from pilot plant experiments at a later point in this chapter.

4.1.5   The Pilot Plant in Detail

After discussing the possibilities concerning the choice of pilot plant setup and mixing elements, the pilot plant setup used in this work will now be presented in detail. As mentioned before, the reactor consists of two zones:

- A tubular recycle loop reactor with high recycle ratio (recycle : feed = 45:1)
- A conventional tube reactor

At the end of the reaction zone, there is a nitrogen-pressurized membrane flash valve from where the polymer solution is flashed into a two-phase heat exchanger, which leads into devolatilization chamber. From the devolatilization chamber, the devolatilized polymer melt is discharged by a rotary gear pump and sent in two strands to the granulator.

There are four independent heating zones in the pilot plant, which can be identified in figure 4.9. The loop reactor, the first and the second part including the flash valve are each heated by a 4kW Karl Juchheim laboratory oil thermostat. The preheater and the devolatilization chamber including the gear pump are heated by a 10kW HTT industrial oil thermostat. The heat transfer medium in all thermostats is a synthetic oil on dibenzyltoluene basis (Shell Aseol Trans-SH) with a temperature resistance up to 350°C.

The whole reactor is constructed with double-jacketed, stainless steel (316 / 1.4401) tubes with diameter DN 20 and equipped with Sulzer SMXL respectively SMX static mixing elements.

The latter are employed in places where advanced mixing is required (e.g. feed inlet, solvent inlet in beginning of tube).

The pilot laboratory facilities are classified as explosion protected zone (Ex II T2) and, therefore, especially equipped as regards electrical outlets, lights and electronic / reactor parts.

Feed preparation

The feed solution is prepared on the first floor of the pilot lab. Raw materials are employed as received, i.e. in the case of monomer and solvent directly from the barrel. The necessary amounts of monomer and solvent are weighed separately on a high-precision balance (Witronic, $m = 1\text{-}100\,\text{kg}$, $\Delta m = 1\,\text{g}$) before initiator and chain transfer agent are added. The feed solution is then transferred into a 60-L stainless steel tank with EKATO stirrer, from where it is fed into the reactor in the basement. The solvent / initiator solution is taken downstairs to a smaller stainless steel reservoir, where it is degassed with Argon and later on dosed into the tube reactor.

The reaction zone

From the feed preparation tank on the first floor, the non-degassed monomer solution already containing initiator and chain transfer agent is transferred by a two-piston pump (Bran&Lübbe N-J32) via a Coriolis flowmeter (Promass 60E DN2, Endress&Hauser) into the loop reactor at position 1. The inlet pressure is measured at the feed pump.

The physical volume of the loop was determined to be $V_{loop} = 907$ ml by measuring the amount of solvent needed to fill it entirely in the cold state.
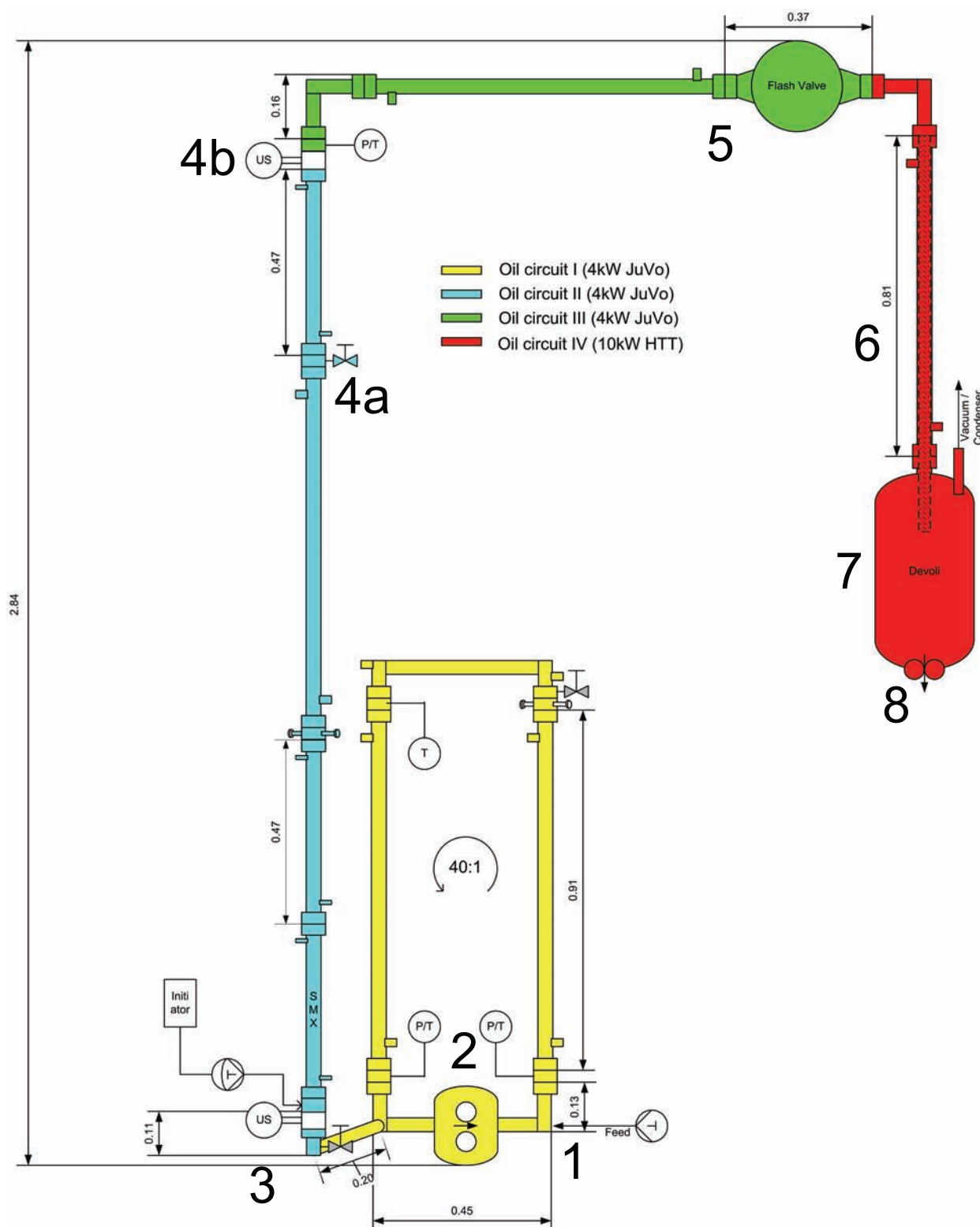
Figure 4.9: Detailed scheme of the pilot plant setup used in this work

Within the recycle loop, the solution is pumped counterclockwise around by a high-speed gear pump (Witte VAH-25,6 ED, position 2) at a recycle flow to feed flow ratio of approximately

45:1. The displaced volume per turn of the pump head corresponds to 25.6 ml, therefore an average rotation frequency of n > 50 min^{-1} is needed. The high recycle ratio is necessary in order to have (near-)CSTR conditions in the loop. In fact, it was shown by Zacca and Ray [83] that, as a rule of thumb, above recycle ratios of 30:1, loop reactors behave as a CSTR (with regards to conversion and molecular weight distribution). The limiting point in this consideration is the life-time of the initiator, which must be higher than the time the solution needs to go around the loop. At a recycle pump rotation speed of ω = 50 min^{-1} the cycle time in the loop is approximately 0.7 min. Ideally, the half-life time of the initiator at given reaction temperatures is higher than this value.

The temperature inside the reactor is measured by means of several thermocouples (type K) and there are two pressure transducers (Dynisco PT 435A / TPT 432A) that measure the pressure drop in the loop at the gear pumps entry and exit. A small sapphire window allows optical inspection of the flowing reaction mixture inside the reactor. Samples can be taken through a sampling valve at the loops exit. In the same place (position 3), there is also the ultrasound probe for inline conversion measurement, which will be referred to later (see "Ultrasound Polymerization Monitoring" on page 115). The results from the ultrasound measurement can, thus, be directly compared to offline sampling.

Connected to the exit of the recycle loop is a partially vertical, partially horizontal tube reactor of the same diameter and a total length of approximately l = 3.5 m. The volume of the tube reactor was determined to be V_{tube} = 1147 ml. Within this tube, the conversion reaches its maximum. As seen in the preceding subchapter, the "zero-shear" viscosity increases by a factor 10^3 for an increase in polymer fraction from w_p = 0.5 to 0.8 (T = 150 °C, $\overline{M}_w$ = 100 kg/mol). It is, therefore, regarded as necessary to add a solvent to this part of the reactor, by which the viscosity can be kept at acceptable values. This is done by continuously injecting the desired amount of solvent punctually in the center of the reactor stream. For an exact and constant dosing of the necessary amount of solvent, a membrane microdosing pump is used (LEWA MLM/M210/3mm). In order to achieve sufficient mixing of the low-viscous solvent with the highly-viscous polymer solution from the loop, only the first half a meter of tube is equipped with SMX mixing elements, the rest of the tube reactor contains SMXL mixing elements. Together with the solvent a second initiator can be added in order to obtain higher conversions in the tube if needed. A second sapphire window is installed after one meter of tube and after approximately 2/3 of the total tube length, a sec-

ond sampling valve and, half a tube length further, a second ultrasound probe together with temperature and pressure measurement were built into the reactor for conversion monitoring in the tube (position 4a and 4b).

The Devolatilization Zone

Figure 4.10 shows the membrane flash valve at the end of the tube reactor (position 5 in figure 4.9), where the reaction mixture is flashed from the pressure in the reactor to the reduced pressure in the devolatilization chamber. A sandwich membrane, the outer part made out of chemically resistant steel and the inner one from spring steel, is pressed by nitrogen (p = 10 - 100 bars) against the opening from the reactor and the outlet opening. This steel-on-steel contact is designed for viscous solutions only, which is the reason why for a solvent this valve does not hold the pressure in the reactor. Therefore, it is activated in the moment when there is polymer in the reactor. However, depending on the viscosity of the polymer, it can happen that the valve does not close anymore but that the pressure in the reactor is held back by the polymer, which fills the system. In this case, the flash point (i.e. the point were the pressure abruptly drops from p > 20 bars to p < 1 bar) can move from the valve to a later position within the preheater.
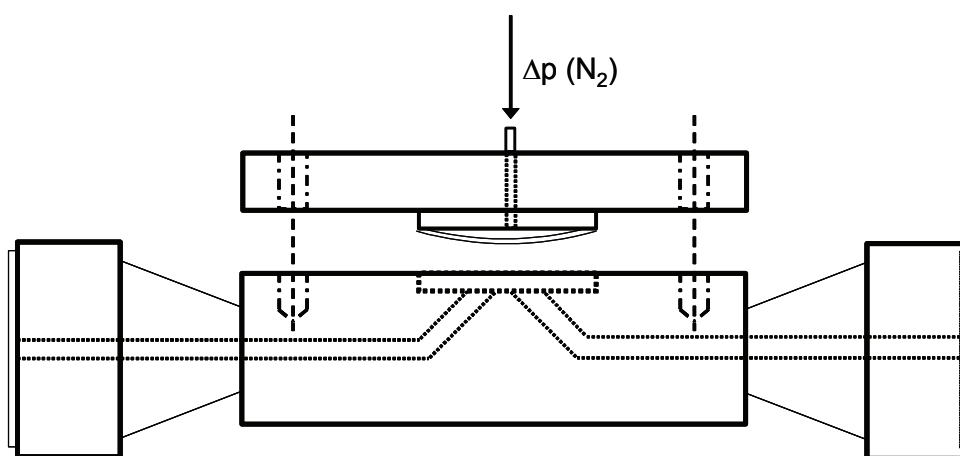
Figure 4.10: Schematic drawing of the flash valve between reactor and preheater

As mentioned before, the polymer is transferred from the flash valve into a two-phase preheater, where it is heated to devolatilization temperature. Basically, there are two different strategies of preheating, which were examined before in this research group [6, 75]: One is to heat up the polymer solution under pressure, while maintaining one phase only ("one-phase preheating").

The other is to first flash the solution and then heat it up, thus creating two phases in the preheater ("two-phase preheating"). In the first case both, polymer *and* volatiles, need to be heated to devolatilization temperature and, since at the moment of the flashing the temperature abruptly decreases due to the occurring evaporation, this temperature needs to be higher than for the two-phase preheating, where - ideally - the introduced energy is immediately used to evaporate the volatile components. The thermal stress on the polymer can, thus, be lowered significantly. Another advantage of the two-phase setup is that, since the preheater is equipped with SMXL mixing elements, the polymer foam formed during flashing is not static but thoroughly mixed for better removal of volatiles from the viscous melt. Figure 4.11 illustrates the principle of the two-phase preheater. In reality, it contains two DN10 tubes equipped with SMXL mixing elements. The presented flow pattern is, therefore, to be considered as schematic only.
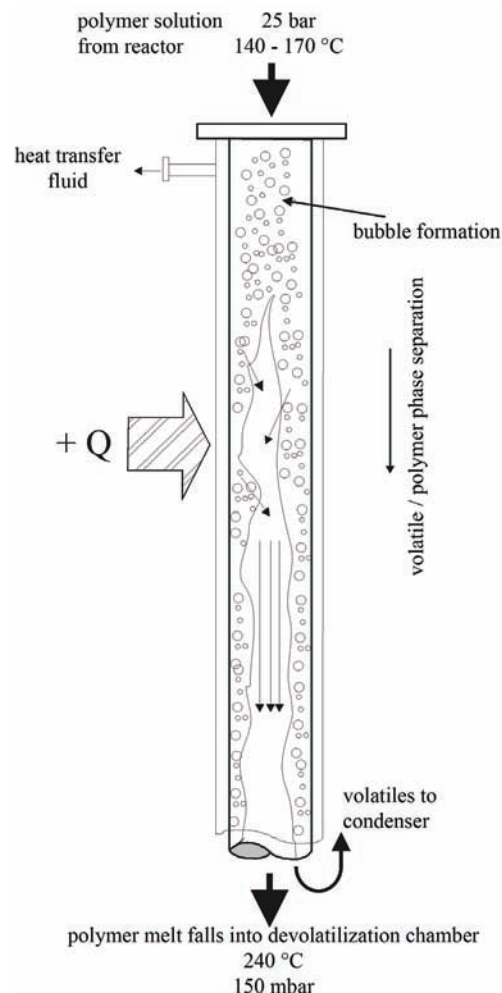
Figure 4.11: Schematic depiction of two-phase preheater for devolatilization of the polymer melt

The exit of the preheater reaches approximately 20-30cm into the devolatilization chamber, as indicated in figure 4.9. From here, the polymer foam falls to the conical bottom of the chamber, where it remains for a given residence time depending on the speed of the gear pump (MAAG Vacorex 45/45). The exact residence time could not be determined but is estimated to be of several minutes. To the devolatilization chamber is connected a vacuum pump (Leybold SOGEVAC SV40) via a condenser, where the volatiles are condensed and recovered from the reactor. For larger plant sizes, they could be separated from each other by distillation and recycled into the process. Given the small size of the pilot installation in this work, the volatiles were disposed of as waste.

Product Granulation

From the discharge gear pump, the polymer leaves the devolatilization in two strands through a nozzle designed in this work (exit diameter ~ 1 cm, see figure 4.12). These strands are pulled over a distance of ~ 3,5 m, supported by three rollers, into the granulator (Rieter Primo60E, with low speed gear for small throughputs), which - for reasons of security - had to be placed outside the lab. This distance is enough for the polymer melt to cool down to a temperature at which the viscosity is high enough for cutting (from T = 250 °C at the gear pump exit to ~ 50°C at the granulator entry). In the granulator, the strands are cut by a rotating knife into cylindric pieces with the approximate dimensions 1 x 3 mm, depending on the speed of granulator and gear pump. The placement of the granulator behind the devolatilization as well as the granulator, itself, are depicted in figure 4.13 (a) and (b).
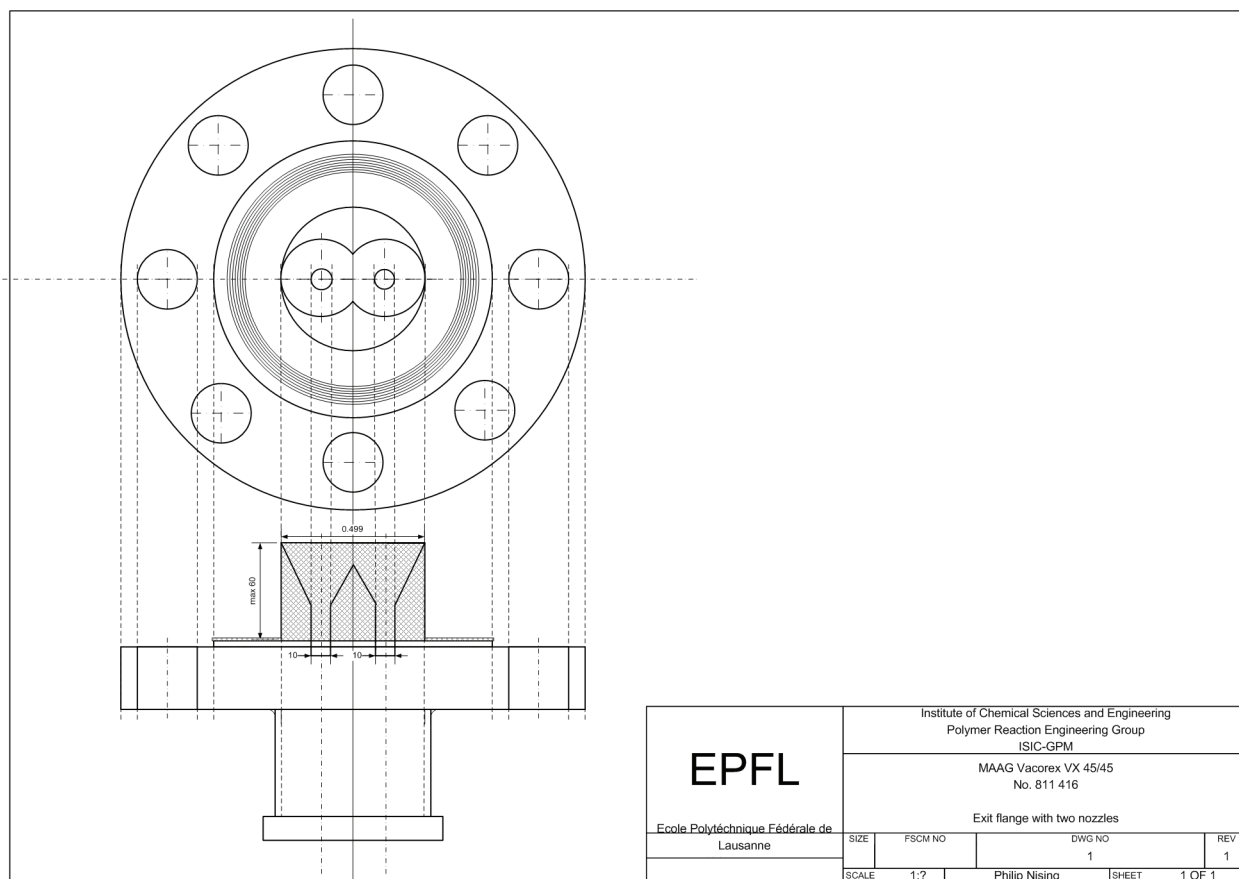
Figure 4.12: Gear pump exit nozzle designed to create two polymer strands for granulation
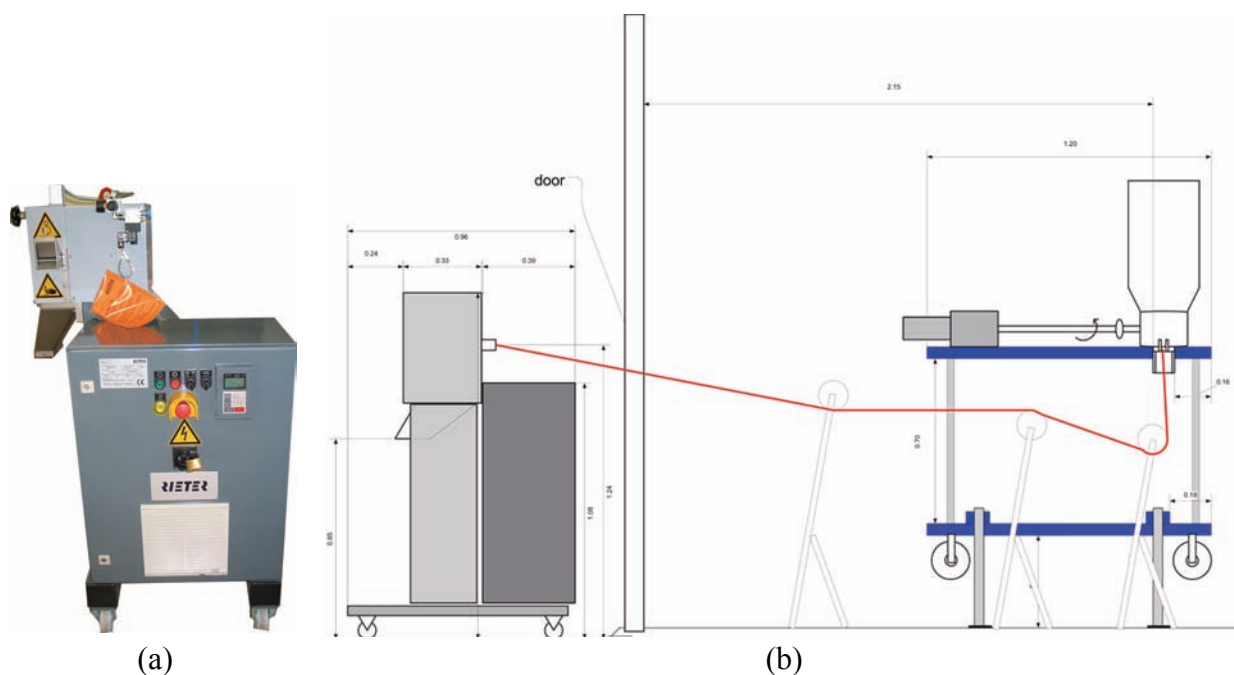
Figure 4.13: (a) Rieter granulator Primo60E with special gear for small throughputs (polymer strand path from devolatilization to granulation

The final product

The final product from the pilot plant polymerization process is a polymer with a molecular weight in the range of M_w = 70'000 - 180'000 g/mol, depending on the reaction conditions, and a residual volatiles' concentration of below 80 ppm for butyl acetate and below 10'000 ppm for monomer, which is quite satisfying considering the simplicity of the devolatilization facility (one-step flash, no moving parts, relatively low vacuum). Compared to commercial product (see figure 4.14), the polymer has a bit of a brownish discoloration, which has two reasons: one is that the vacuum chamber is not entirely gas-tight. Therefore, oxygen gets into the devolatilization, which causes oxidative degradation of the polymer at these temperatures (> 200 °C). The second reason is the relatively short duration of production and the rather small production rate. It was observed that for the long-term experiments over 20 hours and for experiments with higher flowrates, the coloration of the polymer became much less. This is confirmed by the fact that even in industrial polymerizations, the commercial grade polymer sometimes is achieved only after one day of production when a plant shut-down and restart was performed. A detailed discussion of the product quality obtained from the different pilot plant experiments is provided later on in this chapter.
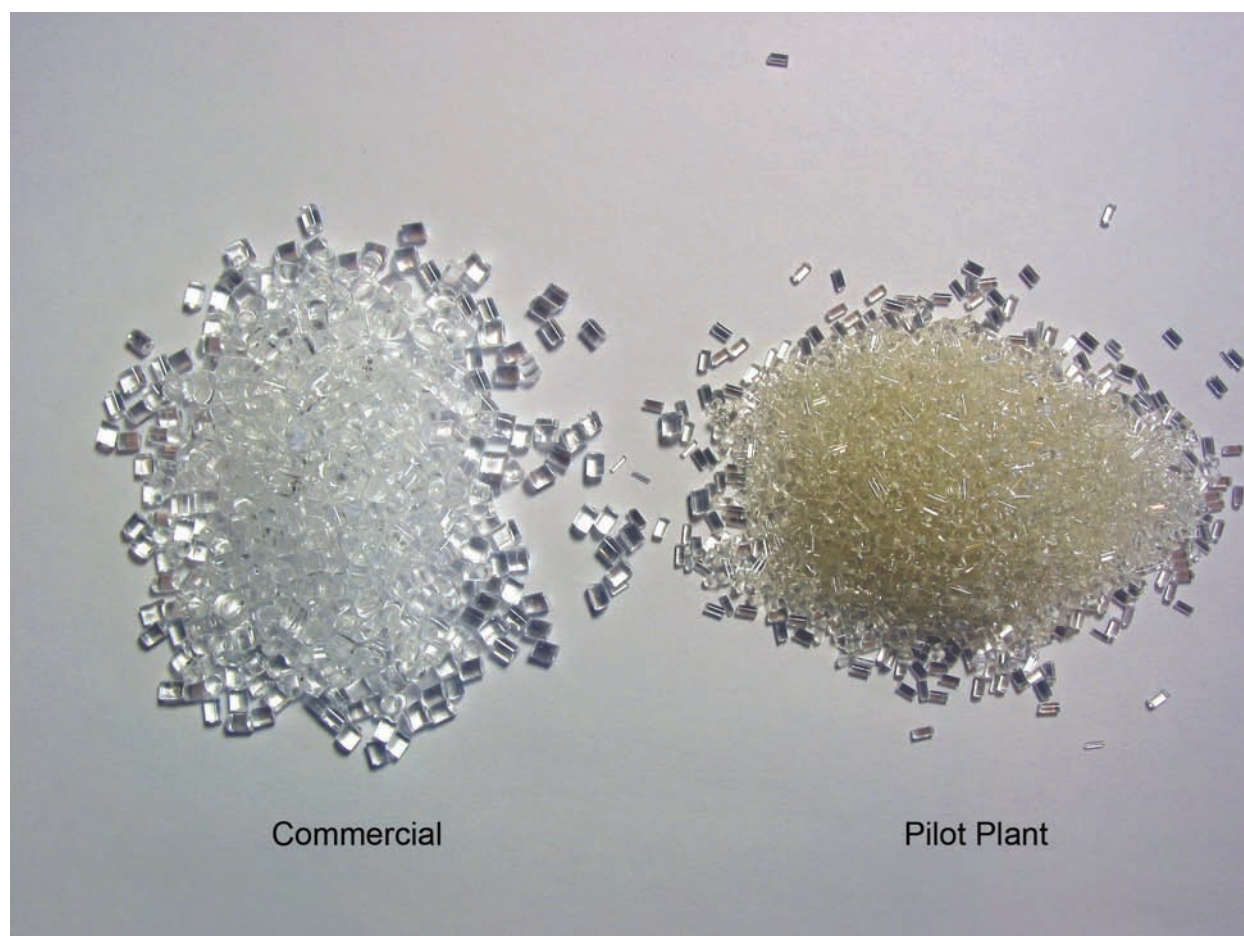
Figure 4.14: Commercial and pilot plant pellets in comparison

4.2   Ultrasound Polymerization Monitoring

One of the key points in process development is the process monitoring. Every process plant, no matter how small or simple it is, needs to be surveyed continuously with regards to process safety and product quality. Even marginal changes in the running process must be detected in the shortest possible delays, so that countermeasures or preventive actions can be taken. The classical way to monitor a reaction is to take samples in regular intervals and to analyze them by offline methods. And even though no production plant will ever work without product samples being taken every now and then, the clear disadvantages of this technique are that

- sampling takes time and - in most cases - human interaction

- in order to take a sample, the process often needs to be "disturbed", e.g. by opening a valve, thus changing the pressure and flow in the reactor
- especially for viscous products like polymers a uniform sample of the reactor contents are difficult to obtain

It must, therefore, be the aim of every process engineer to find and employ adequate methods for the inline monitoring of reactions and processes. Presently, there are a large number of solutions available on the market. A good overview can be found in Ullmann's Encyclopedia of Industrial Chemistry [84]. Among the simplest are namely density and conductivity measurements, whereas on the side of the more complicated ones there are, for example, inline GC or FTIR measurements. Ultrasound can be located somewhere in the middle as regards expenditure of equipment and, more important, investment. An important prerequisite for its application is a sufficiently large difference in speed of sound values for raw material and product. Examples for different applications are shown in table 3. The application of speed of sound measurement to qualitative reaction monitoring of polymerizations has already been described by Cavin et al. [7, 8] for styrene, by Zeilmann [85] for the MMA polymerization and by Dinger [86] for Butadiene/ Styrene polymerization. The quantitative reaction monitoring, i.e. the direct "inline" determination of the monomer conversion from the speed of sound measurement, has, on the other hand, not yet been described by any author.

Due to the complexity of polymerization reaction systems, the direct calculation of conversion from the speed of sound measurement is not at all trivial. In the following, the efforts that were undertaken in this work at establishing a working conversion monitoring for the high temperature polymerization of MMA are presented.

Table 3: Ultrasound velocities of monomers and polymers at 20 °C [84]

Species	Monomer	Polymer
Butyl acrylate	1233 m/s	1375 m/s
Styrene	1354 m/s	2120 m/s
Vinyl acetate	1150 m/s	1853 m/s
Vinyl chloride	897 m/s	2260 m/s

4.2.1   The Measurement Principle

Sound waves of frequencies above $\nu = 20'000$ Hz are called *ultrasound* (for comparison: the spectrum of audible sound waves for the healthy human ear ends at $\nu = 17'000$ Hz). Under the term *speed of sound* is understood the velocity, with which sound waves propagate through different media, i.e. water or air.

The longitudinal speed of sound waves in liquids depends on the density and the adiabatic (= isentropic) compressibility of the fluid[1]:

$$c^2 = \frac{1}{\overline{\kappa}_s \overline{\rho}} \tag{EQ 4.9}$$

For mixtures, κ_s and ρ can be calculated as follows (additivity):

$$\overline{\rho} = \sum_i \phi_i \rho_i \qquad\qquad \overline{\kappa}_s = \sum_i \phi_i \kappa_{s,i} \tag{EQ 4.10}$$

where ϕ_i is the volume fraction, ρ_i the density and κ_i the adiabatic compressibility of the pure component i. The volume fraction ϕ_i is expressed as a function of the mass fraction as follows:

$$\phi_i = \frac{w_i / \rho_i}{\sum_i w_i / \rho_i} \tag{EQ 4.11}$$

Additionally, the speed of sound is linearly depending on the pressure:

---

1. The propagation of sound waves is, thermodynamically speaking, a propagation of density changes in an infinitesimally small volume of the medium. A density and, thus, a volume change inflicts an increase in temperature and pressure and can be described by the following complete differential:

$$\frac{d\rho}{\rho} = -\frac{dV}{V} = -\frac{1}{V} \cdot \left.\left(\frac{\partial V}{\partial p}\right)\right|_T \cdot dp - \frac{1}{V} \cdot \left.\left(\frac{\partial V}{\partial T}\right)\right|_p \cdot dT$$

with the isothermal compressibility $\kappa_T = -\frac{1}{V}\left.\left(\frac{\partial V}{\partial p}\right)\right|_T$ and the thermal expansion coefficient $\beta = \frac{1}{V}\left.\left(\frac{\partial V}{\partial T}\right)\right|_p$.

However, in the case of sound wave propagation, the volume change of this infinitesimal volume is so fast that the dissipated heat cannot be removed (i.e. it is adiabatic). Furthermore, the change is small enough to be considered reversible. It is, therefore, an isentropic change of state and the compressibility becomes the

isentropic compressibility $\kappa_S = -\frac{1}{V}\left.\left(\frac{\partial V}{\partial p}\right)\right|_S$

117

$$c = c_0 + \alpha \cdot p \text{ with } c_0 = c\big|_{p = 1bar} \qquad \text{(EQ 4.12)}$$

From eqs. 4.9 to 4.12 follows for the speed of sound of a three-component system (monomer, polymer, solvent):

$$c_0 = \frac{\sqrt{\left(\dfrac{w_m \kappa_m}{\rho_m} + \dfrac{w_p \kappa_p}{\rho_p} + \dfrac{w_s \kappa_s}{\rho_s}\right)}}{\displaystyle\sum_i \frac{w_i}{\rho_i}} - \alpha \cdot p \qquad \text{(EQ 4.13)}$$

This equation can, unfortunately, not be solved explicitly for the polymer content w_p. However, by means of three-dimensional fitting of theoretical values of c_0 for different solution compositions, an analytical expression of the form $X = f(c, T)$ can be determined, which allows the calculation of monomer conversion from the ultrasound signal for a given temperature, solvent content and pressure.

The density and compressibility data for MMA, PMMA and butyl acetate can be found in literature respectively be determined by ultrasound measurement, itself. For the high temperature process, literature data for the compressibility proved to be rather imprecise. Therefore, it was redetermined by ultrasound measurements at elevated temperatures. The corresponding data can be found in "Calibration of the measuring system" as well as in appendix 5 and a detailed presentation of the results concerning the conversion measurement will be presented in the following ("Results for the ultrasound reaction monitoring").

4.2.2   The Measuring Equipment

The ultrasound equipment used in this work are two high-temperature, high-performance Liquisonic® flange sensors (DN25, PN100, T<200°C, 1.4571/316Ti, see figure 4.15), manufactured by Sensotech (Magdeburg, D). They are controlled by a Liquisonic® Controller 30, which also serves as interface for the transfer of the measured signal to external data acquisition. With regards to previous projects, the temperature resistance has been significantly improved. Ten years ago, the application of ultrasonic technology was limited to temperatures below 100°C. Therefore, it is namely due to Sensotech's advances in technology that the implementation of ultrasound measurement in this high-temperature project is possible.

In order to reduce the dead volume inside the probe, plastic parts were introduced from both sides occupying most of the volume around emitter and receptor (several issues arouse from this feature, which will be discussed further down in this chapter).
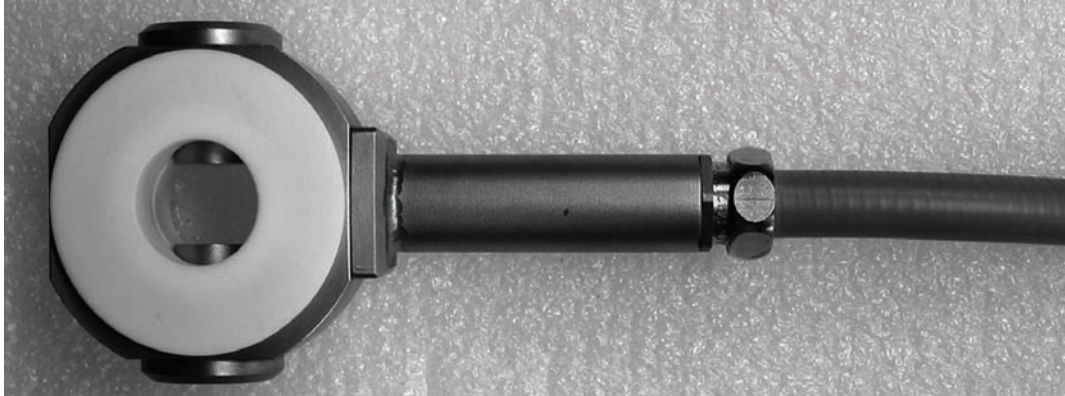
Figure 4.15: Liquisonic® flange sensor DN25

The functioning of the flange sensor is depicted in figure 4.16. On one side of the probe, a transducer emits pulsated sound waves of a given pressure amplitude (proportional to the applied voltage U_0) and frequency, orthogonal to the flow direction. The signal reaches the receptor, where it creates a voltage again proportional to its amplitude. The speed of sound can be determined by the time necessary to travel from the emitter to the receiver, whereas the attenuation of the signal δ is calculated from the change of amplitude (eqs. 4.14 and 4.15). However, for conversion monitoring in polymerization systems, only the speed of sound measurement is of importance.

$$u_z = \frac{x}{\Delta t}$$

(EQ 4.14)

$$\delta = \frac{1}{x} \cdot \ln\frac{A_0}{A_x} = \frac{1}{x} \cdot \ln\frac{U_0}{U_x}$$

(EQ 4.15)
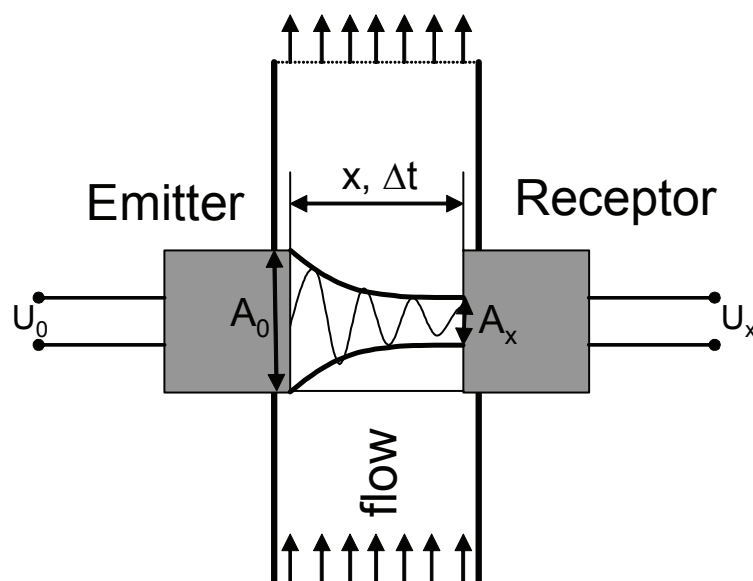
Figure 4.16: Principle of speed of sound measurement (A_0 and A_x are the signals emitter respectively receiver amplitudes)

A limiting factor in reaction monitoring by ultrasound measurement is the presence of gas bubbles. Especially at elevated temperatures, when the medium is close to or above its boiling point (i.e. in absence of sufficient pressurization), the measurement fails periodically. As mentioned above, the pressure in the reactor is built-up by a membrane valve at the end of the tube reactor (see figure 4.10), which is designed for viscous solution. In the start-up of the pilot installation it may happen that, when the reactor is filled with solvent only and heated up, the pressure in the reactor is not sufficient to avoid boiling. Only from the moment when the first polymer reaches the valve and the solution becomes more viscous, pressure builds up and boiling is prevented. Therefore, mostly in starting phases, the ultrasound signal might be disturbed. This phenomenon is presented in figure 4.17, where the reactor is heated with a small solvent flow from $T = 125°C$ to $T = 135°C$. At a given point the measured speed of sound periodically falls off abruptly and then rises back up to its initial value. From the moment when there is polymer in the reactor ($t > 17'000$ s), the signal is stable even with increasing temperature as the pressure augments.

A second limiting factor is the ultrasound velocity, itself, which decreases drastically with increasing temperature. For very high temperatures ($T = 170\text{-}180°C$), the ultrasound velocity of pure MMA is smaller than 600 m/s, a value below which the measurement becomes difficult from

a physical point of view due to structure-born sound disturbances (elastic vibration of solid material, i.e. probe material) and which was enforced electronically as lower measurement limit to avoid inaccuracies. Therefore, at these temperatures, measuring is only possible in the presence of polymer in the system, which causes an increase in ultrasound velocity big enough to be again above the limit.
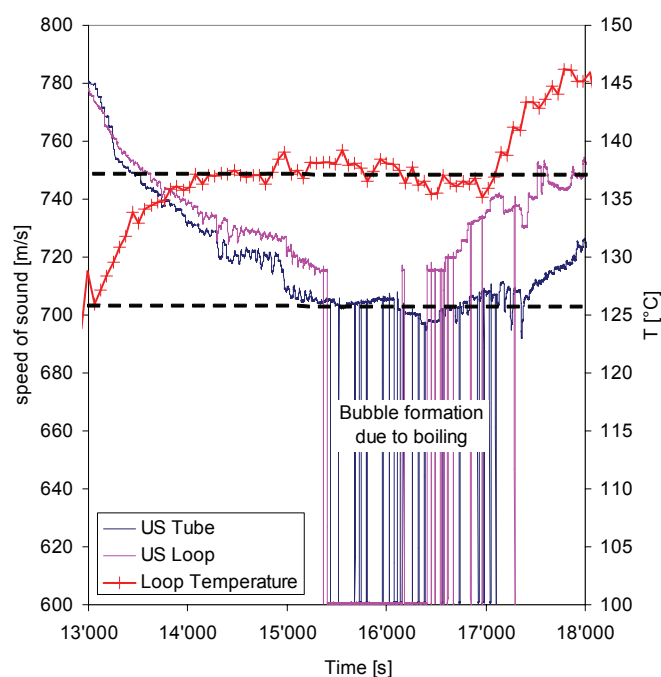
Figure 4.17: Loss of ultrasound signal due to bubble formation

Another probe specific problem is fouling and dead volumes. Since the cylinder-like transducers penetrate the medium and the flow is slowed down due to the widening of the diameter in the sensor, the formation of polymer layers is favoured. For this reason, special filling pieces have been developed with the aim to fill this empty volume and to incorporate the transducer cylinders except for their emitting / receiving surface.

Several problems were encountered as to the use of these pieces. First to mention is the choice of a suitable material, which resists the process conditions. In contrast to recommendations from industry, poly (vinylidene fluoride), PVDF, was found to be not a good candidate since it dissolved already after a few heating cycles to large extents in the reaction medium (compare parts before and after use shown in figure 4.18), leading to severe problems with reactor leaking. The dissolved PVDF was later found in the produced PMMA as encapsulated droplets.

Poly (tetrafluor ethylene), PTFE, exhibits better chemical resistance and is mostly stable under the given process conditions. It is the material used predominantly in this work. Its disadvantage is the rather strong swelling when exposed to hot MMA and other organic solvents. This effect is depicted in figure 4.19. After various days of experiments, the inner wall of the PTFE parts is completely swollen up, offering ideal conditions for fouling. In fact, MMA can penetrate the pores of the swollen PTFE and polymerize, thus making the material burst. Although stable for the duration of the set of experiments carried out in this work, in a continuous process these parts would most probably have to be changed regularly causing increased maintenance expenses. Nevertheless, at this moment it is the only solution found for this problematic. Finally, the best way to avoid material problems at this location is to go without any plastic parts and to employ either probes of the same diameter as the reactor tubing or to employ a different probe geometry (immersion probe etc.).

Figure 4.18: PVDF filling parts before (left) and after use. The material has been completely dissolved by the reaction media.
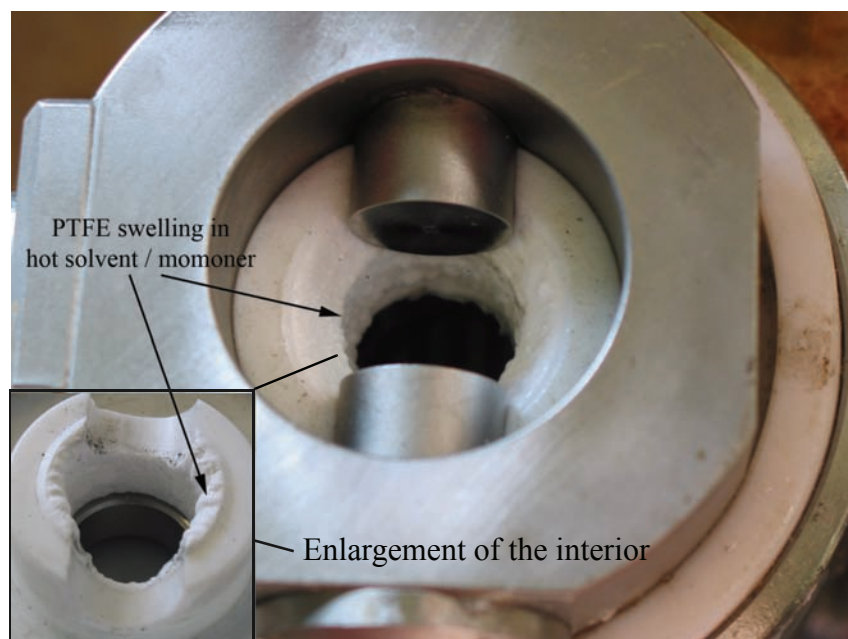
Figure 4.19: Swelling of PTFE filling parts observed after several days of experiments

4.2.3 Calibration of the measuring system

The following parameters need calibration respectively careful examination before reliable measures of the speed of sound can be realized:

- the pressure dependence factor α
- the compressibility at elevated temperatures

For these calibrations, the ultrasound signal was determined for different, calibrated solutions of monomer, polymer and solvent in an independent, pressurizable and heatable measuring cell (see figure 4.20 for schematic setup). This cell consists of an ultrasound probe that is fixed between two double-jacketed flange pieces heated with an oil circuit and connected to a nitrogen gas cylinder for pressurization. The calibration solution is filled into the cell, which is consecutively closed hermetically, heated to the desired temperature and pressurized with N_2. The speed of sound is measured by an online acquisition system and stored by a special software (Sonic Works, Sensotech). From the measured speed of sound and the composition of the calibration solution, the parameter α as well as the compressibility for butyl acetate and MMA were adjusted. The results of this fitting can be found on the following pages.
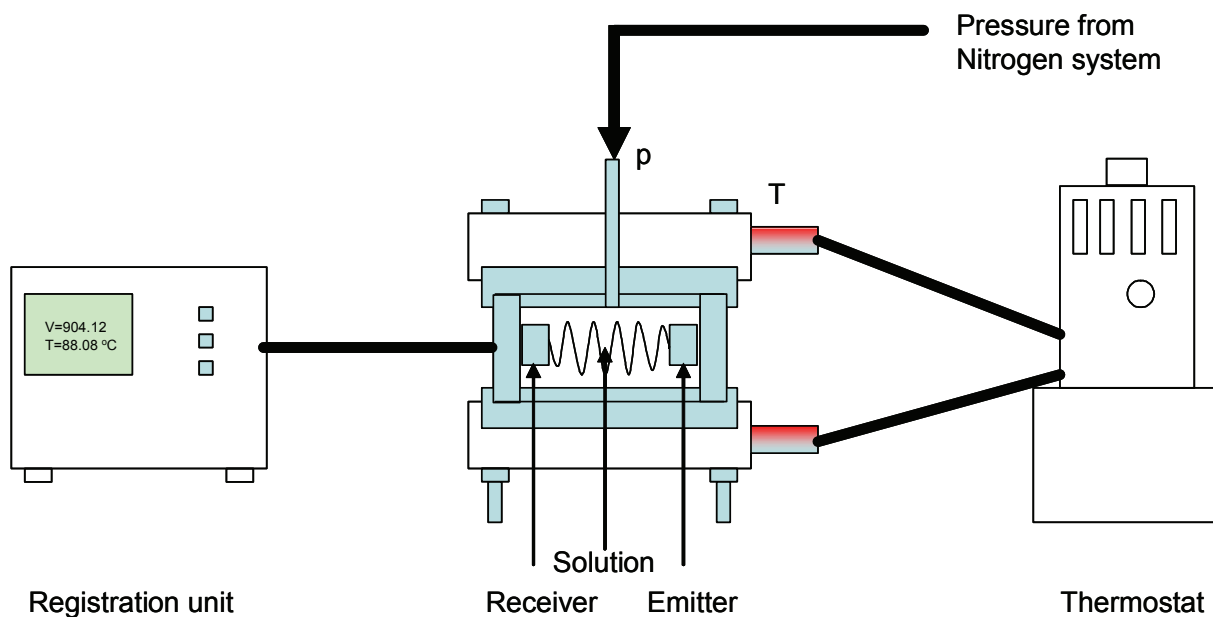
Figure 4.20: Schematic setup of the calibration cell for the ultrasound measurement

For the parameter α, a linear dependence on temperature and polymer content was assumed:

$$\alpha = \alpha_0 + A_1 \cdot T + A_2 \cdot w_p \qquad \text{(EQ 4.16)}$$

The equation parameters α_0, A_1 and A_2, which resulted from the fitting to experimental data are presented in table 4. The corresponding graphic is depicted in figure 4.21. Note that the range of the fitting is limited due to the high viscosity: it was simply not possible to produce a calibration solution with more than 30% polymer content and fill it into the cell at room temperature. As concerns the temperature, the measurement is limited to 120°C, since despite the pressurization the solutions started bubbling (probably due to dissolved N_2), which made the measurement impossible.

Table 4: Fitting parameters for the α curve fitting (values with complete digits as determined by Tablecurve can be found in Annex 8)

Parameter	Value
α_0	0.406
A_1	0.004
A_2	-0.395
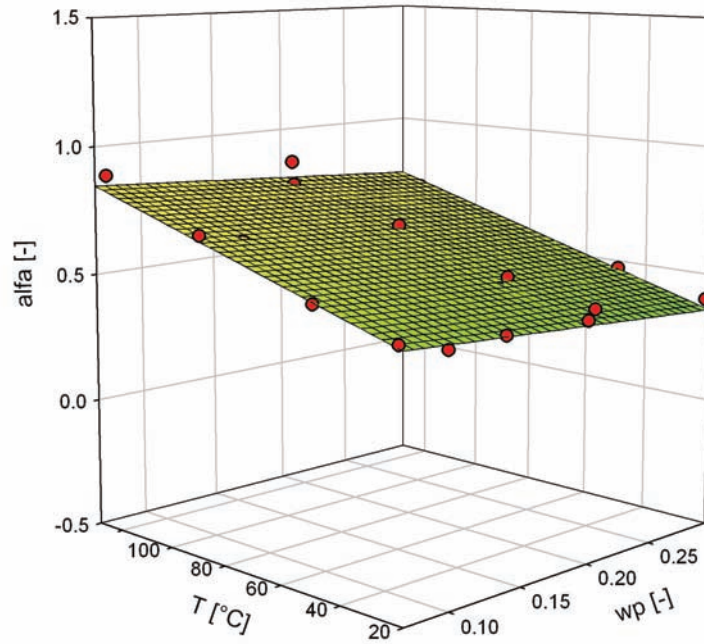
Figure 4.21: Fitting of α for different temperatures and polymer fractions

The compressibility data for butyl acetate, MMA and PMMA found in literature is rather scarce and only validated for low temperatures [87-89]. Zeilmann was the first to publish values for temperatures of up to 130 °C [6]. However, his values seem to slightly mismatch the data obtained in this work, which might be due to the different measurement equipment. Therefore, the determination of butyl acetate and methyl methacrylate compressibilities was redone in this work. The value for the polymer, on the other hand, was not readjusted as it lead to satisfying results. The density data, which is needed for this calculation is taken from literature (see appendix 5).

For the pure compounds, the compressibility can be determined directly from the speed of sound using equation 4.17 (which follows from eqs 4.9 and 4.12).

$$\kappa_s(T) = \frac{\rho(T)}{(c - \alpha \cdot p)^2} \qquad \text{(EQ 4.17)}$$

This calculation was done for several temperature points, leading to the following compressibilities for butyl acetate and MMA:

MMA

Butyl Acetate
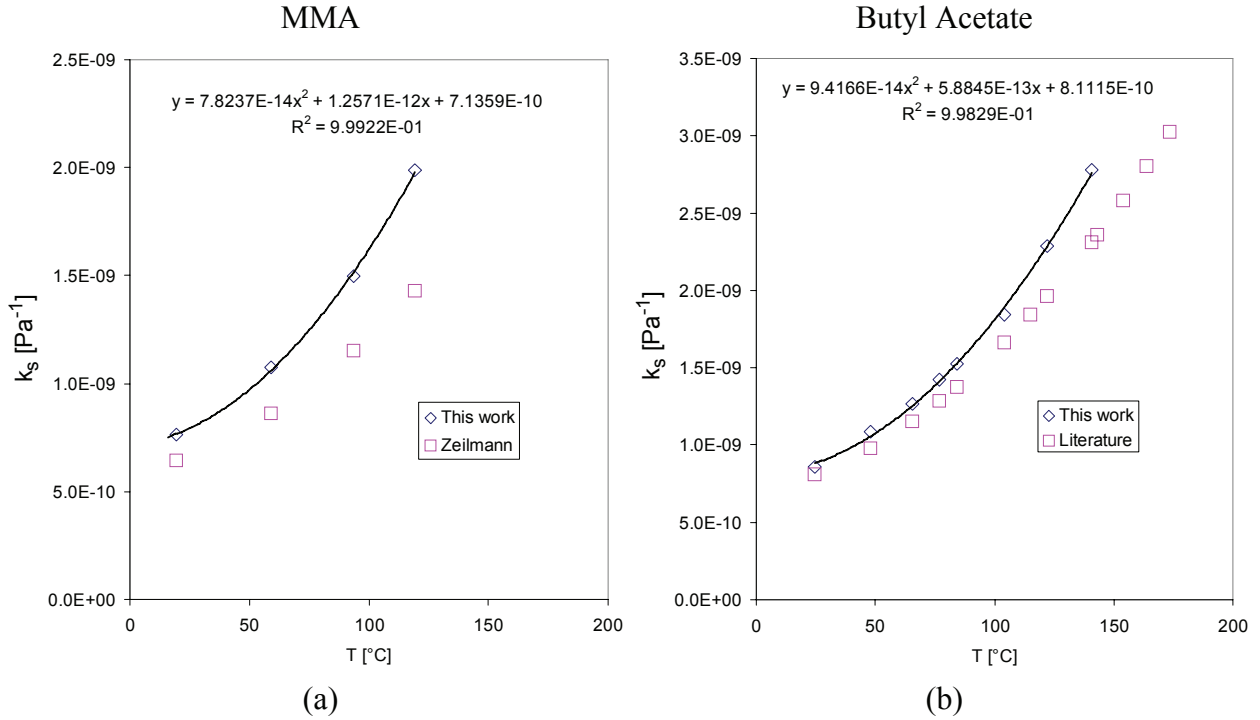
Figure 4.22: Determination of the compressibility for monomer and solvent from experimental data and comparison to literature data (a) [6] (b) [89]

The compressibility for several temperatures of the polymer was taken from literature [47] and fitted as done by Zeilmann with Tablecurve. The temperature dependence follows a more complicated, exponential mathematical expression, since the compressibility undergoes a major change when passing the glass transition temperature T_g.

$$\ln \kappa_{s, PMMA} = \frac{A + B \cdot T + C \cdot T^2}{1 + D \cdot T + E \cdot T^2 + F \cdot T^3}$$

(EQ 4.18)

Table 5: Fitting parameters for the $\kappa_{s,PMMA}$ curve fitting (values with complete digits as determined by Tablecurve can be found in Annex 8)

A $[Pa^{-1}]$	B $[Pa^{-1}{}^\circ C^{-1}]$	C $[Pa^{-1}{}^\circ C^{-2}]$	D $[Pa^{-1}{}^\circ C^{-1}]$	E $[Pa^{-1}{}^\circ C^{-2}]$	F $[Pa^{-1}{}^\circ C^{-3}]$
-22.22	0.37	$-1.57 \cdot 10^{-3}$	-0.016	$6.7 \cdot 10^{-5}$	$1.57 \cdot 10^{-8}$

126
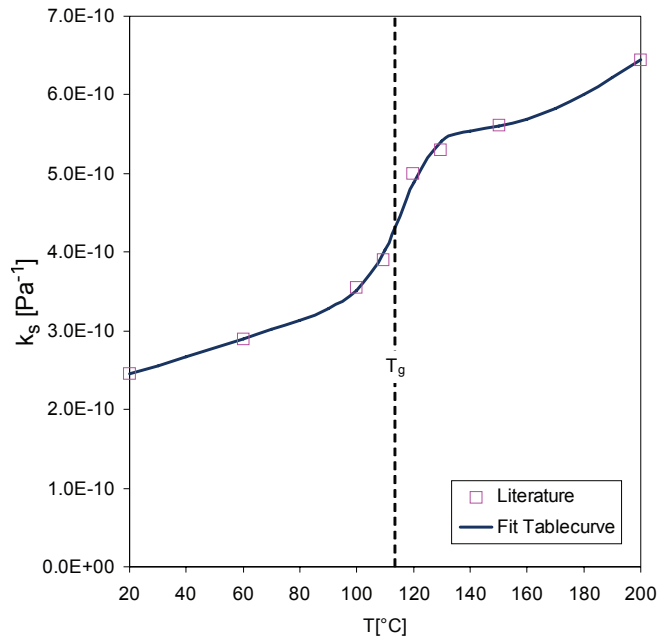
Figure 4.23: Compressibility fit for PMMA based on literature data [47]

With equation 4.13 and the compressibility and density data, it is now possible to calculate the ultrasound propagation velocity for any combination of temperature, pressure and polymer respectively solvent fraction. However, the calculation is quite complicated and it does not allow the inverse calculation, i.e. from a given ultrasound propagation velocity and temperature / pressure to a polymer content. This is due to the character of namely equation 4.13, which is not solvable unambiguously for w_p. In order to overcome this difficulty, a three-dimensional fit is needed, which yields an analytically unambiguous equation. The fitting can be done with Tablecurve 3D on the basis of theoretical values calculated according to above formulas, with the limitation of a fixed solvent fraction and neglecting the difference of speed of sound between MMA and the comonomer MA. The calculation of conversion from the speed of sound is, therefore, only precise when the solvent content is constant or zero (in steady state) and the corresponding fitting parameters are used. In the startup phase of the pilot plant, when the solvent initially present in the reactor is displaced by the feed solution, the measurement is not correct. In the following graphics (figure 4.24 (a) and (b)), the fitting is shown for the example of a reaction without solvent ($w_s = 0$) and at p = 25 bar.
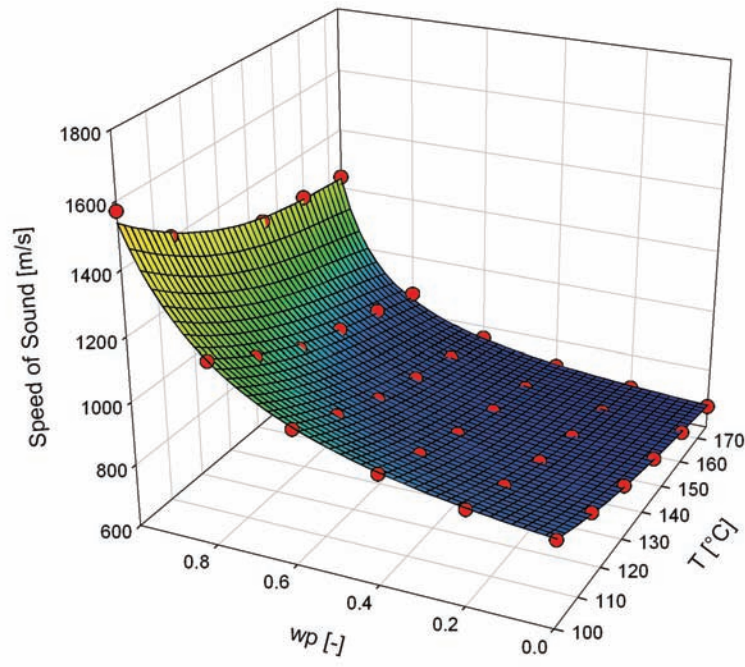
$$c\left[\frac{m}{s}\right] = \frac{a + b \cdot T + c \cdot T^2 + d \cdot T^3 + e \cdot w_p + f \cdot w_p^2}{1 + g \cdot T + h \cdot w_p + i \cdot w_p^2}$$

(a)
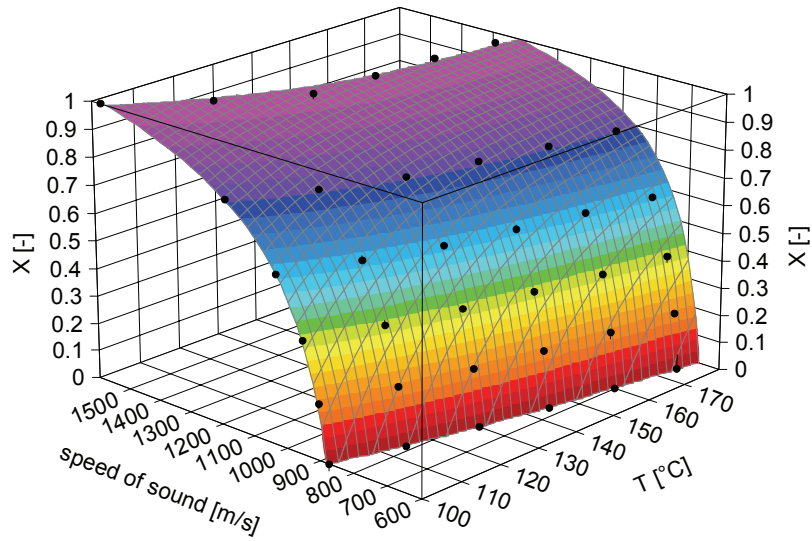
$$X = \frac{a + b \cdot T + c \cdot T^2 + d \cdot T^3 + e \cdot c}{1 + f \cdot T + g \cdot T^2 + h \cdot c + i \cdot c^2}$$

(b)

Figure 4.24: 3D-fitting for $w_s = 0$, $p = 25$ bar with fitting equation (a) w_p, T to speed of sound (b) speed of sound, T to conversion

The parameters for the fitting of these two cases are the following:

Table 6: Fitting parameters for the fittings presented in figure 4.24 (values with complete digits as determined by Tablecurve can be found in Annex 8)

Parameter	w_p to *speed of sound*	*speed of sound* to X
a	1808.1 [-]	1.96
b	$-18.5 \left[\frac{1}{{}^\circ C}\right]$	$-0.016 \left[\frac{1}{{}^\circ C}\right]$
c	$0.093 \left[\frac{1}{{}^\circ C^2}\right]$	$8.11 \cdot 10^{-5} \left[\frac{1}{{}^\circ C^2}\right]$
d	$-0.00018 \left[\frac{1}{{}^\circ C^3}\right]$	$-1.61 \cdot 10^{-7} \left[\frac{1}{{}^\circ C^3}\right]$
e	-159.6 [-]	$-0.001 \left[\frac{s}{m}\right]$
f	-151.66 [-]	$-0.0014 \left[\frac{1}{{}^\circ C}\right]$
g	$-0.002 \left[\frac{1}{{}^\circ C}\right]$	$-2.56 \cdot 10^{-6} \left[\frac{1}{{}^\circ C^2}\right]$
h	-0.29 [-]	$-0.0012 \left[\frac{s}{m}\right]$
i	-0.26 [-]	$1.062 \cdot 10^{-7} \left[\frac{s^2}{m^2}\right]$

It should be pointed out again at this point that these values are only valid for the mentioned cases. For different solvent contents, the fitting needs to be redone. In both cases, the values are related to the pressure-corrected *speed of sound* value, so the correction function (equation 4.12) still needs to be considered when using the fit (for example: before applying the fit to a *speed of sound* value in order to calculate the conversion at this point, it needs to be corrected with the adequate pressure value).

4.2.4 Results for the ultrasound reaction monitoring

Apart from a quantitative determination of the conversion in the reactor (inline conversion measurement), which will be presented later on, the ultrasound technique gives access to other important (qualitative) information. It is, for example, possible to observe the stability of a continuous process or its dynamic behavior during condition changes (i.e. start-up, shut-down, temperature change etc.).

The process monitoring by ultrasound is illustrated in figure 4.25 for the example of a polymerization at T = 140 °C (curve shown for the loop probe). During the initial heating phase with a very low solvent flowrate, the speed of sound decreases continuously until the final reaction temperature is reached. This decrease is only due to the change in density and compressibility of butyl acetate with increasing temperature. As soon as the feed stream is switched from solvent to monomer solution, the polymerizations starts and the polymer volume fraction increases. The consequence is an increasing speed of sound signal. Once the solvent is displaced and the reactor is in hydrodynamic and kinetic steady-state, the signal becomes constant. In the presented case, the time necessary to reach steady state is t = 150 min, i.e. 5 residence times at the flowrate of F = 1.8 kg/h.
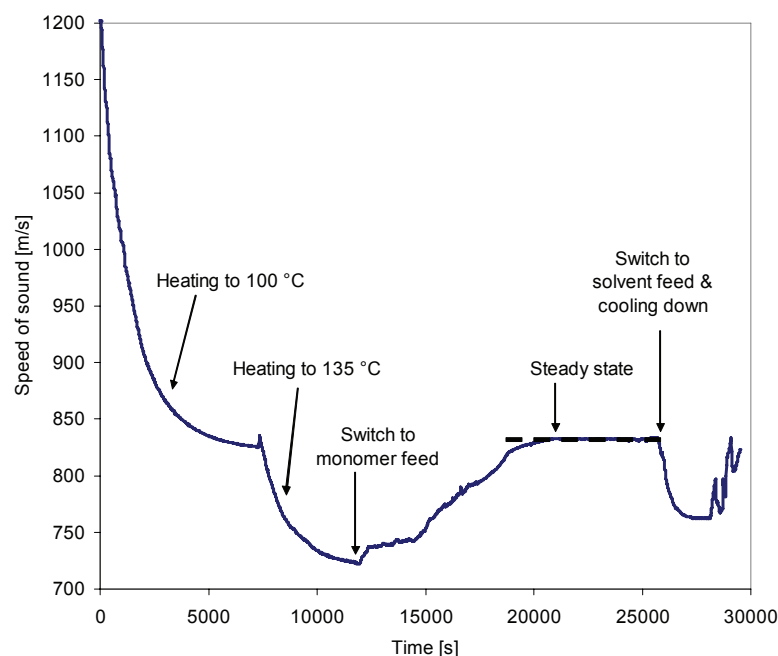
Figure 4.25: Ultrasound process monitoring example for the loop probe in experiment no. 2 (see appendix 7)

At the end of the experiment, the feed stream is again switched back to solvent and the flowrate is increased. This is reflected in a drop of the speed of sound signal at first instance, followed by an increase once the temperature drops significantly due to cooling down of the reactor.

The qualitative information obtained by ultrasound is, therefore, very valuable for the observation of the process and the early detection of slight changes, i.e. in temperature, pressure or feed flow.

With the calibration and fitting from subchapter 4.2.3, the evaluation of the ultrasound signal can be taken one step further to the direct determination of monomer conversion in the reactor. The limitation, as mentioned above, is the composition of the reaction mixture apart from monomer and polymer. This is due to the fact that, in the presence of a solvent for example, equation 4.13 contains 5 unknown variables: w_p, w_m, w_s, T and p. These five can be reduced to four by the fact that $w_p = 1 - w_m - w_s$. Temperature and pressure are known, too, which leaves two unknowns for only one equation: w_m respectively w_p and w_s. In the case of the copolymerization, even a third one, w_{m2}, has to be taken into account.

The conversion determination from ultrasound is, therefore, only possible if either another measurement technique gives access to, for example, the solvent content, or if the solvent and comonomer content are constant, respectively, can be neglected. As to the comonomer content, it can be neglected for the present consideration, since it's weight fraction in the feed is rather low (< 5%) and it's speed of sound very similar to the one of MMA. The solvent, however, has a strong influence on the measurement in the beginning of the reaction, as long as it has not been displaced yet by the monomer feed solution (compare figure 4.26). Until the solvent content in the loop reactor has reached negligible levels (which is the case only shortly before reaching steady-state), the measurement of the conversion is, thus, not reliable.
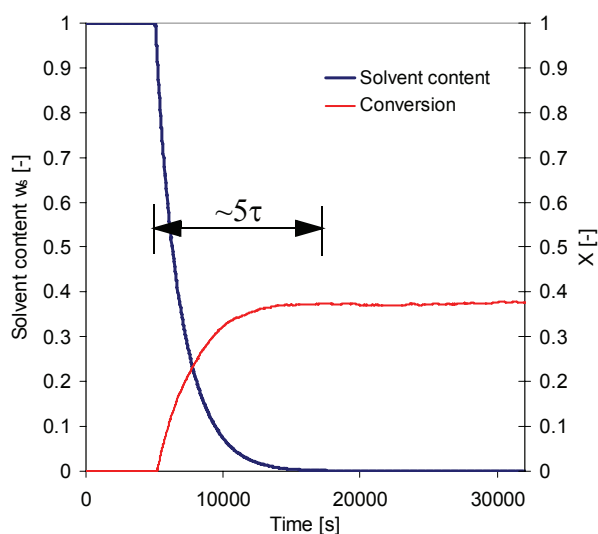
Figure 4.26: Modeled solvent content and monomer conversion in the loop reactor over reaction time for a typical pilot plant experiment

The following images present the results obtained for the direct, i.e. "inline" conversion measurement at the exit of the loop reactor. The data was taken from several experiments with different process conditions (for the experiment numbers see appendix 7). For the temperature value the value measured by a thermocouple integrated in the US-probe was taken, which was lower than the actual reactor temperature by ~5°C. This temperature difference can be attributed to the fact that the US-probes are not actively heated and that the isolation might not be sufficient to prevent a cooling down of the polymer solution.

The problem with the unknown solvent content in the beginning of the reaction is clearly visible in these graphs. Until the moment when the major part of the solvent has been displaced out of the loop reactor, the conversion calculation delivers negative results. This is, as explained beforehand, due to the lower speed of sound of butyl acetate, which pushes the calculated values for the conversion below zero in figure 4.24 (b).
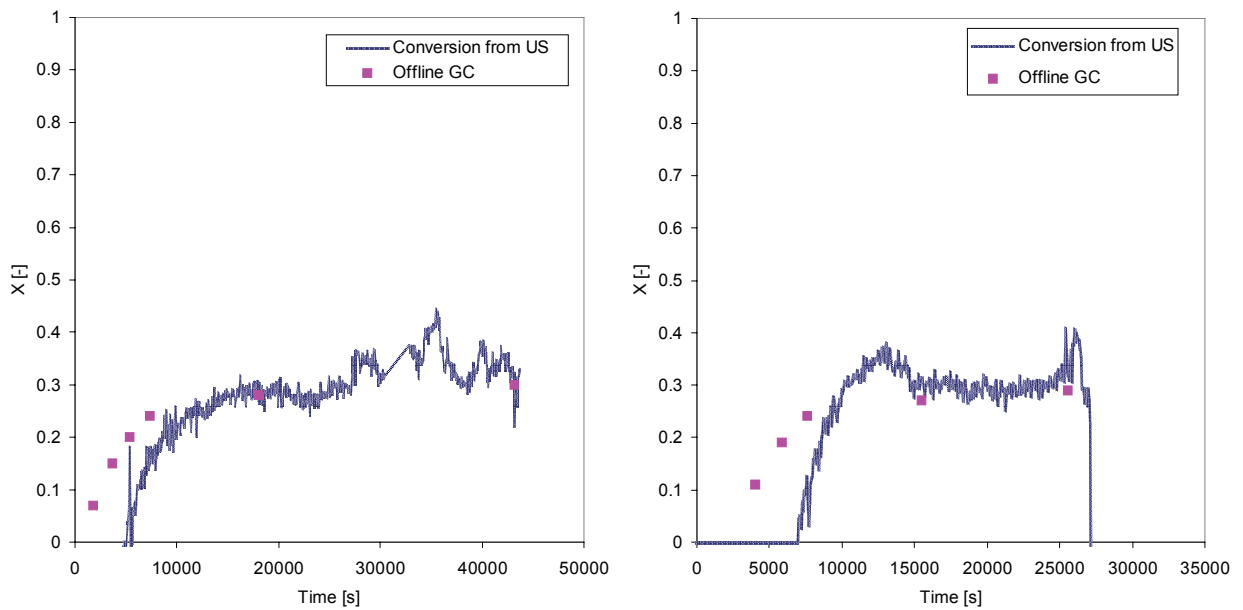
(a) Exp. 10a: 150 °C, 1.5% MA, 250ppm TBPIN *(b) Exp. 11: 150°C, 3.5% MA, 250ppm TBPIN*
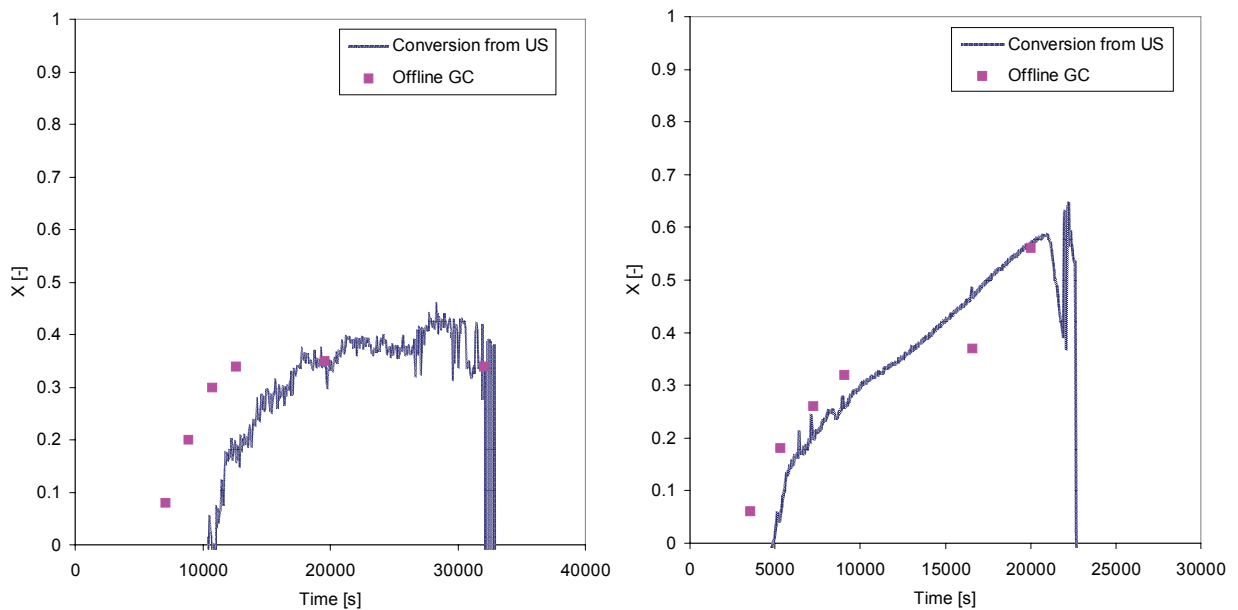
(c) Exp. 17: 170 °C, 5.5% MA, 400ppm TBPIN *(d) Exp. 7: 120 °C, 1.5% MA, 400ppm TBPEH*
Figure 4.27: (a)-(d) Conversion monitoring with Ultrasound (US) for different experiments

Once the loop reactor contains only monomer and polymer in significant amounts, the picture changes and the calculated conversion evolution is in very good agreement with offline measured conversion points. While graphs (a) to (c) in figure 4.27 show experiments that reach steady state more or less after the expected 5 residence times (~ 2.5h), graph (d) contains the results from

a somewhat particular experiment. It was carried out at 120 °C, i.e. at the lower end of the temperature scale used in this work, and with an elevated initiator concentration (400 ppm). The combination of higher viscosity at this temperature and the slightly higher conversion lead during the course of experiment to the triggering of the gel effect. Both, ultrasound conversion measurement and offline GC clearly show the runaway of the reaction, which - after 5 hours - had to be aborted due to an excessive increase in pressure drop.

Since the conversion measurement by offline GC is not available right away during the experiment but needs at least several hours for the analysis to be done, the reason for this pressure increase inside the reactor could not be figured out immediately. Only the ultrasound measurement enabled the controller to realize the reactor instability with the tendency of a reaction runaway and to react by aborting before the situation got out of control (e.g. plugging of the reactor, bursting of sealings etc.).

It can, therefore, without doubt be stated that the inline conversion measurement by ultrasound is an important and useful tool for the monitoring of polymerization reactions.

Some improvements will need to be done concerning the reliability of the measurement, as for some experiments, the signal was seriously disturbed by inexplicable fluctuations of the speed of sound (figure 4.28), leading to a misinterpretation of the conversion by almost 20%.
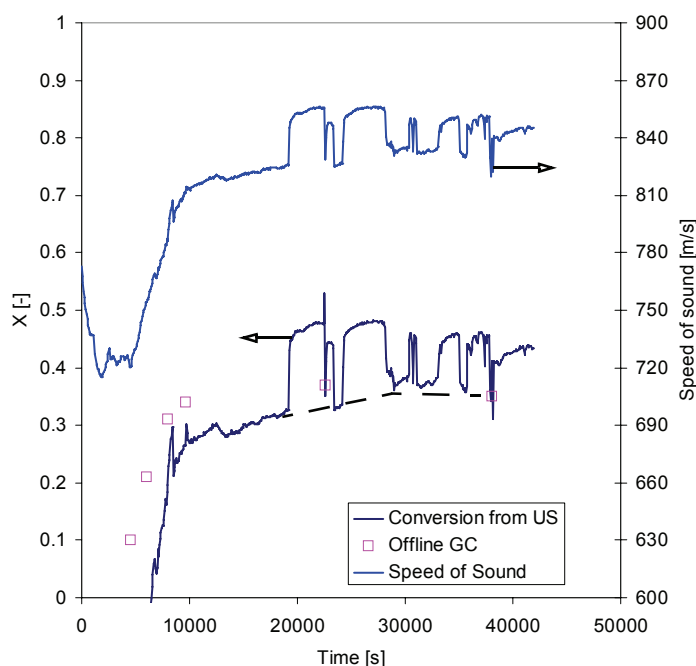
Figure 4.28: Fluctuations of the speed of sound signal during an experiment (140 °C, 3.5% MA, 250ppm TBPEH)

These fluctuations, which were characterized by a sudden increase of the measured speed of sound signal by 30 to 50 m/s, followed by a drop of the same size after a certain period of time, do not have their origin in pressure nor temperature changes, as proven in figure 4.29. The reason must, therefore, lie in the measurement, itself. It may, for example, be conceivable that a film layer of polymer forms on the sensors surfaces, which is flushed away irregularly. In this way, the ultrasound signal would correspond to a higher polymer weight fraction in the volume element between both sensors. However, the ultrasound signal is very sensitive to various external influences and in the end, it might also be a problem of the sensors' electronics at these temperatures. Concerning the interpretation of the curves presented in figure 4.28 it should be pointed out that without the fluctuations the signal would have continued on the dotted line and not on an average value inbetween the peaks.
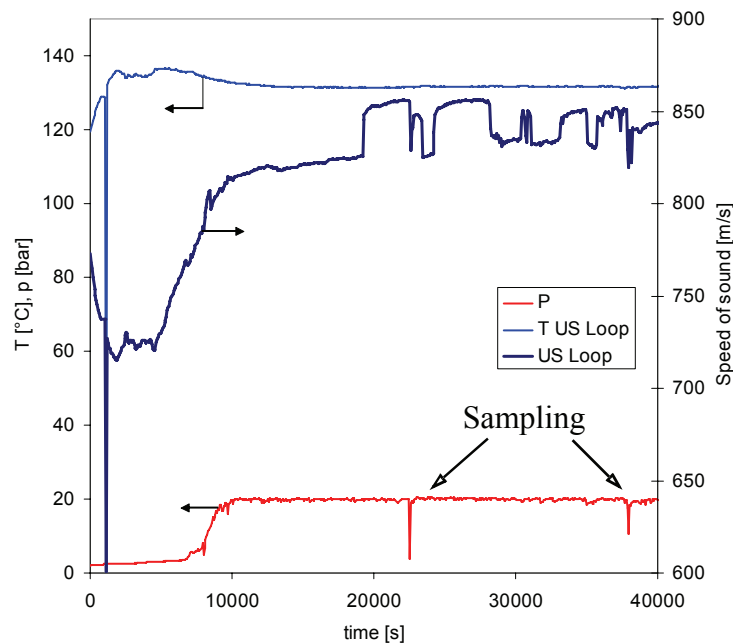
Figure 4.29: Speed of sound, pressure and temperature for the same experiment as in figure 4.28

4.3 Verification of the High-Temperature Kinetics

4.3.1 Results from the Pilot Plant

A complete list of all pilot plant experiments carried out in this work, together with the corresponding process conditions and a result overview can be found in appendix 7. Altogether, 23 experiments were accomplished under different conditions (i.e. 5 different temperatures, 3 different comonomer and chain transfer agent contents) and evaluated concerning monomer conversion, molecular weight and final product quality. The latter was characterized in collaboration with the analytical department of the industrial partner by determining:

- the molecular weight
- the residual volatiles (monomer and solvent)
- the comonomer weight fraction in the polymer
- the tacticity
- and the thermostability of each sample.

The aim for all experiments was to obtain monomer conversions of $\underline{X_{Loop} = 50\%}$ in the loop and an additional $\underline{X_{tube} = 30\%}$ in the tube reactor while maintaining the molecular weight of the final polymer in the region of $\underline{M_w = 100'000 \text{ g/mol}}$, which is an average value for commercial molding compound PMMA.

This goal was practically achieved for most experiments. The effective conversion range in the loop reactor lies around $X_{Loop} = 40 - 50\%$, except for some experiments where the conversion stayed particularly low (around 30%). For the tube, the conversion was determined at two points: the first at the sampling valve after two-thirds of the tube length, the second from the condensate samples, which corresponds to the total conversion over the whole process. The aim of achieving 30% conversion in the tube was only partly achieved, namely for the experiments with DTBP as initiator in the tube. For those with TBPIN (No. 1-5), the conversion was rather 20 than 30%, which is connected to its faster decomposition kinetics. At the injection point, the initiator is dosed into the tube as dilute solution in butyl acetate. This low-viscous liquid needs to be mixed thoroughly with the polymer melt from the loop reactor, which - at 40 - 50% conversion - is significantly more viscous (approximately by a factor 1000). If the decomposition of the initiator is -

relatively speaking - faster than the mixing, the produced radicals cannot be used efficiently for monomer initiation, which equals a very low efficiency factor. Therefore, the obtained conversion is significantly lower than it would be expected for a homogenous solution with the same amount of initiator. DTBP as a very slowly decomposing initiator does not exhibit this problem.

The molecular weight could be successfully adjusted to a region of Mw = 100'000 g/mol ± 20'000 g/mol. It was considerably higher only for experiments at 120 °C (No. 6-8), where it increased to Mw = 120'000 g/mol, and for those where the chain transfer agent was reduced on purpose (No. 4-5, Mw = 140'000-150'000 g/mol). With increasing temperature, the molecular weight slightly decreased as expected from theoretical considerations.

The tacticity of the final polymer was rather uniform for all experiments carried out in this work. The average distribution was 5 : 43 : 52 with respect to iso- : hetero- : syndiotactic polymer.

Concerning the residual volatiles concentration (VOC), the values were quite constant as well for the different experiments. This is not astonishing considering that the devolatilization conditions were always the same (p = 150mbar). With the one-step static flash devolatilization, the values presented in table 7 were obtained for the final polymer, which are very satisfying considering the simplicity of the devolatilization process, although they do not meet the requirements for commercial polymer yet (< 1000 ppm).

Table 7: Residual volatiles in the final polymer (one-step flash, p = 150mbar)

	Content in the final polymer	
	average	maximum
MMA	< 4500 ppm	< 8000 ppm
BuAc	< 100 ppm	< 1200 ppm
Dimer	< 33 ppm	< 100 ppm

4.3.2 R-parameters

For the kinetic description of copolymerizations according to the ultimate model (i.e. only the final monomer unit of an active chain is considered as influencing the propagation mechanism), there are four propagation reactions to take into account:

Propagation

$$P_{1,n}{}^{\cdot} + MMA \longrightarrow P_{1,n+1}{}^{\cdot} \qquad k_{p11}$$
$$P_{1,n}{}^{\cdot} + MA \longrightarrow P_{2,n+1}{}^{\cdot} \qquad k_{p12}$$
$$P_{2,n}{}^{\cdot} + MA \longrightarrow P_{2,n+1}{}^{\cdot} \qquad k_{p22}$$
$$P_{2,n}{}^{\cdot} + MMA \longrightarrow P_{1,n+1}{}^{\cdot} \qquad k_{p21}$$
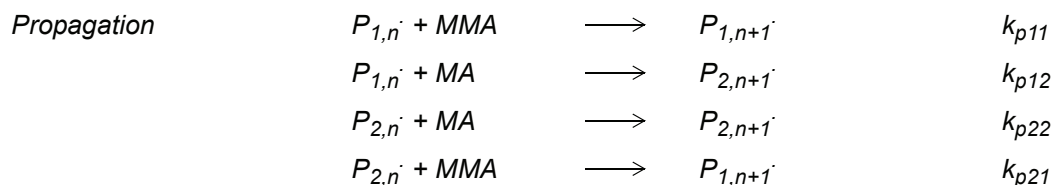
where $P_{1,n}{}^{\cdot}$ and $P_{2,n}{}^{\cdot}$ represent the MMA, respectively MA terminated chain radicals.

As to the rate coefficients, it is either necessary to know all four of them separately, or to express the cross-propagation (e.g. propagation of an MMA-terminated chain with an MA monomer) by so-called reactivity ratios or "r-parameters":

$$r_{12} = \frac{k_{11}}{k_{12}} \text{ and } r_{21} = \frac{k_{22}}{k_{21}} \qquad \text{(EQ 4.19)}$$

These r-parameters express the probability for an active polymer chain to react with either the one or the other monomer for a binary copolymerization. They are determined experimentally by the Tüdös-Kelen-approach [90], which is a further-development of the equations derived by Lewis-Mayo and Fineman-Ross [91].

For the relative change of monomer consumption as a function of the instantaneous monomer ratio *[MMA]/[MA]*, it can be written

$$\frac{d[MMA]}{d[MA]} = \frac{1 + r_{12} \cdot [MMA]/[MA]}{1 + r_{21} \cdot [MA]/[MMA]} = \frac{[MMA]}{[MA]} \cdot \frac{r_{12} \cdot [MMA] + [MA]}{r_{21} \cdot [MA] + [MMA]} \qquad \text{(EQ 4.20)}$$

This equation also describes the instantaneous polymer composition for small conversion changes.

For the determination of the r-parameters from experimental data, equation 4.20 needs to be linearized by setting *y = d[MMA]/d[MA]* and *x = [MMA]/[MA]*:

$$y = x \cdot \frac{1 + r_{12}x}{r_{21} + x} \quad \text{and further to} \quad \frac{(y-1)}{x} = r_{12} - r_{21} \cdot \frac{y}{x^2} \tag{EQ 4.21}$$

This equation can be further simplified by introducing $G = \frac{x(y-1)}{y}$ and $F = \frac{x^2}{y}$:

$$G = r_{12}F - r_{21} \quad \text{respectively} \quad \frac{G}{F} = r_{12} - \frac{r_{21}}{F} \tag{EQ 4.22}$$

Equation 4.22 is also called the Fineman-Ross equation. Tracing G against F or G/F against $1/F$ gives r_{12} as the slope and r_{21} as the intercept or vice-versa, respectively.

However, this method is not very well balanced since the slope of a straight line fitted through experimental data is overly influenced by points at the far end of the scale. The result might, therefore, change for experiments with different concentration values [MMA] or [MA], or when, for example, the monomer indices are inverted and the calculation is repeated. Kelen and Tüdös propose an equilibration algorithm in order to equally weigh the experimental points from the whole range of concentration values in form of equation 4.23:

$$\frac{G}{\alpha + F} = \left(r_{12} + \frac{r_{21}}{\alpha}\right) \cdot \frac{F}{\alpha + F} - \frac{r_{21}}{\alpha} \tag{EQ 4.23}$$

where α denotes a constant ($\alpha > 0$), which is arbitrarily defined by the authors to be $\alpha = \sqrt{min(F) \cdot max(F)}$. By introducing

$$\eta = \frac{G}{\alpha + F} \quad \text{and} \quad \xi = \frac{F}{\alpha + F} \tag{EQ 4.24}$$

equation 4.23 can be written

$$\eta = \left(r_{12} + \frac{r_{21}}{\alpha}\right) \cdot \xi - \frac{r_{21}}{\alpha} \tag{EQ 4.25}$$

The variable ξ can only take values in the interval $(0, 1)$, therefore tracing the variable η against ξ delivers the parameters r_{12} and r_{21} as intercepts.

The described method is only valid in approximation for very small conversions, because otherwise equation 4.20 would have to be integrated.

In case of the continuous recycle loop reactor at steady state, where the conversion does not increase over time, the concentration difference between the feed and the reactor solution can be employed instead. Thus, the expression for *y* in equation 4.21 becomes:

$$y = \frac{d[MMA]}{d[MA]} = \frac{\dfrac{[MMA]_{feed}}{1 + \varepsilon \cdot X} - [MMA]}{\dfrac{[MA]_{feed}}{1 + \varepsilon \cdot X} - [MA]} \qquad \text{(EQ 4.26)}$$

The feed concentration must be corrected by the volume contraction ε, which occurs during the polymerization reaction, so that it can be compared to the concentration in the reactor.

In literature, the following r-parameters can be found for the monomer pair MMA / MA measured at low temperatures (< 80 °C) except for one value at 130 °C:

Table 8: r-parameters for MMA / MA from literature

r_{12}	r_{21}	$T_{exp.}$	Source
1.8 ± 0.4	0.35 ± 0.1	65 °C	[92]
2.3 ± 0.5	0.47 ± 0.1	130 °C	[92]
2.36 ± 0.32	0.42 ± 0.08	50°C	[93]
2.15	0.4	80°C	[94]

However, it was observed in this work that the amount of comonomer (MA) incorporated in the final polymer increases with temperature. As a matter of fact, the amount of methyl acrylate in the polymer approaches the feed concentration with increasing temperature as depicted in figure 4.31, which means that the r-parameters have to change, too. The literature values are, therefore, not correct for the temperature range of interest as they lead to too low MA contents in the polymer (compare figure 4.30).

Experiment	MA content in Copolymer (modeled)	MA content in Copolymer (experimental)
160 °C 3% MA	1.5 wt%	2.3 wt%

(a)
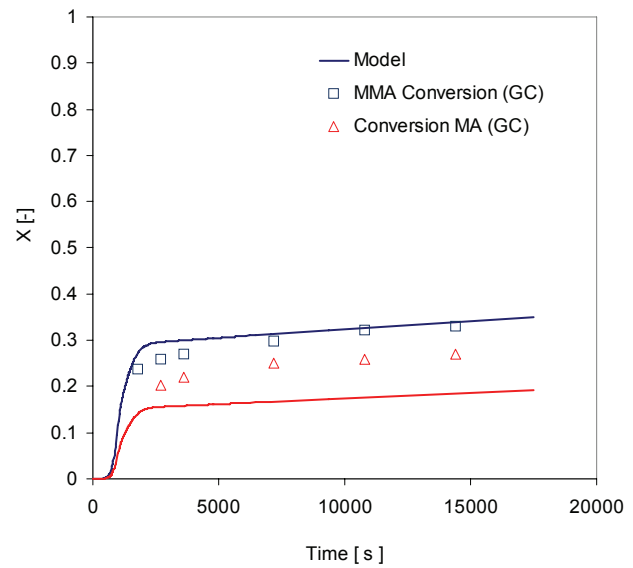
(b)

Figure 4.30: Testing of literature r-parameters (r_{12} = 2.3 and r_{21} = 0.47)
(a) Experimental and modeled copolymer composition for loop experiment
(b) Modeled and Experimental MMA/MA Conversion for batch experiment (150°C)

In order to refine, respectively, redetermine the r-parameters for temperatures in the region of 140 - 170 °C, pilot plant experiments with varying MA feed concentration (1.5, 3.5 and 5.5 weight-%) were carried out and the results analyzed according to the above described method. The MA content could not be increased further due to two reasons: Firstly, the reaction rate and heat of the MA polymerization is much more intense and an experiment with more than the mentioned amounts could be difficult to handle in the available installations. Secondly, the propagation rate for MA is not necessarily constant for high MA concentrations as has been shown by Nagy and Tüdös [95], which would open a completely new problematic of determining the dependence of k_{p22} on the acrylate concentration. For these reasons the use of higher concentrations was renounced in this work.

However, the problem with low MA concentrations is the precision in the determination of r_{21}. Since for the investigated cases, MMA is the dominant monomer, the influence of the reactivity ratio for MA-terminated polymer chains does not play a major role for the consumption of MA monomer. While for r_{12} more or less reproducible values could be found, the ones for r_{21} varied considerably inbetween different experiments and, accordingly, their reliability is uncertain.
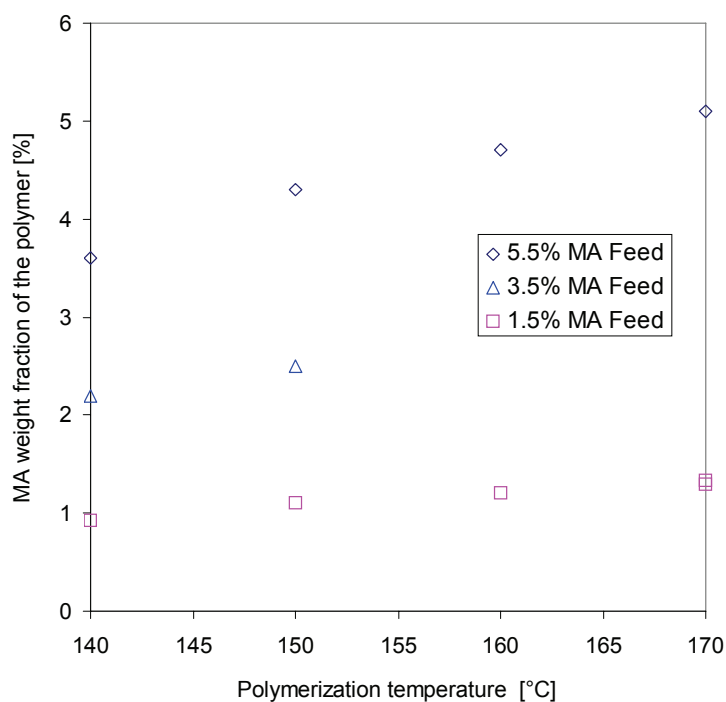
Figure 4.31: MA content in the final polymer depending on temperature and feed composition

A complicating factor was the correct determination of the MA conversion for the loop samples from the pilot plant. Due to the considerably lower boiling point of methyl acrylate (bp. = 80 °C), it evaporates more easily from the sample solution while being transferred from the sampling tube into screw cap vials (unfortunately, with the sampling technique used in this work, the samples cannot be shock-frozen directly). As a result of this sampling error, many samples exhibited a slightly higher conversion for MA than for MMA, which is unrealistic with regards to literature data and the fact that the acrylate weight fraction in the final polymer was always below the feed weight fraction of MA, which proves that the acrylate is consumed more slowly than the methacrylate. However, with $X_{MA} \sim X_{MMA}$ or even $X_{MA} > X_{MMA}$, the results obtained for the r-parameters following the described method are misleading.

In the end, only for two data series (at 160 °C and 150 °C) the obtained experimental data could be used for the determination of r-parameters. The analysis results are presented in table 9 and table 10.

Table 9: Results from three copolymerization experiments at T = 160 °C

	1.5% MA Feed	3.0% MA Feed	5.5% MA Feed
Final polymer composition	1.2 wt% MA	2.3 wt% MA	4.7 wt% MA
MMA loop conversion	44.8 %	30.3 %	35.2 %
MA loop conversion	38.2 %	25.7 %	31.9 %

Table 10: Results from two copolymerization experiments at T = 150 °C

	1.5% MA Feed	5.5% MA Feed
Final polymer composition	1.1 wt% MA	4.3 wt% MA
MMA loop conversion	45.3 %	36.7 %
MA loop conversion	48.1 %	39.5 %

With the results from this tables, the r-parameters could be estimated graphically according to the Kelen-Tüdös method by calculating and tracing η and ξ. For comparison, the y in equation 4.21 was calculated from both, the final polymer composition and the loop sample composition, even if the use of the polymer composition is not fully correct as the polymer sample was taken at the end of the pilot reactor and the polymer composition still changes during the course of polymerization in the tube reactor.

The graph containing the tracing of η over ξ is depicted in figure 4.32 for the example of the experiment at 160 °C. The resulting r-parameters for T = 160 °C are $r_{12} = 1.55$ and $r_{21} = 3.59$ for the calculation based on the loop sample data and $r_{12} = 1.89$ and $r_{21} = 3.07$ for the polymer composition data. For 150 °C, on the other hand, the values were determined from the loop sample concentration to be $r_{12} = 1.47$ and $r_{21} = 0.79$.
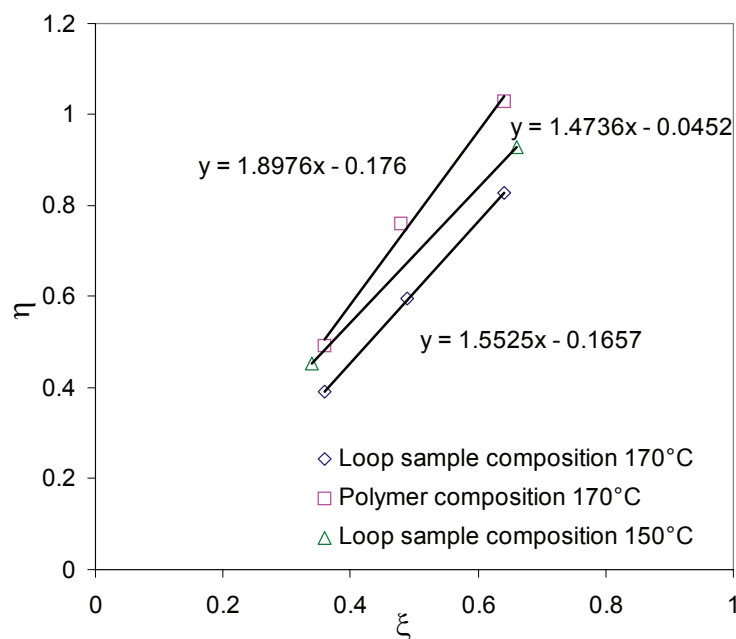
Figure 4.32: Kelen-Tüdös plot for the determination of r-parameters (160 °C and 150 °C data from table 9)

It is obvious that the value for r_{21} at 160 °C is far off the expected scale in comparison to literature data (table 8) and it is also in contradiction to the fact that MMA is preferably incorporated in the growing chains (i.e. $r_{21} < 1$!). This is due to the problem that with the experimental conditions in this work, i.e. the extremely low MA content, it is not possible to unambiguously solve the copolymerization balance equation with the employed graphical method, as it will be demonstrated in the following:

From the r-parameters determined by the above method and those from literature, it is possible to draw a phase diagram of the monomer and polymer composition in terms of MMA content (see figure 4.33). It can be seen that for the pair of parameters determined beforehand by the Kelen-Tüdös method ($r_{12} = 1.55$ and $r_{21} = 3.59$), an azeotropic course of the curve is obtained, whereas for the literature values from Grassie [92] determined at 130 °C, the curve does not cross the 45° line corresponding to equal feed and polymer composition. Regarding the measured data points in the upper right corner, it becomes evident that there exist several combinations of r_{12} and r_{21} that lead to a satisfying description of the found polymer compositions. For the experiments carried out at 150 °C, the found pair of r-parameters happens to fulfill the requirement $r_{21} < 1$. However, the solution $r_{12} = 1.55$ and $r_{21} = 3.59$ for 160 °C would lead to completely unrealistic

results at higher MA concentrations. It must, therefore, be found a way to force the Kelen-Tüdös fit to stay in the upper region of the diagram, i.e. to limit the allowed values for r_{21} to values smaller than one.

One way to do so is the introduction of a "dummy point" at the other end of the scale. Adding a fictitious feed composition of $x_{MMA} = 0.05$ / $x_{MA} = 0.95$ and a corresponding copolymer composition of $y_{MMA} = 0.07$ / $y_{MA} = 0.93$ for the fitting, i.e. a value far away from the region of interest in this work, leads to the desired result that the curve will have to pass on top of the 45° line without falsifying the measured data.
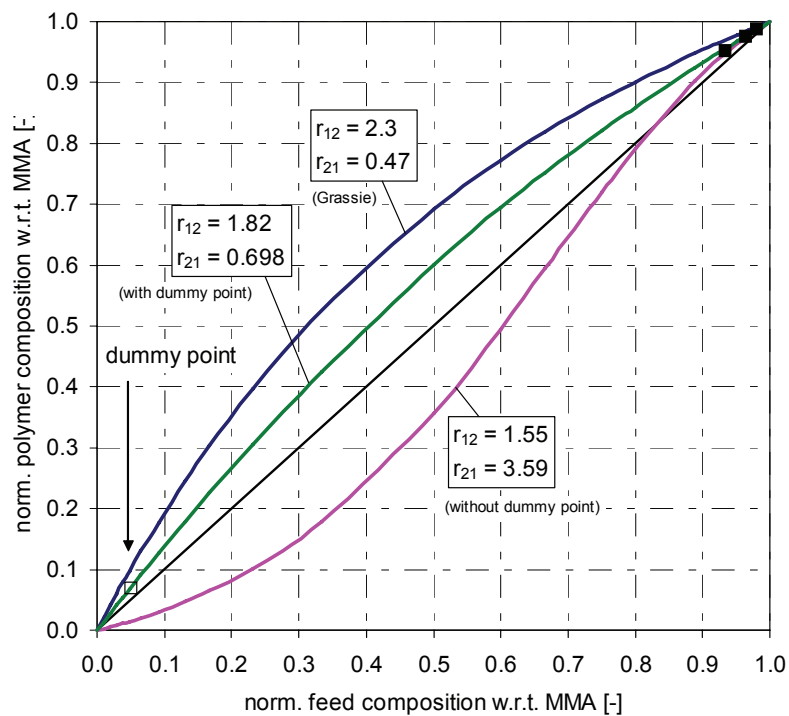
Figure 4.33: Phase diagram of the feed and polymer composition for different pairs of r-parameters (i.e. different solutions of the copolymer balance)

Re-evaluating the experimental data by means of the Kelen-Tüdös approach with this added dummy point yields, in fact, a value < 1 for r_{21}, while the measured data points for high MMA concentrations are still well matched by the curve. Figure 4.34 shows the Kelen-Tüdös graph from figure 4.32 for the loop sample composition at 150 °C and 160 °C with the added dummy points for a low MMA concentration. The slope of the 160 °C data fit has changed significantly with regards to figure 4.32 and the line is now almost parallel to the one for the 150 °C data. From

the way how the 160 °C line now crosses the three measured points it is now obvious why without the dummy point unrealistic values are obtained.
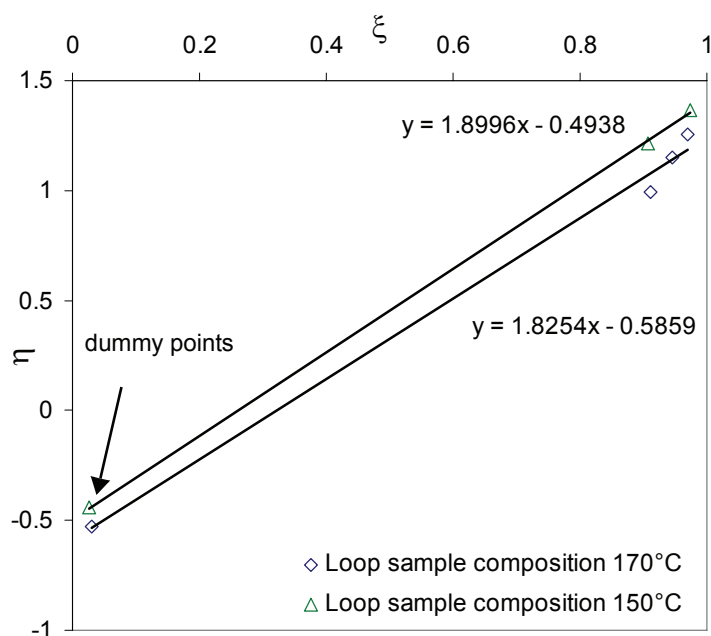
Figure 4.34: Kelen-Tüdös plot for the determination of r-parameters using a dummy point (x=0.053/y=0.111)

The r-parameters obtained from the curves in figure 4.34 are listed in table 11. Due to the missing experimental values for higher MA concentrations, these r-parameters can only serve as an indication of their order of magnitude. In order to determine them with higher certainty, experiments over the whole range of MA concentrations would need to be carried out. The problem in doing so is that for high acrylate concentrations, the propagation rate constant k_{p2} is no longer constant but a function of the acrylate content [95], which complicates significantly the determination of the reactivity ratios.

Table 11: r-parameters for the MMA/MA-system at 150 °C and 160 °C determined from experimental data by using a dummy point for correction of the r_{21}-value

	150 °C	160 °C
r_{12}	1.899 ± 0.02	1.825 ± 0.1
r_{21}	0.457 ± 0.02	0.698 ± 0.1

To verify the estimated parameters, they were put in the kinetic model for the MMA/MA copolymerization in PREDICI and the thus calculated copolymer composition as well as MMA and MA conversion compared to experimental data. The results are presented in the following.

Table 12: Modeled and experimental copolymer compositions for different conditions

			Copolymer composition		
Experiment	T	MA feed content	modeled		Exp.
No.	[°C]	wt-%	mol-%	wt-%	wt-%
10	150	1.5	1.1	1.0	1.1
12	150	5.5	4.1	3.6	4.3
13	160	1.5	1.3	1.1	1.2
14	160	3	2.6	2.3	2.3
15	160	5.5	4.8	4.2	4.7
16	170	1.5	1.3[a]	1.2[a]	1.3
17	170	5.5	4.9[a]	4.3[a]	5.1

a. Calculated with the r-parameters for 160 °C
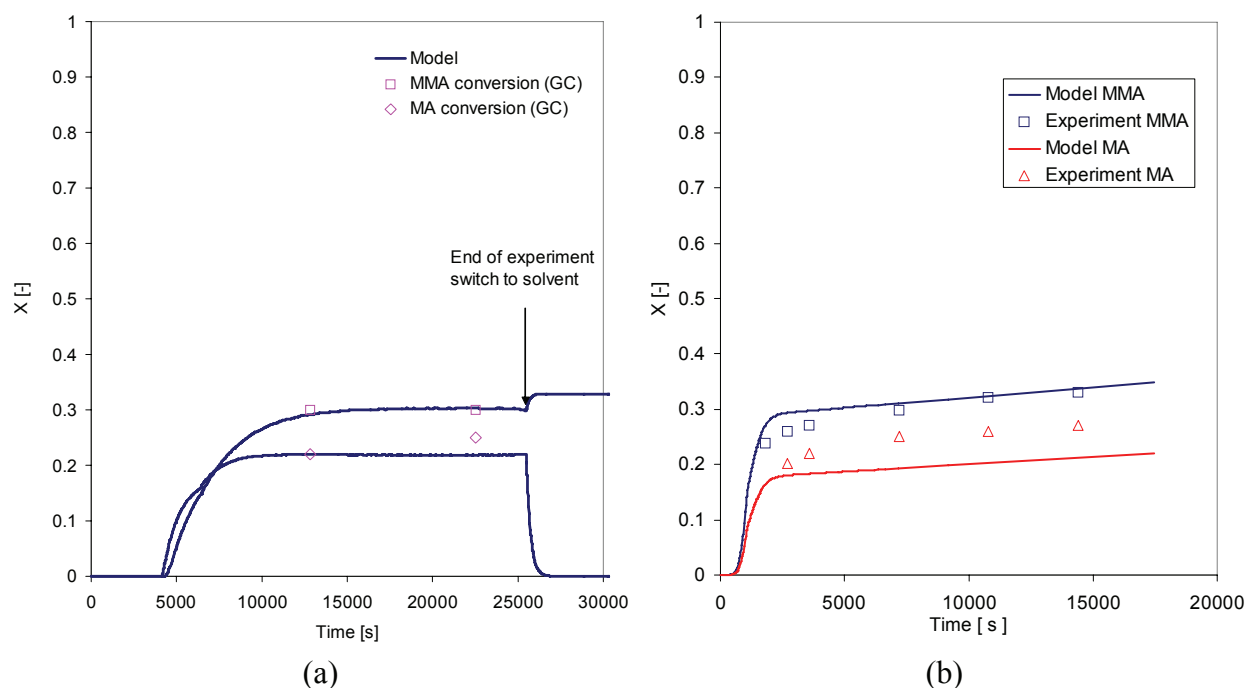
Figure 4.35: (a) MMA and MA conversion for loop experiment (No. 14, 160 °C, 3% MA)
(b) MMA and MA conversion for batch experiment (150 °C, 3% MA)

Table 12 contains the feed and polymer composition data from several copolymerization experiments at different temperatures and comonomer feed ratios. The agreement between modeled and analyzed copolymer composition is rather good, although for 150 °C and 170 °C the model underestimates the MA content of the polymer. For the first case, this might be a hint that the r_{21} value determined at 150 °C (r_{21} = 0.457) is too low. At 170 °C, on the other hand, the incorporation of MA in the chain is stronger than at 160 °C as seen above (figure 4.31). Therefore, with the 160 °C parameters used in the modeling, the MA polymer content is underestimated. Another explanation for the discrepancies is that the polymer composition was determined for the final polymer, i.e. from reactor exit, whereas the modeled values are for the loop exit. During the continuing polymerization in the tube reactor, the concentration of MA increases as it consumed slowlier than MMA. Therefore, the MA fraction in the copolymer will be higher in the final polymer than in the loop sample, which is correctly mirrored by the results in table 12.

Figure 4.35 contains the conversion evolution at 160 °C for the loop reactor (a) and for 150 °C in the batch reactor (b). In the left graphic, the agreement is very good for the obtained r-parameters. For the 150 °C batch experiment, on the other hand, the model underestimates as already for the polymer composition the reactivity of MA and predicts a lower MA conversion

than actually measured. This is a second indication that the r-parameters at 150 °C need to be readjusted.

It should be kept in mind, though, that for the investigated cases, the copolymer composition is mainly governed by the r_{12}-value, since MMA is the dominating monomer and that this r_{12}-value could be determined quite reliably in this work. For polymerizations with higher MA concentration, the results might be less precise due to the uncertainty connected with the determination of r_{21}. It is, therefore, necessary to consider further experiments with higher MA fractions in order to improve the precision of r_{21}.

Another important issue to take into account when further increasing the temperature (>170 °C), is the depolymerization. Due to the depolymerization mechanism (unzipping, see chapter 5 "Thermal stability"), which only works for methacrylates and is stopped by the occurrence of acrylates in the chain, the incorporation of acrylate becomes more pronounced at high temperatures: while the effective propagation rate for MMA needs to be corrected by the depolymerization

$$k_{p1, effective} = k_{p, 1} - \frac{k_{dp}}{[MMA]}$$

(EQ 4.27)

the propagation of the acrylate is, in first approximation[1], not influenced by this mechanism. This is the reason why the acrylate fraction increases disproportionally much for very high temperatures, an issue that is not taken into account by the r-parameters.

4.3.3 Chain Transfer Constants

In order to correctly predict the molecular weight distributions in the modeling, the chain transfer constants for all transfer reactions are needed at the given temperature range. For the transfer to monomer and solvent, these are taken from literature or assumed to be constant (see appendix 3). However, in the presence of a strong chain transfer agent, like the n-dodecanethiol used in this work, their influence on the molecular weight can be neglected without any remark-

---

1. This is valid for the "ultimate" model only. For the "penultimate" model, i.e. when the second-last element of the active radical chain is taken into account, too, the depolymerization needs to be considered. However, this would lead too far concerning the frame of this work.

able deterioration of the model precision. The transfer constants for thiols are, indeed, by almost a factor 10^4 higher than the ones for monomer and solvent transfer [47].

The value of the transfer constant for n-dodecanethiol (DDT) can be found in literature [96]:

$$C_{DDT} = \frac{k_{CTA}}{k_p} = 0.678$$

(EQ 4.28)

However, as for so many rate constants found in literature for the MMA polymerization, the temperature range of its determination is 20 °C < T < 80 °C and it cannot be said for sure if the same value applies to higher temperatures. The aim was, therefore, to redetermine the chain transfer constant for the system MMA/DDT from the results of high-temperature experiments.

Several experiments at various concentration ratios [CTA]/[MMA] were carried out and the results treated by two different methods. A detailed description of these methods can be found in an article by De la Fuente and Madruga [97].

The first one is the *Mayo*-method. It is generally known that, according to the *Mayo equation*, the degree of polymerization $\overline{DP}_n$ in the presence of a transfer agent is related to the one of a polymerization without transfer agent $\overline{DP}_{n,0}$ as follows:

$$\frac{1}{\overline{DP}_n} = \frac{1}{\overline{DP}_{n,0}} + C_{CTA} \cdot \frac{[CTA]}{[M]}$$

(EQ 4.29)

where C_{CTA} is the transfer constant, *[CTA]* the concentration of the transfer agent and *[M]* the concentration of the monomer. The transfer constant is determined graphically rather than from two points only, by tracing $\frac{1}{\overline{DP}_n}$ against $\frac{[CTA]}{[MMA]}$.

Usually, the number-average degree of polymerization is to be taken. However, the exact determination of the number-average molecular weight $\overline{M}_n$ is usually flawed with a rather large error due to a very pronounced baseline sensitivity as regards the peak integration in SEC measurements. The determination of the weight average molecular weight $\overline{M}_w$ is much more robust and less sensitive to the choice of the baseline. De la Fuente and Madruga propose, therefore, to take the weight-average molecular weight divided by a factor 2 for the Mayo-plot, which holds true for most CTA regulated polymerizations[1]. In this work, calculations with both values were

compared to each other and no significant difference could be found, as will be shown later in this subchapter.

An alternative method for the determination of C_{CTA} is developed in the paper of De la Fuente and Madruga, which is based on the shape of the number average molecular weight distribution of the produced polymer. For a system where the chain transfer to initiator, monomer and solvent can be neglected compared to that of the CTA, the molecular weight distribution at any instant will follow an exponential decay as presented in equation 4.30 [97].

$$\lim_{\substack{M \to \infty \\ [I] \to 0}} P(M) = B \cdot \exp\left(-\frac{k_{CTA} \cdot [CTA] \cdot M}{k_p \cdot [MMA] \cdot M_0}\right) \tag{EQ 4.30}$$

where $P(M)$ is the number distribution of molecular weight M, M_0 the monomer molecular weight and B a proportionality constant. The number distribution $P(M)$ can be obtained by SEC measurement of the polymer from the calibrated SEC molecular weight distribution $Wf\ (log\ M)$:

$$P(M) = W_f(\log M) \cdot \frac{\log e}{M^2} \tag{EQ 4.31}$$

By plotting the number-average molecular weight distribution obtained in equation 4.31 as *ln P(M)* against the molecular weight M, a straight line is obtained for the region of the distribution that is controlled by the CTA, whose slope Λ corresponds to

$$\Lambda = -C_{CTA} \cdot \frac{[CTA]}{[MMA] \cdot M_0} \tag{EQ 4.32}$$

Analogous to the Mayo plot, the C_{CTA} value is obtained graphically from the slope of the plot Λ against $\frac{[CTA]}{[MMA]}$ for experiments with different CTA content, in order to obtain a higher precision than for only one experiment. Figure 4.36 contains the plotting of *ln P(M)* against M, from which the slopes Λ presented in table 13 were determined.

---

1. The polydispersity $PD = \dfrac{\overline{M_w}}{\overline{M_n}}$ is usually in the region of 2 for radical polymerizations with chain transfer agent.

Table 13: Results from pilot plant experiments for the determination of the DDT chain transfer constant at T = 140 °C (Initiator [TBPEH] = 250ppm)

Exp. No. (appendix 7)	$10^3 \dfrac{[CTA]}{[MMA]}$	$\overline{M}_n$ [g/mol]	$\overline{M}_w$ [g/mol]	$PD = \dfrac{\overline{M}_w}{\overline{M}_n}$	$\Lambda \cdot 10^5$
4	1.13066	84'187	162'070	1.93	-1.04
1	1.69599	51'264	106'303	2.07	-1.55
5	2.82665	35'328	73'022	2.07	-2.54
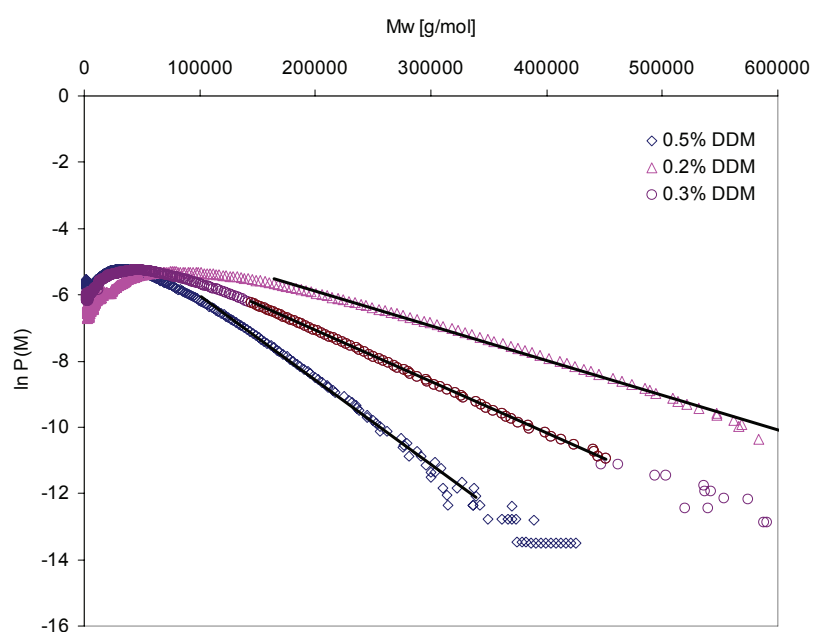
Figure 4.36: Plot ln P(M) against M according to equation 4.30

With the values from table 13, the following two graphs can be drawn, leading directly to the chain transfer constant for n-dodecanethiol (slopes):
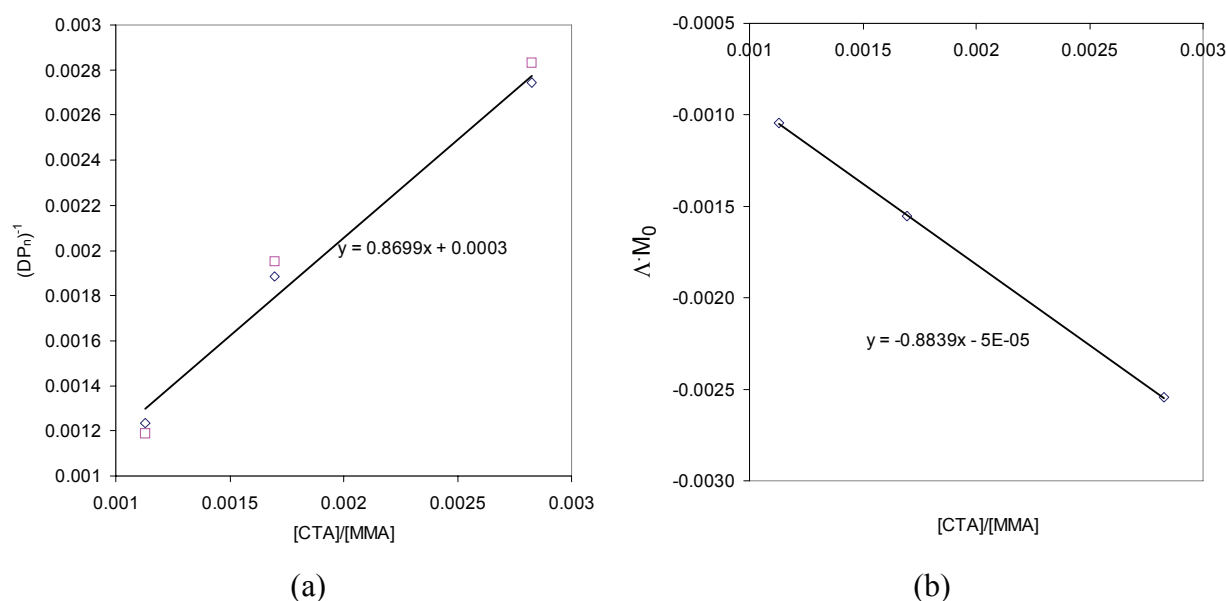
*Figure 4.37: (a) Mayo plot for M_n resp. M_w values from table 13
(b) Plot of the slopes from the lnP(M) plot against [CTA]/[MMA]*

The results for the chain transfer constant from both methods match very well. However, compared to literature values, they are slightly higher. This means that the transfer reaction becomes more important at higher temperatures than it is the case below 100 °C.

It should be pointed out that in order to achieve correct values for the chain transfer constant, the MMA and CTA concentrations in the loop reactor at steady state have to be taken into account in eqs. 4.29 and 4.30. Unfortunately, it was not possible during the course of this work to determine the CTA concentration in the loop samples by analytical methods. Therefore, it was estimated using the kinetic model developed in this work, for which the transfer constant from literature ($C_{DDT} = 0.678$ at 80°C) was used. This is, of course, a simplification but due to the expected relatively small increase of C_{DDT} with temperature, it was reckoned that this does not have a huge impact on the conversion / concentration and that, therefore, the determination of C_{DDT} is sufficiently exact.

Table 14: Values for the chain transfer from n-dodecanethiol to MMA at T = 140 °C

	Mayo method	MWD method
$C_{DDT} = \dfrac{k_{CTA}}{k_p}$	0.870 ± 0.018	0.884 ± 0.01

4.4   Modeling the pilot plant

With the kinetic model established in PREDICI®, which is described in detail with all kinetic constants and reaction steps in appendix 3, it is possible to predict many process variables for the continuous pilot plant, among which are the monomer conversion, the molecular weight and the speed of sound to be expected for the corresponding reaction conditions. In this chapter, first the validation of the model with experimental data is presented, before in a second part, a parameter variation is carried out in order to demonstrate the utility of a working model for process development.

The model for the continuous polymerization process had to be split into two parts: one CSTR model, describing the recycle loop (for recycle ratios > 30 [83] this is admissible), and one tube reactor model for the second part of the reactor. While for the CSTR model, dynamic simulations of the startup and switch-off phase are possible, the tube model only allows the modeling of steady state.

The connection between both models is realized by means of a so-called "initial data sheet" containing all necessary parameters from the exit of the CSTR reactor at steady state. This data sheet is loaded into the tube model and defines all concentrations and molecular weight profiles at position 0 of the tube reactor. An additional feed is included for the injection of solvent and second initiator into the tube.

4.4.1 Model validation for the continuous polymerization

The validation of the model with experimental data is carried out in the following by means of the results from several different pilot plant experiments. Due to the vast amount of data acquired during the series of pilot plant trials and the repetition that would be connected to a presentation of all different pilot plant experiments, only few exemplary experiments are presented here.

One major point concerning the modeling of the pilot plant process is the correct prediction of the monomer conversion. The data presented in figure 4.38 proves the good agreement of the model with the experimental results for three pilot plant experiments at 150 °C, 160 °C and 170 °C for the loop and the tube. It is clearly visible how with increasing temperature, the conversion in the loop is slightly increased, too. In the tube reactor, the curve at 170 °C flattens quite quickly due to initiator burn-out ($\tau_{1/2}$(DTBP) ~ 10 min). For 150 °C, on the other hand, the maximum conversion is not reached at the end of the tube, which means that initiator is still present and the polymerization can continue in the preheater of the devolatilization (T = 250 °C). This is not desirable due to the high radical flux created, which might influence the thermal stability of the polymer.
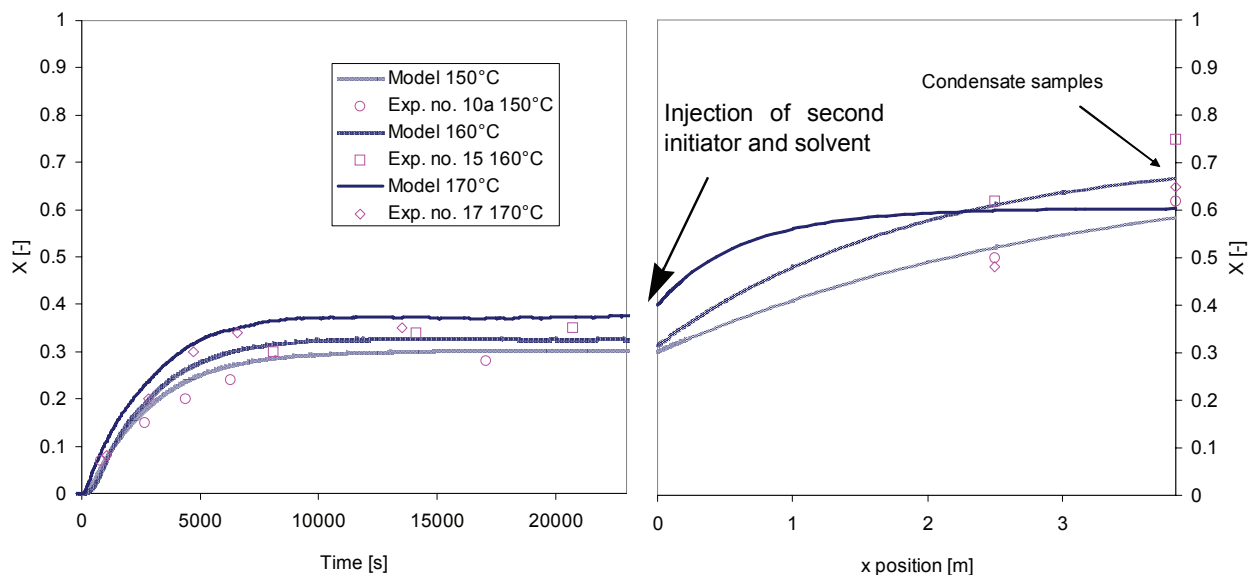
Figure 4.38: Conversion evolution, modeled and experimental data, for pilot plant experiments no.10a, 15 and 17 (150°C, 160 °C, 170°C)

Figure 4.39 shows the conversion evolution for a polymerization carried out at 140 °C with 250ppm TBPEH as initiator. As the graph reveals, the polymerization is entering the gel effect region and does not arrive at steady state. In fact, the experiment was stopped after 6 hours before the conversion increase was becoming too dramatic. However, the process simulation could have revealed before carrying out the experiment that the chosen conditions would lead to an unstable reactor behaviour with the risk of autoacceleration. In a larger scale production plant with a much higher inertia than the pilot plant, these process conditions could have had severe consequences. This demonstrates how important it is to have a working model, which makes it possible to predict the course of an experiment before actually running it.
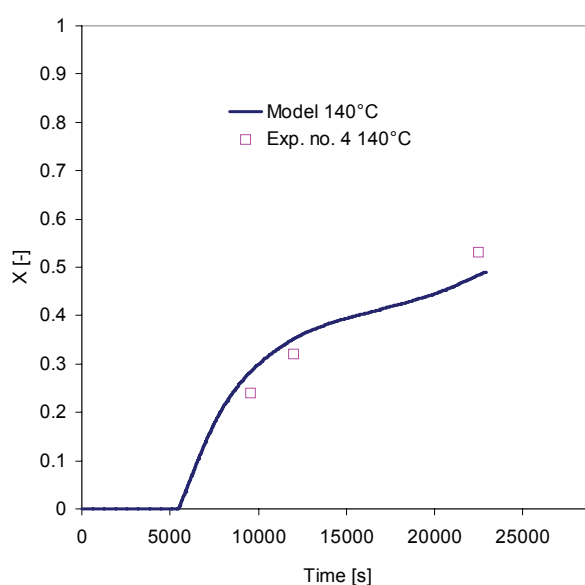
Figure 4.39: Conversion evolution for experiment no. 4 at 140 °C with reduced chain transfer agent (0.2% DDT), exhibiting a commencing gel effect

The model was also validated concerning the molecular weight prediction. PREDICI® not only allows the calculation of average molecular weights, but also the complete distribution modeling. In figure 4.40, the evolution of the average molecular weight in number, respectively in weight, in both reactors (loop and tube) is presented for experiment no. 15 (160 °C). Both molecular weight values rise quickly to a steady value, which is in good agreement with the values determined by GPC from several samples over time. Due to the addition of a second initiator to the tube reactor, the values decrease slightly with increasing conversion in the tube. As last sampling point the value from the polymer at the reactor exit is taken.

The same good agreement is found for the simulated and measured M_w distributions, as shown in figure 4.41. The predicted ultrasound signal, which is based on the theoretical speed of sound for the reaction mixture composition calculated by the model, follows the measured signal rather closely, too. The difference in the beginning of the reaction (after the feed-switch) illustrates the difference between the ideal reactor behaviour of the model and the real reactor, which "follows" the ideal curve with a little delay. When the reactor reaches steady state, the values match very well again. However, a little later after the first sample has been taken, the measured signal increases further by ~30m/s whereas the predicted signal does not change anymore. The measured increase might be due to the formation of a polymer film on the probe heads as discussed in the section dealing with the ultrasound technique in this chapter.
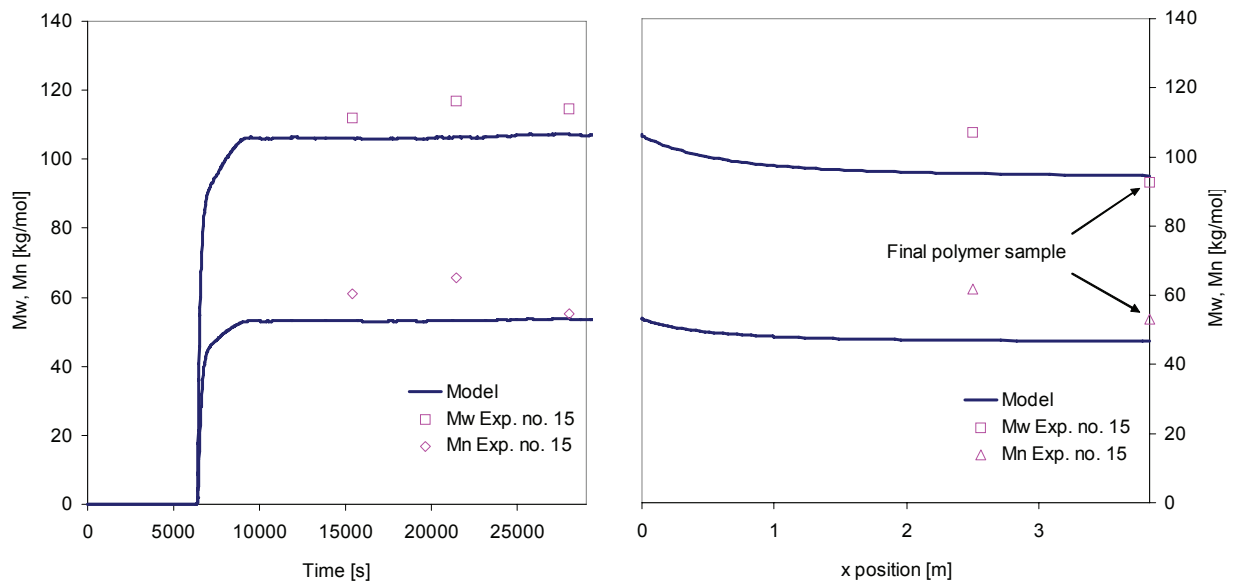
Figure 4.40: Molecular weight evolution, modeled and experimental data, for pilot plant experiment no.15 (160 °C, 3%MA, 250ppm TBPIN loop, 250ppm DTBP tube, 22% BuAc im tube)
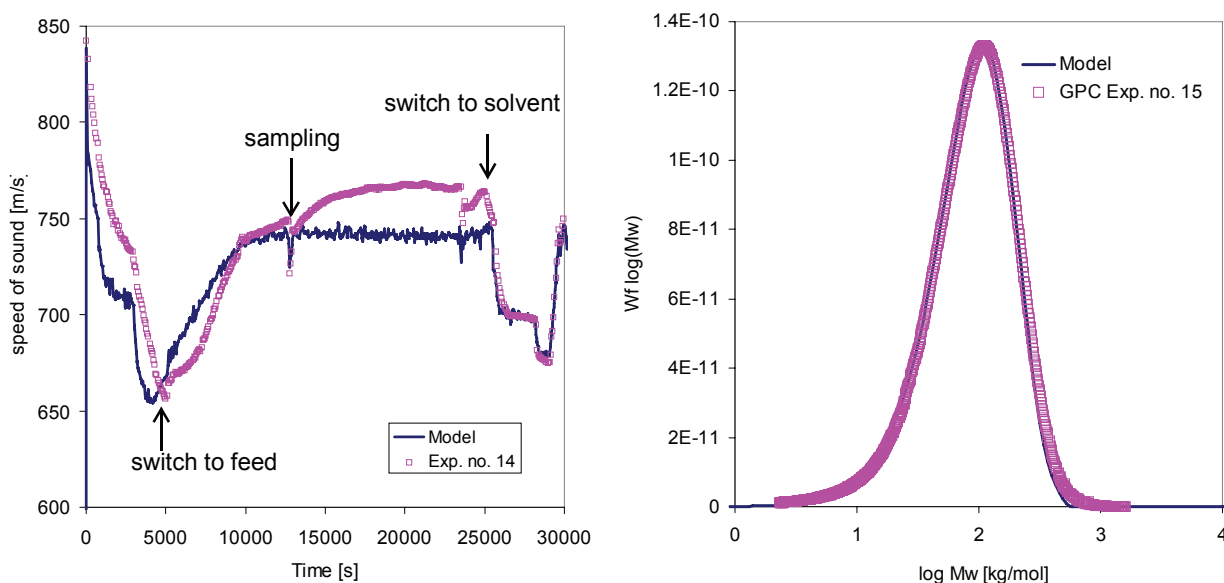
Figure 4.41: Ultrasound signal and molecular weight distribution (at loop exit), modeled and experimental data, for experiment no. 14 (150 °C, 3%MA, 250ppm TBPIN) resp. no.15 (160 °C, 3%MA, 250ppm TBPIN)

4.4.2 Variation of process parameters - Model predictions

With the working kinetic model for the continuous polymerization process, it is possible to run through several scenarios of varying process parameters in order to say something about the process stability or to predict possible courses of reactions. This is to be done in the following for the example of the loop reactor. For the demonstration of the possibilities one has with a kinetic model, the parameters residence time, temperature, amount of initiator and solvent content were varied and the results evaluated with respect to the impact of each variation on conversion and molecular weight with special attention focused on the triggering of the gel effect.

Varying the residence time

Depending on the initiator, which is employed, as well as on the temperature of the reactor, changing the residence time can have severe consequences for the stability of a process. In the presented example, a polymerization at 140 °C with 250ppm of TBPIN is modeled and the residence time varied from ~10 to ~80 minutes. A change of the residence time can, for example, be caused by a technical problem or operators error with the feed pump(s) (result: higher residence times) or by the formation of polymer films inside a tubular reactor due to fouling (result: lower

residence times). For this example, a relatively slowly decomposing initiator (TBPIN) is compared to a faster decomposing one (TBPEH) in order to demonstrate the effect on conversion.

It can be seen from figure 4.42 that the polymerization is stable for residence times up to ~33 minutes. However, above this value, the reaction enters the autoacceleration zone and the conversion is continuously driven to higher values. Further reducing the residence time leads to a strong reaction acceleration followed by almost full conversion, which, in reality, would be impossible to handle due to viscosity issues. For the faster decomposing initiator TBPEH, this effect is slightly less pronounced, in particular for very high residence times.
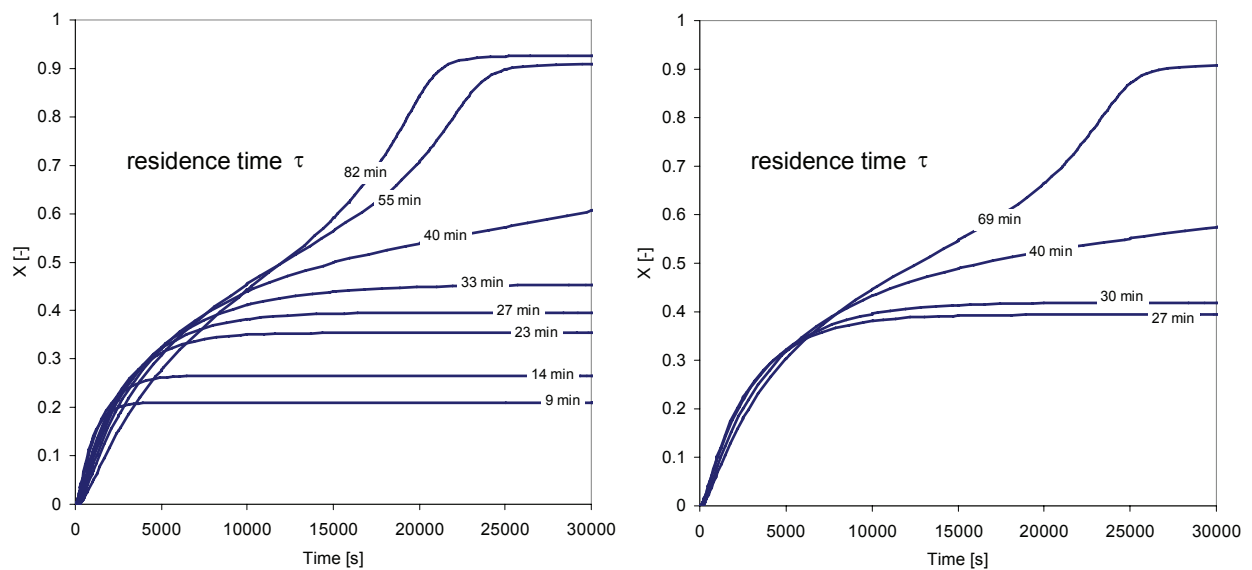
Figure 4.42: Conversion evolution in the loop reactor as a function of the residence time (140 °C, 0.3% DDT, left: 250ppm TBPIN, right: 250ppm TBPEH)

The scenario of a decreasing feed stream, causing higher residence times can be taken one step further to the case of a complete failure of the feed pump. In this case, the recycle loop will behave like a batch reactor and follow a different reaction path. Again, depending on initiator and temperature, a feed pump failure can have drastic consequences on the heat production and conversion respectively viscosity evolution in the reactor.

The simulation results for this failure scenario are shown in figure 4.43, where a complete cut of the feed flow occurs at t = 10'000 s. The same calculations have been carried out for three initiators with different decomposition characteristics: TBPEH, TBPIN and DTBP. The latter decomposes extremely slowly at T = 140 °C, which is the reason for the high monomer conver-

sion obtained after the failure of the feed pump. While for TBPEH and TBPIN the risk concerning a reaction runaway is practically zero due to the quick consumption of initiator after cutting the feed flow, this risk is extremely high for DTBP. Additionally, the time to react after a possible pump failure and to take countermeasures is rather low (~10% conversion increase per 10 minutes).

It is, therefore, indispensable to carefully choose the right initiator for a given temperature in order to reduce the risk that the polymerization is taken to high conversions in case of a major residence time variation by, for example, a feed pump failure.
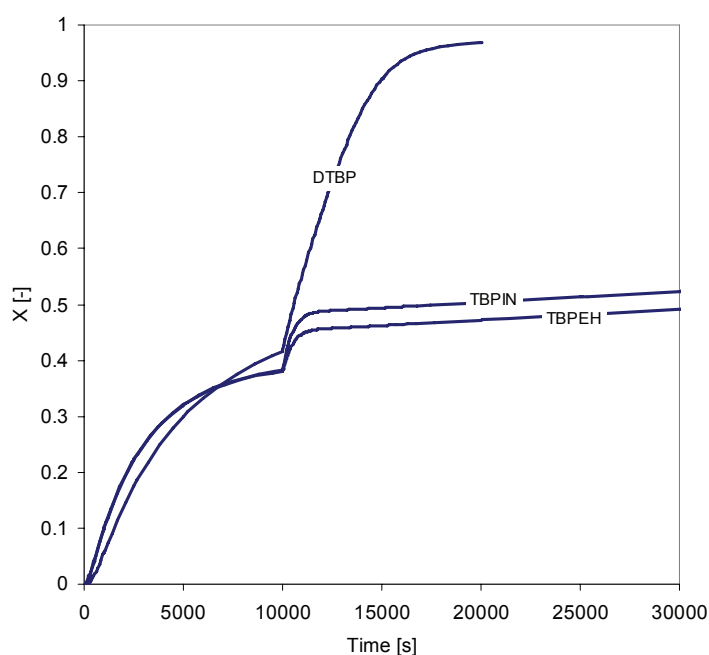
Figure 4.43: Conversion evolution in the loop reactor after an assumed feed pump failure for different initiators (140 °C, 0.3% DDT)

Varying the temperature

Varying the process temperature has a less important effect on the process. On the one hand, this is due to the fact that lowering the temperature automatically reduces the decomposition rate of the thermal initiator, which leads to a reduction of monomer conversion. On the other hand, increasing the temperature leads, depending on the chosen initiator, either to a quick initiator burn-out, or to a conversion limitation due to the depolymerization.

Figure 4.44 contains two graphs showing the conversion evolution over time as a function of temperature for TBPIN, respectively DTBP. In the case of TBPIN, the variation is not very intense, which is due to the rather quick initiator burnout above 150 °C ($t_{1/2, \text{TBPIN}}$ = 1 min at 160 °C). For DTBP, the difference is much more visible. At 140 °C, the decomposition of DTBP is very slow and the conversion, therefore, not very high. However, increasing the temperature to 160 °C pushes the conversion to a region where the reaction slowly enters the autoacceleration, which is noticeable by the constant increase of conversion. Above this, what could be called "turnover point", the conversion drops again due to the starting depolymerization (not due to initiator burnout: for comparison, $t_{1/2, \text{DTBP}}$ = 1 min at 190 °C!).
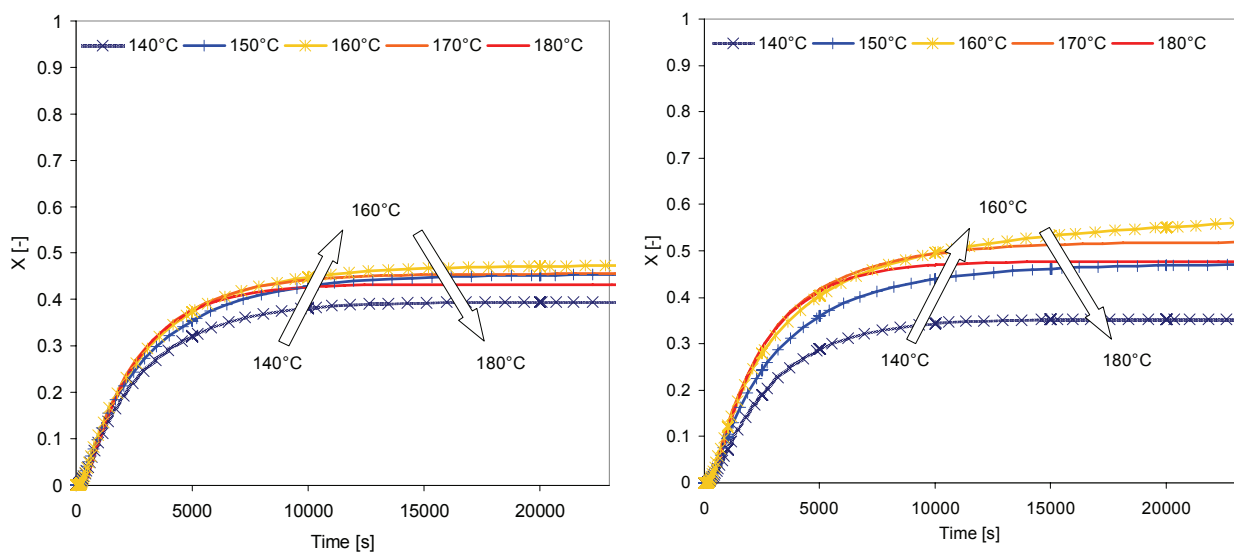
Figure 4.44: Conversion evolution in the loop reactor as a function of the temperature
(τ = 27 min, 0.3% DDT, left: 250ppm TBPIN, right: 250ppm DTBP)

Note that the above presented cases are valid for the variation of the reaction temperature under isothermal conditions. They do not describe the variation of temperature due to the reaction heat in case of a failure of the reactor's heating, respectively cooling circuit.

Varying the initiator concentration

Increasing the initiator concentration has, as expected, a very strong impact on the conversion evolution in the reactor. For the example shown in figure 4.45, the initiator concentration of the feed flow was stepwisely increased from 150ppm TBPIN to 600ppm. The results illustrate that above a concentration of 400ppm, the reactor behaviour becomes unstable and the reaction

goes into the gel effect. The influence on the molecular weight distribution is that the amount of polymer increases (in analogy to the conversion). The average molecular weight remains rather unchanged due to the presence of chain transfer agent. Only a small drift to lower molecular masses can be observed with increasing initiator concentration.

This example proves once again the importance of process modeling, making it possible to estimate a tolerance interval for the initiator concentration to guarantee a safe and stable reactor behavior, which is particulary important before changing the process conditions, e.g. the type of initiator or temperature.
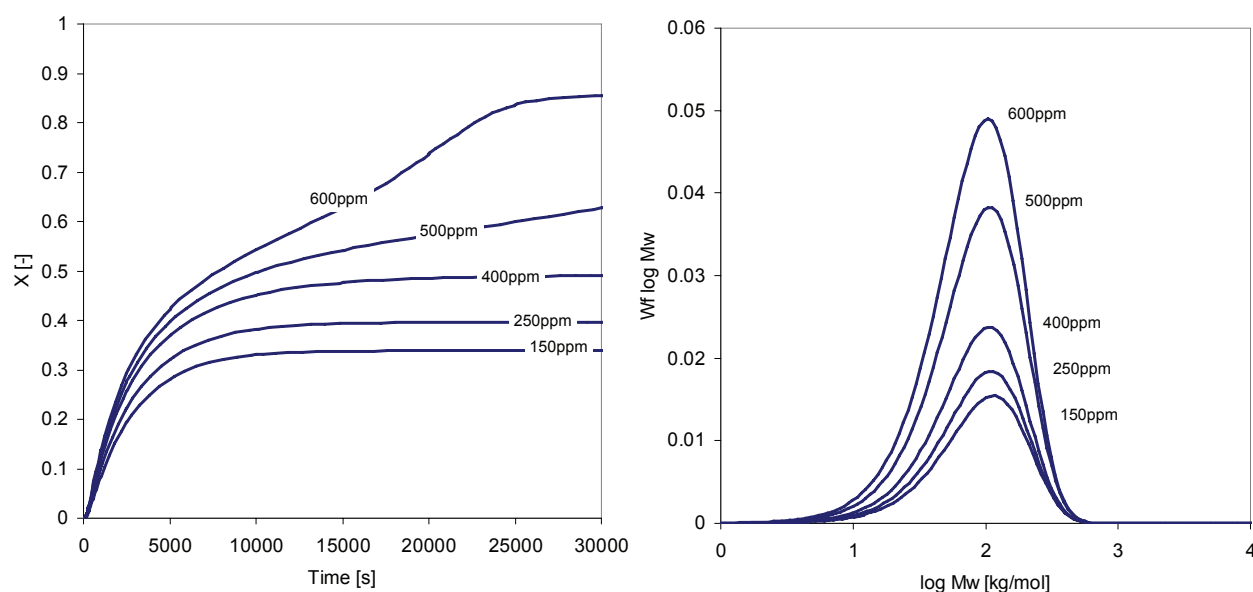
Figure 4.45: Conversion evolution and molecular weight distribution in the loop reactor as a function of the initiator concentration (T = 140 °C, τ = 27 min, 0.3% DDT)

Varying the chain transfer agent concentration

The chain transfer agent influences the reaction mostly by changing the molecular weight of the produced polymer and, thus, the viscosity of the reactor contents. Reducing the CTA feed concentration too much can lead to a strong increase in molecular weight, which can trigger the gel effect. In this work, the CTA concentration was at all times adjusted in a way to obtain a polymer of approximately 100 kg/mol in M_w.

How strong the impact of reducing the CTA feed concentration can be is illustrated in figure 4.46. A reduction from 0.3% to 0.1% causes an increase in molecular weight by 80% from ~100 kg/mol to ~180 kg/mol, by which the viscosity of the reaction mixture rises in a way that the

polymerization goes straight into the gel effect. The amount of chain transfer agent added to the feed solution must, therefore, be carefully evaluated before carrying out a reaction if problems arising from the strong viscosity increase are to be avoided.
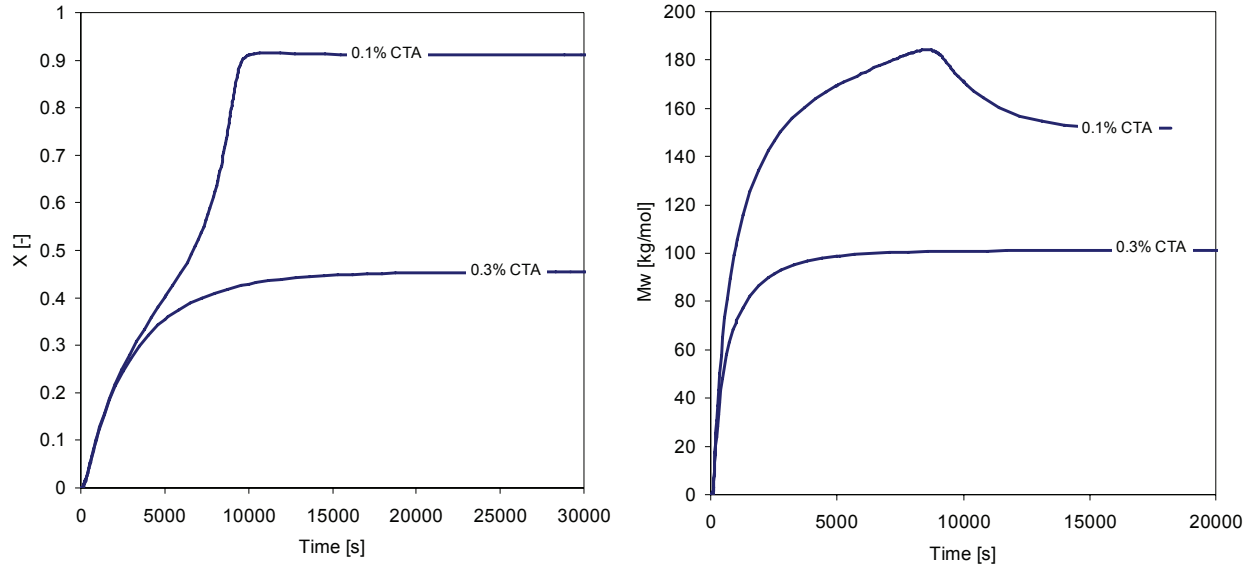
Figure 4.46: Conversion and molecular weight evolution in the loop reactor as a function of the DDT concentration (250ppm TBPIN, T = 150 °C, τ = 27 min)
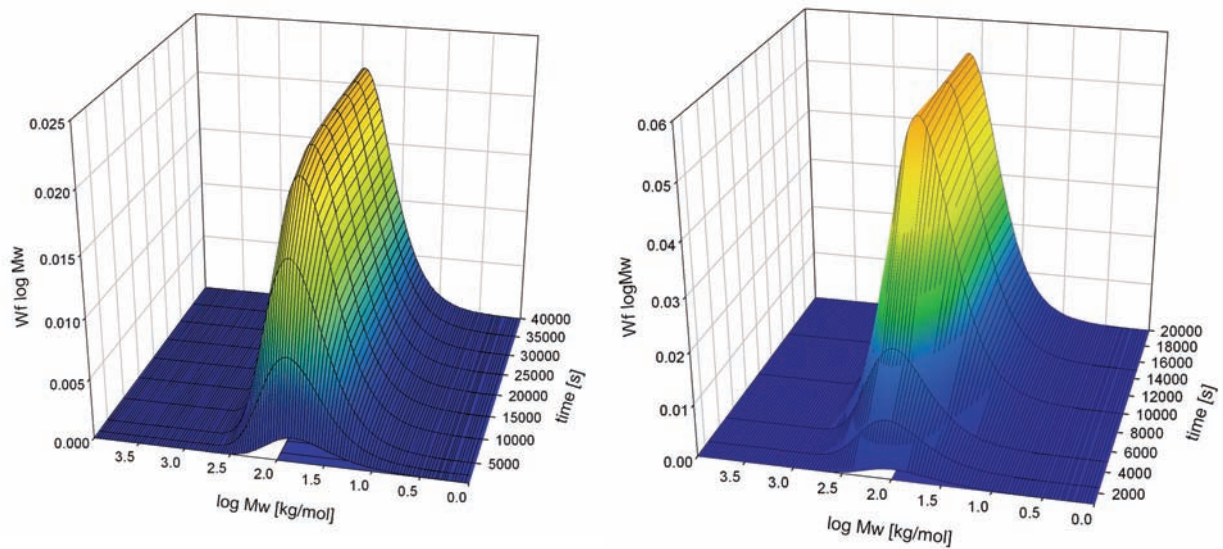
Figure 4.47: 3D-graphs of the molecular weight distribution evolution with 0.3% (left) resp. 0.1% (right) DDT (250ppm TBPIN, T = 150 °C, τ = 27 min)

Influence of the solvent content

Finally, also adding a solvent can help in making a process more stable. As seen in chapter 3, the gel effect is attenuated considerably in the presence of solvent, which is caused by the strong reduction of the viscosity due to the lower polymer fraction.

In figure 4.48, two different cases are compared, one without any solvent in the reactor feed, the other one with 20% butyl acetate. Apart from lowering the polymer fraction, the solvent also has an influence on the molecular weight, which is decreased by approximately 20% by the solvent addition. The reason for this decrease is the transfer reaction between solvent and active polymer chains (analog to the transfer to monomer and CTA) on the one hand, and the lower monomer concentration on the other.

Despite its positive impact on the reaction stability in terms of avoiding a strong gel effect, the use of solvent in early stages of polymerization is usually unwanted due to, inter alia, the lower reaction rate and possible side reactions (e.g. the above-mentioned transfer reactions).

Generally speaking, minimizing the solvent content, respectively avoiding its addition completely, has the advantage of an easier devolatilization in the end of the process.
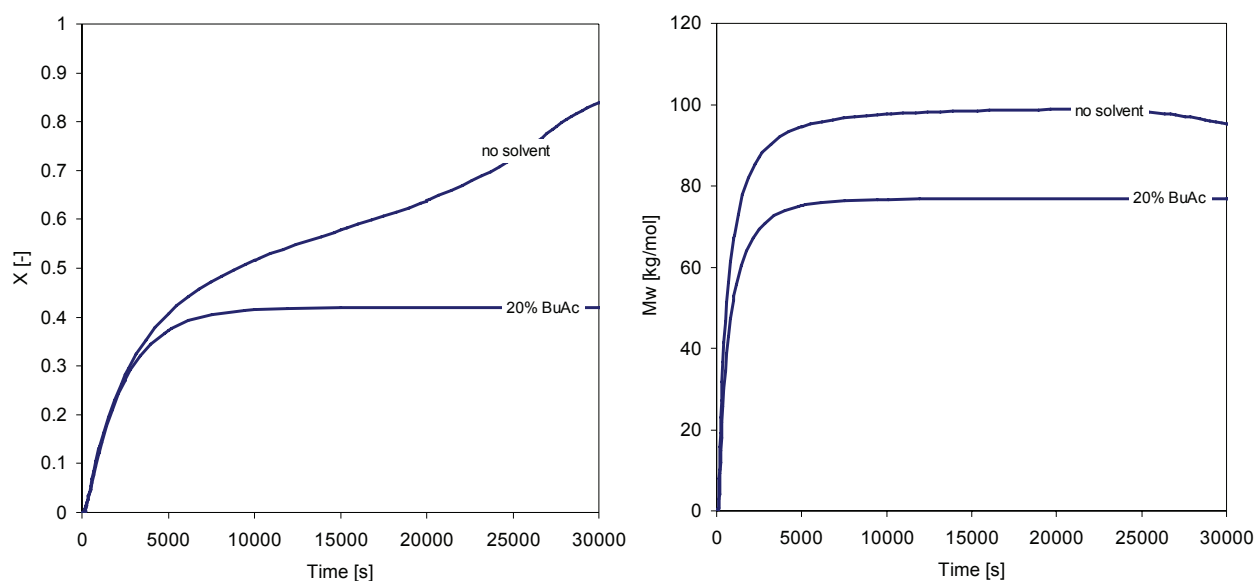
Figure 4.48: Conversion evolution in the loop reactor as a function of the solvent content (400ppm TBPIN, T = 150 °C, τ = 27 min)

4.5   Discussion

The present chapter is the most extensive one in this report. This is due to the fact that it contains a variety of topics and information related to the pilot plant process.

On the first pages, the pilot plant setup has been described in detail and the advantages of a combination of recycle loop and tube reactor was pointed out with regards to a classic setup of CSTR and tube reactor. At the same time, the static mixing elements and their characteristics were presented. The concept of chosing mixing elements with the same specific heat transfer coefficient as found in industrial scale reactors simplifies the scale-up from pilot plant to industrial production size.

Connected to every polymerization reaction is a more or less pronounced viscosity increase with rising polymer fraction. In the case of PMMA, this increase can be of several orders of magnitude. A model from literature was presented for the prediction of the viscosity and the pressure drop in the tubular reactor. By means of this model, it is possible to estimate the viscosity evolution with increasing conversion and molecular weight.

One major aim of this work was the implementation of a method for the inline conversion measurement based on ultrasound technology. The pilot plant had been equipped with two probes for the speed of sound measurement of the polymer solution at high temperatures. A problem arising from the determination of the monomer conversion from the speed of sound has been a rather large discrepancy between the measured values and speeds of sound calculated from theory. It was found that by readjusting the compressibility data for solvent and monomer, which had been found in literature only for low temperatures, this offset could be avoided. The equation for the calculation of the speed of sound for a mixture of known composition can, unfortunately, not be solved explicitly to yield the polymer weight fraction as a function of speed of sound and temperature. This limitation could be overcome by fitting calculated speed of sound values as a function of solution composition and temperature, leading to an analytical expression for the direct conversion calculation from measured speed of sound and temperature. The correct functioning of this measurement technique was demonstrated by comparison of conversion data from ultrasound to offline measured values from GC measurements. A limitation that could not be resolved is the restricted ability to measure in the presence of solvent. Since the above mentioned fitting is limited to three dimensions (speed of sound, temperature and polymer fraction / conversion), it is

impossible to include the influence of the solvent on the measured speed of sound in the calculation. Therefore, the conversion measurement can only be precise if the solvent fraction is constant or zero. If solvent is to be used in the process, the fitting presented in this work needs to be redone considering the influence of a constant amount of solvent on the speed of sound. However, it was shown in this chapter, that the ultrasound technology is a powerful tool for the monitoring of the process stability in polymerization reactions.

In several pilot plant experiments, the feasibility of the high temperature polymerization of MMA was demonstrated as well as the influence of various process parameters on the product quality investigated. Generally, a polymer of approximately 100 kg/mol and a residual volatiles' concentration of ~4000ppm was obtained with the process conditions applied in this work. The total monomer conversion was X = 40-50% in the recycle loop and X = 20-30% in the tube reactor (corresponds to 60-80% overall conversion).

From experiments with different comonomer, respectively chain transfer agent concentration, the reactivity ratios for the system MMA/MA and the transfer constant for n-dodecanethiol could be determined at high temperature. For the calculation of these parameters certain simplifications and assumptions had to be made in order to overcome limitations related to the narrow measuring range (r-parameters) or to missing CTA concentration values (transfer constant). After all, for the reactivity ratios of the system methyl methacrylate / methyl acrylate, the values $r_{12} = \mathbf{1.825 \pm 0.1}$ and $r_{21} = \mathbf{0.698 \pm 0.1}$ were found for T = 160 °C and MA fractions below 10% by the Kelen-Tüdös method. For higher acrylate fractions, more experiments need to be carried out to refine the r_{21}-parameter, which, in this work, could only be determined by the addition of an auxiliary "dummy" point positioned at an MA fraction close to one. The chain transfer constant for n-dodecanethiol at T = 140 °C was determined by means of the Mayo-plot and by a method found in literature (de la Fuente and Madruga) to be $\mathbf{C_{CTA} = 0.88 \pm 0.01}$.

Finally, the validity of the kinetic model established in this work for the continuous polymerization process was proven by comparison to experimental data. The agreement between modeled and measured data in terms of conversion evolution and molecular weight distribution modeling is very satisfying. Last but not least, the importance of process modeling in polymer reaction engineering was pointed out by a parameter variation study. With the help of the pilot plant model, several scenarios of changing process parameters were simulated and the influence of each parameter on process stability and comportment was evaluated.

Short Summary:

- The continuous polymerization of MMA at high reaction temperatures is discussed and results from several pilot plant experiments are presented
- With the reaction conditions applied in this work, a PMMA with a molecular weight of Mw = 100 kg/mol is obtained at high monomer conversion
- For inline conversion monitoring, a technique based on speed of sound measurement was successfully implemented and tested
- From the experimental data it was possible to determine two important kinetic parameters: the reactivity ratios for the comonomer system MMA/MA and the chain transfer constant for n-dodecanethiol at high temperature
- The validity of the kinetic model established during this work in PREDICI® was proven by comparison to experimental data. With the help of this model, a parameter variation was carried out to predict the response of the process to several scenarios of changing process conditions.

CHAPTER 5

Thermal stability and Depolymerization

As practically all organic substances, also polymers have a rather limited thermal stability. The thermal stability of a molecule is normally directly dependent on the bond energy of the molecule's constitutional bonds. Different from smaller molecules, polymers suffer basically from an especially low bond energy, which is due to the non-uniform movements of the polymer chains above the glass transition [98] that weaken the chain bonds. In the case of PMMA, the activation energy for random chain scission is with approximately 233 kJ/mol [99] significantly lower than for C-C bonds in small organic molecules (326 kJ/mol [100]).

But the thermal degradation of PMMA is particular for yet another reason: the unzipping mechanism. Unlike other polymers, the non-oxidative degradation of PMMA yields mostly monomer and it is, thus, possible to recover as much as 98% methyl methacrylate from the pyrolysis of PMMA, as presented in table 1 for a recycling study found in literature. The mechanism is called unzipping because the molecular structure of PMMA allows an intramolecular radical transfer from the chain end to the penultimate chain link, setting free one monomer molecule after the other, like in a zipper:

(EQ 5.1)
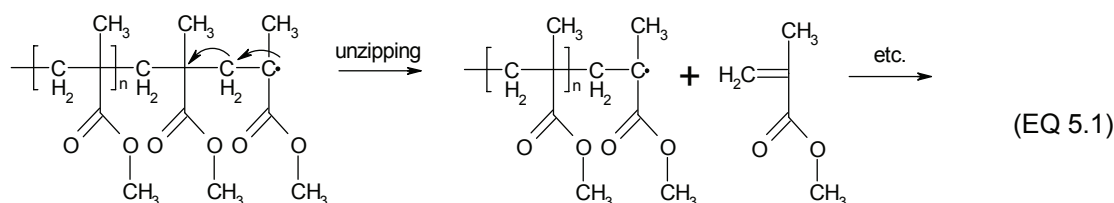
This means that once a polymer chain has been activated by chain scission, the created chain radicals "unzip" either completely or until they are terminated by combination or disproportionation with another radical.

Table 1: Degradation products for the pyrolysis of PMMA [101]

Analysis (wt%)	450 °C	490 °C	590 °C
Gas	**1.37**	**2.63**	**42.46**
Methane	11.8	10.3	9.2
Ethene	4.7	4.4	5.87
Ethane	3.4	2.6	1.6
Propene	1.3	6.8	16.3
Iso-butene	0.21	1.85	4.9
CO_2	75.8	55	20.4
CO	0.78	14.3	31.9
Liquid	**98.48**	**97.08**	**57.27**
Methanol	0.03	0.07	0.06
Methylisobutanol	0.11	0.13	0.54
MA	0.28	0.34	2.18
MMA	98.66	98.34	95.8
MMA-dimere	0.14	0.26	0.51
Char	**0.15**	**0.29**	**0.27**

It is the same mechanism that applies for the depropagation reaction in the MMA polymerization, which has already been mentioned with regards to the conversion limitation at high temperature in Chapter 3. It is, therefore, logical to discuss both issues together within this chapter.

5.1   Depropagation of poly (methyl methacrylate) chains

The radical polymerization of MMA, unlike for example polycondensation reactions, is a reversible reaction and is determined by the equilibrium between the propagation and the depropagation reaction, depicted in equation 5.2.

$$P_n^{\bullet} + M_1 \underset{k_{dp}}{\overset{k_p}{\rightleftharpoons}} P_{n+1}^{\bullet}$$

(EQ 5.2)

For low temperatures, the depropagation rate is very small and can be neglected in comparison to the propagation rate: the equilibrium is pushed to the far right hand side of equation 5.2. With increasing temperature, however, the depropagation becomes more important and, above 170 °C, it causes remarkable conversion limitations due to the decrease of the "effective" propagation rate, as can be seen in figure 5.1, where the simple propagation rate k_p is compared to the propagation rate corrected by the term for the depropagation over a large temperature range[1]:

$$k_{p,\,effective} \;=\; k_p - \frac{k_{dp}}{[M]} \qquad\qquad \text{(EQ 5.3)}$$
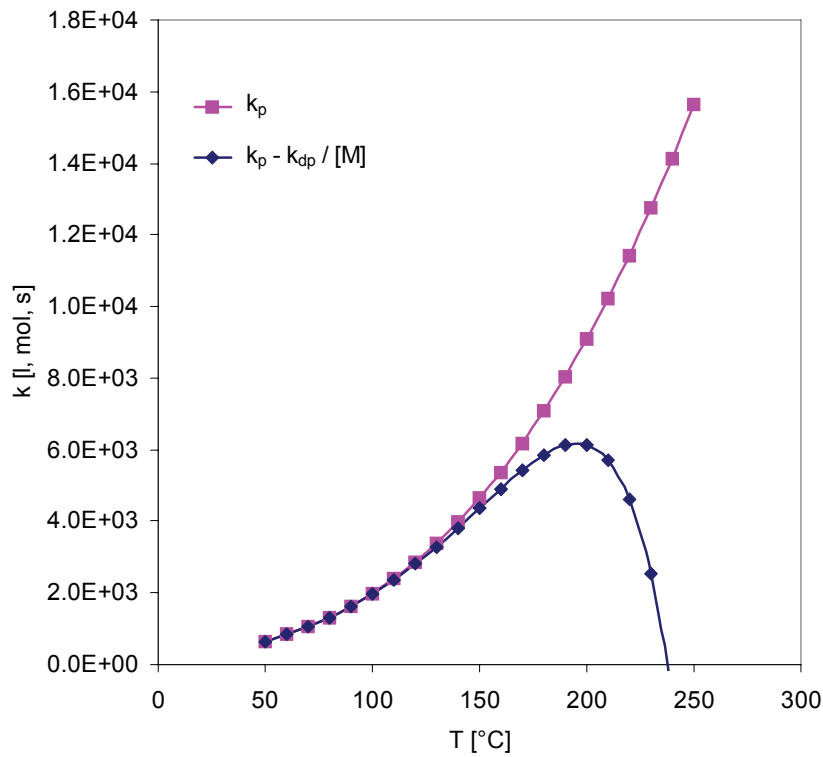
Figure 5.1: Comparison of effective and theoretical propagation rate for MMA depending on the temperature of polymerization

---

1. As monomer concentration *[M]* is taken its bulk concentration at the corresponding temperature and the following rate coefficients have been employed for this presentation:

$k_p \;=\; 2.67 \cdot 10^6 \cdot \exp\!\left(-\dfrac{22.4\,kJ/mol}{RT}\right)\left[\dfrac{l}{mol \cdot s}\right]$ (IUPAC), $k_{dp} \;=\; 2.4 \cdot 10^{12} \cdot \exp\!\left(-\dfrac{73.3\,kJ/mol}{RT}\right)\left[\dfrac{1}{s}\right]$ (this work)

Once the system reaches the ceiling temperature, i.e. the temperature where propagation and depropagation rate are the same, the apparent rate of polymerization is zero. This means that the propagation still takes place but for each element that is added to the chain, one is taken away at the same time. Thus, the net chain growth is zero.

Kinetically, an equilibrium between two reactions like propagation and depropagation is expressed by equation 5.4:

$$k_p(T_c) \cdot [P_n'] \cdot [M] = k_{dp}(T_c) \cdot [P_{n+1}']$$

(EQ 5.4)

from which the equilibrium constant can be isolated:

$$K(T_c) = \frac{k_p(T_c)}{k_{dp}(T_c)} = \frac{[P_{n+1}']}{[P_n'] \cdot [M]} \approx \frac{1}{[M]}$$

(EQ 5.5)

From a thermodynamic point of view, propagation and depropagation are in the equilibrium state at ceiling temperature, which in terms of the standard Gibbs enthalpy of polymerization ΔG_p^0 can be written as

$$\Delta G_p^0(T_c) = \Delta H_p^0 - T\Delta S_p^0 = -RT_c \cdot \ln K(T_c) \text{ (at constant pressure)}$$

(EQ 5.6)

where ΔH_p^0 is the standard enthalpy and ΔS_p^0 the standard entropy of polymerization (for PMMA these values are -57.8 kJ/mol respectively -117 J/mol K [47]). From equations 5.5 and 5.6 follows for the calculation of the ceiling temperature:

$$T_c = \frac{\Delta H_p^0}{\Delta S_p^0 + R \cdot \ln[M]} = 494K \sim 221°C$$

(EQ 5.7)

Note that the concentration *[M]* is the equilibrium concentration of MMA at T_c. Usually, *[M]* is taken as unit concentration (*[M] = 1 mol/l*) [102] and T_c is then the temperature above which it is not possible to form polymer from unit or lower concentration. This means that if the polymerization started at T_c, it would proceed until the monomer concentration reaches the equilibrium concentration. Conversely, polymer chains that are made at a lower temperature and con-

secutively heated to T_c will depolymerize until the equilibrium concentration of the monomer in the system is reached.

With the help of equation 5.7, also the equilibrium monomer concentration for any given temperature can be calculated, assuming that ΔH_p^{0} and ΔS_p^{0} do not exhibit any temperature dependence:

$$\ln[M]\big|_{equilibrium} = \frac{\Delta H_p^{0}}{RT} - \frac{\Delta S_p^{0}}{R} \qquad \text{(EQ 5.8)}$$

Together with the relation $[M] = \dfrac{[M]_0 \cdot (1 - X)}{1 + \varepsilon \cdot X}$ and equation 5.8, the equilibrium conversion at a given temperature T can be calculated:

$$X_{equilibrium} = \frac{[M]_0 - [M]_{eq}}{[M]_0 + \varepsilon \cdot [M]_{eq}} \qquad \text{(EQ 5.9)}$$
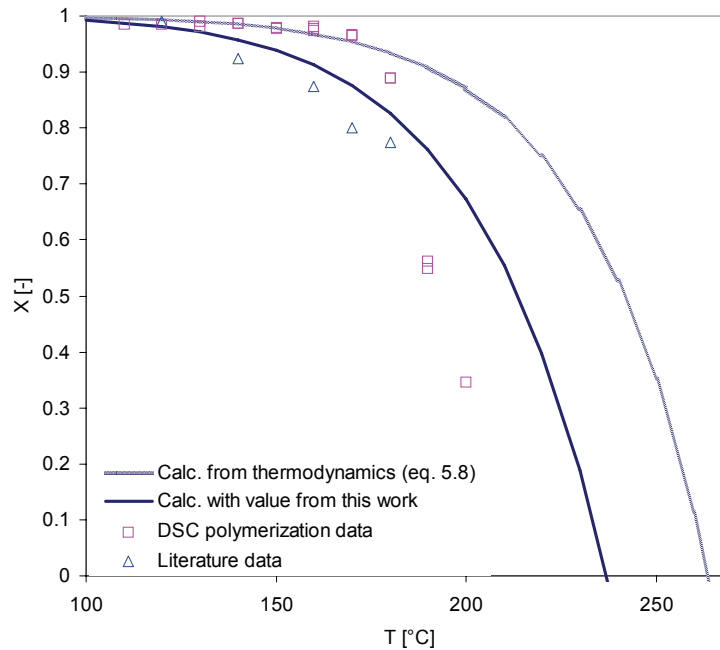
Figure 5.2: Equilibrium conversion for MMA at different temperatures according to equation 5.9 in comparison to experimental data from this work (DSC polymerizations with 1000ppm DTBP as initiator) and literature [103]

However, when tracing the equilibrium conversion against temperature, which has been done in figure 5.2, it becomes evident that, above 170 °C, the calculated values are much too high compared to experimental and literature data. In fact, for DSC batch polymerizations, the maxi-

mum attainable conversion drops quickly to zero between 170 °C and 210 °C while the calculated values remain quite high until approximately 230 °C and reach zero conversion at ~260 °C. This might be due to the simplifications made in the above considerations, e.g. that the chain radicals $[P_{n+1}{}^{\cdot}]$ and $[P_n{}^{\cdot}]$ have the same reactivity (equation 5.6). If, for example, the reactivity of $[P_{n+1}{}^{\cdot}]$ is lower than for $[P_n{}^{\cdot}]$, the equilibrium conversion will be lower, too. Also the fact that other, irreversible reactions (like chain termination) take place at the same time influences the thermodynamic equilibrium and prevents the use of the purely theoretical development made up to here for the estimation of the depropagation rate constant, which is the real aim of this.

In order to determine a depropagation rate constant for MMA radical chains, it is therefore more appropriate to do this with respect to experimental data rather than based on the theoretical curve in figure 5.2. Also literature provides values for k_{dp} as shown in table 2, but unfortunately, values from both sources did not deliver satisfying results in the modeling of this work. The value of Chiu et al. underestimated the conversion limitation by depropagation, whereas the Fleury relations for the calculation of X_{equ} and k_{dp} resulted in a too strict reduction of the final monomer conversion.

Table 2: Literature values for the depropagation rate of MMA radical chains

Source	k_{dp}
Chiu et al. [58]	$k_{dp} = 6.48 \cdot 10^{11} \cdot \exp\left(\dfrac{-76.4[kJ/mol]}{RT}\right)\left[\dfrac{1}{s}\right]$
Fleury [5]	$k_{dp} = k_p \cdot [MMA]_0 \cdot (1 - X_{equ}) \cdot \dfrac{\rho_{equ}}{\rho_0}$ $X_{equ} = 1 - \exp\left[23.66 - \dfrac{11282.7}{T[K]}\right]$ (fitted by Fleury)

With the technical possibilities to fit rate constants to experimental data in PREDICI$^{®}$ and the data from several high temperature polymerizations at 170 °C and 180 °C, a new value for k_{dp} was determined, which leads to a correct description of the conversion limitation in the frame of the modeling used in this work.

Figure 5.3 shows the results of the fitting for two DSC batch polymerizations at 170 °C and 180 °C in comparison to experimental data. The values for k_0 and E_A of the depropagation rate obtained in this way are presented in table 3.
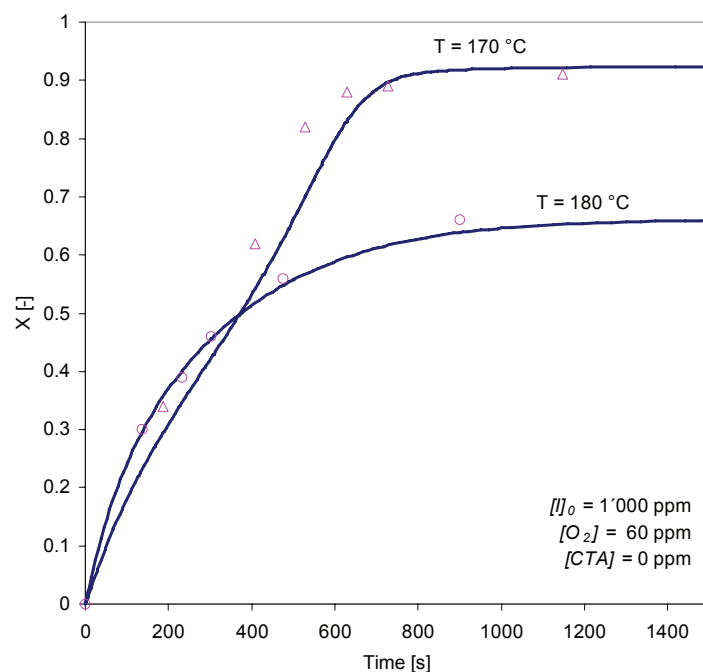
Figure 5.3: Results for the conversion limitation by depolymerization using the k_{dp} value estimated in this work

Table 3: Values for the depropagation rate obtained in this work by fitting to experimental data

	k_0	E_a
k_{dp}	$2.4 \cdot 10^{12}$ [1/s]	73.3 [kJ/mol]

5.2　Thermal stability of the polymer

The previous part of this chapter has dealt with the depolymerization reaction of live polymer chains. Yet, once a chain is terminated, the depolymerization is not an issue anymore since the termination is an irreversible reaction. So, in order for the above mentioned unzipping mechanism to take place, the "dead" polymer chain needs to be activated by chain scission. Once this has happened, the activated chain undergoes the same depolymerization reaction as described in

175

section 5.1., as postulated by Grassie and Melville [104]. The thermal degradation of PMMA is, therefore, nothing else than a depolymerization initiated by chain scission, with the chain scission being the rate determining step.

For radically polymerized PMMA, chain scission can occur at different places of the molecule. Basically there are three main bond types, each exhibiting a different thermal stability. Therefore, PMMA degrades in three steps with increasing temperature, as it was demonstrated by previous research studies carried out in this laboratory [43] as well as by many other authors [99, 105-117].

The three most important bond types in order of increasing thermal stability are:

- head-to-head bonds that form by combination termination of two active polymer chains
- unsaturated end groups that form by disproportionation termination of two active polymer chains
- random C-C bonds of the main chain

Apart from these three types of bonds, other weak linkages can be introduced into the polymer chains depending on, for example, the process conditions and impurities. However, their occurrence is too random and non-reproducible in order to relate them to any thermal degradation step as the above mentioned ones. In general, it can be said that the more regular a polymer chain is, the more thermally stable it will be.

The following figure 5.4 shows a typical result from the thermogravimetry of PMMA, which has been polymerized at 140 °C and not been stabilized or heat-treated after polymerization. The three degradation steps are easily recognizable. Remarkable is the low starting point for the head-to-head degradation at little above 150 °C. This temperature is far from the ceiling temperature of MMA, which means that the monomer set free by the degradation can repolymerize with the active chains [109], while for the two other steps, both taking place beyond 220°C, the chain scission leads inevitably to a complete unzipping of the whole chain.
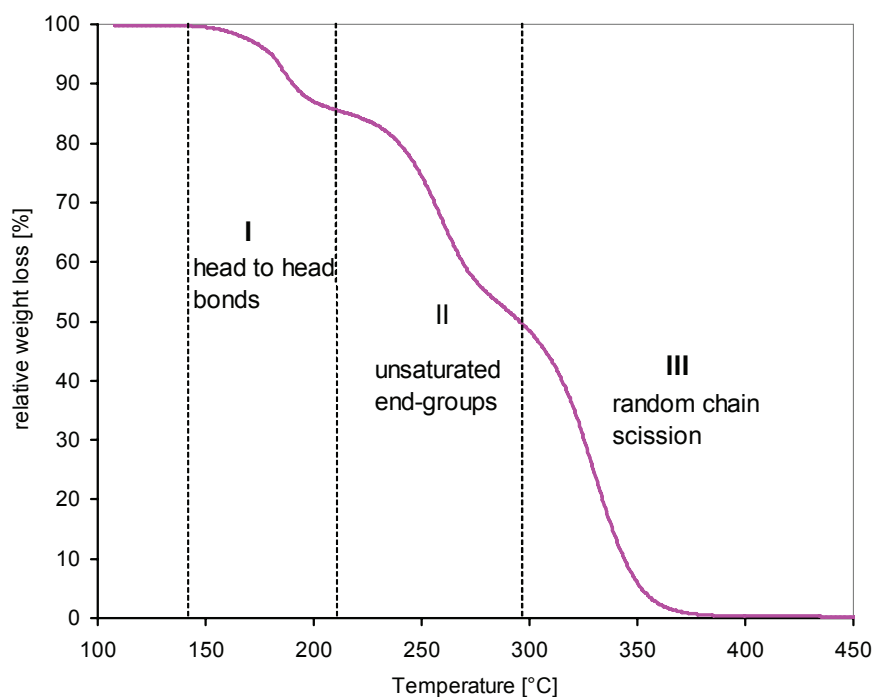
Figure 5.4: Typical TGA thermogram of the degradation of radically polymerized PMMA (polymerization temperature 140 °C)

Thermal stability of a polymer is an important characteristic for the product quality. Especially for molding compounds, as the PMMA produced in this work, that have to be molten in an extruder at temperatures between 250 °C and 300 °C before they can be injected into a mold to produce parts with the desired shape, the minimization of weight losses due to thermal degradation is a major concern. The example presented in figure 5.4 would be completely unsuitable for this application, since the weight loss at 250 °C exceeds already 30% and at 300 °C only less than 50% are left. The volatiles created during the degradation pollute the final work piece and make its use for most applications impossible.

The development of an efficient stabilization strategy has therefore been subject to intensive research in the past, which is illustrated by more than 4000 patents[1] on this topic. The most popular solution for improving the heat stability of methacrylates is the copolymerization with small amounts of acrylates. The unzipping mechanism presented in equation 5.1 can only work with a

---

1. Number of patents found in SciFinder 2006 by searching for the keywords "methacrylate", "moldability" and "thermal stability"

methyl group in the alpha position of the acrylate. As soon as this methyl group is replaced by a hydrogen atom, the unzipping stops [118]. This is, for example, the case for methyl acrylate but also works for any other acrylate comonomer:

(EQ 5.10)
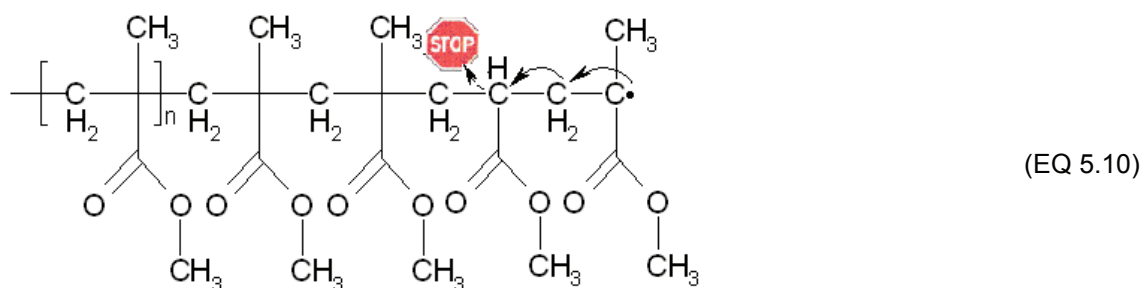
The stabilization with a comonomer is simple and cheap and it does not significantly change other product properties of the polymer, since already small amounts of comonomer are sufficient for stabilization reasons. This is the reason why nowadays practically no homopolymerized PMMA is sold but only copolymers with various comonomer contents.

Another possibility to make PMMA thermally more stable is the use of chain transfer agents. This group of substances, which are mostly of the thiol type, has already been mentioned at other occasions in this work, namely with regards to the thermal initiation and the gel effect. Apart from their primary application in polymerization reactions, i.e. to control the molecular weight, they also have an important stabilizing effect on the polymer. In fact, the principle of chain transfer is the termination of active polymer chains by transferring the radical from the chain to the transfer agent in exchange for a hydrogen atom, which terminates the active chain. Thus, the probability that polymer chains contain weak bonds is considerably lower. Since the chain transfer is in concurrence with the other termination reactions it is: the higher the amount of chain transfer agent, the less termination by combination or disproportionation occurs and the more stable the polymer. An additional side-effect is the presence of residual thiols in the final polymer. As the degradation of PMMA is a process involving radicals, thiols being radical scavengers can capture active radicals and, thus, slow down the degradation by unzipping.

Finally, also the polymerization conditions can have a major impact on the thermal stability of the polymer. As said before, the uniformity of the polymer chains is a key to good resistance against thermal stress. Increasing the radical flow during a polymerization reaction, e.g. by over-

dosing thermal initiators, or increasing polymerization rate and temperature can have a negative effect on the structure of the polymer.

In the following, the efficiency of the above-mentioned stabilization strategies and their impact on the polymer stability is discussed with the help of results obtained in this work for the batch and the continuous polymerization of MMA under various conditions. During the next paragraphs it should be kept in mind that there is a major difference between samples from the batch experiments and those from the pilot plant. The samples from the DSC were all polymerized to full conversion with rather high amounts of DTBP as initiator (1000ppm). Furthermore, they were not exposed to higher temperatures than the reaction temperature, unlike the pilot plant samples that have already passed the devolatilization at 250 °C. It is, thus, to be expected that the DSC samples exhibit a generally lower thermal stability than the pilot plant samples. The latter will, therefore, be discussed separately at the end of this chapter and in the next sections the influence of each reaction parameter will be evaluated only qualitatively based on DSC samples.

5.2.1 Effect of the polymerization temperature

PMMA starts to decompose by scission of head-to-head bonds at approximately 150 °C (see figure 5.4). Increasing the polymerization temperature to above this value will, therefore, have the effect of eliminating this type of bond in the polymer. Additionally, also the ratio between termination by combination and disproportionation, γ, is more and more in favour of the disproportionation with increasing temperature. This means that for polymerization temperatures higher than 150°C, the degradation by head-to-head scission should be significantly reduced, whereas the scission at unsaturated chain ends should become more important. In thermogravimetrical experiments, exactly this phenomena can be observed, as shown in figure 5.5 (a). Presented are the results from TGA experiments with three homogenous PMMA samples from DSC batch polymerizations carried out at different temperatures. It is evident how increasing the temperature improves the thermal stability for temperatures below 250 °C. The other side of the coin is that, in particular for 190 °C polymerization temperature, the thermal lability between 250 °C and 300 °C, i.e. the weight loss during the second degradation step, is drastically increased. This is explainable by the fact that at this polymerization temperature, very short chains are polymerized, which terminate almost exclusively by disproportionation at this temperature ($\gamma = k_{tc}/k_{td} = 0.034$). Therefore, the ratio of unsaturated end groups to random C-C bonds is rather high.

The influence of temperature on thermal stability is, therefore, also a consequence of the changing molecular weight: at low temperatures, rather long polymer chains are produced. This means that the ratio between possibly instable bonds to C-C chain bonds is lower than for shorter chains and, therefore, the probability that a chain molecule breaks at a weak bond decreases. In figure 5.5 (b), this is illustrated by the comparison of three polymers that were polymerized at lower temperatures and which exhibit a quite important difference in molecular weight.
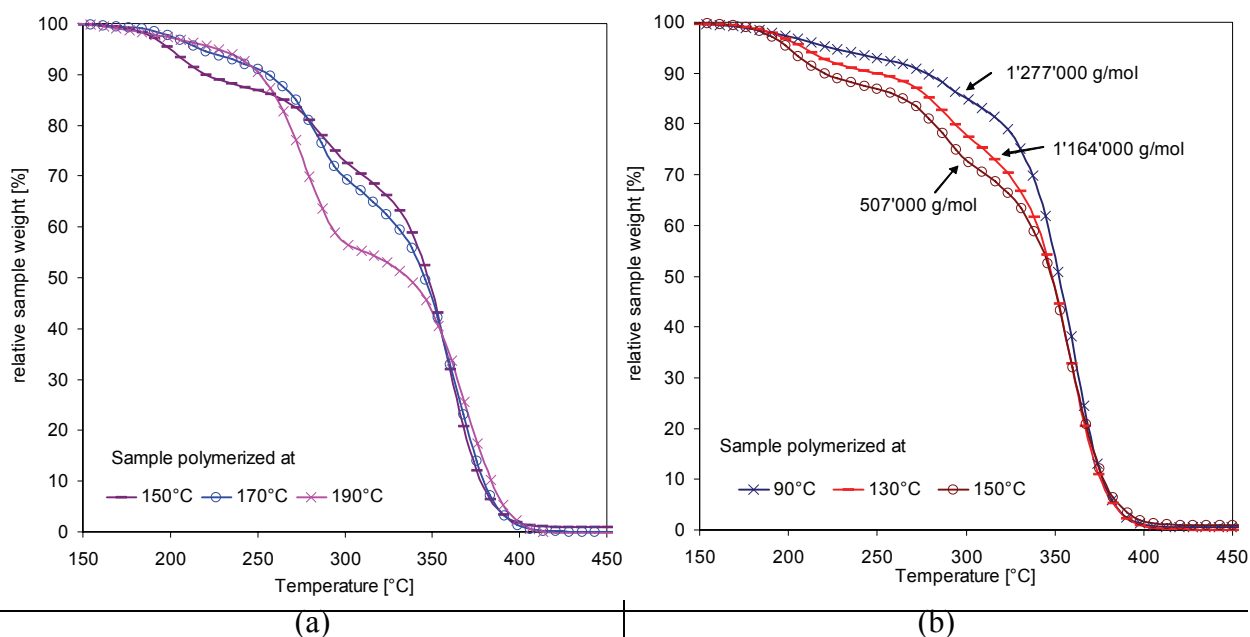
Figure 5.5: Influence of (a) the polymerization temperature and (b) the molecular weight on the thermal stability of PMMA (1000ppm DTBP, no CTA, no solvent)

5.2.2 Effect of the comonomer

According to the theory discussed beforehand and as illustrated in equation 5.10, the addition of small amounts of acrylates as comonomer prevents the polymer chains from complete unzipping after being activated by chain scission. Depending on the amount of acrylate added to the reaction mixture, the fraction of acrylate molecules that are incorporated in the chains increases and, at the same time, the thermal resistance of the polymer should become better. The maximum amount of comonomer is limited, however, by the fact that too much comonomer can seriously deteriorate the polymer properties (mechanical strength etc.).

Figure 5.6 illustrates the impact of increasing comonomer concentration in the reaction mixture on the thermal stability of the resulting polymer for the example of methyl acrylate. The

samples were all polymerized at 140 °C in DSC batch polymerizations. Already 2% of MA are sufficient to improve the thermal stability by more than 10% with respect to the weight loss between 250 °C and 350 °C. For 5% MA, the overall weight loss below 300 °C is less than 10%.
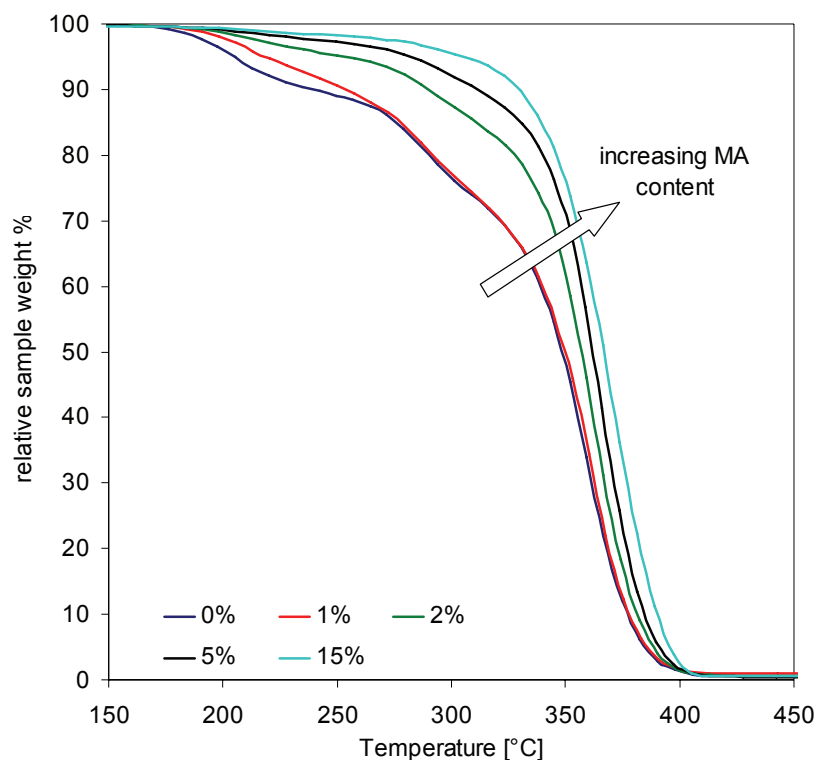
Figure 5.6: Influence of comonomer (methyl acrylate) and its amount on the thermal stability of PMMA (DSC batch polymerization T = 140 °C, 1000ppm DTBP, no CTA, no solvent)

Increasing the temperature of the copolymerization from 140 °C to 170 °C deteriorates the thermal stability and the weight loss increases again, in particular in the region of the unsaturated end group scission (figure 5.7). At first sight, this is in contradiction to the fact observed in Chapter 4, "R-parameters" on page 138 that with increasing temperature more comonomer is incorporated in the polymer chains. This should make the polymer more resistant according to figure 5.6. The only possible explanation is an augmenting occurrence of weak linkages (i.e. unsaturated end groups) in the polymer chains at 170 °C analog to section 5.2.1. It will have to be seen later if the same phenomenon can be observed for the samples from the continuous pilot plant process or in the presence of a chain transfer agent.
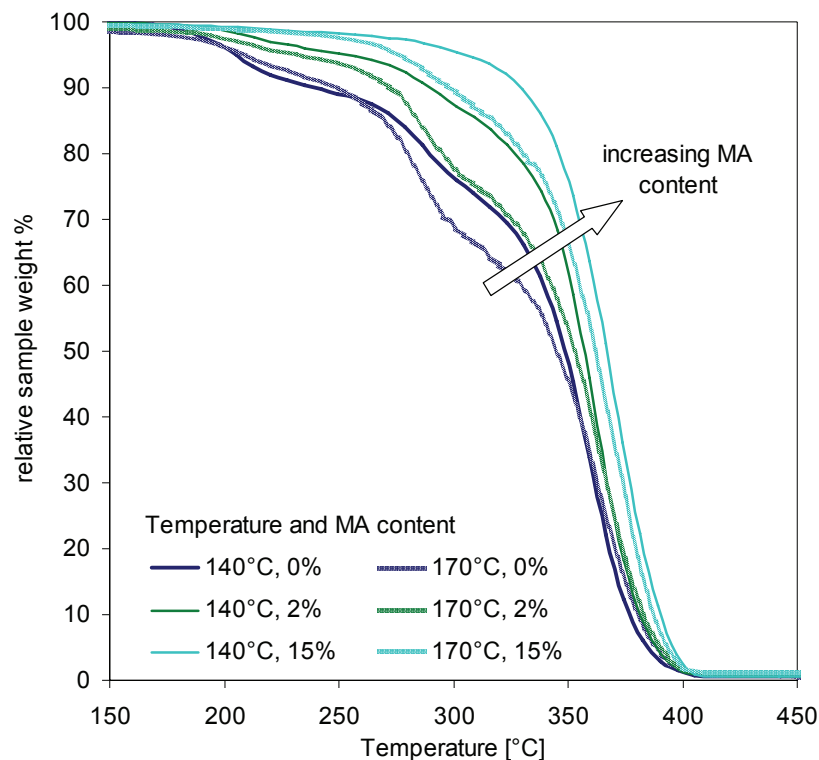
Figure 5.7: Influence of comonomer (methyl acrylate) and its amount on the thermal stability of PMMA (DSC batch polymerization T = 140 °C resp. 170 °C, no CTA, no solvent)

Finally, in order to verify the assumption for the stabilization mechanism of acrylates, i.e. that the mechanism is really depending on the alpha substituent as presented beforehand, several different acrylates and alkyl-substituted acrylates were tested as comonomer in the polymerization of MMA. An as a matter of fact, the comonomer acts only as stabilizer if the alpha-position of the acrylate is not substituted. In figure 5.8 are presented the results from four polymerizations, one without any comonomer, one with butyl methacrylate, one with methyl acrylate and one with butyl acrylate. The curves for both acrylates and both methacrylates are overlapping each other. The stabilizing effect is only achieved for the two acrylates. This result is an important piece of evidence for the supposed stabilization mechanism of equation 5.10.
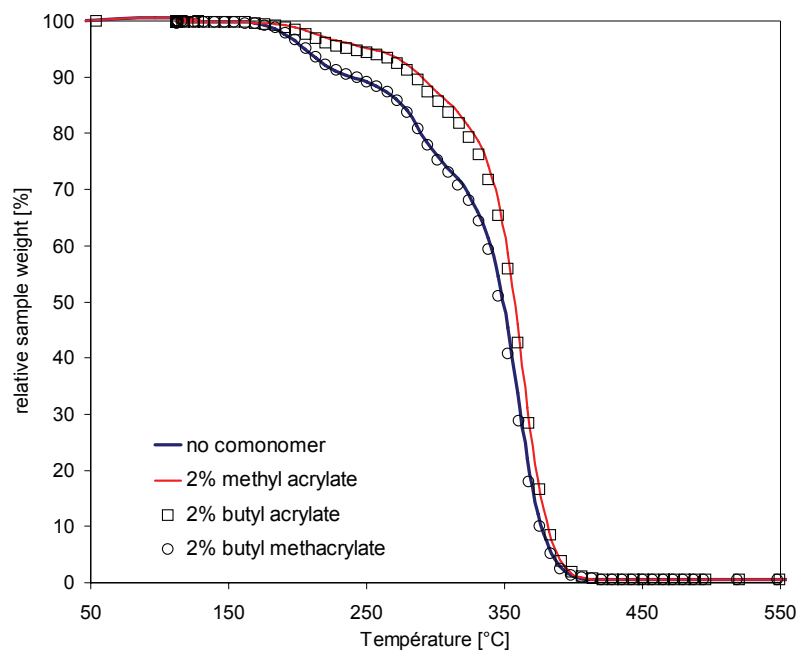
Figure 5.8: Influence of the choice of comonomer on the stabilization of PMMA (DSC batch poly-merization at T = 140 °C, 1000ppm DTBP)

5.2.3   Influence of the chain transfer agent

The stabilizing effect of the thiol added to the polymerization as chain transfer agent is less pronounced than expected (see figure 5.9). Although the experiments with no, respectively, 500 - 3000ppm CTA added cannot be directly compared due to a large change of the molecular weight, it can be said that with increasing CTA concentration, the thermal stability in the temperature range of 150 °C to 250 °C gets worse while it improves for the region above 250 °C. The degradation by unsaturated end group scission almost completely disappears and the thermogram flattens between 220 °C and the beginning of the random chain scission at 330 °C. The increased weight loss around 200 °C might be due to the fact that the chain transfer agent can also act as initiator, which, at high CTA concentrations, can lead to the formation of significant amounts of polymeric chains with thioether end groups, which exhibit a low thermal stability.
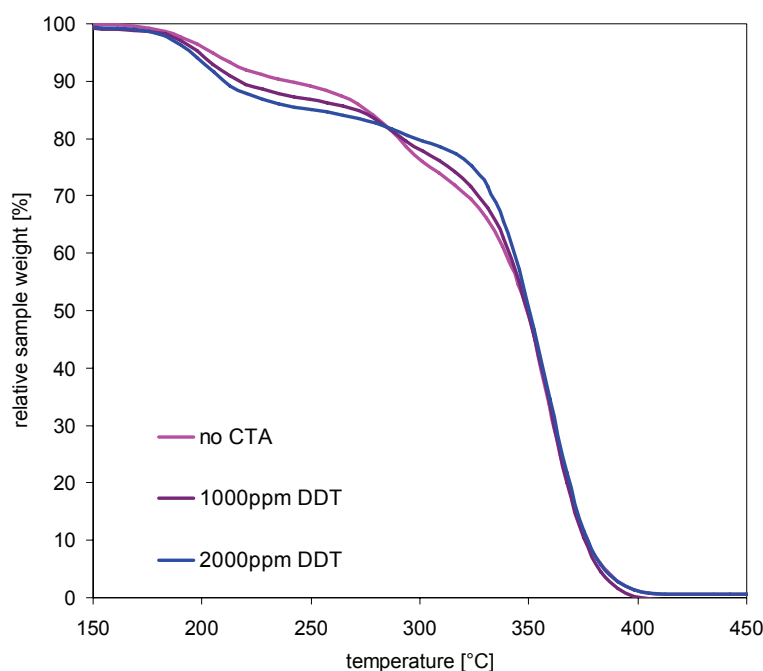
Figure 5.9: Influence of the chain transfer agent (n-dodecanethiol) on the stability of the polymer (DSC batch polymerization at 140 °C, 1000ppm DTBP)

5.2.4   Results from the pilot plant polymerization

The polymer samples coming from the pilot plant were analyzed in the analytical facilities of the industrial partner according to a method validated for commercial polymers. This allowed the direct comparison between the product from the pilot scale reactor to industrial scale produced PMMA. The specifications concerning the thermal stability of a product are given by characteristic values, which quantify the weight loss at certain criteria and can be easily compared for different samples. These criteria are:

- T_d: the temperature where the total weight loss is of 2% of the sample

- $T_{v0.05}$, $T_{v0.1}$, $T_{v0.2}$: the temperature where the rate of weight loss is of 0.05%/min, 0.1%/min, respectively 0.2%/min

- T_{max}: the temperature of maximum rate of weight loss

Apart from the relative weight loss suffered at a given temperature, also the rate of weight loss is important, since the exposure of the polymer to elevated temperatures is usually kept rather short in extrusion.

Figure 5.10 shows the typical result from a thermogravimetrical analysis of a commercial grade PMMA molding compound of excellent thermal stability: below 300°C, the polymer sample loses less than 0.2% of its weight per minute.
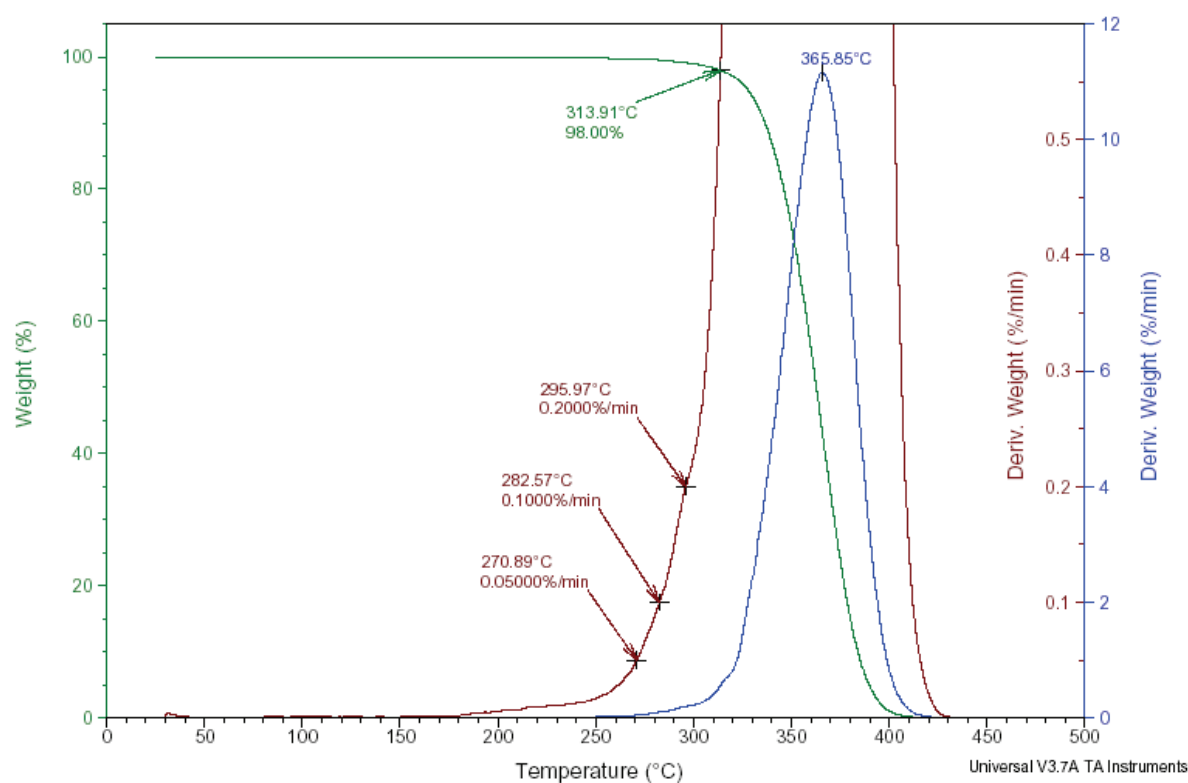
Figure 5.10: Thermogravimetry of a commercial grade PMMA with characteristic values T_d, $T_{v0.05-0.2}$ and T_{max}

These values were not quite reached for the polymers produced in the pilot process during this research study, as will be presented in the following. Especially the weight loss rates $\mathbf{T_{v0.05}}$, $\mathbf{T_{v0.1}}$, $\mathbf{T_{v0.2}}$ were reached at considerably lower temperatures (compare table 4), which might be due to the fact that the pilot plant polymer contains rather large amounts of residual monomer, at least in comparison to commercial polymer, which has to be much better degassed at the end of the production process in order to meet environmental and toxicological requirements for consumer products.

Another reason might be oxidative degradation caused by gas leaks in the devolatilization chamber (this has been discussed in Chapter 4, "The final product" on page 114), which does not

only cause a brownish coloration of the polymer but can also lead to instable bonds in the polymer chains (e.g. by formation of (hydro)-peroxides).
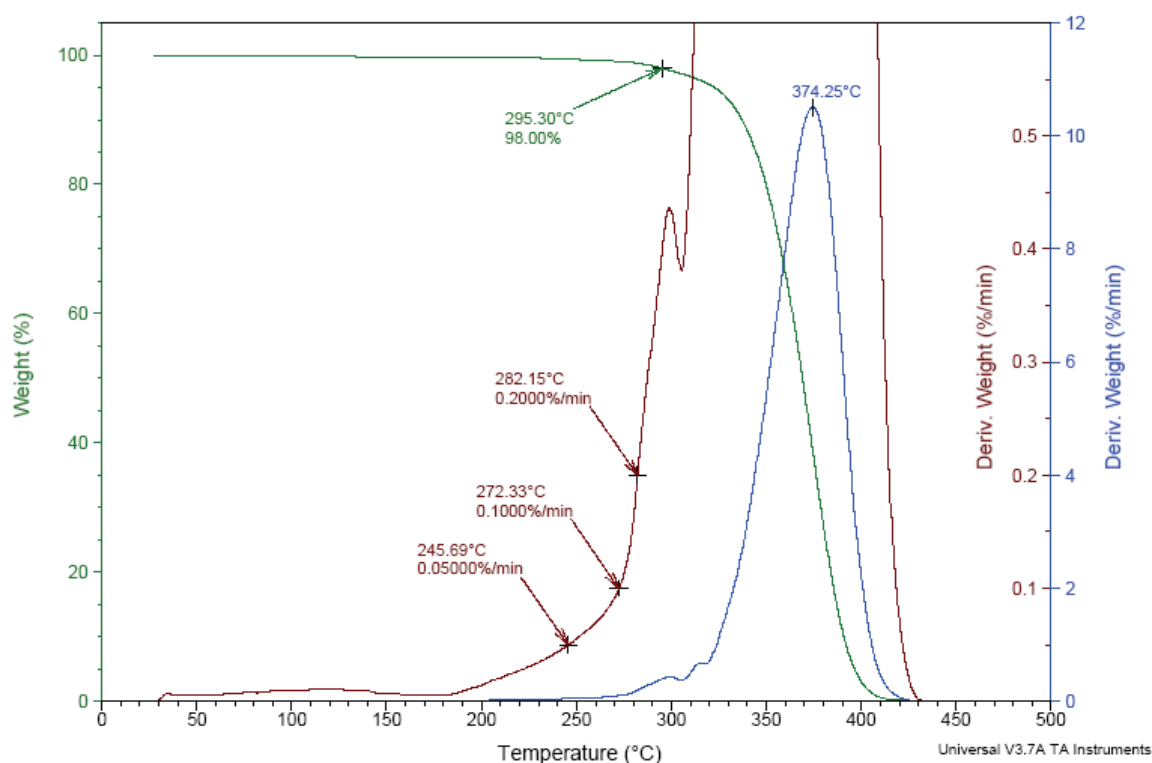
Figure 5.11: Thermogravimetry of a pilot plant sample (Exp. no 15) with characteristic values T_d, $T_{v0.05\text{-}0.2}$ and T_{max}

For a clearer structure, only three values are compared for the following evaluation of the thermal stability: $T_{d2\%}$, $T_{v0.1}$ and T_{max}.

One important trend already observed for the DSC batch polymerizations could be confirmed: the thermal stability is considerably improved by the addition of acrylate comonomer. Polymer samples containing no or little comonomer exhibit a lower T_{max} and $T_{v0.1}$ values than the samples with 5.5% MA. The $T_{d2\%}$ value is difficult to compare for the different samples since it is an integral value and depends, for example, on the amount of volatiles evaporated already at lower temperatures.

A second important observation is that also increasing the polymerization temperature improves the thermostability, even if the improvement is much less important than for the addition of comonomer. This is, at first sight, in contradiction to the results from batch polymerized

polymer samples (see figure 5.7), where increasing the temperature deteriorated the thermal stability. The explanation for these different observations is the presence of chain transfer agent in the pilot plant experiments, which reduces the number of weak linkages in the polymer chains, in particular the unsaturated chain ends:

For polymerizations without CTA, the amount of unsaturated chain ends increases together with the temperature. This means that, although at high temperatures the formation of head-to-head-bonds is more unlikely and the polymer gets more stable in the corresponding temperature region, the higher number of unsaturated chain ends deteriorates the overall thermal stability of the polymer. Adding a chain transfer agent, however, solves this issue by reducing the number of these unsaturated chain ends.

At the same time, as it was seen in Chapter 4, the chain transfer constant, too, increases with temperature, which means that the effectiveness of the transfer reation becomes even better for higher temperatures. This might be the explanation for the improvement of the thermal stability observed with increasing temperature.

The chain transfer agent, itself, also seems to have a rather significant influence, at least for high concentrations. At 140 °C, all T-values except the T_{max} increase by ~10 °C from [CTA] = 0.2 % to [CTA] = 0.5 %. This is in correspondence with figure 5.9, which shows that the weight loss above 200 °C is much smaller for samples that had been polymerized with a high CTA load.

Compared to the commercial standard, the thermostability of the analyzed polymer samples is rather poor in terms of the rate of weight loss below 300 °C. As mentioned above, only T_{max} could be significantly improved for polymerization temperatures above 150 °C with regards to the commercial polymer.

Table 4: Results for the thermal stability of different pilot plant samples

Exp. No.	T [°C]	MA [%]	CTA [%]	$T_{d2\%}$ [°C]	$T_{v0.1\%/min}$ [°C]	$T_{v0.2\%/min}$ [°C]	T_{max} [°C]
6	120	0	0.3	290	266	275	364
7	120	1.5	0.33	269	238	257	371
4	140	0	0.2	282	257	263	363

Table 4: Results for the thermal stability of different pilot plant samples

Exp. No.	T [°C]	MA [%]	CTA [%]	$T_{d2\%}$ [°C]	$T_{v0.1\%/min}$ [°C]	$T_{v0.2\%/min}$ [°C]	T_{max} [°C]
1	140	0	0.3	279	257	265	363
5	140	0	0.5	292	269	274	363
2	140	1.5	0.3	280	254	264	365
3	140	5.5	0.3	294	270	280	370
9	150	0	0.3	291	268	275	368
10	150	1.5	0.3	292	268	275	370
12	150	5.5	0.3	296	273	284	374
13	160	1.5	0.25	290	269	278	370
14	160	3	0.25	289	277	277	373
15	160	5.5	0.25	295	272	282	374
19	170	1.5	0.2	285	267	273	373
17	170	5.5	0.2	292	271	279	376
Commercial PMMA				314	282	296	366

5.3   Discussion

This chapter deals with the thermal stability and the depolymerization that are investigated for the case of PMMA. Since both phenomena depend on the unzipping of polymer chains, they are discussed in the same context. It was shown that due to the depropagation reaction, which is in thermodynamical equilibrium with the propagation of radical chains, the monomer conversion at temperatures above 170 °C is limited significantly. For the kinetic description of the depropagation, the rate constants for the calculation of k_{dp} were determined by means of fitting to experimental data. Using this k_{dp} it is possible to include the depropagation reaction in the model for PMMA polymerization derived in this work and to correctly predict the conversion limitation at different temperatures.

Also terminated polymer chains, i.e. the final polymer, can undergo thermal degradation by unzipping. The prerequisite is the activation of chains by scission of constitutive bonds in the polymer molecules. This can happen at different positions in the chains, i.e. for different bond

types exhibiting different thermal stabilities, and each type breaks in a characteristic temperature range. For homogeneous PMMA, the thermal degradation usually takes place in three steps, corresponding to three bond types that are particular for this kind of polymer: head-to-head bonds, unsaturated chain ends and the random C-C bonds of the polymer backbone.

One aim of the present work is to improve the thermal stability of the final polymer and to investigate different strategies of stabilization: the addition of an acrylic comonomer to prevent the polymer chains from complete unzipping, the addition of chain transfer agent to reduce the occurrence of weak bonds in the chains caused by non-uniform termination processes, and finally to increase the polymerization temperature in order to avoid completely the formation of thermally weak linkages in the molecules. The different influences on the thermostability were discussed at first instance by comparing TGA-curves for different polymer samples from batch polymerizations. Secondly, the thermostability results for different pilot plant polymer samples were evaluated.

The results showed that each of the three factors positively influences the thermal stability of the polymer, most of all the addition of a comonomer. Furthermore, by adding different acrylic and methacrylic comonomers to the reaction mixture, it could be proven that the alpha methyl group of the methacrylate is responsible for the unzipping mechanism and that by introducing small amounts of acrylic groups into the polymer chains, the thermal degradation can be significantly reduced.

The quality of the pilot plant polymer in terms of thermostability does not reach the high standards of commercial polymer. However, the slightly worse thermal resistance below 300 °C can be explained by the rather high residual monomer content and by oxidative processes taking place in the devolatilization, which, despite the efforts made during this research study, could not be made entirely gas tight. Additionally, the duration of each pilot plant experiment was by far too short to obtain a polymer that compares in terms of molecular uniformity to a commercial product, where the production process runs for long periods in steady state. However, it is remarkable that the value of T_{max}, i.e. the temperature of maximum rate of weight loss, is shifted upward by ~5-10 °C compared to the commercial polymer when the polymerization temperature is higher than 150 °C.

Short Summary:

- The depolymerization reaction has to be taken into account for the correct prediction of the monomer conversion at high temperature

- The value of the depolymerization rate constant was determined by fitting to experimental data

- PMMA thermally decomposes in three steps, which are due to the scission of (in the order of their thermal stability): the polymer chain at head-to-head bonds, unsaturated chain ends and random C-C bonds.

- The thermal stability of PMMA is influenced by the following parameters: presence of acrylic comonomers, presence of chain transfer agent, polymerization temperature

- Each effect is discussed by means of experimental results from batch and continuous polymerizations.

Conclusions and Perspectives

Anyone who has never made a mistake
has never tried anything new.
<div align="right">- Albert Einstein (1879-1955)</div>

The present Ph.D. thesis focused on the continuous high temperature polymerization of methyl (methacrylate) at pilot scale, its kinetic description and a study of the impacts of various process parameters on the obtained polymer. Its major aims are listed in the introduction of this report on page 7 and the summarized conclusions will be presented in the same order together with the perspectives, i.e. issues that, according to the authors opinion, might need to be refined or be interesting subject of further investigations in future.

Generally, it can be stated that the high temperature polymerization aiming for the production of PMMA molding compounds is technically feasible and yields certain advantages in comparison to a lower temperature process. The most important features are

- a better and safer handling of the process due to reduced viscosity
- less risk to enter the gel effect and, therefore, higher kinetic reactor stability
- higher reaction rates and, therefore, higher space time yields
- reduced need for chain transfer agent and initiators
- increased thermal stability of the polymer

A major disadvantage of a high temperature process might be an increased energy demand for heating and more expensive equipment to resist the more severe process conditions. Unfortunately, the time frame of this work did not allow a study of the economical consequences of increasing the temperature. It might be an important aspect of future investigations to weigh the additional costs against the benefits concerning process and product quality.

In the following, the results from all different parts of this work will be summarized with respect to the different chapters they were discussed in.

Self-Initiation at high temperature

Acrylic monomers are subject to a rather pronounced spontaneous initiation. In the case of MMA it was demonstrated that, depending on the process conditions, monomer conversions as high as 30% can be observed in absence of any intentionally added initiator. The source of this self-initiation is mainly the formation and decomposition of a polymeric peroxide (the so-called MMA-peroxide or PMMAP), which forms from physically dissolved oxygen in the monomer and the monomer, itself. However, there are other mechanisms contributing to the initiation at high temperature. These are the initiation by **chain transfer agent** as well as the "true" **thermal initiation** of the monomer (i.e. no other species involved). At very high temperatures (> 170 °C), also the **dimerization** and formation of higher MMA oligomers influences the monomer conversion, but these reactions follow a different mechanism and do not directly take part in the initiation of the radical polymerization. The importance of all different initiating mechanisms was compared for the temperature range 140 °C - 180 °C and related to each other.

The **formation** and **decomposition** of **MMA-peroxides** have been extensively investigated in this work, which resulted in the determination of reaction rate constants for both of them. As a part of the peroxide formation investigations, a method for the determination of organic peroxides by UV spectrophotometry was developed. The MMA-peroxide could be successfully synthesized in sufficiently large quantities to allow its characterization by advanced analytical methods (GPC, TGA, NMR). It was found that it consists of copolymeric chains of the alternating structure ~MMA-OO-MMA-OO~ with molecular weights of approximately $M_w = 5'000\text{-}8'000$ g/mol (determined by GPC). They form quickly and in significant amounts at temperatures between 50 °C and 100 °C and start decomposing above ~110 °C. It is, therefore, legitimate to compare

them to high-temperature decomposing thermal initiators. Although their efficiency as initiator is rather low ($f \sim 0.2$), their presence even in small quantities is enough to cause considerable monomer conversions.

The information obtained from studying the spontaneous initiation of MMA were implemented in a **kinetic model** for the description of the high temperature kinetics and **validated** by comparison to **experimental data** from batch polymerizations with and without initiator.

A point, which needs to be improved for future studies is the determination of oxygen in monomer and solvent. In this work, it was tried to determine the concentration of oxygen in MMA under different conditions. However, the analytical method is quite complicated due to the strong disturbing effect of atmospheric oxygen, so that in the end only a concentration estimate for the saturation concentration at one temperature could be realized. This estimate (~ 60-80 ppm O_2 at $18\,°C$) is, nevertheless, in agreement with literature values for other acrylic monomers.

Gel effect at high temperatures

Since the characteristic of the gel effect changes drastically at high temperatures with respect to the gel effect observed at temperatures below $100\,°C$, it was necessary to find suitable model equations to describe it in the kinetic model for the batch and the continuous process. Unfortunately, most existing models that can be found in the specialized literature are rather limited concerning their interval of validity and their applicability to continuous polymerization. The challenge was, therefore, to find a suitable basic gel effect model and to refine it in a way so that it meets the requirements of this work. This could be realized by **modifying** the widely-known **Chiu, Carrat and Soong (CCS-) model**. The modification consisted mainly in eliminating the dependency on the initiator concentration and to relate the change of the **termination rate constant** directly to the **molecular weight**, instead. The new model equation could then be fitted to experimental data obtained in this work as well as to literature data.

The correct prediction of the high temperature gel effect with this adapted modeling approach could be proven for batch and continuous polymerization experiments within the experimental conditions used in this work and, at the same time, the results allowed investigating the influence of **changing different process conditions** (CTA, T, solvent etc.) on the **shape** and **intensity** of the **gel effect** and the correct consideration of this influence by the model.

Continuous High Temperature Polymerization

The major challenge in this work was the design and construction of a complete pilot plant installation for the continuous polymerization of MMA. The final setup used for the polymerization experiments presented in this report consisted of a **recycle loop** combined with a single **tube reactor** equipped with Sulzer SMXL/SMX static mixing elements. The pilot plant was operated for 5 - 10 hours experiments, depending on the quantity of polymer needed. The mean residence time in each reactor part was of ~ 30 min. The **obtained polymer** had a **molecular weight** of approximately **100 kg/mol** and was analyzed for its thermal stability and residual volatiles' concentration.

Moreover, the pilot plant was equipped with two **ultrasound probes** for speed of sound measurements of the polymer solution. This technique allowed the **inline conversion measurement** based on a mathematical treatment of the obtained speed of sound values as a function of temperature and pressure. The realization of a correct conversion measurement required the reevaluation of **compressibility** data for MMA and butyl acetate taken from literature. Unfortunately, there was no possibility to determine at the same time the solvent fraction in the reactor. The equation for the calculation of the speed of sound had, therefore, to be reduced assuming an either constant or zero solvent fraction. Since in the beginning of the reaction the solvent that is present in the reactor during heating needs to be displaced, which takes approximately 5 residence times, this assumption does not hold true and the conversion measurement is only correct at, respectively, close to steady state. An improvement for the future would be the combination of ultrasound measurement with other analytical methods in order to have access to the solvent concentration. Thus, the number of unknowns in the ultrasound equation could be reduced and monomer conversion measurement would be possible independently of the solvent fraction present in the reactor.

For the modeling of the continuous polymerization in loop and tube reactor, a kinetic model was established in PREDICI®. This model allowed the correct prediction of conversion and molecular weight distribution as well as a parameter study for various process parameters.

The data obtained from experiments in the loop reactor with varying amounts of CTA and comonomer allowed the determination of the **chain transfer constant** for **n-dodecanethiol** as well as the **reactivity ratios** for the system **MMA / MA** at the investigated temperature range. In

order to obtain these values, some simplifications respectively assumptions had to be made. For the chain transfer constant, the concentration of thiol in the reactor could not be determined analytically and had, therefore, to be estimated. The determination of the r-parameters for MMA and MA by the **Kelen-Tüdös** method turned out to be difficult due to a too limited variation of the comonomer fraction (1 - 5 wt-%), leading to unrealistic results for the reactivity of the comonomer. Only by the addition of a fictive point on the other end of the concentration scale it was possible to come to realistic values for the reactivity ratio of MA-terminated chains. The results showed that future experiments should be carried out with higher MA weight fractions of at least 20% in order to obtain more precise values for the r-parameters.

Finally, the **thermal stability** and the **depolymerization** of PMMA were discussed. They both base on the same degradation mechanism of active polymer chains, the so-called **unzipping**, which can be stopped by the incorporation of acrylate monomers in the polymer chain. This is the reason why the thermal stability of PMMA can be significantly **improved** by the addition of **methyl acrylate**. The change of thermal stability with changing process parameters (temperature, chain transfer agent, comonomer concentration) was discussed for samples from batch and continuous polymerizations. It was found that increasing the process temperature has only a slightly improving impact on the thermal stability. On the other hand, it is strongly improved by the addition of methyl acrylate as comonomer or a n-dodecanethiol as chain transfer agent. This is due to the stopping of the unzipping mechanism at comonomer units in the chain, respectively due to more uniform chains with less instable bonds in the case of a chain transfer regulated polymerization.

After all, the results of the present Ph.D. thesis are motivating for further studies concerning the high temperature polymerization of MMA. It could be shown that in many regards, increasing the reaction temperature yields interesting improvements of process and product properties. And although the pilot plant setup used in this work as well as the process conditions will have to be further optimized in order to obtain a final product with the degree of sophistication of a modern commercial PMMA concerning its optical and thermal qualities, the results concerning the kinetics and parameter studies will, hopefully, be valuable for future research and process optimization in industry.

Analytical Techniques and Method Development

In this work, various techniques have been employed for all the different analytical tasks. Since most of them are relevant for several chapters of this thesis, it was chosen to bundle their description in one Annex and to refer hereto within each chapter. In the following are explained in detail each analytical technique used in this work as well as the corresponding methods, many of which had to be developed in the frame of this study.

1.1   Headspace Gas Chromatography

Gas chromatography (GC) is the method of choice for the analysis of volatile compounds. The general concept is widely known and not presented again at this point. When it comes to polymers or polymer containing mixtures, the use of standard gas chromatography is, however, not possible. The simple reason for this is that polymers are not volatile and must, therefore, not be injected into the evaporator of a GC, where they would simply get stuck and block the injector port with time.

A technical solution for this problem is the so-called headspace gas chromatography (HS-GC), the principle of which is rather simple: Before the injection into the GC, itself, the polymer is separated from the volatiles to be analyzed. In the case of the dynamic headspace technique,

this is done by evaporating the volatiles during a first phase at elevated temperature into a stream of inert gas (in general the carrier gas of the GC), condensing them by means of a cold trap containing an adsorbent, and in a second phase, evaporating them quickly (ideally as a peak function) from the trap into a capillary leading to the GC column. Figure 1.1 shows the schematic cycles of headspace GC analysis. Since the sample amount in the sample tube is naturally much larger than in conventional GC, where usually 1-5µl of liquid sample are injected, there are two split valves to reduce the quantity of sample transferred to the GC in order to avoid saturation.
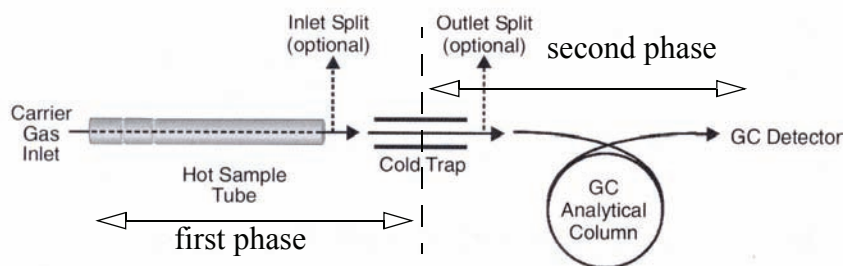
Figure 1.1: Principle of the head-space thermal desorption GC

The device employed in this work is a Perkin-Elmer ATD Thermal Absorber with sampling robot in combination with a Perkin Elmer Autosystem GC with FID detector. The device settings are summarized in table 1.

Table 1: Device settings for the Headspace-GC

Evaporation temperature	120 °C
Time of evaporation from sample tube	30 min
Temperature of the cold trap	- 30 °C
Inlet split factor	10:1
Outlet split factor	20:1
Desorption temperature of the trap	130°C
Desorption interval	2 min
Temperature of the transfer capillary	130°C
GC program	80-120°C, 2.5°C/min
GC capillary column	SUPELCO SPB-1 30m, ⌀0.53mm, 0.1µm film
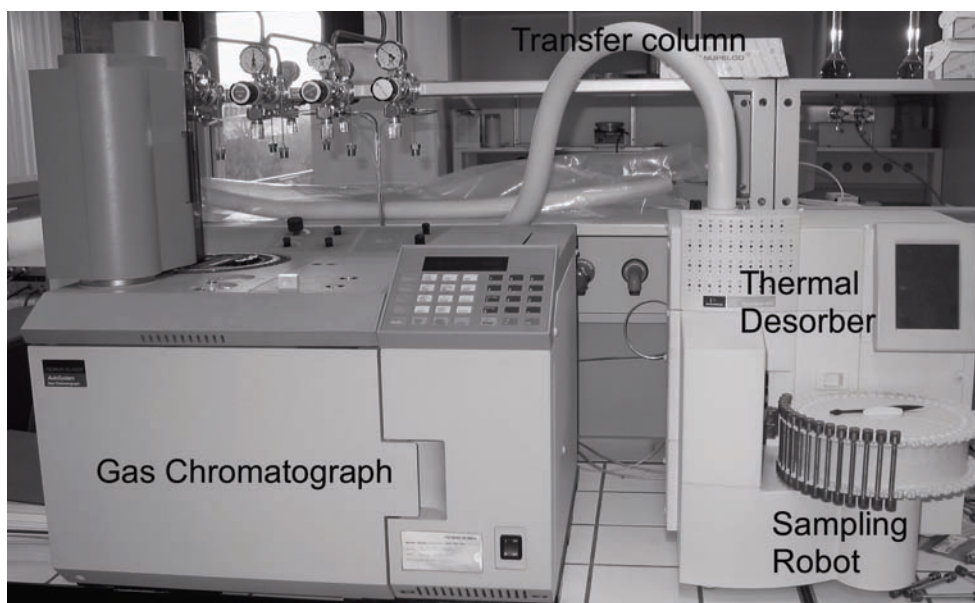
Figure 1.2: Picture of the Perkin-Elmer ATD Thermal Desorber HS-GC system

Sampling system

Samples need to be prepared in device-specific stainless steel tubes that are compatible with the sampling robot and the evaporation furnace. The fixation of the sample in the tube is either done with the help of an adsorbent in the case of liquid samples, or with a piece of glass wool in the case of viscous samples. The absorbent, respectively, the glass wool is placed in a PTFE inliner and held back by two glass wool stoppers. The whole inliner is fixed with two stainless steel springs.

It must be taken care that the contents of the tube are loose enough so that the desorption gas stream can still pass. Especially if the adsorbent or the glass wool stoppers are too compressed, the free flow of the gas is disturbed and the measurement can be faulty.

On the sample robot, the tubes are sealed with stick-on caps. These caps must close the tubes tightly, otherwise volatiles may evaporate from the tube while waiting for analysis, hence making the measurement incorrect.
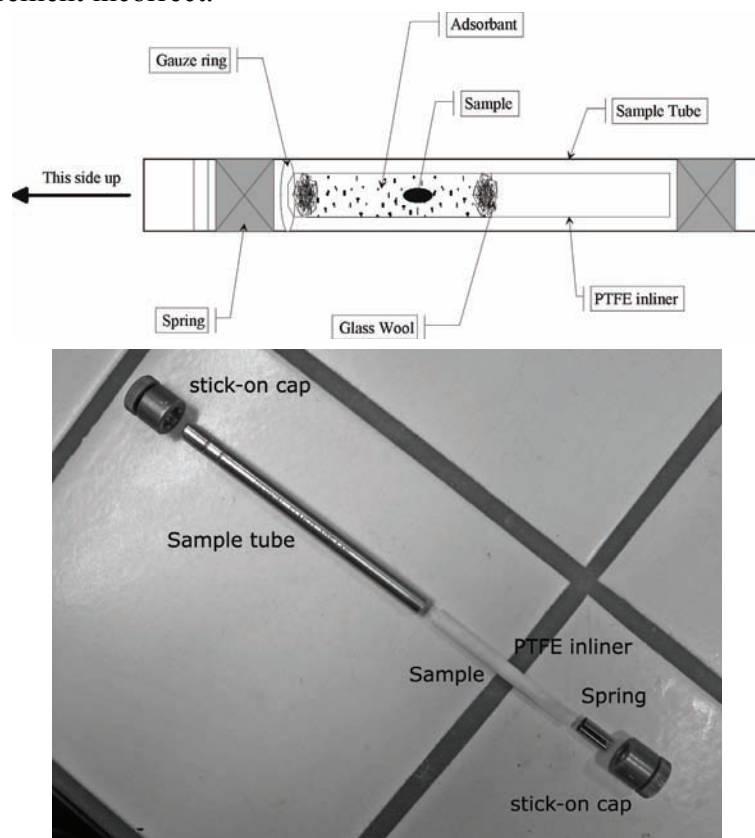
Figure 1.3: Principle of sampling tube and fixation of the sample

Sample preparation

Liquid, no polymer containing samples (e.g. condensate, calibration) are injected with a syringe directly onto the adsorbent in the sampling tube. The injected volume is in the range of V = 1-20µl, depending on the type of sample.

For viscous samples, as those from the pilot plant, a weighted amount of sample is first dissolved in 400µl DMF for improved evaporation of the volatiles in the headspace device. The evaporation directly from the polymer matrix would take by far more time than evaporation from a dilute solution of polymer and volatiles. 10µl ethyl benzene are added as internal standard and the sample is left on a stirring table for 30 minutes. Consecutively, 20µl of the sample solution are transferred with a micropipette on a piece of glass wool in the sample tube. The glass wool fixes

the sample and holds back the polymer matrix during the evaporation. After each injection, the glass wool is renewed and the PTFE inliner cleaned.

HS-GC Calibration

The HS-GC was calibrated in the same range as the samples to be analyzed. Different, known amounts of an analyte containing solution were injected as described above into an adsorbent containing sampling tube. From the GC peak response and the known sample amount, a calibration curve could be established for each analyte. Figure 1.4 shows the calibration curve for the four analytes of interest.

Calculation

With the help of the calibration equation and the corresponding calibration parameter $K_{analyte}$ the amount of each analyte present in the sample tube (i.e. 20μl of the sample solution) can be determined.

$$m_{analyte}[mg] \ = \ K_{analyte}\left[\frac{mg}{\mu Vs}\right] \cdot A_{peak}[\mu Vs] \tag{EQ 1.1}$$

In order to know its exact amount in the entire sample, it has to be correlated to the internal standard (ethyl benzene). Therefore, it is multiplied with a correlation factor Ω, which is the quotient of the amount of EB added as internal standard and the amount found for the sample tube.

$$\Omega \ = \ \frac{m_{IS}[mg]}{m_{EB}[mg]} \tag{EQ 1.2}$$

The amount of analyte in the entire sample becomes, thus,

$$m_{analyte}^{sample}[mg] \ = \ K_{analyte}\left[\frac{mg}{\mu Vs}\right] \cdot A_{peak}[\mu Vs] \cdot \Omega \tag{EQ 1.3}$$
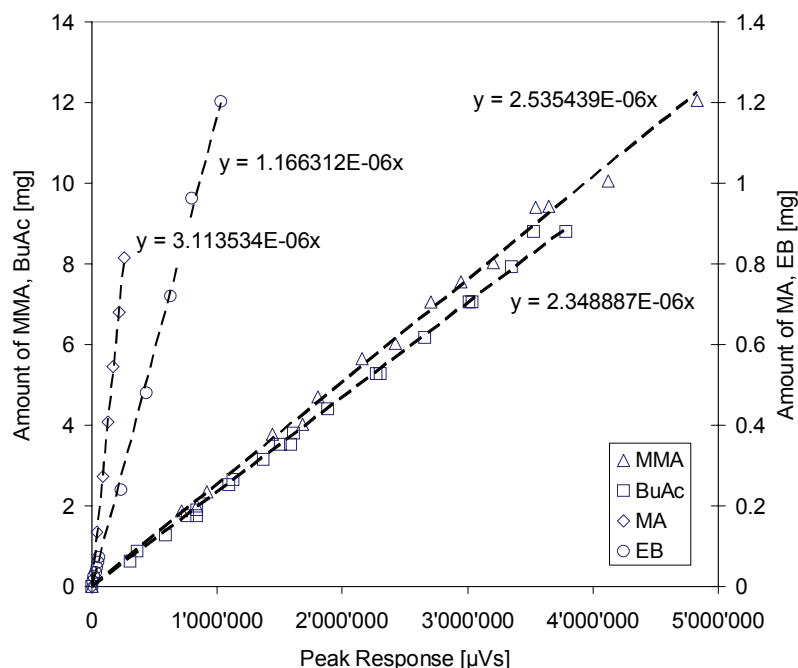
Figure 1.4: GC calibration curves for MMA, MA and BuAc

In order to calculate the monomer conversion of a sample, the amount of monomer needs to be correlated to an initial amount of monomer m_0, i.e. at zero conversion.

$$X(MMA) = \frac{m_0(MMA) - m(MMA)}{m_0(MMA)} \qquad \text{(EQ 1.4)}$$

There are basically two ways of determining m_0. If there is solvent present in the process, it can be considered as inert, i.e. its weight fraction does not change during the reaction (it must not change during the sampling, neither, i.e. by evaporation!). The initial amount of monomer is then:

$$m_0[mg] = \frac{m_{MMA}^{sample}[mg]}{w_s} \qquad \text{(EQ 1.5)}$$

In the absence of solvent, the amount of sample dissolved in DMF must be weighted and can be considered as m_0, assuming there are no other monomers present. In the case of the copolymerization, the amount must be multiplied by the monomer weight fraction of the initial mixture.

The residual volatiles' concentration is determined in the same way: a known amount of polymer is dissolved in 400µl DMF and analyzed as described in the HS-GC. The found amount of volatiles is divided by the sample weight and the residual volatiles' concentration is obtained.

1.2　　　Size Exclusion Chromatography

Another very important kind of analysis in polymer reaction engineering is the determination of the molecular weight. The technique of choice is the Gel Permeation Chromatography. In the Wikipedia online encyclopedia [119], it is defined as follows:

"Gel permeation chromatography (GPC), also known as size exclusion chromatography (SEC), is a chromatographic method in which molecules are separated based on their size. This method is most widely used in the analysis of polymer molecular weights (or molar mass). The term GPC was used in the beginning of polymer analysis when people used glass columns filled with gels to perform GPC. Nowadays more and more automated and high pressure liquid chromatographic columns are used. Therefore GPC is an old terminology and size exclusion chromatography (SEC) is the correct expression for the determination of molecular weights.

In SEC, a column (steel cylinder typically 10 mm in diameter and 500 to 1000 mm in length) is packed with a porous material (typically silica or crosslinked polystyrene) and solvent is forced through the column (at rates typically 1 ml/min and pressures of 50 to 200 bar). A sample is dissolved in the same solvent that is running through the column and is then introduced into the solvent stream going through the column. A detector monitors the concentration of sample exiting the end of the column. Inside the column, molecules are separated based on their hydrodynamic volume (the volume the molecule occupies in a dilute solution). For polymers this can vary greatly with the particular solvent and the temperature. By studying the properties of polymers in particular solvents and by calibrating each column setup with samples of known molecular weight, it is possible to get a relative distribution of molecular weights for a given polymer sample. Using this data, it is possible to calculate number average molecular weight, weight average molecular weight, polydispersity, as well as higher order molecular weights within a useful level of accuracy.

Inside the column, molecules are separated by whether or not they can fit within the pore size of the packing material. When columns are created they are packed with porous beads with a

specific pore size so that they are most accurate at separating molecules with sizes similar to the pore size. As a molecule flows through the column it passes by a number of these porous beads. If the molecule can fit inside the pore then it is drawn in by the force of diffusion. There it stays a short while and then moves on. If a molecule can not fit into a pore then it continues following the solvent flow. For this reason, in a GPC column, molecules with larger size will reach the end of the column before molecules with smaller size. The effective range of the column is determined by the pore size of the packing. Any molecules larger than all the pores in a column will be eluted together regardless of their size. Likewise, any molecules that can fit into all the pores in the packing material will elute at the same time.

It is important to remember that the only absolute measure in SEC is volume of the molecule (hydrodynamic volume), and even that measurement has certain error built into it. Interactions between the solvent, packing, and or the sample will affect the measurement as will concentration due to sample-sample interactions. Calculating the molecular weight from this molecular size introduces even more error into the system. SEC is a useful tool for determining molecular weight in polymers, but it is essential that the column and instrumentation be carefully equilibrated and properly calibrated for the results to be trusted."

The device used in this work is a Viscotek Triple Detection SEC TDA300 with refractive index, viscosity and light scattering detector. Measurement parameters are provided in table 2.

Table 2: Measurement parameters for the SEC molecular weight analysis

Solvent / Eluent:	THF (GPC grade, Fisher Scientific T/0709/PB17)
Flowrate:	1 ml/min
Sample concentration	approx. 1 - 20 mg/ml
Sampling volume:	100 µl
Column set:	2 x PSS (Germany) linear M SDV 8x300 5µm 1 guard column
Column temperature:	35°C

Polymer standards:	*For conventional calibration:*
	    PSS ReadyCal PMMA standards (series) (800 - 1'180'000 g/mol)
	For triple detection:
	    PSS Polystyrene standards (one at a time) (60'000 - 470'000 g/mol)
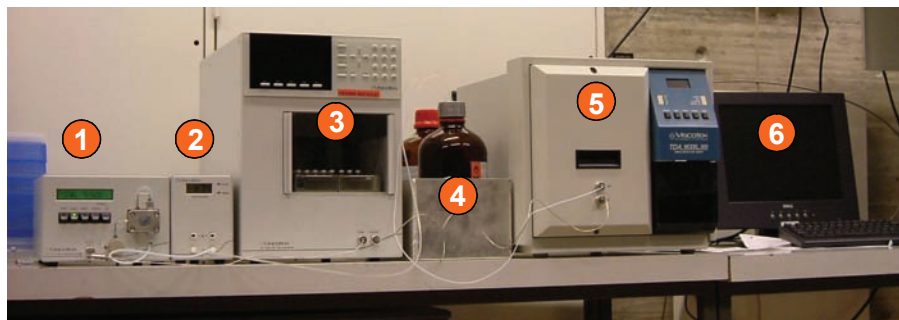
Figure 1.5: Viscotek SEC-System with (1) HPLC pump, (2) Degasser, (3) Autosampler, (4) Eluent storage, (5) Detector unit, (6) Computer for data acquisition

Sample preparation

The polymer sample (viscous or solid) is weighted and, depending on the sample size, 1 - 5 ml THF (GPC grade) are added so that a final concentration in the range of 1 - 20 mg/ml is obtained. In the following, the solution is left on a stirring table overnight until complete dissolution of the polymer (optical inspection). For very high molecular weight or branched polymers it might be necessary to leave them on a heated stirring table (T ~ 40 °C) in order to shorten the time necessary for dissolution.

The knowledge of the exact sample concentration is necessary for the determination of the polymer content by RI. Since the RI determines a concentration corresponding to the polymer peak (it does not "see" the low-molecular volatiles), the polymer content respectively the conversion can be determined by the equation:

$$w_p = \frac{c_{polymer}[mg/ml]}{c_{totalsample}[mg/ml]} \quad \text{and} \quad X = \frac{w_p}{1-w_s} \tag{EQ 1.6}$$

Triple Detection (SEC^3)

The fractionated polymer molecules undergo three different analyses:

First of all the *refractive index detector* (RI). By means of the refractive index, the concentration of each polymer fraction can be determined, as the refractive index increases linearly with concentration:

$$\frac{dn}{dc} = 0.083 \quad \text{(for linear PMMA)} \tag{EQ 1.7}$$

It is measured against a reference cell filled with eluent in order to eliminate the refractive index of the solvent.

Secondly, the *intrinsic viscosity* of the polymer fraction is determined by a *relative visco-simeter*. It is based on a differential Wheatstone bridge and measures the pressure drop over a capillary. The eluent flow coming from the refractometer containing the polymer is separated into two equivalent flows. One is delayed in the following by a retention column, the other flows unhindered to the capillary. The pressure drop in the capillary depends on the viscosity of the fluid. Since on one side, the polymer has already reached the capillary, whereas on the other side it is held back in the retention volume, a pressure difference is measurable between both arms of the Wheatstone bridge. This pressure difference (DP) is proportional to the viscosity of the polymer fraction passing the capillary at the very moment.

Thirdly, a *right-angle laser light scattering detector* (RALS) is installed in the detector unit, which measures the absolute molecular weight, molecular size, density and conformation, and can furthermore provide structural information on branching and aggregation.
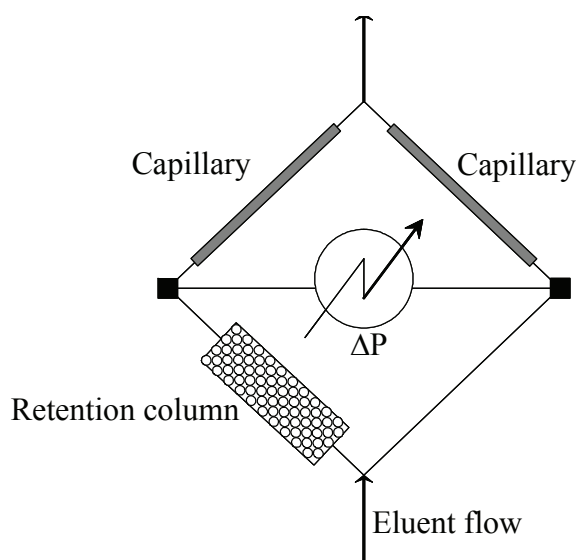
Figure 1.6: Measuring principle of the relative viscosimeter (Wheatstone bridge)

From the information of all three detectors, the molecular weight distribution of the polymer sample can be determined from one single injection. The major advantage is that only one standard (usually polystyrene) is needed in order to once in a while calibrate the detectors instead of a series of standards of the same polymer as the sample, as for the conventional calibration.

Furthermore, the precision of the measurement is supposed to be higher than that of the conventional calibration since information of three independent measurements is taken into account for the calculation of the molecular weight [120]. In figure 1.7 is shown a typical SEC triple detection spectrum with the responses from refractometer (RI), viscosimeter (DP) and light scattering (LS).
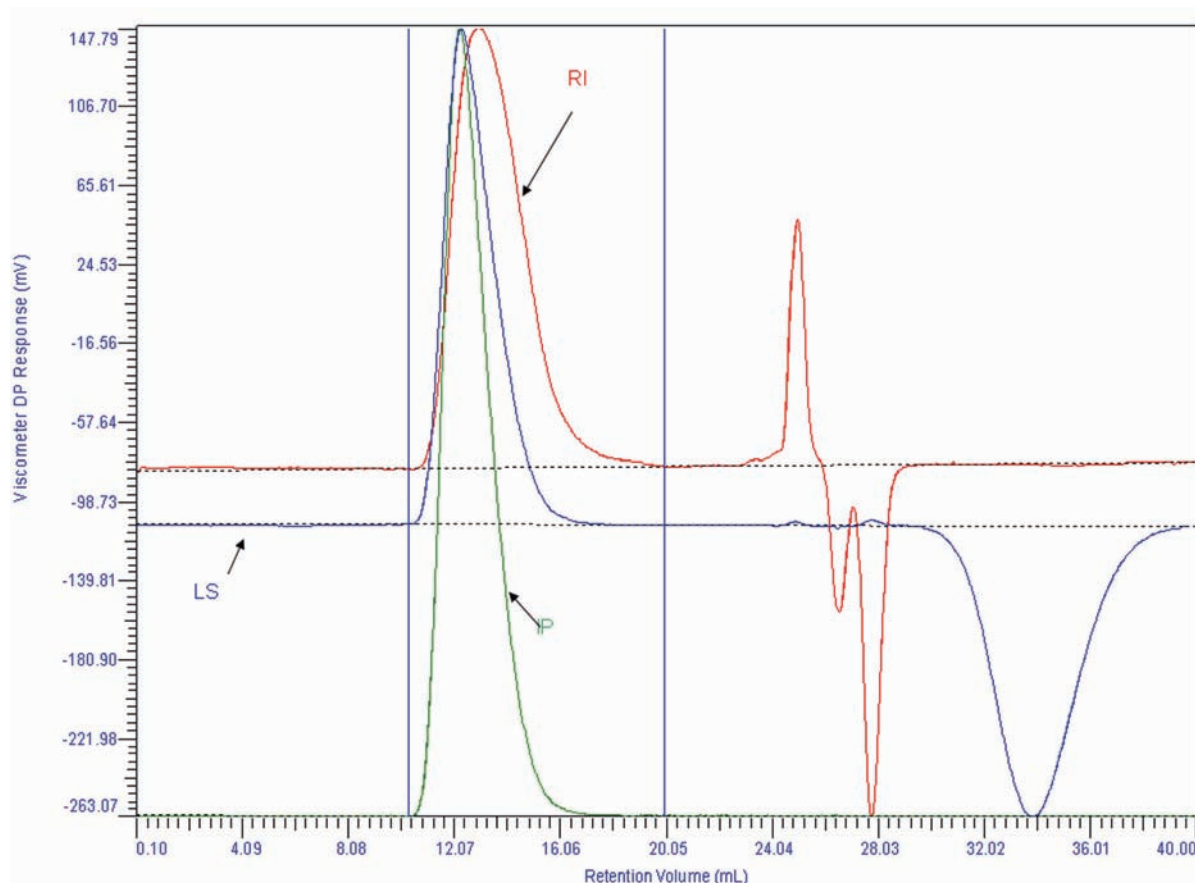
Figure 1.7: SEC Triple Detection spectrum of a PMMA sample

Conventional Calibration

For the conventional calibration, only the *RI* detector is used. By comparing the peak to a series of standards (calibration curve), the molecular weight distribution can be calculated. This method is illustrated in figure 1.8. It is the simplest way of analyzing the molecular weight and does not need complicated calculations like the triple detection method. However, the disadvantage is that, due to different interactions of each polymer with columns etc., standards of the exactly same polymer as the analyzed one are needed, which - in the case of more exotic poly-

mers than PMMA - can be difficult to find. Furthermore, the molecular weight changes with different standard origins. It can occur that by changing the producer of the standards, the measured molecular weight increases by as much as 10%. On this account, the triple detection provides a more independant measure of the molecular weight.
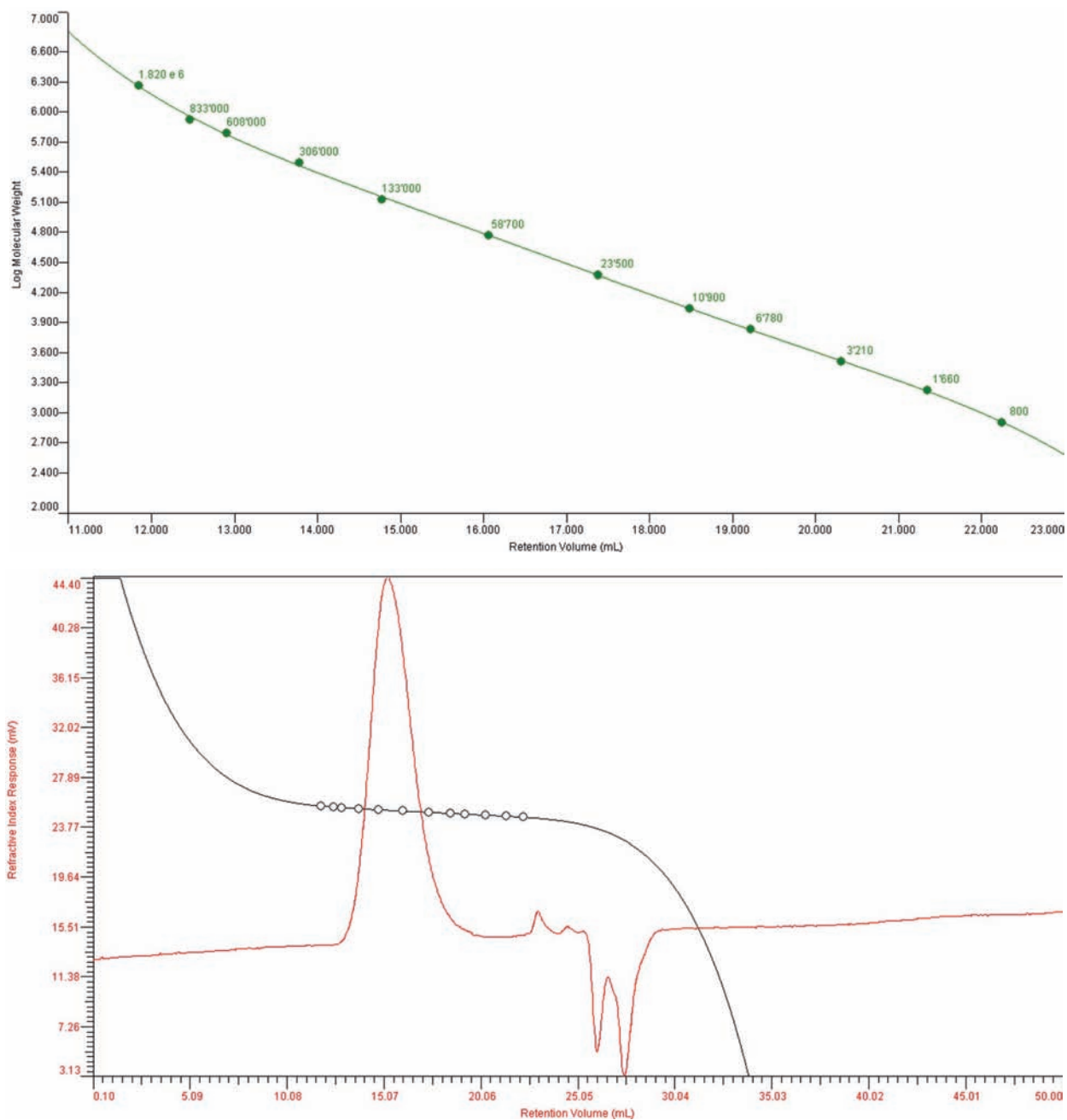
Figure 1.8: Conventional GPC analysis

1.3   Differential Scanning Calorimetry

Calorimetry is the science of measuring the heat of chemical reactions or physical changes. Differential scanning calorimetry (DSC) is a thermoanalytical technique in which the difference in the amount of heat required to increase the temperature of a sample and reference are measured as a function of temperature. Both the sample and reference are maintained at very nearly the same temperature throughout the experiment. The basic principle underlying this technique is that, when the sample undergoes a physical transformation such as phase transitions, more (or less) heat will need to flow to it than the reference to maintain both at the same temperature. Whether more or less heat must flow to the sample depends on whether the process is exothermic or endothermic. There are two main types of differential scanning calorimeters: *heat flux DSC* and *power compensation DSC*.

In a *heat flux calorimeter*, the heat transported to the sample and reference in a furnace is controlled while the instrument monitors the temperature difference between the two.

In *power compensated calorimeters*, separate heaters are used for the sample and reference. Both the sample and reference are maintained at the same temperature while monitoring the electrical power used by their heaters (see figure 1.9).
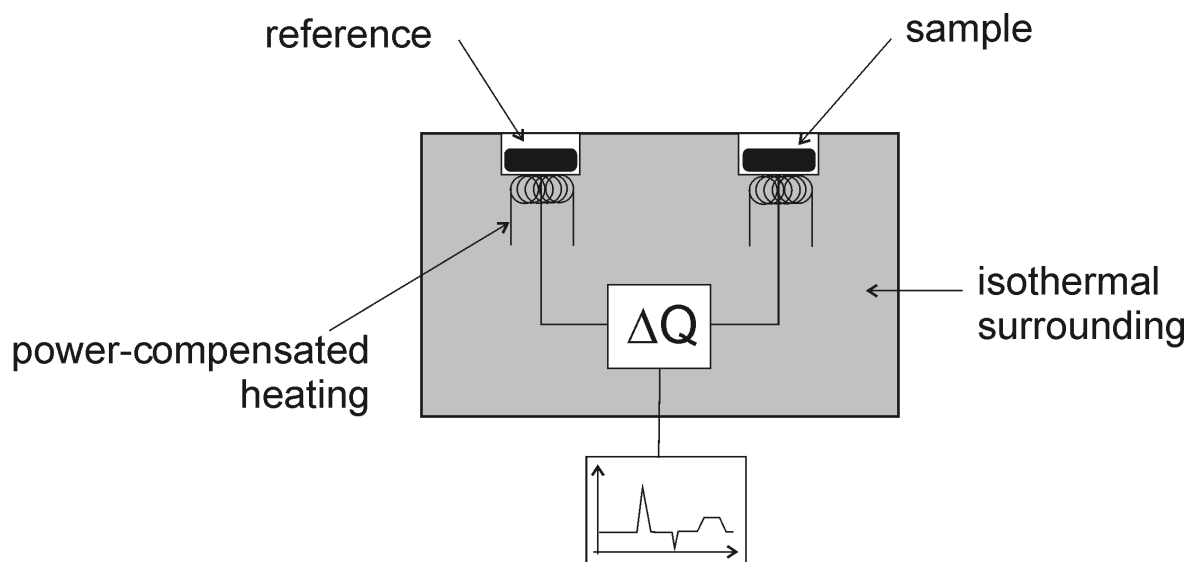
Figure 1.9: Principle of the Power-compensated DSC

The calorimeter employed in this work is a power-compensated Perkin Elmer Pyris1 DSC (figure 1.10 b) with cryostat (IP Intracooler unit) for sub-ambient measurements. Sample solutions of usually 20µl are filled into 60µl stainless steel medium pressure crucibles (figure 1.10 a), which resist pressures of up to 40 bars.

(a)   (b)

Figure 1.10: (a) Medium-pressure stainless steel crucibles consisting of bottom, cover and O-Ring, (b) Perkin-Elmer Pyris1 DSC with Intracooler

The DSC was mainly used to polymerize samples at different temperatures, but also to determine peroxide decomposition kinetics and glass transition temperatures T_g. For the polymerizations, an isothermal temperature programm was used with an initial heating rate of 40 °C/min until reaction temperature. The conversion at time t can be determined by two methods: one is to stop the reaction by throwing the crucible into liquid nitrogen and measuring the conversion by GC analysis. In order to obtain also the molecular weight at time t, the experiment needs to be repeated under the exact same conditions and this time GPC analysis is done with the sample.

Another way to obtain the conversion is integration of the heat flow curve. Assuming that the reaction reaches full (= 100 %) conversion at the end, the conversion at time t can be calculated from the heat flow curve by equation 2.21 on page 28. This method has the advantage that the experiment only needs to be done once and that the reaction does not need to be stopped each time, which causes a certain error of the measurement. On the other hand, by assuming full conversion, this method is not fully correct, neither, which is in particular the case for high temperatures, where the calculation needs to be corrected by the "real" final conversion that is reached for the given temperature.

For the peroxide decomposition, a temperature scan was employed with constant heating rates between 1 and 10 °C/min. From these scans, the decomposition kinetics can be determined as explained in chapter 2.

1.4   Thermogravimetry-Mass spectroscopy

Thermogravimetry is a method for the determination of the thermostability of substances. A sample is continuously weighted on a high-precision microbalance in an oven while the oven temperature is constantly increased. The sample weight - temperature curve characterizes the substance's behaviour at elevated temperatures, i.e. sample degradation ("thermostability") or weight-loss by evaporation of water or other volatile compounds.

In order to get a more detailed picture of weight-loss mechanisms, this method can be combined with gas-phase analytical techniques for the analysis of volatile (decomposition) compounds that might evaporate from the sample, such as *Fourier Transform Infrared Spectroscopy (FTIR)* or *Mass Spectrometry (MS)*.

The device used in this work is a *Mettler-Toledo TGA/SDTA851e SF*, connected over a heated transfer capillary to a *Pfeiffer Vacuum Thermostar Mass Spectrometer* (see figure 1.11).
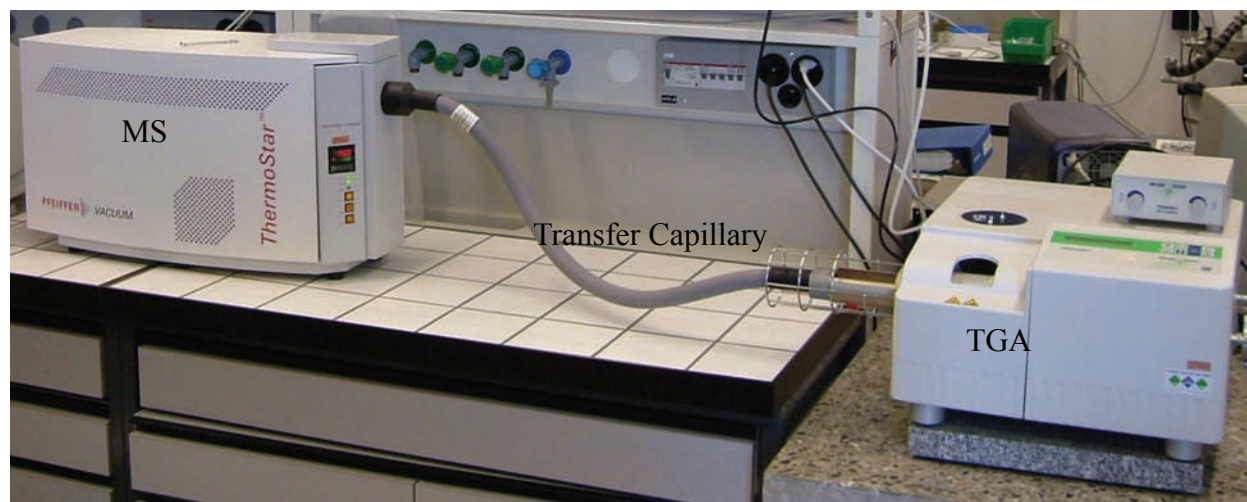
Figure 1.11: Mettler TGA/SDTA851e system coupled with a Pfeiffer Vacuum Thermostar Mass Spectrometer

With the TGA, measurements up to 1100 °C are possible. The polymer samples (5-30mg) are filled into 70µl alumina crucibles (sapphire crucibles for peroxide decomposition measurements). Heating rates typically vary between 1 and 10 °C/min. For better comparability of different polymer samples, it is common to define specific criteria for the weight loss (i.e. 2%), the rate of weight loss (i.e. 0.2 %/min) or the maximum weight loss rate and compare the temperatures where each sample reaches these values (illustrated in figure 1.12). In industry, these criteria represent important indicators of the product quality.

(a)	(b)
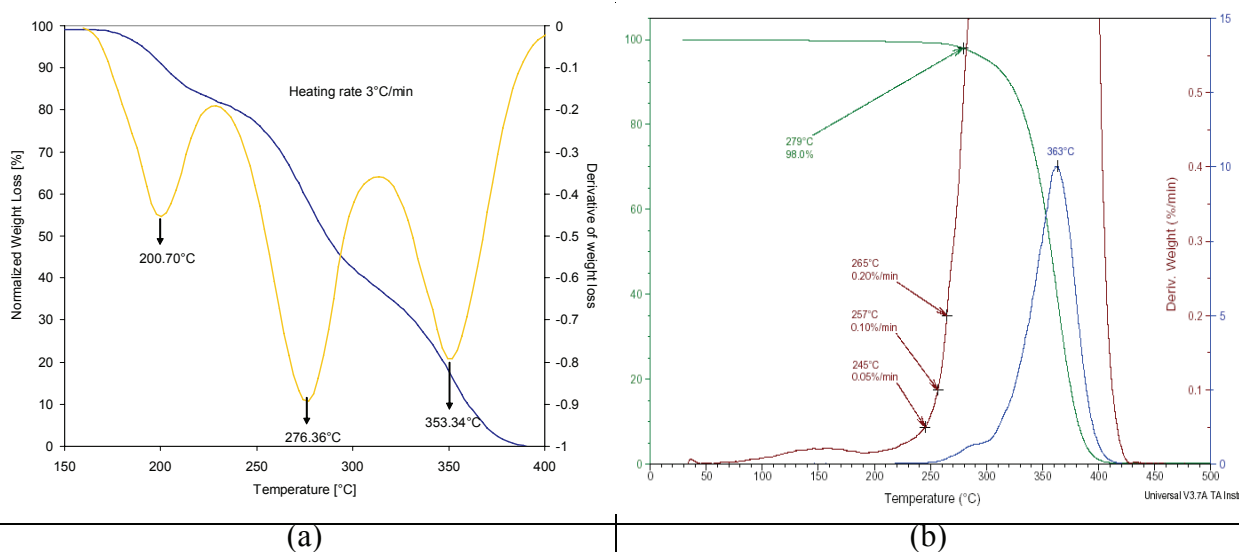
Figure 1.12: Examples of TGA-measurements of PMMA
(a) untreated polymer from DSC experiment
(b) heat-treated polymer from pilot process

The mass spectrometer used in this work is a gas phase quadrupol mass spectrometer with electron ionization (EI) and a detection range of 1-200 amu (C-SEM/Faraday detector). By means of mass spectrometry, it is possible to analyze the molecular weight of compounds evolved from the decomposing sample, i.e. MMA in the case of PMMA homopolymer or methyl pyruvate for PMMAP. It is possible to measure an entire spectrum of masses with time (spectrum mode) or to follow user-defined masses with time (tracking mode). Figure 1.13 shows the example of the TGA-MS analysis of PMMA in tracking mode with two typical masses corresponding to MMA ionization fragments (41 and 69 g/mol). It is visible that during the three degradations steps mainly MMA is set free from the sample. This is in agreement with the known fact that PMMA thermally decomposes to more than 90% back into MMA [121].
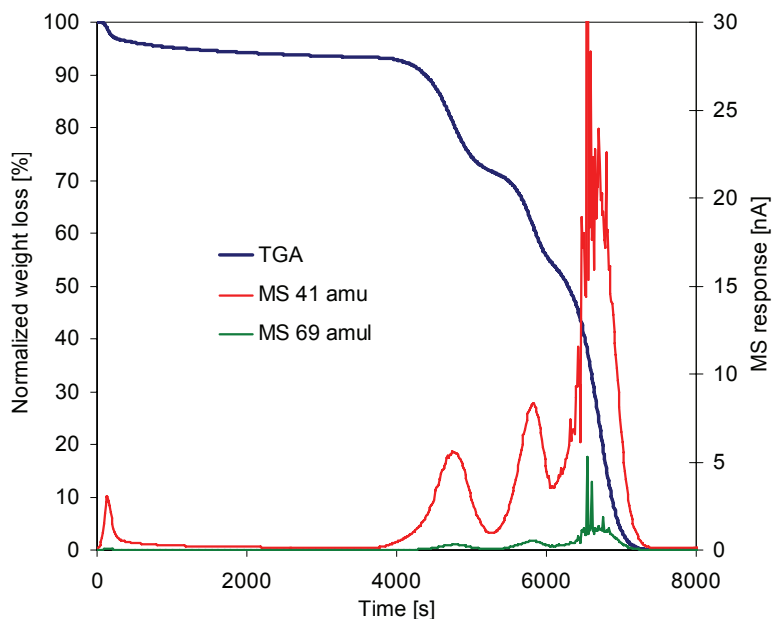
Figure 1.13: Example for a coupled TGA-MS experiment of PMMA with two characteristic MS-responses for MMA (t < 4000 s: isothermal step 110 °C, t > 4000 s: temperature scan 5 °C/min)

1.5   Organic Peroxide Determination by UV

The method of choice for the determination of peroxides is iodometry.

$$R{-}O{-}O{-}R \;+\; 2\,I^{-} \;\xrightarrow{\;H^{+}\;}\; 2\,R{-}OH \;+\; I_2$$

$$I_2 \;+\; S_2O_3^{2-} \;\longrightarrow\; S_4O_6^{2-} \;+\; 2\,I^{-}$$

(EQ 1.8)
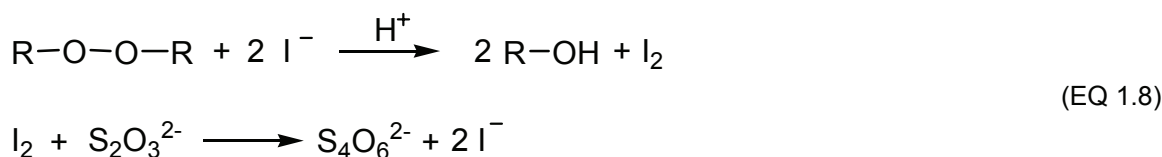
However, most classical iodometrical methods work only in aqueous solutions, especially when using starch as indicator for lower detection limits. Unfortunately, MMA is neither soluble in water nor in most polar solvents. And neither iodine salts nor thiosulfates, both necessary for this type of method, are soluble in unpolar solvents. In addition, oxygen can have - depending on the method - a strong, disturbing effect on the measurement. Therefore, a new iodometrical method was needed to reliably determine MMA peroxides in organic phase and down to concentrations of several ppm.

It was quite clear from the beginning that, in spite of a titration of the iodine with thiosulfate, a more elegant spectrophotometrical analysis would be advantageous. Iodine exhibits a char-

acteristic absorption at a wavelength of 360nm and can, therefore, be easily determined that way. The only problem was to find a suitable sample preparation method for the reliable quantification of peroxides.

At first, a standard method for the determination of peroxides was tried. The peroxide containing sample was dissolved in a mixture of chloroform and methanol [25:75] and a 5% methanolic solution of NaI was added. Since the oxidation is rather slow under these conditions, the solution had to be heated to 55°C for two hours. Afterwards, the iodine was titrated with a methanolic thiosulfate solution.

The first problem that arose from this method was the solubility of the salts in methanol. NaI and thiosulfate dissolve very poorly, which makes it difficult to produce a 5% solution. Secondly, the reaction time of 2 hours at 55°C is too long to yield reproducible results, especially since the reactive system seems to be considerably influenced by air, leading to strongly varying results. Other analytical methods can be found in literature, working with a variety of different solvents, e.g. isopropanol [22] or even in two phase systems with water.

The deciding information was found in an article from 1946: Nozaki [34] used acetic anhydride as solvent and reported the following advantages with regards to other solvents:

- High solubility for NaI
- No important influence of atmospheric oxygen
- High reactivity of iodine with organic peroxides

Acetic anhydride was, therefore, chosen as solvent for further experiments and found to be suitable for the peroxide determination by UV spectroscopy. The exact procedure is described in the following.

1.5.1 Method description

Spectrophotometrical Iodometry is done with a Hewlett-Packard HP8452A spectrophotometer at the maximum iodine absorption wavelength of 360nm. The samples are analyzed in a 1cm quartz cuvette and prepared as described in the following:

- 0.5 g of NaI (Fluka, p.a.) are dissolved in 10 ml of acetic anhydride (Fluka, p.a.) in glass vial with clip cap
- 5 ml of the peroxide containing sample are added

- The solution is stirred during 15minutes and directly analyzed with the spectrometer

The calibration of the system is done with benzoyl-peroxide (Acros, 25% residual water) solutions in MMA. To be sure that the MMA does not already contain any peroxides, it was pre-polymerized at 100°C for 5 hours under reflux and argon atmosphere. In order to keep the molecular weight and, thus, the viscosity low, 10 wt-% of dodecanethiol (Fluka, p.a.) were added as chain transfer agent. In a following step, the monomer was separated from the polymer by vacuum distillation under argon atmosphere. Throughout all further handling, the argon atmosphere was carefully kept to prevent any oxygen from contaminating the system.

 Benzoyl peroxyde (BPO)
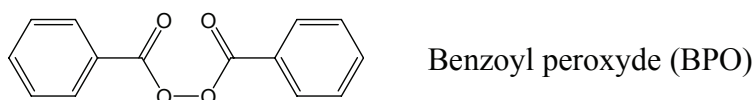
For the calibration, two solutions of 8.85 mg and 84.9 mg BPO (25% residual water) in 10 ml of the above MMA were prepared. This corresponds to a concentration of 0.66375 mg/ml, respectively, 6.3675 mg/ml of pure BPO in MMA. Different amounts of these solutions were subsequently added to 5ml MMA each and analyzed as described above.

Table 3: Calibration solutions for the UV-peroxide determination

Stock Solution 1:				
	mg BPO$_{aq.}$	**mg BPO**	**V [ml]**	**c [mg/ml]**
	8.85	6.6375	10	0.6637
Calibration solutions (* w.r.t. 5ml MMA + V(BPO)):				
	µl BPO[1] added	**c [mg/ml]***	**c [mol/l]**	**Abs [AU]**
1	0	0	0	0.15
2	10	0.00132	$5.5 \cdot 10^{-6}$	0.20
3	20	0.00264	$1.1 \cdot 10^{-5}$	0.26
4	40	0.00527	$2.2 \cdot 10^{-5}$	0.36
5	60	0.00787	$3.3 \cdot 10^{-5}$	0.47

Table 3: Calibration solutions for the UV-peroxide determination

Stock solution 2:				
	mg BPO$_{aq.}$	**mg BPO**	**V [ml]**	**c [mg/ml]**
	84.9	63.675	10	6.3675
Calibration solutions (* w.r.t. 5ml MMA + V(BPO)):				
	µl BPO^2 added	**c [mg/ml]***	**c [mol/l]**	**Abs [AU]**
6	10	0.01271	$5.25 \cdot 10^{-5}$	0.61
7	20	0.02537	$1.05 \cdot 10^{-4}$	1.00
8	50	0.06304	$2.60 \cdot 10^{-4}$	2.30
9	70	0.08791	$3.63 \cdot 10^{-4}$	3.08

These calibration points lead to the following calibration curve and relation between UV absorption and peroxide concentration:
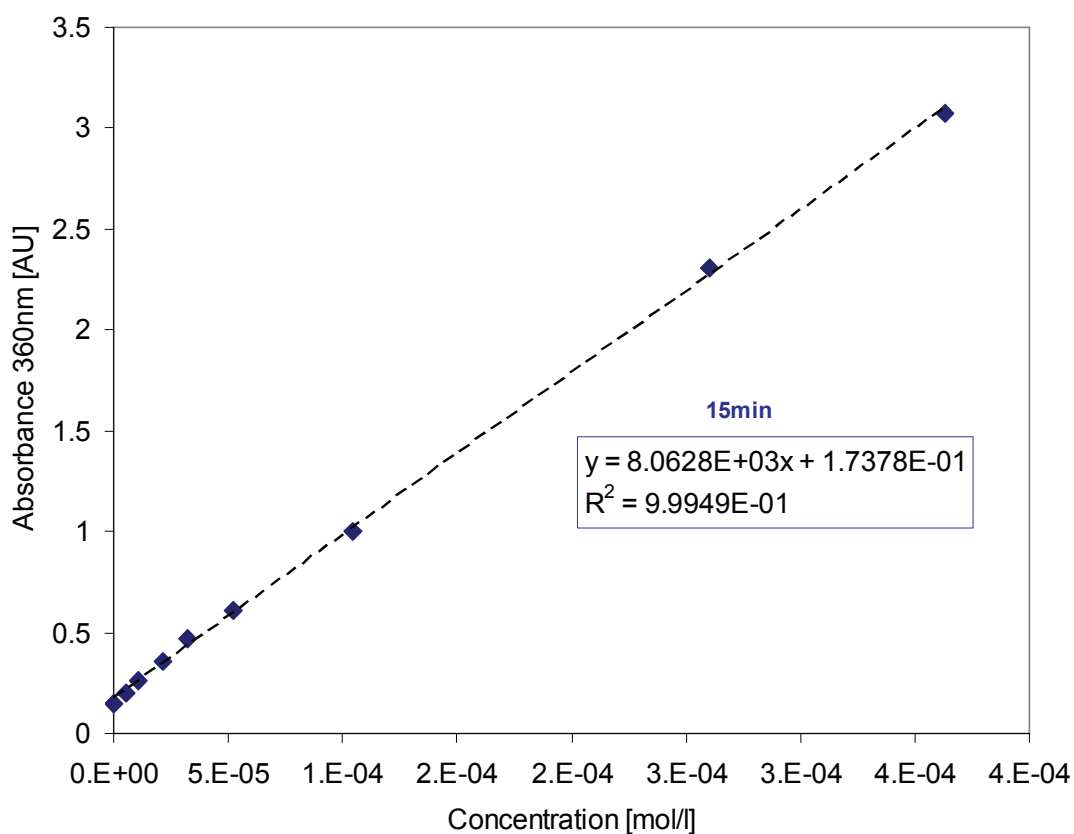
Figure 1.14: Calibration curve for the UV peroxide quantification

$$Conc\left[\frac{mol}{l}\right] = 1.24026 \cdot 10^{-4} \cdot ABS - 2.1553 \cdot 10^{-5} \qquad \text{(EQ 1.9)}$$

The error of oxidation by air after 24h is approximately 2 to $4 \cdot 10^{-5}$ mol/l. For concentrations above $3.115 \cdot 10^{-4}$ mol/l (i.e. 80 ppm BPO), the signal saturates quickly and the solution has to be diluted in a 1:10 ratio.

Figure 1.15: Hewlett-Packard 8452a Photospectrometer
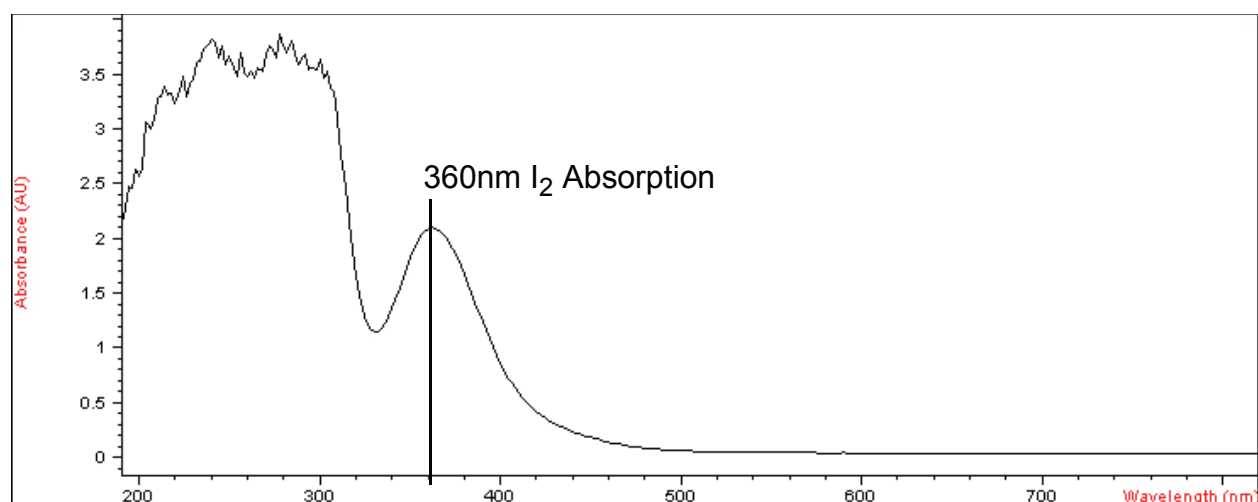
Figure 1.16: UV-spectrum of the iodine containing MMA solution

1.6 Oxygen determination in organic solvents

UV-Spectrophotometry was also employed for the determination of oxygen in the monomer. Since the saturation concentration for physically dissolved oxygen in MMA is crucial for the whole topic of MMA peroxides, it was considered as necessary to try to get a more reliable value than the assumed 60-80 ppm. However, the determination is not at all trivial and succeeded only

partially. The basic method was found in literature: Scherzer and Langguth [35] determined the temperature dependent oxygen concentration for tripropylene glycol diacrylate (TPGDA) and found a strong decrease in oxygen with increasing temperature (see figure 1.17). Another, similar method is provided by Gou et al. [122], but was not considered in this work.
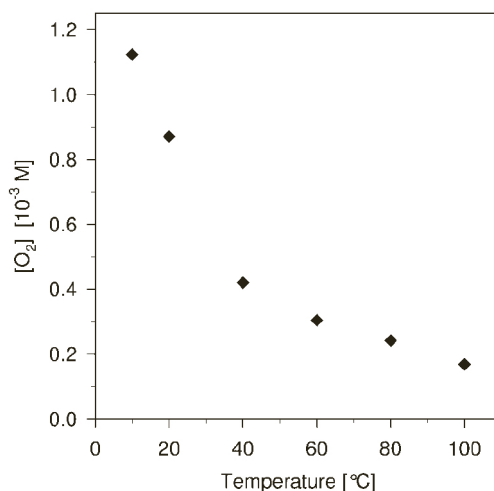
Figure 1.17: Temperature-dependent oxygen concentration in TPGDA [35]

Their method proceeds as follows:

- The monomer is saturated with air at the desired temperature
- It is then shock-frosted with a dry-ice / acetone mixture (-90 °C)
- The gas phase over the frozen monomer is purged with inert gas (*He*)
- The monomer is defrosted and purged continuously with inert gas
- The inert gas is conducted through a washing bottle with an ammoniacal containing solution of *Cu-(I)-Cl* (0.01 mol/l)
- The *Cu-(I)* ion is oxidized by the O_2 driven out of the monomer and the created *Cu-(II)* ion forms a complex with ammonia ($Cu(NH_3)_4^{2+}$)
- This complex can be detected by UV-spectrophotometry at $\lambda = 600$nm and, thus, the oxygen content of the monomer be quantified.

As simple as it sounds, several problems were encountered while trying to reproduce this method: firstly, it was not possible to completely freeze the monomer with a dry-ice / acetone mixture. Only with liquid nitrogen was this possible. Secondly, atmospheric oxygen had a strongly disturbing effect, especially during the sampling from the washing bottle and during the

preparation of the Cu(I)-solution. Thirdly, the residence time of the inert gas stream in the washing bottle was not long enough for a complete conversion of the contained oxygen with Cu-(I). A second washing bottle with the same Cu-(I)-solution, which was connected in series to the first one, also showed blue coloration after a short time.

Therefore, the experimental setup and the method, itself, had to be refined several times. In particular, the measurement at different temperatures with consecutive freezing of the monomer had to be abandoned due to the narrow time frame available for this measurement. The monomer was, therefore, taken directly at room temperature. The final experimental setup can be seen in figure 1.18. It consists of a three-neck round flask with funnel, a washing bottle with sampling valve at the bottom and two gas syringes for the displacement of the inert gas within the installation. The oxygen-saturated monomer was filled in the inertized system through the funnel, while a small stream of inert gas (*He*) was maintained to minimize the error caused by introduced atmospheric oxygen. In the following, a volume of ~ 100 ml *He* was pumped in several cycles forth and back through the monomer and the washing bottle with Cu-(I)-solution with the help of two three-way valves. Samples were taken over time from the washing bottle and analyzed immediately on the UV-spectrophotomer (same as used for the peroxide determination), which had been calibrated beforehand with ammoniacal Cu-(II)-solutions.
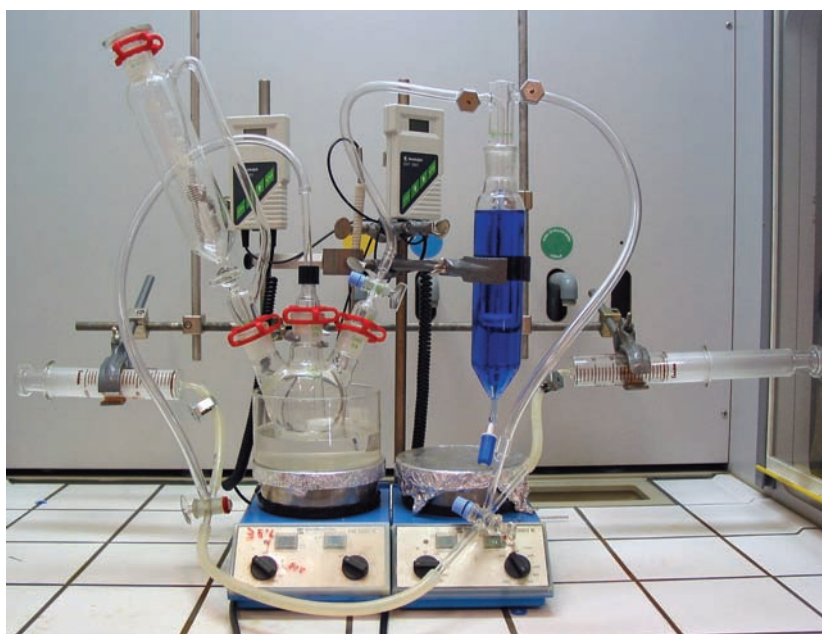
Figure 1.18: Experimental setup for the determination of oxygen in MMA

The results were strongly varying, although the expected order of magnitude for the oxygen concentration could be very well confirmed. Figure 1.19 shows the results for two experimental series obtained with monomer at room temperature (~ 18 °C). The extrapolated saturation value is supposed to be between 80 and 100 ppm, which is slightly higher than the value estimated from batch and DSC experiments by simulation (60 ppm).
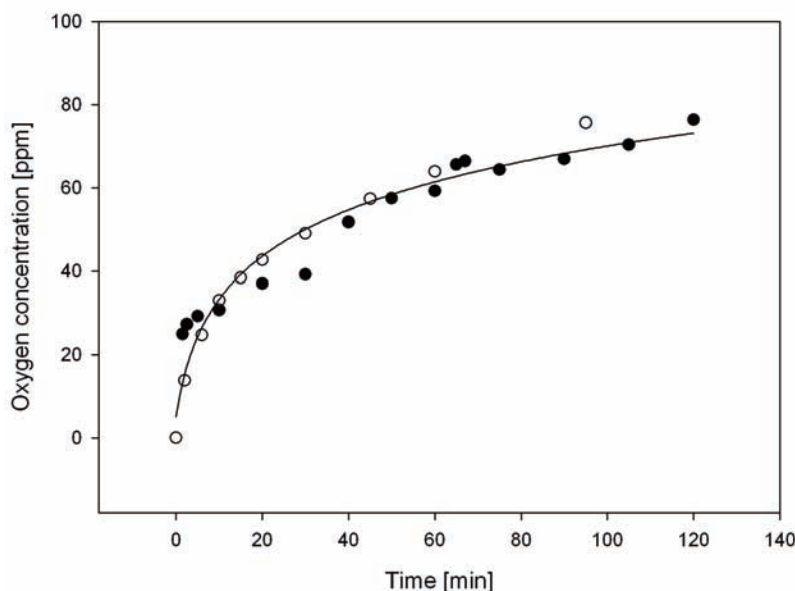
Figure 1.19: Detected oxygen concentration at room temperature (18 °C) over bubbling time (experiment was carried out twice, compare hollow and filled circles)

Another attempt to determine the oxygen concentration in the monomer feed of the pilot plant was undertaken by means of a special electrochemical probe (Orbisphere) designed to measure in organic solvents. However, the membranes used in this probe were not resistant enough for the rather aggressive butyl acetate used in this work and, therefore, the measurement did not lead to stable values. Additionally, the probe only allowed the measurement of a partial pressure for oxygen, which, in order to calculate the concentration of O_2 in MMA, would require the knowledge of solubility data.

Finally, it was tried to estimate the oxygen concentration in MMA with ASPEN PLUS by means of a one-step flash (1 bar, 25 °C) with a two-phase monomer / air feed stream and one liquid and one gaseous exit stream. The equilibrium concentration of O_2 in the monomer was estimated to be ~115 ppm, which is - although of the same order of magnitude - much higher than the values determined by the methods mentioned beforehand.

Experimental procedures

2.1 Monomer purification

For certain experiments, the monomer could not be taken directly from the barrel but had to be purified prior to its use. This was done in several manners, depending on the necessary purity.

Removing the stabilizer

In order to remove the stabilizer (20 ppm MEHQ), the monomer was washed with 2N-NaOH and rinsed with deionized water until the aqueous phase was neutral (pH = 6-7).

Prepolymerization

In the case of the UV calibration, it was necessary to be sure that the monomer used for the calibration solutions did not contain any peroxide. Therefore, a prepolymerization was carried out at 100°C during 5 hours under argon atmosphere. A large amount of chain transfer agent (~ 10 wt-%) was added to the monomer in order to keep the viscosity low. Following the prepolymerization, the monomer was distilled as described in the next paragraph.

Vacuum distillation

The distillation of MMA was carried out under argon atmosphere at reduced pressure (~ 150 mbar) and at T = 45 °C. A The monomer was distilled over a column for better separation and fractionated in three distillate fractions, of which only the middle one was kept. Depending on the use of the monomer in the following experiments, it was either kept under argon atmosphere or in a flask closed only with a drying tube in order to garantuee contact with air (e.g. for MMA-peroxide formation experiments).

2.2　PMMAP synthesis

For the synthesis of PMMAP, 250 ml of distilled monomer are heated to 70 °C under reflux and molecular oxygen from a gas cylinder bubbled through it for several hours (4 - 7 h). A picture of the setup can be found in chapter 2, figure 2.5. In a following step, the monomer was removed from the flask at a rotary evaporator until a viscous residue was obtained. This residue was reduced as far as possible in vaccuum (~ 1 mbar), dissolved in chloroform ($CHCl_3$) and precipitated twice in 20 times the volume of cold petrol ether (bp. 40-60 °C) for purification. From the petrol ether, the precipates were separated by centrifugation. The final product was a white, sticky powder. Its quantity depends largely on the duration and the temperature of the formation experiment. It varied from 8 to 125 mg for 3h at 60 °C and 7h at 70 °C, respectively. In the latter experiment, also the molecular weight of the peroxide and its amount compared to the parallely formed PMMA was higher. It can, therefore, be said that with increasing temperature and duration of oxygen bubbling, the amount and molecular weight of the formed peroxides increases. However, it has to be considered that with increasing temperature, also the decomposition of the peroxide gets more important.

2.3　Batch experiments

The batch experiments for verification of the kinetic model were carried out in a stainless steel bench-scale reactor. The general procedure for each experiment is presented in the following:

Preparation:

- Chemicals (monomer, solvent, CTA) are weighed and filled in the reactor

- Screw cap vials are stored in the deep freezer to cool them to -18 ^{o}C

Reaction:

- t = 0 min: The reactor is pressurized to p = 10 bar and the reaction subsequently started by heating (heating ramp = 3.5 ^{o}C / min.) to the desired reaction temperature

- t = 15 min: First sample; The immersion tube is purged with 10 ml reaction mixture before another 10 ml of the reaction mixture are taken for sampling into a frozen screw cap vial and immediately stored at -18 ^{o}C

- t = 30 - 240 min: Samples are taken in regular intervals as described before. For certain experiments, the initiator solution is filled into the funnel and added under pressure to the reaction mixture at a preset time.

- t = 240 min: Reaction is stopped by cooling down; the rest of the reaction mixture is disposed and the reactor is cleaned

Analysis:

- Samples are analyzed by GPC and GC for conversion respectively molecular weight analysis

2.4 Pilot Plant experiments

For the pilot plant experiments, always the same procedure was followed during startup, running and shut-down. This procedure is described in the following as detailed as possible.

Heating Phase

- Firstly, the pilot plant was heated up by setting the temperature on the thermostats to 120 °C for the reaction zone and to 260 °C for the devolatilization.

- During the heating up of the pilot plant, the feed solution was prepared. Therefore, the necessary amounts of monomer, initiator and CTA, which had been calculated before-hand for the planned duration of the experiment, were weighed and mixed in a stain-

less steel recipient. From this recipient, they were transferred into a 60-litres stainless steel tank through a hose by reducing the pressure inside the tank. From this tank, the feed solution is transferred directly into the pilot plant.

- When the reactor has reached the set temperature, a small solvent flow (0.5 kg/h) is established and the recycle pump activated. The membrane valve is set to 10 bars to evoke a slight pressurization of the reactor. At the same time, the pressure in the devolatilization chamber is reduced (150 mbar) so that the solvent is correctly removed and condensed.

- The computer with Dasylab is switched on for data acquisition

Startup phase

- With the solvent flow established, the temperature is set to reaction temperature and the feed flow switched from solvent to monomer feed. The flowrate is set to the desired value (e.g. *1.84 kg/h* for a residence time of *30 minutes* in the loop)

- During this phase, the beginning reaction can be followed by ultrasound and by an increase in pressure.

- As soon as polymer falls into the devolatilization chamber (approximately after 1 hour at the given feed flowrate), the discharge gear pump is activated.

- Samples are taken regularly from positions at the loop exit, at 2/3 length of the tube and from the condensate and the final polymer. During the sampling, the second feed pump, which pumps solvent and initiator into the tube reactor, is deactivated to avoid a backflow into the loop sample. The reactor samples are taken through heated valves, on which hermetic, 10cm stainless steel tubes with 12mm diameter are screwed. Before mounting the tubes, the valves are purged (tube valve before, then loop valve). For the sampling, the valves are left open until the sampling tubes are hot over their whole length. The sample is consecutively transferred from the tubes into 25ml screw cap vials (Schott) and immediately frozen at -18°C.

- At steady state, the polymer is transfered as two strands to the granulator and processed to granules.

- In regular intervals, the condensate recipient is emptied.

Shut-down phase

- At the end of the experiment, the feed flow is again switched from monomer solution to solvent and the flowrate increased to 10 kg/h. Thus, the polymer / monomer solution is pushed out of the reactor. The flowrate is varied several times from 10 to 5 kg/h in order to improve the rinsing of the plant.

- Once the polymer stops falling into the devolatilization chamber, which is generally the case after 1 hour, the solvent flow and the reactor temperature are decreased to 0.5 kg/h and 120 °C, respectively.

- Both gear pumps, the one in the recycle loop and at the exit, are stopped.

- For the final shut-down, the temperature of all thermostats is lowered to <20°C, the cooling water circuits are openend, the membrane valve depressurized, the vacuum of the devolatilization cut and the solvent flow stopped.

- At last, the condensate recipient is emptied, the data acquisition is halted and all equipment switched off.

A-XXX

ANNEXE 3

Modeling with Predici®

PREDICI® stands for <u>P</u>olyreaction <u>D</u>istributions by <u>C</u>ountable System <u>I</u>ntegration and is the name of an industrially recognized and widely spread simulation package for the treatment of kinetic equations in models of polymerization reactions. The input consists of a complete reaction model with reaction equations and kinetic parameters, together with concentrations and stuff-data of all reactive components and reaction conditions. The software performs a numerical integration of the resulting system of differential equations, based on recent mathematical-numerical methods [123]. For each time step, the complete concentration profile as well as molecular weight distributions of polymeric species are estimated.

The user can - within the limits of available kinds of reaction steps - freely add elementary reactions of all types to the model and define various output-functions (e.g. ultrasound velocity, conversion, etc.), the calculation of which can be based on the estimated process parameters for each time step (e.g. temperature, concentration of a species, etc.).

PREDICI® offers four different reactor models: ideal batch, semi-batch and continuous tank reactor and the ideal plug flow tube reactor. Several CSTR can be combined to a cascade. The combination of CSTR and tube, however, is not possible in the present version. This combination can, yet, be realized by a transfer data sheet, which uses the data of a CSTR exit stream as input for a tubular reactor located in another file.

For each model, recipes can be created for the components defined in the model, which contain the initial composition of the reactor's contents as well as feed streams with arbitrary compositions at user-defined times. This increases significantly the flexibility of each model, as it is enough to change the recipe in order to model another experiment.

The use of PREDICI® for the modeling in this work was motivated by the fact that it is widely present in industry. The model can, therefore, easily (and without huge loss of time to reprogram the equations in another modeling tool) be used by other researchers using the same software and be applied to comparable processes and reactions.
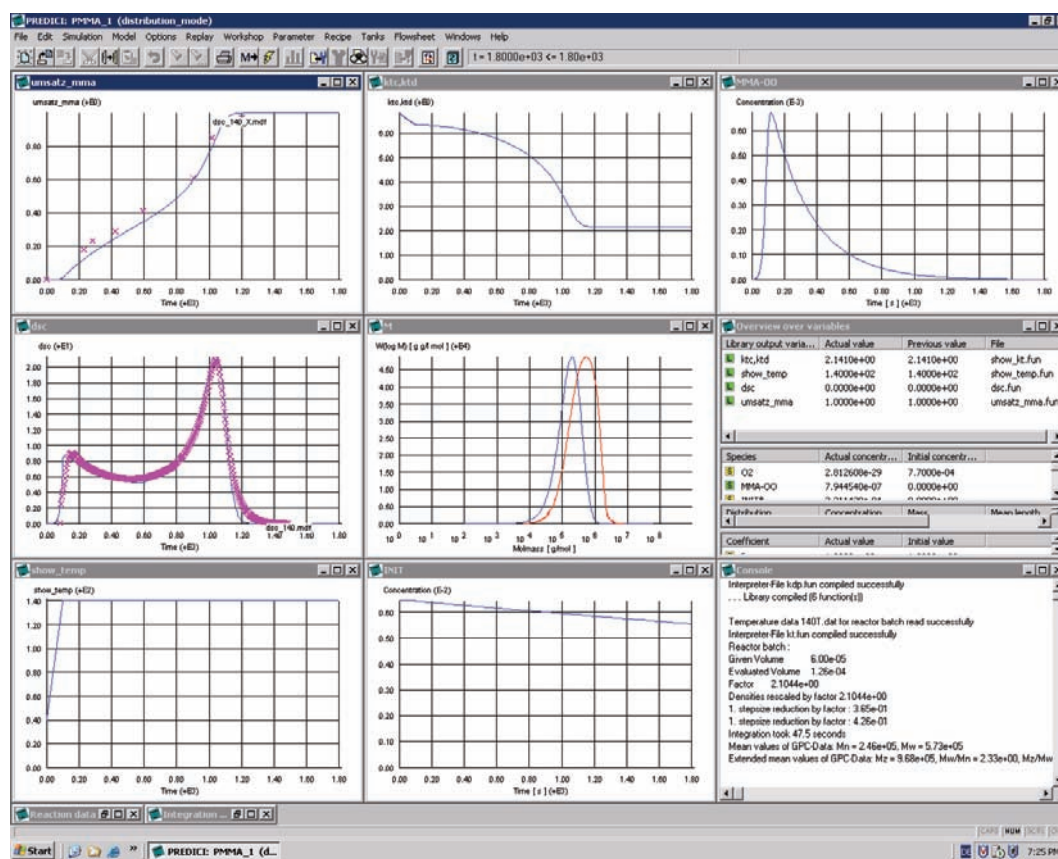
Figure 3.1: Screenshot of the result window for a batch polymerization in PREDICI®

This annex contains all the information ncessary to reproduce the model, which was developed in this work for the methyl methacrylate / methyl acrylate copolymerization at high temperature.

3.1   Reactor

R1   *continuous*

                                  $V_r = 0.907\ l$

                                  T = temperature program following pilot plant data

                                  p = pressure program following pilot plant data

                                  flowrate defined by recipe

Tube   *Tube reactor*

                                  Length L = 3.84 m

                                  Diameter d = 0.02 m

                                  T = constant (as in experiment)

                                  p = constant (as in experiment)

                                  Input flow as defined in "initial data sheet"

                                  Additional solvent / initiator feed defined by recipe

3.2   Reaction equations

Reaction step	Reaction equation			Rate constant
MMA-OO formation	$MMA + O2$	$\longrightarrow$	$MMA\text{-}OO$	$k_{po,f}$
MMA-OO decomposition	$MMA\text{-}OO$	$\longrightarrow$	$2\ f_{po}\ MMA\text{-}OO^{\cdot}$	$k_{po,d}$, f_{po}
MMA-OO initiation	$MMA\text{-}OO^{\cdot} + MMA$	$\longrightarrow$	$P_{1,1}^{\cdot}$	k_{p1}
	$MMA\text{-}OO^{\cdot} + MA$	$\longrightarrow$	$P_{2,1}^{\cdot}$	k_{p2}
Thermal initiation	$2\ MMA$	$\longrightarrow$	$2\ MMA^{\cdot}$	k_{th}
	$MMA^{\cdot} + MMA$	$\longrightarrow$	$P_{1,1}^{\cdot}$	k_{p1}
	$MMA^{\cdot} + MA$	$\longrightarrow$	$P_{2,1}^{\cdot}$	k_{p2}
Initiation by CTA	CTA	$\longrightarrow$	$CTA^{\cdot}$	k_{dt}
	$CTA^{\cdot} + MMA$	$\longrightarrow$	$P_{1,1}^{\cdot}$	k_{p1}

	$CTA \cdot + MA$	$\longrightarrow$	$P_{2,1} \cdot$	k_{p2}
Initiation by Initiator	I	$\longrightarrow$	$2 f I \cdot$	k_i , f
	$I \cdot + MMA$	$\longrightarrow$	$P_{1,1} \cdot$	k_{p1}
	$I \cdot + MA$	$\longrightarrow$	$P_{2,1} \cdot$	k_{p2}
Propagation	$P_{1,n} \cdot + MMA$	$\longrightarrow$	$P_{1,n+1} \cdot$	k_{p1}
(ultimate model)	$P_{1,n} \cdot + MA$	$\longrightarrow$	$P_{2,n+1} \cdot$	k_{p1}, r_{12}
	$P_{2,n} \cdot + MA$	$\longrightarrow$	$P_{2,n+1} \cdot$	k_{p2}
	$P_{2,n} \cdot + MMA$	$\longrightarrow$	$P_{1,n+1} \cdot$	k_{p2}, r_{21}
Depropagation	$P_{1,n} \cdot$	$\longrightarrow$	$P_{1,n-1} \cdot$	k_{dp}
Transfer to monomer	$P_{1,n} \cdot + MMA$	$\longrightarrow$	$D_n + P_{1,1} \cdot$	k_{f1}
	$P_{1,n} \cdot + MA$	$\longrightarrow$	$D_n + P_{2,1} \cdot$	k_{f12}
	$P_{2,n} \cdot + MA$	$\longrightarrow$	$D_n + P_{2,1} \cdot$	k_{f2}
	$P_{2,n} \cdot + MMA$	$\longrightarrow$	$D_n + P_{1,1} \cdot$	k_{f21}
Transfer to solvent	$P_{1,n} \cdot + LM$	$\longrightarrow$	$D_n + P_{1,1} \cdot$	C_S
	$P_{2,n} \cdot + LM$	$\longrightarrow$	$D_n + P_{2,1} \cdot$	C_S
Transfer to CTA	$P_{1,n} \cdot + CTA$	$\longrightarrow$	$D_n + P_{1,1} \cdot$	C_{CTA}
	$P_{2,n} \cdot + CTA$	$\longrightarrow$	$D_n + P_{2,1} \cdot$	C_{CTA}
Termination	$P_{1,n} \cdot + P_{1,m} \cdot$	$\longrightarrow$	D_{n+m}	$k_{tc,11}$
	$P_{1,n} \cdot + P_{1,m} \cdot$	$\longrightarrow$	$D_n + D_m$	$k_{td,11}$
	$P_{1,n} \cdot + P_{2,m} \cdot$	$\longrightarrow$	D_{n+m}	$k_{tc,12}$
	$P_{1,n} \cdot + P_{2,m} \cdot$	$\longrightarrow$	$D_n + D_m$	$k_{td,12}$
	$P_{2,n} \cdot + P_{2,m} \cdot$	$\longrightarrow$	D_{n+m}	$k_{tc,22}$

3.3 Rate coefficients

Coefficient		k_0 [l, mol, s]	E_a [kJ / mol]	Source
$k_{po,f}$		$1.7691 \cdot 10^6$	73.0	*this work*
$k_{po,d}$		$1.7752 \cdot 10^6$	70.378	*this work*
f_{po}			0.21 [-]	*this work*
k_{p1}		$2.67 \cdot 10^6$	22.36	[124]
				(IUPAC recommended)
k_{p2}		$2.656 \cdot 10^8$	29.726	[94]
k_{th}		$9.54 \cdot 10^{-2}$	90.623	[14]
k_{dt}		$6.78 \cdot 10^7$	128.7	[66]
k_i	*DTBP*	$9.178 \cdot 10^{14}$	147.9	*this work*
	TBPEH	$1.84 \cdot 10^{14}$	123.95	*this work*
	TBPIN	$1.22 \cdot 10^{13}$	124.31	*this work*
f	*DTBP*		0.7 [-]	[47]
	TBPEH		0.61 [-]	*this work*
	TBPIN		0.7 [-]	*this work*
r_{12}			1.59 [-]	*this work*
r_{21}			4.46 [-]	*this work*
k_{dp}		$6.48 \cdot 10^{11}$	76.364	*this work*
k_{f1}		2.024	33.306	*this work*
k_{f12}			$1 \cdot 10^{-4}$ [-]	*this work*
k_{f2}			$1 \cdot 10^{-4}$ [-]	*this work*
k_{f21}			$1 \cdot 10^{-4}$ [-]	*this work*
$C_S = k_I / k_p$			$1 \cdot 10^{-4}$ [-]	*this work*
$C_{CTA} = k_{cta} / k_p$			0.68 [-]	[96]
$k_{t0,11}$		$1.21 \cdot 10^9$	83.66	*this work*[1]
$\gamma = k_{tc} / k_{td}$		$3.956 \cdot 10^{-4}$	-17.168	[63]
$k_{t0,22}$		$9.85 \cdot 10^{10}$	22.148	[94]

---

1. The value for k_{t0}, i.e. the intrinsic termination rate constant for MMA, was determined by plotting the term $\ln \dfrac{k_p}{\sqrt{k_t}}$ (with the IUPAC value for k_p) against 1/T and comparing it to graphs resulting from several literature values. The k_{t0} value was then determined in the way to yield the best fit with literature data.

3.4 Calculations (fun-files)

Initiator efficiency f

```
result1=arg1
result2=arg2
cm=getco(":MMA")
cp=getmy(":dead_polymer",1)+getmy(":active_polymer_1",1)+getmy(":active_polymer_2", 1)
X=eval("X_comp", cm, cp)
rhom=getdensitylow(":MMA")
rhop=getdensityhigh(":dead_polymer")
eps=1-rhom/rhop
Fs=0
Phis=getcf(":BuAc")*getmmlow(":BuAc")/getdensitylow(":BuAc")
if((1-Phis)>0)
{Fs=Phis/(1-Phis)}
Phip=X*(1-eps)/(1-eps*X+Fs)
alpha = 15
beta = 5
result2=setkp("f", getkp("f0")/(1+alpha*Phip^beta))
```

Termination rate constant (gel effect) kt11

```
T=gettemp(":")
ratiokt=getkp("ratio_kt")
kt0=getkp("kt0")
mw=getmw(":dead_polymer")*1000
Tgp=116
A=0.168-8.21e-6*(T-Tgp)^2
B=0.03
R=8.314
c0=7.69577e-09*exp(-4854.97/(T+273.15))
cm=getco(":MMA")+getco(":MA")
cp=getmy(":active_polymer_1", 1)+getmy(":dead_polymer", 1)+getmy(":active_polymer_2", 1)
X=eval("X_comp", cm, cp)
rhom=getdensitylow(":MMA")
rhop=getdensityhigh(":dead_polymer")
```

```
eps=1-rhom/rhop
Phis=getcf(":BuAc")*getmmlow(":BuAc")/getdensitylow(":BuAc")
Fs=0
if((1-Phis)>0)
{Fs=Phis/(1-Phis)}
Phip=X*(1-eps)/(1-eps*X+Fs)
delta=mw^1.75*c0/exp(2.3*(1-Phip)/(A+B*(1-Phip)))
kt=setkp("kt", 1/(1/kt0+delta))
result1=kt*ratiokt/(1+ratiokt)
result2=kt/(1+ratiokt)
```

Termination rate constant (gel effect) kt12

```
t=gettemp(":")
F1=getmolpart("M1")
F2=getmolpart("M2")
kt11=getkp("kt0")
kt22=getkp("kt22_0")
kt0=F1*kt11+F2*kt22
ratiokt=getkp("ratio_kt")
mw=getmw(":dead_polymer")*1000
Tgp=116
A=0.168-8.21e-6*(t-Tgp)^2
B=0.03
c0=7.69577e-09*exp(-4854.97/(t+273.15))
cm=getco(":MMA")+getco(":MA")
cp=getmy(":dead_polymer", 1)+getmy(":active_polymer_1", 1)+getmy(":active_polymer_2", 1)
X=eval("X_comp", cm, cp)
rhom=getdensitylow(":MMA")
rhop=getdensityhigh(":dead_polymer")
eps=1-rhom/rhop
Phis=getcf(":BuAc")*getmmlow(":BuAc")/getdensitylow(":BuAc")
Fs=0
if((1-Phis)>0)
{Fs=Phis/(1-Phis)}
Phip=X*(1-eps)/(1-eps*X+Fs)
if(kt0>0)
```

```
{delta=mw^1.75*c0/exp(2.3*(1-Phip)/(A+B*(1-Phip)))
kt=1/(1/kt0+delta)}
else
{kt=kt0}
result1=kt*ratiokt/(1+ratiokt)
result2=kt/(1+ratiokt)
```

Termination rate constant (gel effect) kt22

```
t=gettemp(":")
kt0=getkp("kt22_0")
ratiokt=getkp("ratio_kt")
mw=getmw(":dead_polymer")*1000
Tgp=116
A=0.168-8.21e-6*(t-Tgp)^2
B=0.03
c0=7.69577e-09*exp(-4854.97/(t+273.15))
cm=getco(":MMA")+getco(":MA")
cp=getmy(":dead_polymer", 1)+getmy(":active_polymer_1", 1)+getmy(":active_polymer_2", 1)
X=eval("X_comp", cm, cp)
rhom=getdensitylow(":MMA")
rhop=getdensityhigh(":dead_polymer")
eps=1-rhom/rhop
Phis=getcf(":BuAc")*getmmlow(":BuAc")/getdensity(":BuAc")
Fs=0
if((1-Phis)>0)
{Fs=Phis/(1-Phis)}
Phip= X*(1-eps)/(1-eps*X+Fs)
if(kt0>0)
{delta=mw^1.75*c0/exp(2.3*(1-Phip)/(A+B*(1-Phip)))
kt=1/(1/kt0+delta)}
else
{kt=kt0}
result1=kt*ratiokt/(1+ratiokt)
result2=kt/(1+ratiokt)
```

Ultrasound calculation (theoretical speed of sound from solution composition)

T=gettemp("dummy")

kappa_m1 = 7.823735E-14*T^2 + 1.257146E-12*T + 7.135903E-10

kappa_m2 = 0.00000000000004*T^2 + 0.000000000002*T + 0.0000000006

kappa_s = 9.416596E-14*T^2 + 5.884506E-13*T + 8.111514E-10

kappa_p=exp((-22.220389+0.36888905*T-0.0015726875*T^2)/(1-
            0.016394164*T+0.000067228059*T^2+0.000000015752519*T^3))

rho_m1 = getdensitylow("M1")

rho_m2 = getdensitylow("M2")

rho_s = getdensitylow("LM")

rho_p = getdensityhigh(":dead_polymer")

p=getpressure("R1")

wp = getmy(":dead_polymer", 1)*getvol("R1")*getmmlow(":MMA") / getmass("R1")

wm1 = getco(":MMA")*getmmlow(":MMA")*getvol("R1") / getmass("R1")

wm2 = getco(":MA")*getmmlow(":MA")*getvol("R1") / getmass("R1")

ws = getco("LM")*getmmlow("LM")*getvol("R1") / getmass("R1")

alpha=0.40604-0.37541*wp+0.00364*T

result1=1/sqrt(1000)*(wp/rho_p + wm1/rho_m1 + ws/rho_s + wm2/rho_m2)/sqrt(wp*kappa_p/rho_p
            + ws*kappa_s/rho_s + wm1*kappa_m1/rho_m1 + wm2*kappa_m2/rho_m2)+alpha*p

Density monomer

T=arg1

rho=(-9.4146E-06*T^3 + 1.3028E-03*T^2 - 1.1552*T + 9.6339E+02)/1000

result1=1/rho-arg3

Density solvent

T=arg1

rho=-2.48E-06*T^2 - 5.28E-04*T + 8.70E-01

result1=1/rho-arg3

Density polymer

T=arg1

rho=-1E-06*T^2 - 0.0002*T + 1.195

result1=1/rho-arg3

A-XL

Determination of the Initiator Decomposition by DSC

In analogy to the determination of the MMA peroxide decay kinetics by DSC (compare chapter 2, "Differential Scanning Calorimetry (DSC)" on page 26), also the decomposition of commercial initiators has been investigated as a part of this work. For standard initiators like di-tert.butyl-peroxide (DTBP) or azo-bis-isobutyro-nitril (AIBN), which are widely used in polymer research, the kinetics of their decomposition are well-known and published in unnumerous scientific articles. When it comes to less common peroxides, as they are used mostly in industrial processes, where it is important to have very specific decomposition characteristics, the situation changes drastically and it gets very difficult to obtain reliable kinetic parameters. Often, the data provided for a component vary between different manufacturers and the conditions under which they had been determined are rarely revealed.

It is, therefore, inevitable for precise modeling of polymerization processes, to determine the exact decomposition kinetics of the employed thermal initiators under controlled experimental conditions. In the following, the results from DSC experiments are presented for the two industrial initiators *tert.butyl-peroxy-2-ethylhexanoat* (TBPEH) and *tert.butyl-peroxy-3,5,5-trimethyl-hexanoate* (TBPIN), as well as for *di-tert.butyl-peroxide* (DTBP) in order to validate the determination method with values from literature.

The experiments were carried out in 60 µl medium-pressure, stainless steel crucibles (see annex 1, "Differential Scanning Calorimetry" on page XIII) with either the pure peroxide or peroxide diluted in butyl acetate. For the mathematical algorithm, which is used by the PerkinElmer software to determine the kinetic parameters, see chapter 2, "Differential Scanning Calorimetry (DSC)" on page 26.

4.1 Tert.butyl-peroxy-2-ethylhexanoat (TBPEH)

The decomposition of TBPEH was measured by DSC in solution (~50% butyl acetate) and for the undiluted peroxide. The DSC results, i.e. heat flow peak and Arrhenius diagram from the peak integration, are shown in figure 4.1 (a)+(b) for the undiluted and in figure 4.2 (a)+(b) for the diluted peroxide.

The kinetic parameters for both cases, as well as values provided by two different producers of TBPEH are presented in table 1.

Finally, the different kinetic parameters are compared by tracing the half life time against temperature in figure 4.3.

Table 1: Kinetic rate constants for the thermal decomposition of TBPEH

	k_0 [s^{-1}]	E_A [kJ mol^{-1}]
DSC pure	$1.312 \cdot 10^{14}$	124.13
DSC (50% BuAc)	$1.847 \cdot 10^{14}$	123.95
Degussa Initiators	$1.840 \cdot 10^{15}$	132.68
Akzo	$9.990 \cdot 10^{13}$	122.96
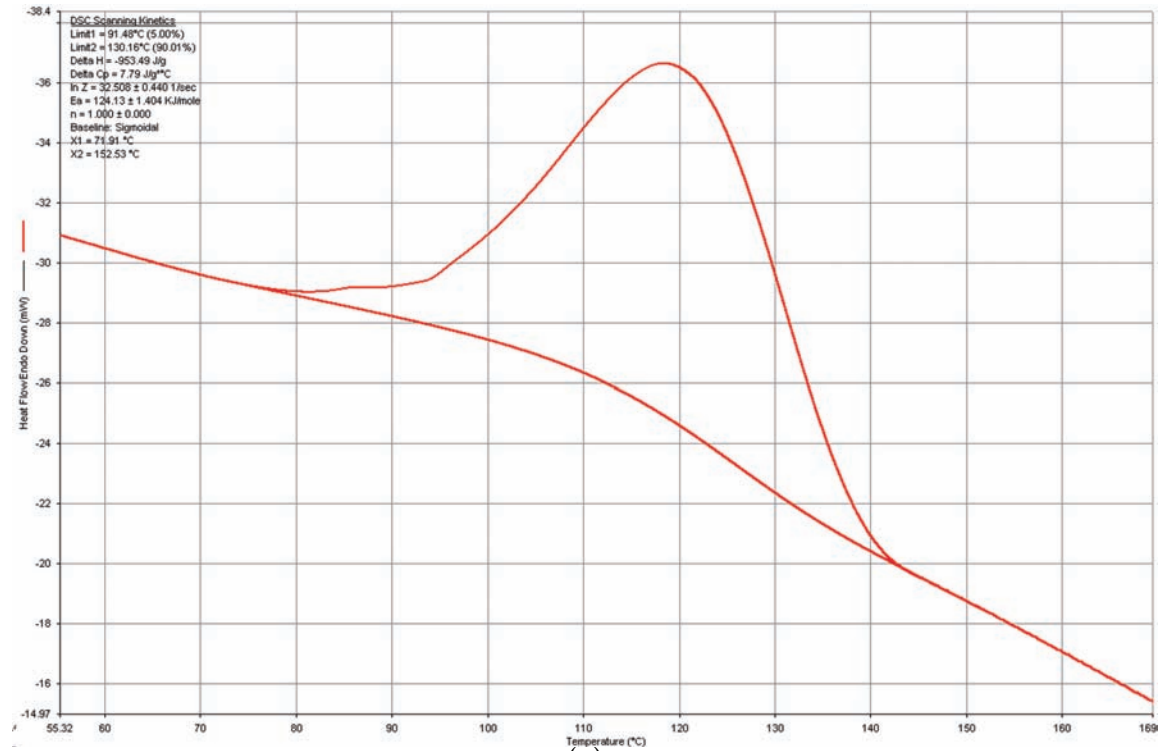
(a)
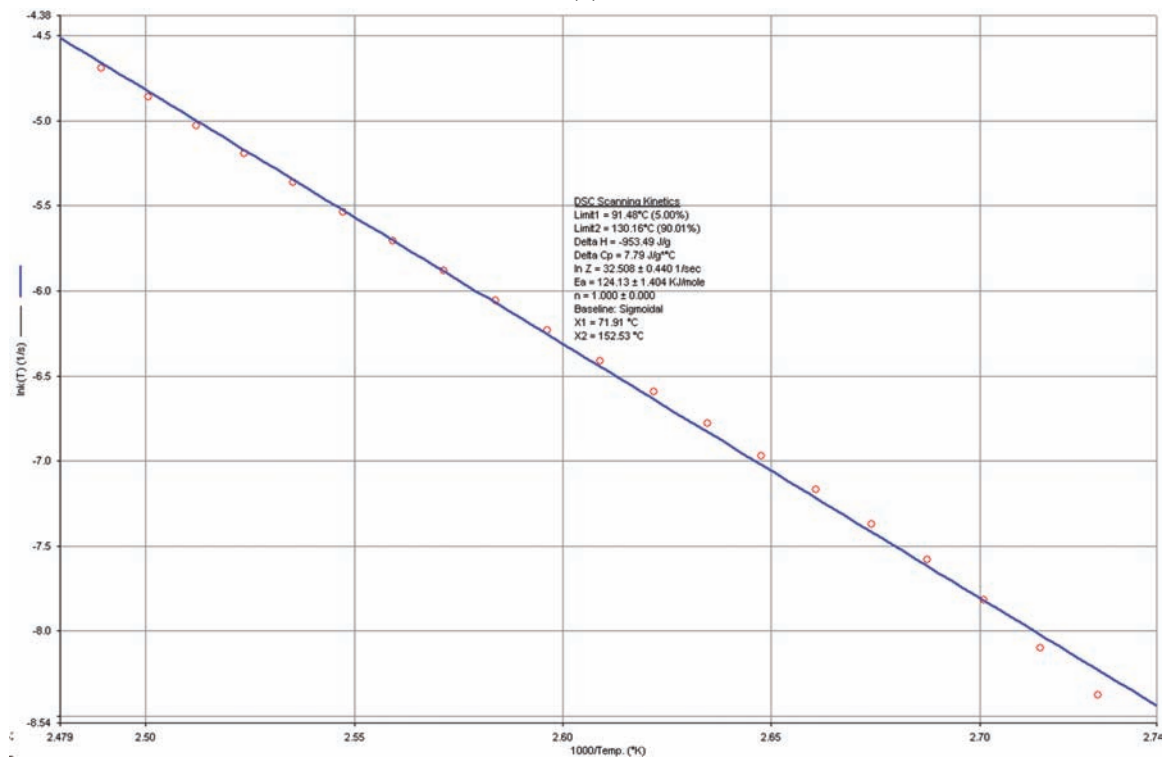
(b)

Figure 4.1: Decomposition of TBPEH (undiluted) measured by DSC
(a) heat flow curve (b) Arrhenius diagram from the integrated heat curve

Figure 4.2: Decomposition of TBPEH (50% BuAc solution) measured by DSC
(a) heat flow curve (b) Arrhenius diagram from the integrated heat curve

(b)

Figure 4.2: Decomposition of TBPEH (50% BuAc solution) measured by DSC
(a) heat flow curve (b) Arrhenius diagram from the integrated heat curve
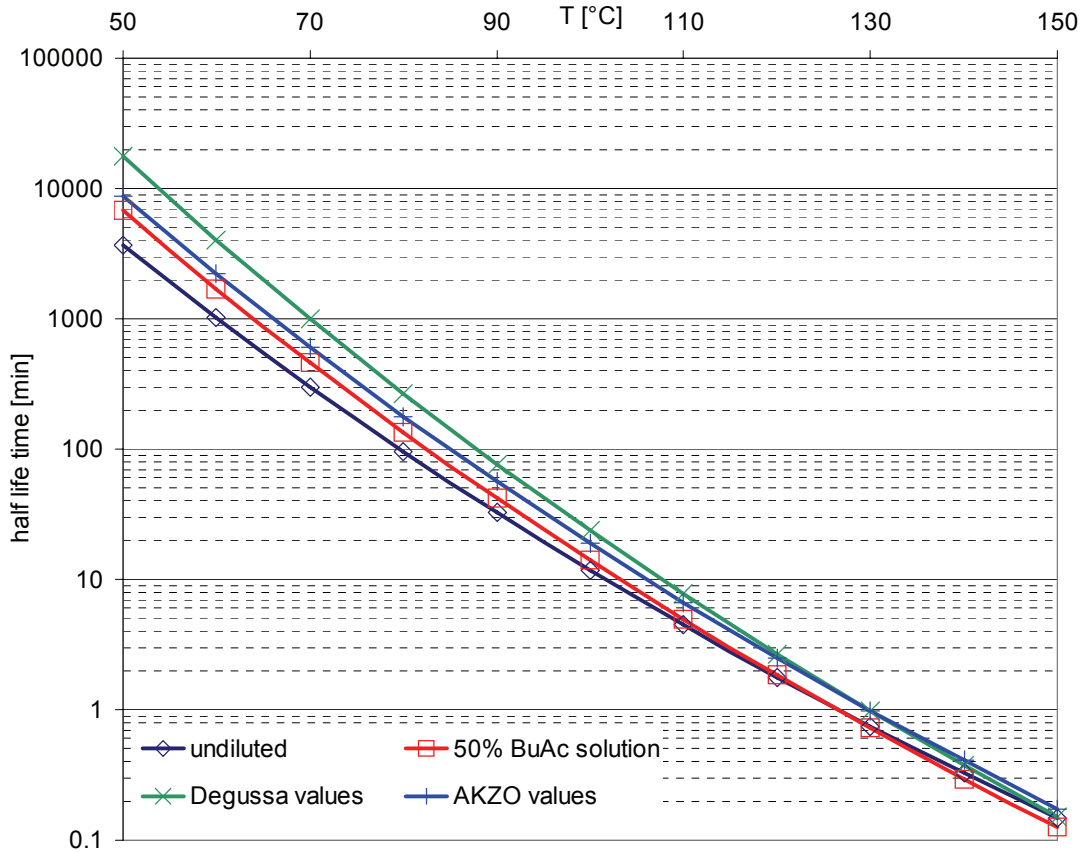
Figure 4.3: Half life times for TBPEH using the kinetic constants from table 1

As shown in the above figure, the kinetics determined for the undiluted TBPEH is the fastest decomposition kinetics. This is an effect often observed for this kind of reaction. It is, therefore, recommendable to measure in dilute solutions. The kinetics determined for a 50% TBPEH solution in BuAc is rather close to the values provided by the two manufacturers, i.e. the curve is almost parallel to the one from DEGUSSA, from where the peroxide was obtained. However, the conditions under which the kinetics were determined by AKZO and DEGUSSA is unknown, which makes it impossible to explain the difference between the three cases.

4.2   Tert.butyl-peroxy-3,5,5-trimethyl-hexanoate (TBPIN)

The same procedure as for TBPEH was followed to determine the decomposition kinetics for TBPIN. The peroxide was measured undiluted and in 50% butyl acetate. The resulting kinetic constants are listed in table 2. The corresponding half life time plot is depicted in figure 4.4 and the DSC results in figure 4.5 (a)+(b) respectively figure 4.6 (a)+(b) for the diluted peroxide.

Table 2: Kinetic rate constants for the thermal decomposition of TBPIN

	k_0 [s^{-1}]	E_A [kJ mol^{-1}]
DSC pure	$1.176 \cdot 10^{10}$	100.03
DSC (50% BuAc)	$1.217 \cdot 10^{13}$	124.31
Degussa Initiators	$2.020 \cdot 10^{15}$	142.88
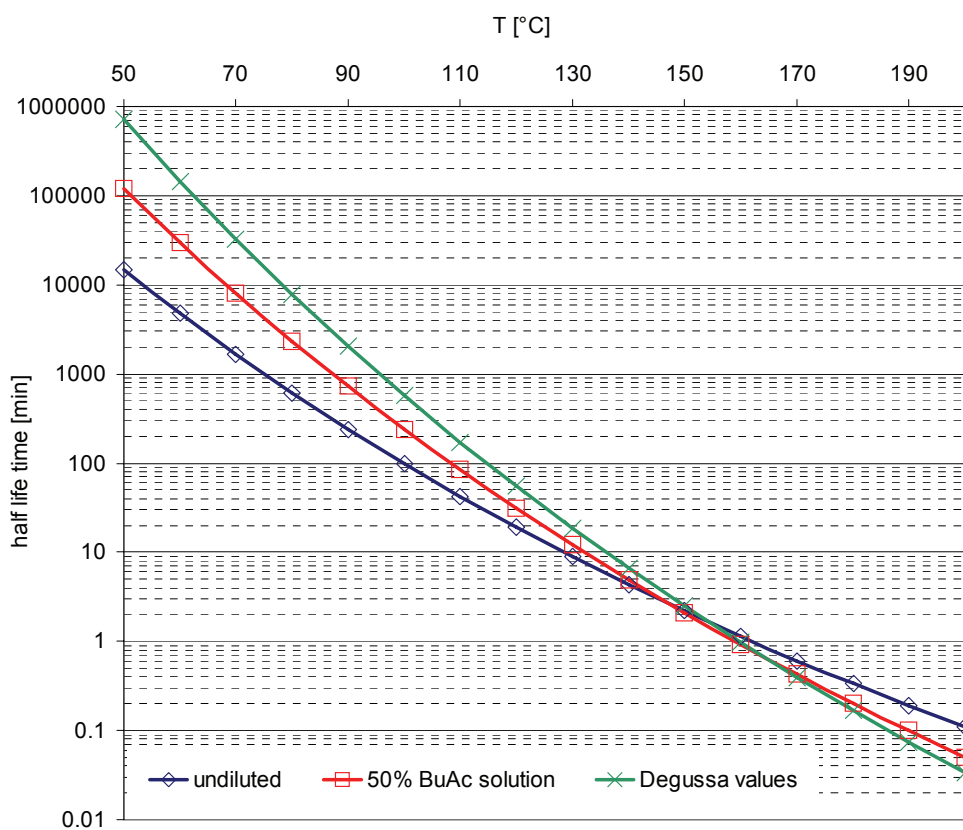
Figure 4.4: Half life times for TBPIN using the kinetic constants from table 2

(a)

(b)
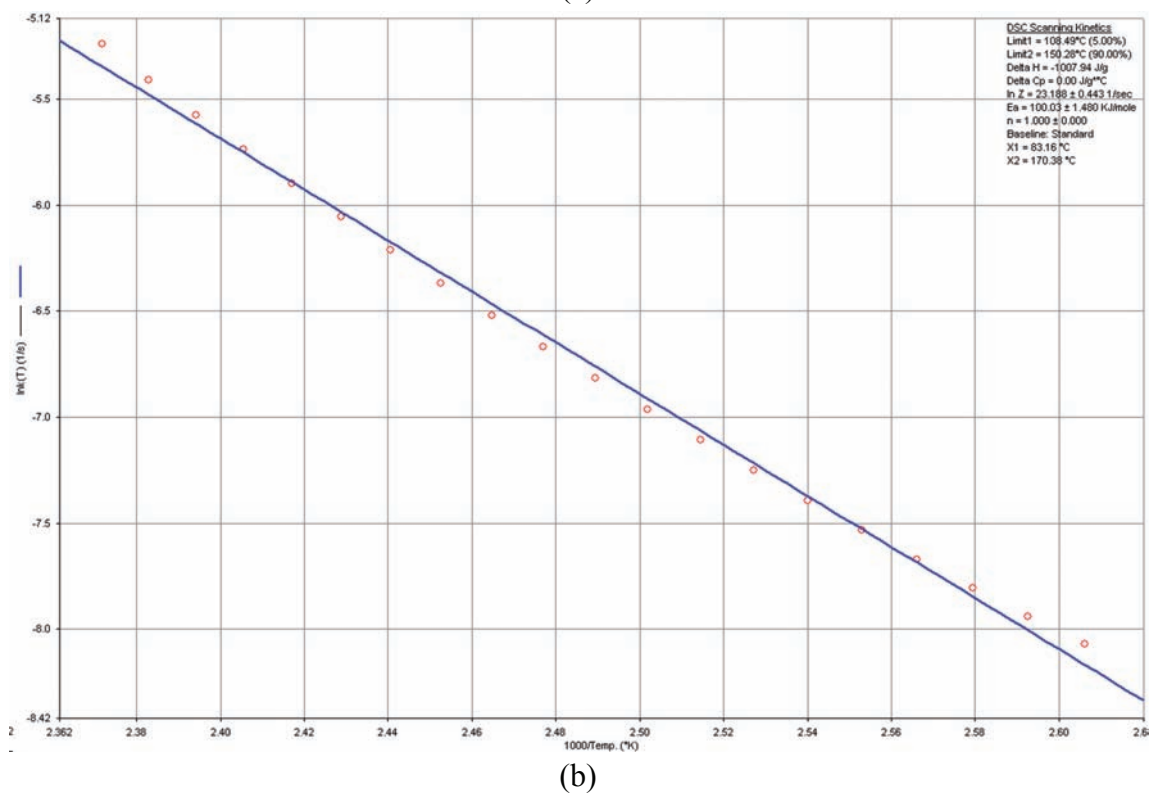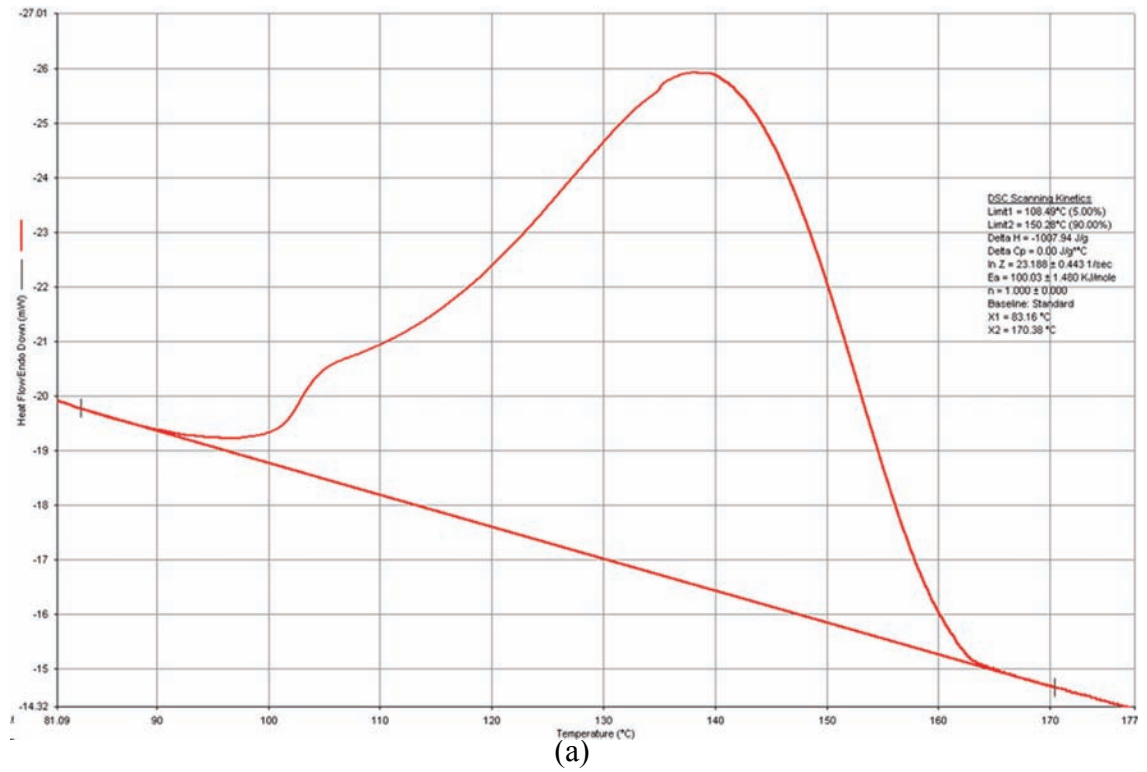
Figure 4.5: Decomposition of TBPIN (undiluted) measured by DSC
(a) heat flow curve (b) Arrhenius diagram from the integrated heat curve

(a)

(b)
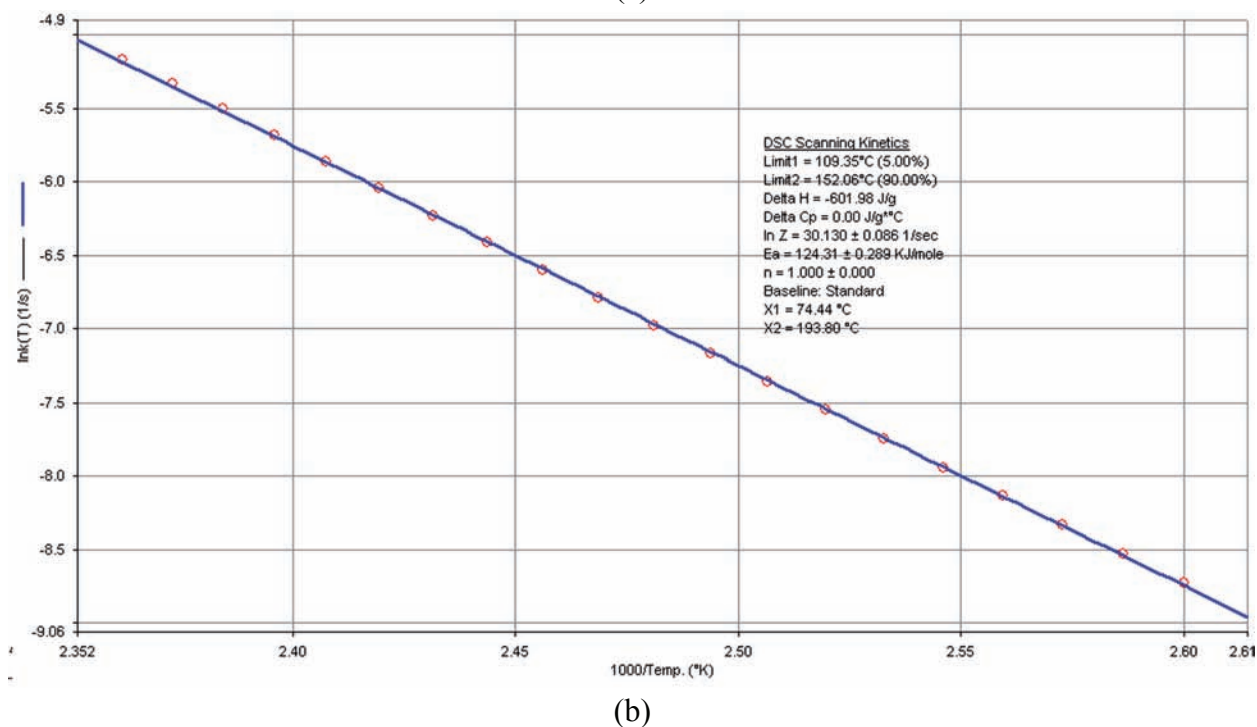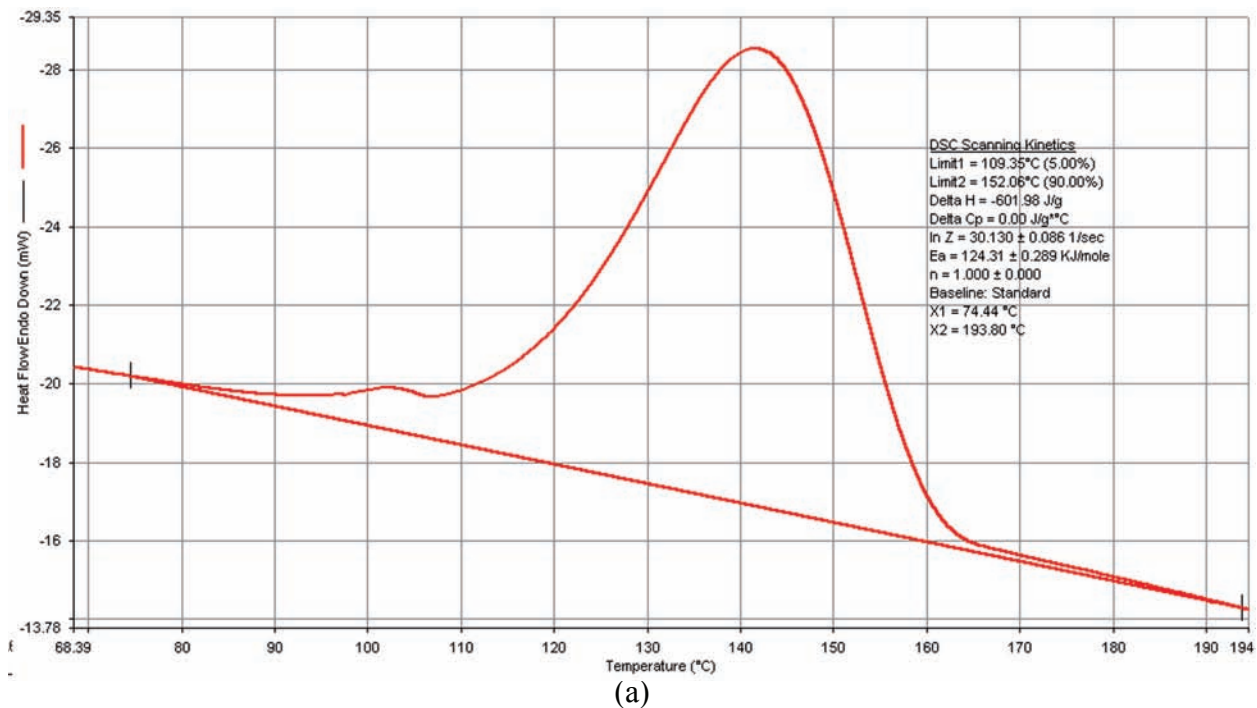
Figure 4.6: Decomposition of TBPIN (50% BuAc solution) measured by DSC
(a) heat flow curve (b) Arrhenius diagram from the integrated heat curve

4.3   Di-tert.butyl-peroxide (DTBP)

Finally, to validate the DSC method, a peroxide with well-known decomposition kinetics (DTBP) was taken as example and the measured decomposition kinetics compared to the one found in literature. DTPB is one of the most popular thermal initiators used in research studies. In industrial polymerizations it is less preferrable since its decomposition mechanism is rather complex and affected by the formation of various side products like aceton, free oxygen and different hydrocarbons [125]. For the other peroxides used in this work, on the other hand, the decomposition mechanism consists of a simple scission of the O-O group into to R-O· radicals.

In this study, the DTBP decomposition was only measured undiluted. The results from this comparison are presented in the following. The activation energy is in very good agreement with literature / manufacturer data. Although measured only undiluted, the half life time curve for the DSC kinetics is very close to the one calculated with the kinetic constants from the other sources.

Table 3: Kinetic rate constants for the thermal decomposition of DTBP

	k_0 [s^{-1}]	E_A [kJ mol^{-1}]
DSC undiluted	$9.178 \cdot 10^{14}$	147.90
Literature [47]	$2.800 \cdot 10^{14}$	146.40
Degussa Initiators	$1.164 \cdot 10^{15}$	150.69
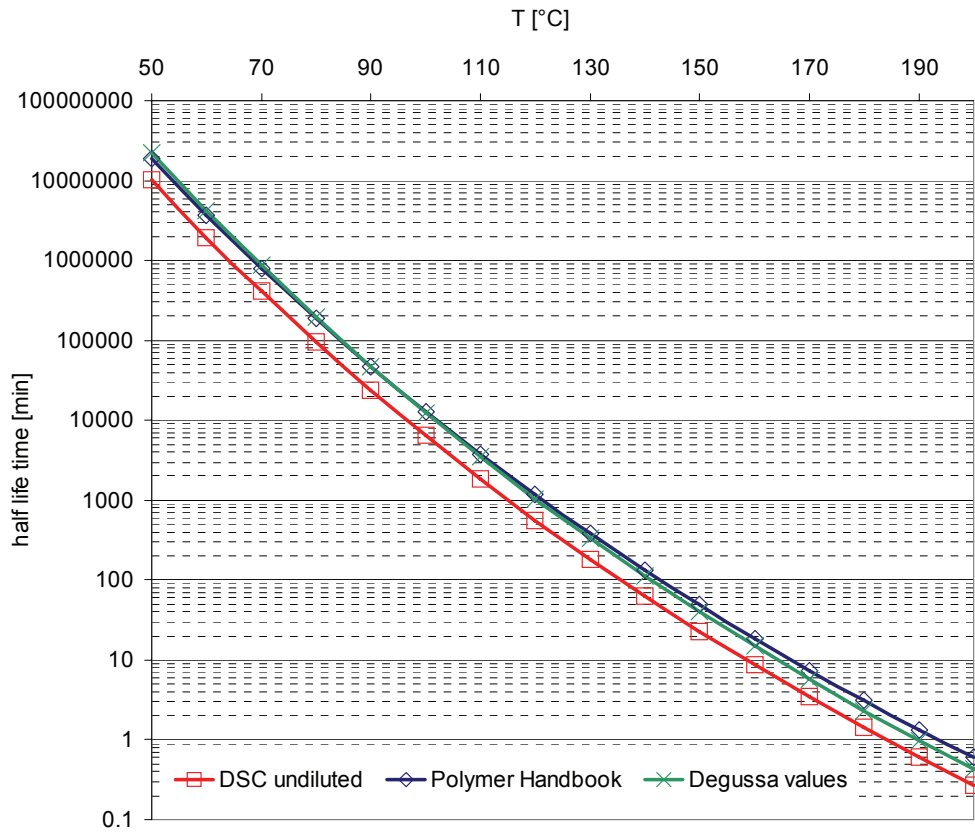
Figure 4.7: Half life times for DTBP using the kinetic constants from table 3

(a)

(b)
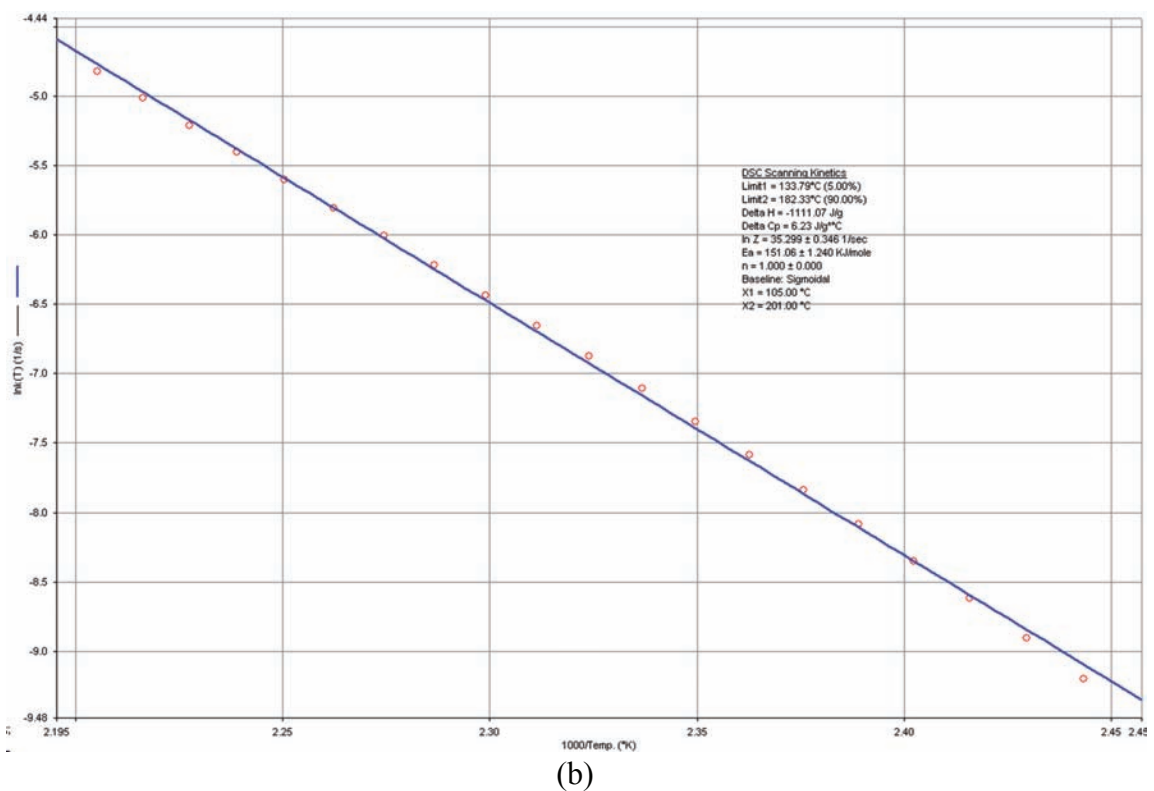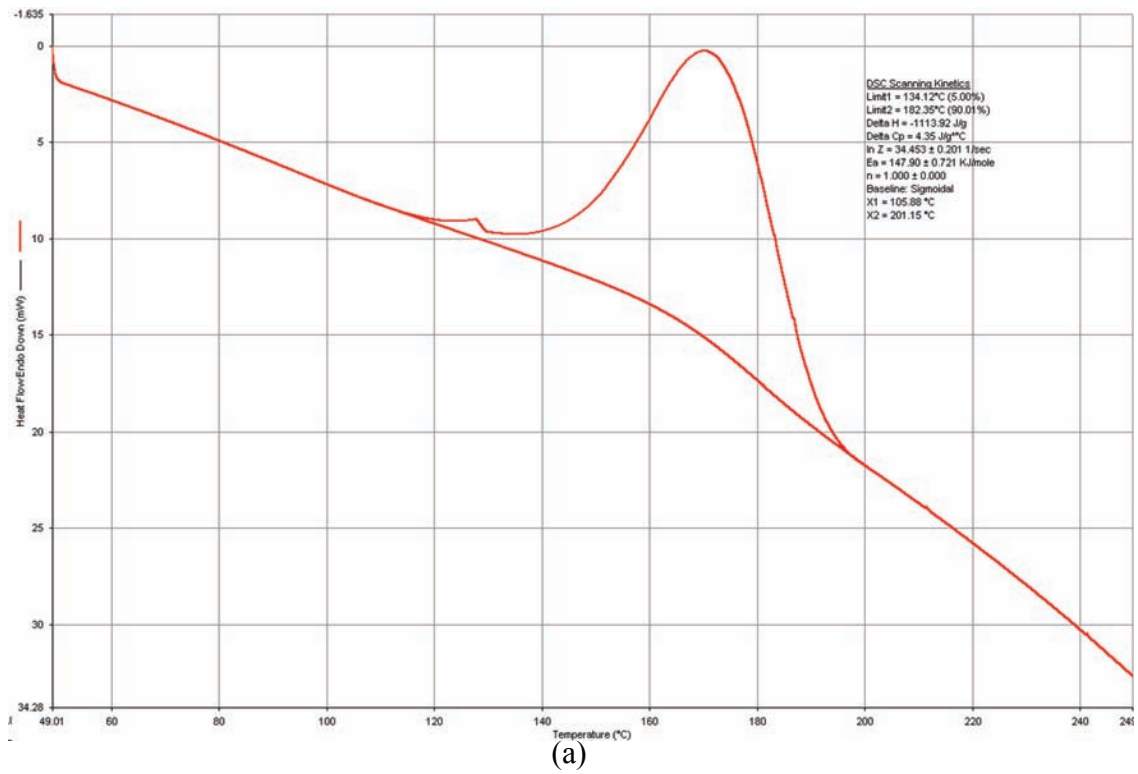
Figure 4.8: Decomposition of DTBP (undiluted) measured by DSC
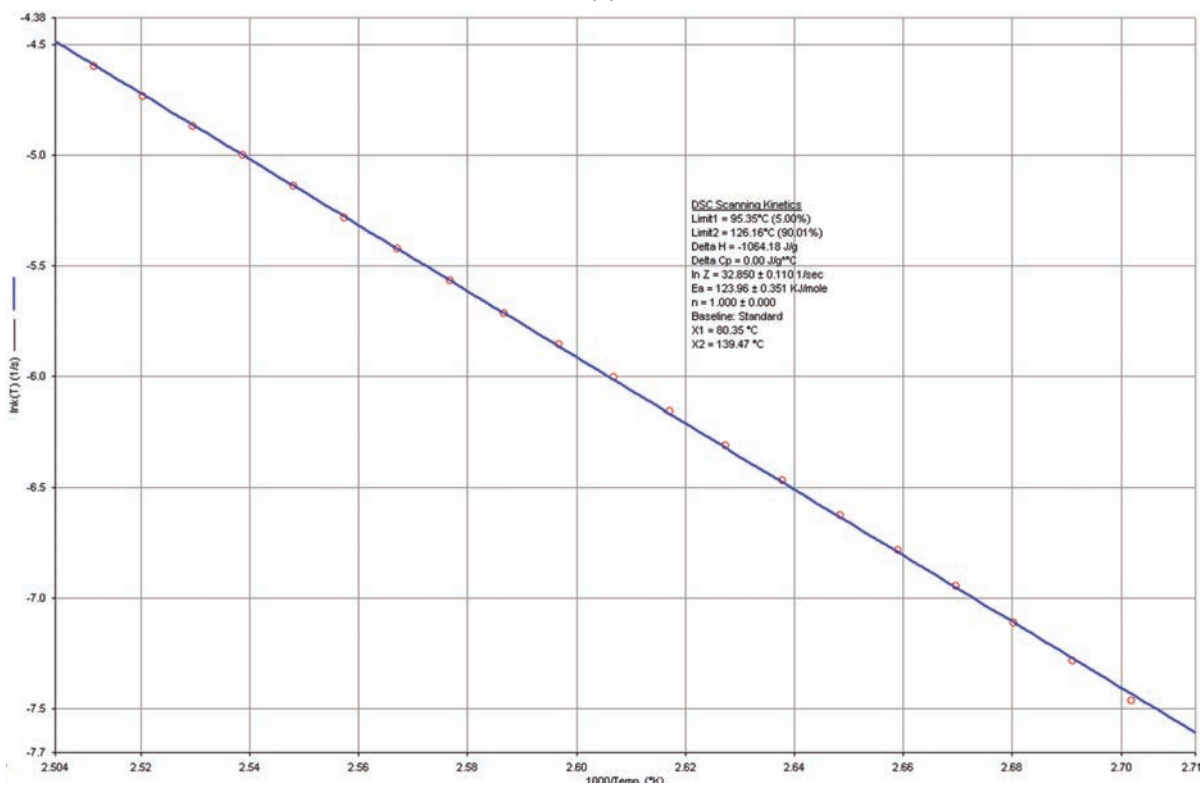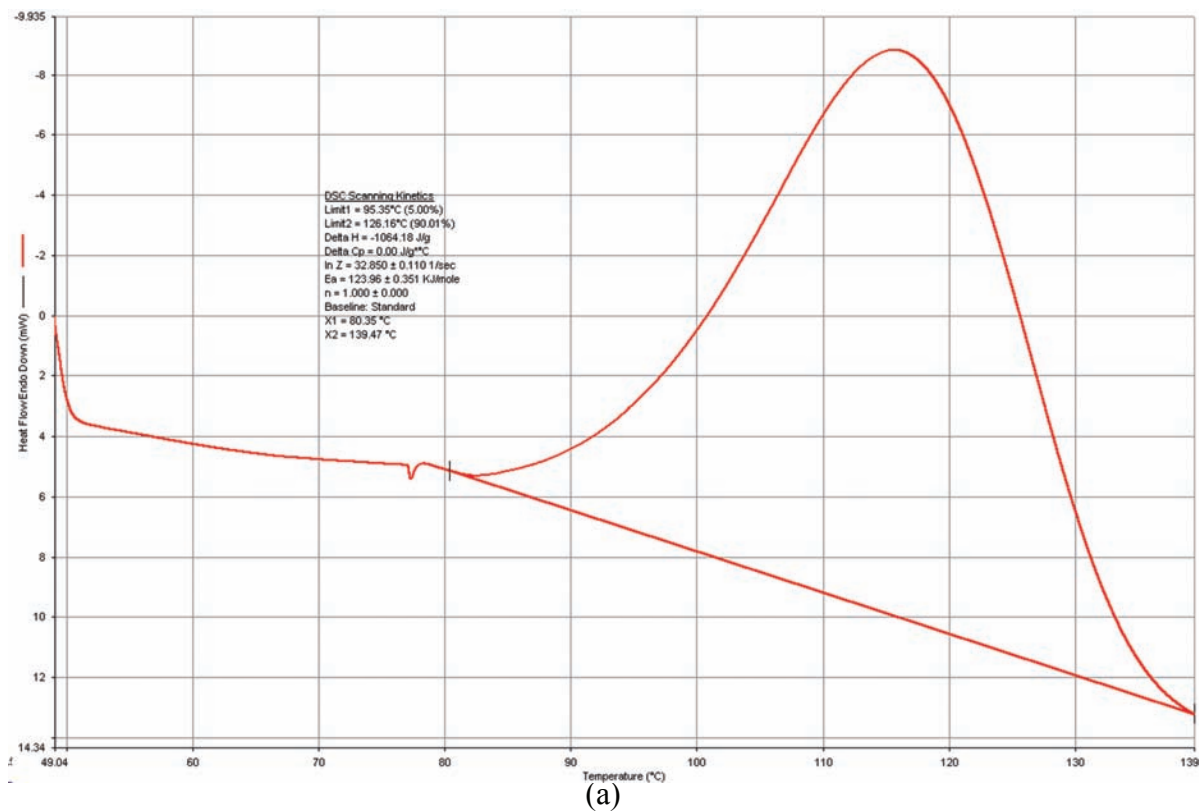*(a) heat flow curve (b) Arrhenius diagram from the integrated heat curve*

Physico-chemical data

5.1 Density of methyl methacrylate

$$\rho_{MMA}(T) = -9.4146 \cdot 10^{-6} \cdot T^3 + 1.3028 \cdot 10^{-3} \cdot T^2 - 1.1552\,T + 9.6339\,10^2$$
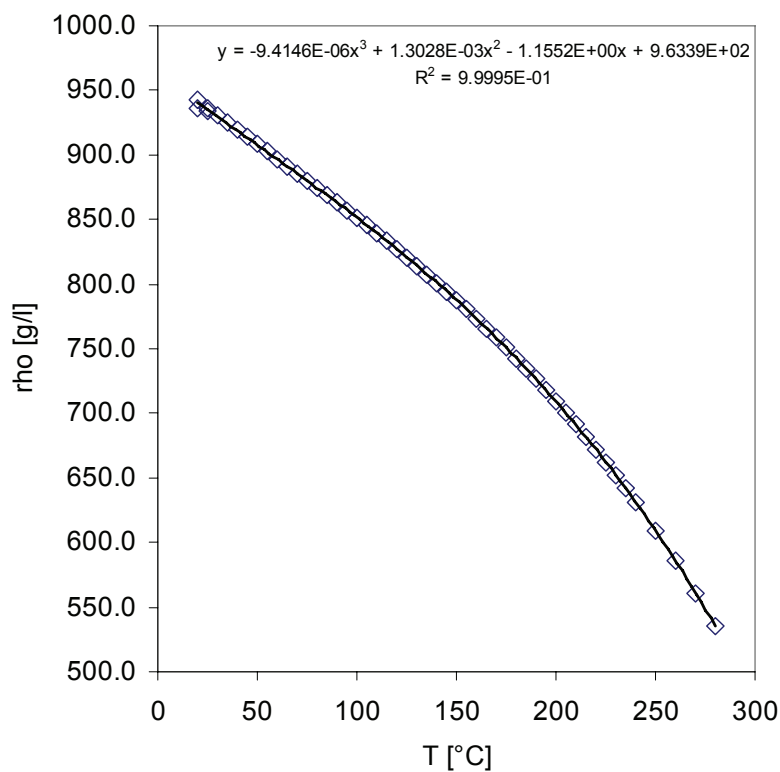
Figure 5.1: Density of methyl methacrylate as a function of temperature [°C], source: measured data from industrial partner

5.2 Density of butyl acetate

$$\rho_{BuAc}(T) = -3.1905 \cdot 10^{-4} \cdot T^2 - 1.0635 \cdot T + 9.0305 \ 10^2$$
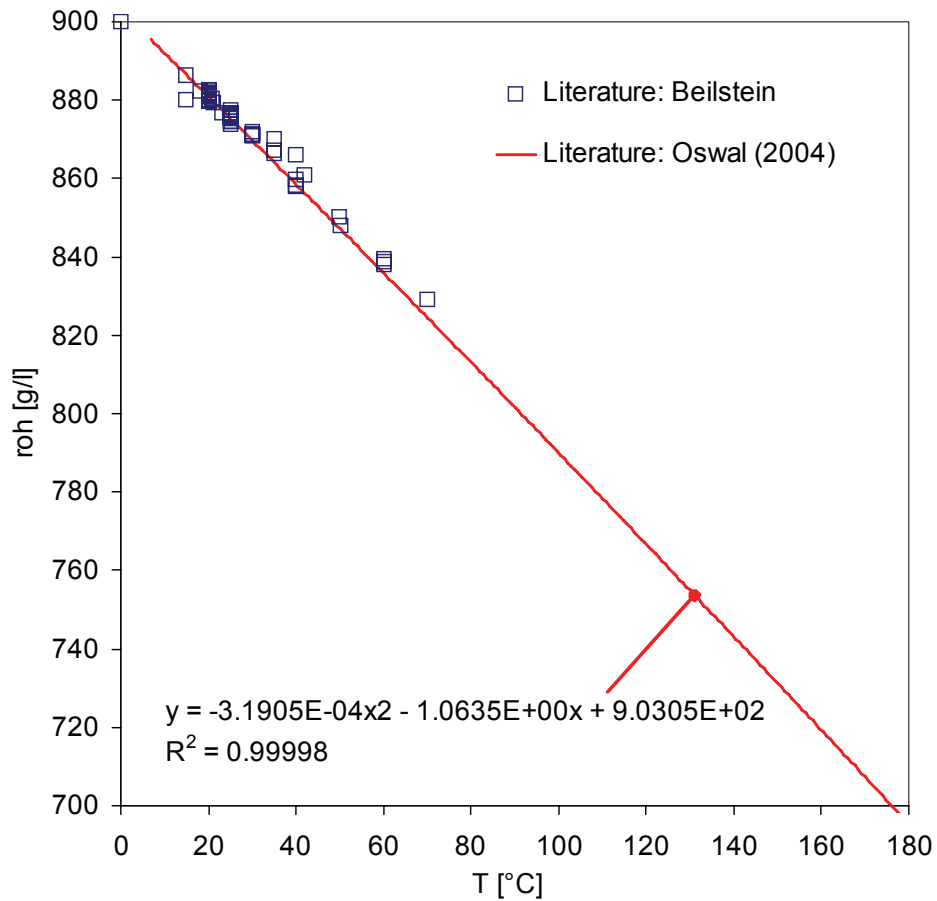
Figure 5.2: Density of butyl acetate as a function of temperature [°C], source: [88] (straight line), [126](squares)

5.3   Density of methyl acrylate

$$\rho_{MA}(T) = -1.1788 \cdot 10^{-3} \cdot T + 0.9774$$
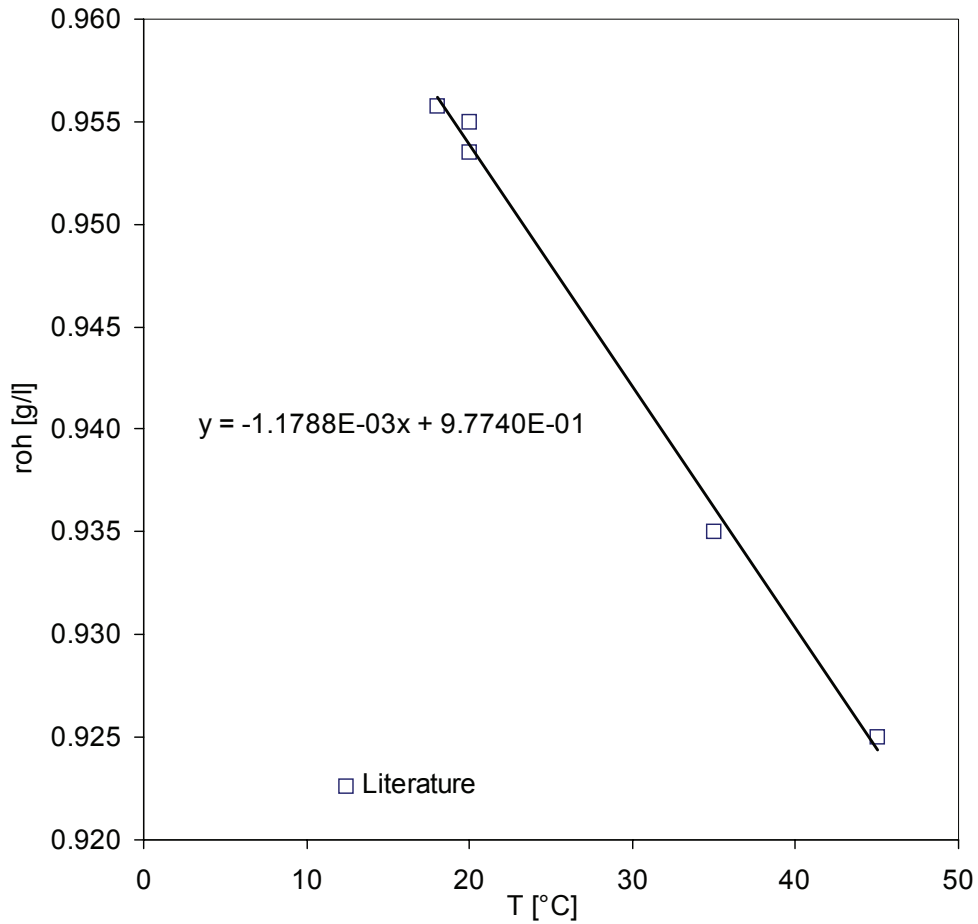
Figure 5.3: Density of methyl acrylate as a function of temperature [°C], source: [47, 127-129]

5.4   Density of poly (methyl methacrylate)

$$\rho_{PMMA}(T) = -0.0014 \cdot T^2 - 0.2309 \cdot T + 1195$$
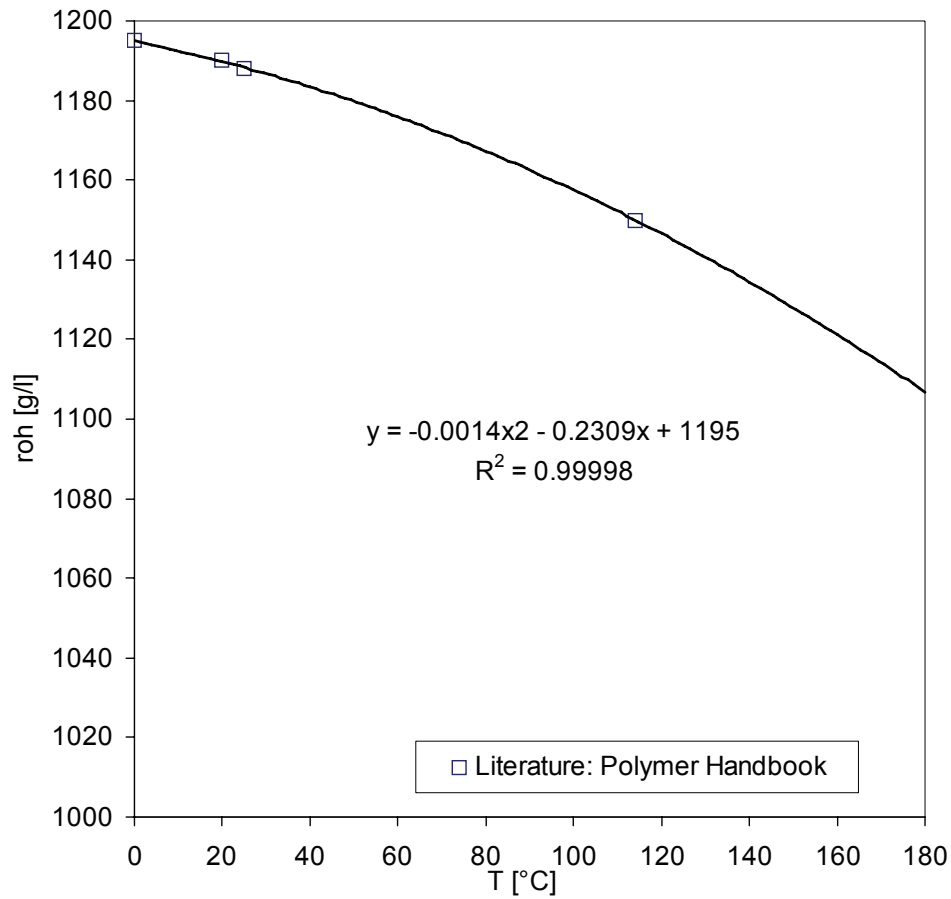
Figure 5.4: Density of poly (methyl methacrylate) as a function of temperature [°C]

5.5 Isentropic compressibility of methyl methacrylate

$$\kappa_{MMA}(T) = 7.8237 \cdot 10^{-14} \cdot T^2 + 1.2571 \cdot 10^{-12} \cdot T + 7.1359 \cdot 10^{-10}$$
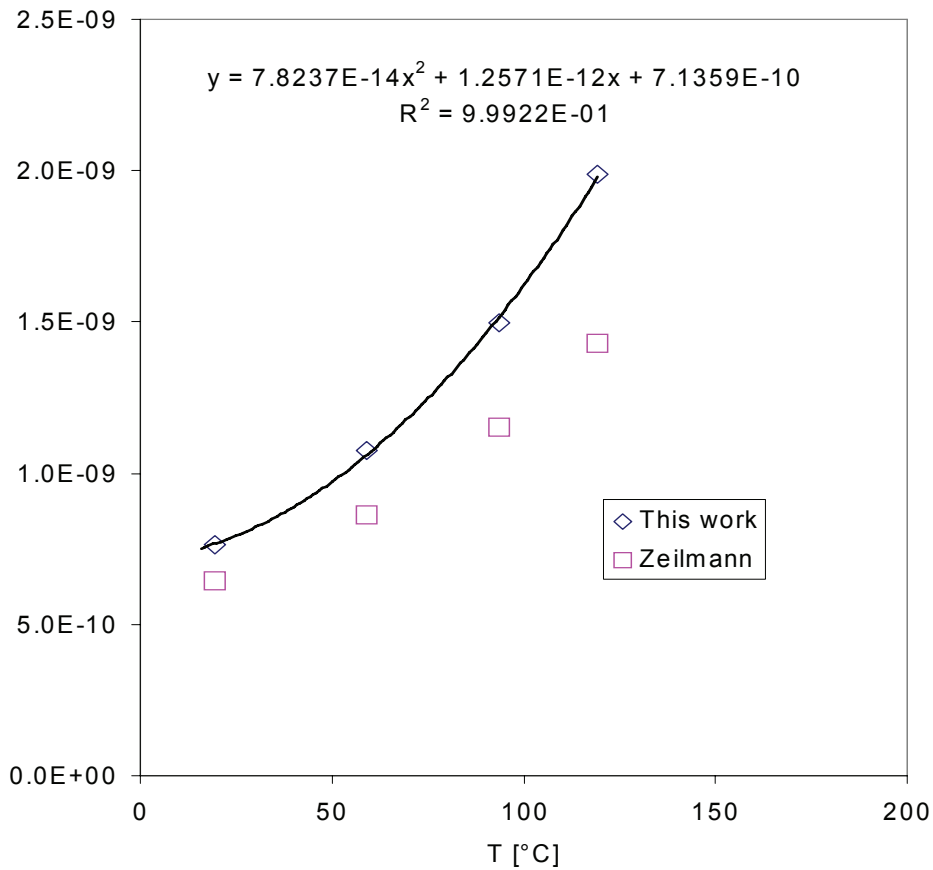
Figure 5.5: Isentropic compressibility of methyl methacrylate as a function of temperature [°C], literature values: [6]

5.6   Isentropic compressibility of butyl acetate

$$\kappa_{BuAc}(T) = 9.4166 \cdot 10^{-14} \cdot T^2 + 5.8845 \cdot 10^{-13} \cdot T + 8.1115 \cdot 10^{-10}$$
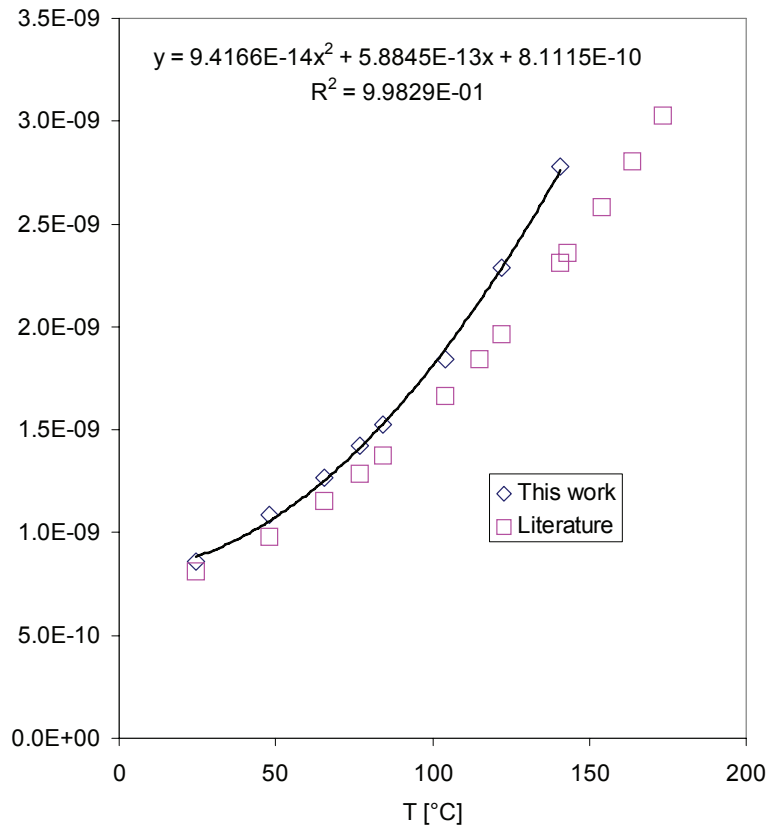
Figure 5.6: Isentropic compressibility of butyl aceate as a function of temperature [°C] Literature values: [89]

5.7 Isentropic compressibility of poly (methyl methacrylate)

$$\ln\kappa_{s,PMMA} = \frac{A + B \cdot T + C \cdot T^2}{1 + D \cdot T + E \cdot T^2 + F \cdot T^3}$$

Table 1: Fitting parameters for the $\kappa_{s,PMMA}$ curve fitting

A [Pa^{-1}]	B [Pa^{-1}°C^{-1}]	C [Pa^{-1}°C^{-2}]	D [Pa^{-1}°C^{-1}]	E [Pa^{-1}°C^{-2}]	F [Pa^{-1}°C^{-3}]
-22.22	0.36889	$-1.57 \cdot 10^{-3}$	-0.01639	$6.723 \cdot 10^{-5}$	$1.57 \cdot 10^{-8}$

Figure 5.7: Isentropic compressibility of poly (methyl methacrylate) as a function of temperature [°C], literature values: [47]

ANNEXE 6

Raw Materials and Qualities

Methyl Methacrylate (MMA)
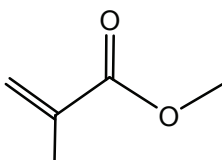
Manufacturer:	Degussa Röhm GmbH & Co. KG, Germany
CAS-No.:	80-62-6
Quality:	> 99.9% GC, stabilized with 25 ppm MEHQ
Molar mass:	100.12 g/mol
Density at 20°C:	ca. 0.943 g/cm3
Viscosity at 20°C:	ca. 0.63 mPa•s
Boiling point (1 atm):	100.3 °C

n-Butyl Acetate (BuAc)
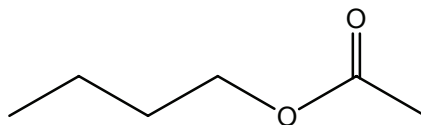
Manufacturer:	Schweizerhall SA, Switzerland
CAS-No.:	123-86-4
Quality:	liquid, technically pure
Molar mass:	116.16 g/mol
Density at 25°C:	ca. 0.881 g/cm3
Boiling point (1 atm):	124-126 °C

Ethyl Benzene (EB)
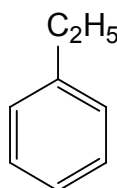
Manufacturer:	BASF AG, Germany
CAS-No.:	100-41-4
Quality:	liquid, technically pure
Molar mass:	106.17 g/mol
Density at 25°C:	ca. 0.867 g/cm3
Boiling point (1 atm):	136 °C

Methyl Acrylate (MA)
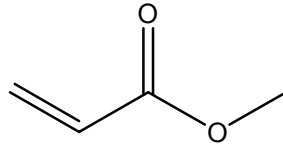
Manufacturer:	FLUKA GmbH&Co KG, Switzerland
CAS-No.:	96-33-3
Quality:	>99% GC, stabilized with 0.0015% MEHQ
Molar mass:	86.09 g/mol
Density at 20°C:	ca. 0.955 g/cm3
Boiling point (1 atm):	80 °C

n-Dodecanethiol (DDT)
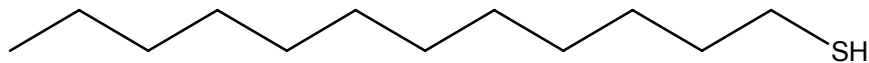
Manufacturer:	Riedel-de-Haëhn, Germany
CAS-No.:	112-55-0
Quality:	> 98% GC
Molar mass:	202.4 g/mol
Density at 25°C:	ca. 0.854 g/cm3
Boiling point (1 atm):	266 - 283 °C

***Tert*.butyl-peroxy-2-ethylhexanoat (TBPEH)**
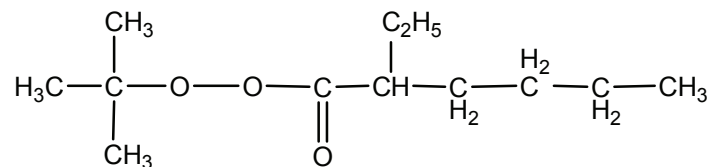
Manufacturer:	Degussa Initiators GmbH & Co.KG, Germany

CAS-No.: 3006-82-4

Quality: liquid, technically pure (99% peroxide content)

Molar mass: 216.3 g/mol

Density at 20°C: ca. 0.90 g/cm3

Viscosity at 20°C: ca. 4 mPa•s

Half life time 10h/1h/1min: 74 °C / 92 °C / 130 °C (0.1 M benzene solution)

Critical temperature: ca. 40°C (SADT[1])

Tert.butyl-peroxy-3,5,5-trimethyl- hexanoate (TBPIN)
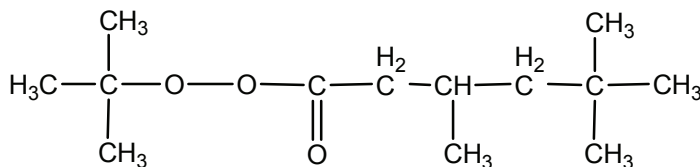
Manufacturer: Degussa Initiators GmbH & Co.KG, Germany

CAS-No.: 13122-18-4

Quality: liquid, technically pure (99% peroxide content)

Molar mass: 230.3 g/mol

Density at 20°C: ca. 0.89 g/cm3

Viscosity at 20°C: ca. 5 mPa•s

Half life time 10h/1h/1min: 100 °C / 119 °C / 160 °C (0.1 M benzene solution)

Critical temperature: ca. 60°C (SADT[1])

---

1. Self Accelerating Decomposition Temperature, SADT

Di-*tert*.butyl-peroxide (DTBP)

$$H_3C - \underset{\underset{CH_3}{|}}{\overset{\overset{CH_3}{|}}{C}} - O - O - \underset{\underset{CH_3}{|}}{\overset{\overset{CH_3}{|}}{C}} - CH_3$$
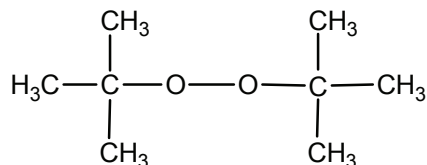
Manufacturer:	FLUKA GmbH&Co KG, Switzerland
CAS-No.:	110-05-4
Quality:	liquid, technical (>95% GC)
Molar mass:	146.2 g/mol
Density at 20°C:	0.794 g/cm3
Viscosity at 20°C:	ca. 0.8 mPa•s
Half life time 10h/1h/1min:	125 °C / 146 °C / 190 °C (0.1 M benzene solution)
Critical temperature:	> 80°C (SADT[1])

N,N-Dimethylformamid (DMF)
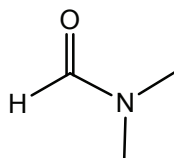
Manufacturer:	Riedel-de-Haëhn, Germany
CAS-No.:	68-12-2
Quality:	>99% GC
Molar mass:	73.09 g/mol
Density at 20°C:	0.944 g/cm3
Boiling point (1 atm):	153 °C

Tetrahydrofuran (THF)
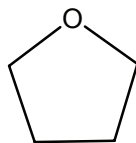
Manufacturer:	FISHER Scientific, Switzerland
CAS-No.:	109-99-9
Quality:	for GPC (>99.99% GC), stabilized with 0.025% BHT
Molar mass:	72.1 g/mol
Density at 20°C:	0.89 g/cm3
Boiling point (1 atm):	66 °C

ANNEXE 7

List of pilot plant experiments

Nr.	Aim	Reactor	T [°C]	VWZ [min]	BUAC [%]	BUAC [%]	MMA [%]	MA [%]	TBPEH [ppm]	TBPIN [ppm]	DTBP [ppm]	n-Dodecylm. [%]	X-Loop [%]	X-Tube [%]	X-total [%]	Mw [g/mol]	PD [-]
1	MA-TH	Loop	140	30	0	0	100	0	250	0	0	0.3	38			112'782	2.5
		Tube	140		20	100	0	0	0	1250	0	0		50		106'534	2.1
Exp.:	5.4.05 + 20.4.05														54	107'499	1.9
2	MA-TH	Loop	140	30	0	0	98.5	1.5	250	0	0	0.3	41			114'863	2.1
		Tube	140		20	100	0	0	0	1250	0	0		53		106'916	2.0
Exp.:	26.04.2005 Kond														62	95'618	1.9
2a	MA-TH	Loop	140	30	0	0	96.5	3.5	250	0	0	0.3	35			119'832	1.7
		Tube	140		20	100	0	0	0	1250	0	0		48		112'235	1.8
Exp.:	14.09.2005 Kond		long duration experiment (10h)												??	100'026	2.1
3	MA-TH	Loop	140	30	0	0	94.5	5.5	250	0	0	0.3	35			110'928	1.9
		Tube	140		20	100	0	0	0	1250	0	0		47		106'494	1.7
Exp.:	21.04.2005 Kond														54	103'007	2.2
4	CTA-I	Loop	140	30	0	0	100	0	250	0	0	0.2	50			162'070	1.9
		Tube	140		20	100	0	0	0	1250	0	0		61		152'746	2.1
Exp.:	27.4.05 + 30.06.2005														??	138'901	2.2
4a	CTA-I	Loop	140	30	0	0	100	0	250	0	0	0.2	54			176'064	2.1
		Tube	140		20	100	0	0	0	0	0	0		51		177'443	1.9
Exp.:	04.07.2005 Kond		Experiment with Inhibitor (250ppm TEMPO) in the tube												??	165'510	2.0
4b	CTA-I	Loop	140	30	0	0	100	0	250	0	0	0.2	45			149'323	1.7
		Tube	140		20	100	0	0	0	1250	0	0		56		140'055	2.1
Exp.:	08.07.2005 Kond		Experiment with 5% EB as internal standard												??	133'446	2.8
5	CTA-I	Loop	140	30	0	0	100	0	250	0	0	0.5	35			73'022	2.1
		Tube	140		20	100	0	0	0	1250		0		50		73'807	1.9
Exp.:	03.05.2005 Kond														??	117'043	2.2
6	MA-TH	Loop	120	30	0	0	100	0	250	0	0	0.3	38			123'954	2.1
		Tube	120		20	100	0	0	*1250*	0	*0*	*0*		52		120'669	2.2
Exp.:	04.05.2005 Kond														62	68'352	2.3
6a	**MA-TH**	**Loop**	**120**	**30**	**0**	**0**	**100**	**0**	**500**	**0**	**0**	**0.3**	**56**			**127'708**	**2.0**
		Tube	**120**		**20**	**100**	**0**	**0**	**1250**	**0**	**0**	**0**		**72**		**116'000**	**2.5**
Exp.:	11.05.2005 Kond		Experiment aborted due to strong pressure increase (consequence: broken sealing)												??	99'268	1.9
7	**MA-TH**	**Loop**	**120**	**30**	**0**	**0**	**98.5**	**1.5**	***400***	***0***	***0***	***0.33***	**56**			**123'195**	**1.7**
		Tube	**120**		**20**	**100**	**0**	**0**	***1000***	***0***	***0***	***0***		**67**		**119'144**	**1.8**
Exp.:	13.09.2005 Kond		again strong pressure increase, aborted at 42bar												??	105'672	1.7
9	MA-TH	Loop	150	30	0	0	100	0	0	250	0	0.3	53			119'553	2.2
		Tube	150		20	100	0	0	0	0	1250	0		65		113'721	2.2
Exp.:	18.07.2005 Kond														78	102'280	2.1
10	MA-TH	Loop	150	30	0	0	98.5	1.5	0	250	0	0.3	52			115'120	1.8
		Tube	150		20	100	0	0	0	0	1250	0		68		110'316	2.1
Exp.:	19.07.2005 Kond														78	96'982	1.8
10a	MA-TH	Loop	150	30	0	0	98.5	1.5	0	250	0	0.3	30			105'695	1.6
		Tube	150		20	100	0	0	0	0	1250	0		50		103'522	1.7
Exp.:	12.09.2005 Kond		long duration experiment (10h)												62	92'048	1.8
11	MA-TH	Loop	150	30	0	0	96.5	3.5	0	250	0	0.3	29			104'927	1.9
		Tube	150		20	100	0	0	0	0	1250	0		49		102'535	1.8
Exp.:	15.09.2005 Kond														63	87'352	1.8
12	MA-TH	Loop	150	30	0	0	94.5	5.5	0	250	0	0.3	50			115'343	1.9
		Tube	150		20	100	0	0	0	0	1250	0		66		108'016	2.1
Exp.:	21.07.2005 Kond														82	86'532	2.2
13	MA-TH	Loop	160	30	0	0	98.5	1.5	0	250	0	0.25	45			126'900	1.8
		Tube	160		20	100	0	0	0	0	1250	0		65		113'607	1.8
Exp.:	03.08.2005 Kond														76	101'144	1.8
14	MA-TH	Loop	160	30	0	0	97	3	0	250	0	0.25	30			114'735	2.0
		Tube	160		20	100	0	0	0	0	1250	0		60		108'224	1.8
Exp.:	05.08.2005 Kond														70	91'146	1.8
15	MA-TH	Loop	160	30	0	0	94.5	5.5	0	250	0	0.25	36			114'638	2.1
		Tube	160		20	100	0	0	0	0	1250	0		62		106'967	1.7
Exp.:	04.08.2005 Kond														75	92'771	1.7
16	MA-TH	Loop	170	30	0	0	98.5	1.5	0	250	0	0.2	26			119'838	1.9
		Tube	170		20	100	0	0	0	0	1250	0		47		98'056	1.9
Exp.:	12.08.2005 Kond														58	85'007	1.9
17	MA-TH	Loop	170	30	0	0	94.5	5.5	0	400	0	0.2	25			110'654	1.7
		Tube	170		20	100	0	0	0	0	1250	0		48		94'330	2.0
Exp.:	16.08.2005 Kond														65	82'852	2.0
18	MA-TH	Loop	170	30	0	0	96.5	3.5	0	600	0	0.2	48			110'876	1.8
		Tube	170		20	100	0	0	0	0	1502	0		56		97'738	1.9
Exp.:	06.09. + 08.09.2005														65	88'058	2.0
19	MA-TH	Loop	170	30	0	0	98.5	1.5	0	500	0	0.2	32			108'121	1.9
		Tube	170		20	100	0	0	0	0	1250	0		52		92'658	1.9
Exp.:	18.08.2005 Kond		long duration experiment (10h)												61	87'541	1.7

A-LXVIII

ANNEXE 5

Tablecurve fitting parameters

5.1 α correction factor

Table 1: Fitting parameters for the α curve fitting

Parameter	Value	Error
α_0	0.40604	± 0.0221
A_1	0.00364	± 0.0002
A_2	-0.39541	± 0.0968

5.2 $\kappa_{s, PMMA}$ - fitting

Table 2: Fitting parameters for the $\kappa_{s,PMMA}$ curve fitting

A [Pa⁻¹]	B [Pa⁻¹°C⁻¹]	C [Pa⁻¹°C⁻²]	D [Pa⁻¹°C⁻¹]	E [Pa⁻¹°C⁻²]	F [Pa⁻¹°C⁻³]
$[Pa^{-1}]$	$[Pa^{-1}°C^{-1}]$	$[Pa^{-1}°C^{-2}]$	$[Pa^{-1}°C^{-1}]$	$[Pa^{-1}°C^{-2}]$	$[Pa^{-1}°C^{-3}]$
-22.22	0.36889	$-1.57 \cdot 10^{-3}$	-0.01639	$6.723 \cdot 10^{-5}$	$1.57 \cdot 10^{-8}$

5.3   UPV-Conversion fit

Table 3: Fitting parameters for the fittings presented in figure 4.24

Parameter	w_p to *speed of sound*	*speed of sound* to X
a	1808.1378 [-]	1.9646026
b	-18.522899 $\left[\frac{1}{°C}\right]$	-0.016100033 $\left[\frac{1}{°C}\right]$
c	0.092598977 $\left[\frac{1}{°C^2}\right]$	$8.1124055 \cdot 10^{-5}$ $\left[\frac{1}{°C^2}\right]$
d	-0.00017919959 $\left[\frac{1}{°C^3}\right]$	$-1.6127687 \cdot 10^{-7}$ $\left[\frac{1}{°C^3}\right]$
e	-159.6025 [-]	-0.001146163 $\left[\frac{s}{m}\right]$
f	-151.65653 [-]	-0.0014100568 $\left[\frac{1}{°C}\right]$
g	-0.0019820557 $\left[\frac{1}{°C}\right]$	$-2.5559475 \cdot 10^{-6}$ $\left[\frac{1}{°C^2}\right]$
h	-0.29202612 [-]	-0.0012009741 $\left[\frac{s}{m}\right]$
i	-0.25516883 [-]	$1.0616658 \cdot 10^{-7}$ $\left[\frac{s^2}{m^2}\right]$

Symbols and Abbreviations

Symbols

Symbol	Description	Unit *(unless specified in the text)*
Bo	Bodenstein number	[-]
C_m	monomer concentration	[mol/l]
C_b	Bulk monomer concentration	[mol/l]
C_{CTA}	chain transfer constant	[-]
d	diameter	[m]
D_{ax}	axial dispersion coefficient	[m²/s]
D_{eff}	Diffusion coefficient	[m²/s]
$\overline{DP}_n$	Degree of polymerization	[-]
e	Euler number	[-]
E_A	activation energy	[kJ/mol]
f	efficiency of a thermal initiator	[-]
ΔH	reaction enthalpy	[kJ/mol]
k	kinetic rate constant	[l, mol, s]
k_d	decomposition rate for thermal initiators	
k_{dt}	rate coefficient for the initiation by CTA	
k_{dp}	rate coefficient for the depolymerization	
k_{CTA}	rate coefficient for the radical transfer to CTA	

k_{H-1} rate coefficient for the formation of dimer

k_p propagation rate coefficient

$k_{po,f}$ formation rate coefficient for PMMAP

$k_{po,d}$ decomposition rate coefficient for PMMAP

k_{t0} intrinsic termination rate coefficient

k_{tc} rate coefficient for the combination termination

k_{td} rate coefficient for the disproportionation termination

k_{th} rate coefficient for the thermal initiation mechanism

$k_f, k_{tr,m}$ rate coefficient for the radical transfer to monomer

K_γ	shear constant	[-]
K	volume specific heat transfer coefficient	[W/m^3 K]
L	length	[m]
m	mass	[kg]
M_w	weight average molecular weight	[kg/mol]
M_n	number average molecular weight	[kg/mol]
Nu	Nusselt number	[-]
n	reaction order	[-]
$\overline{P}$	kinetic chain length	[-]
$P_{i,n}\cdot$	chain radical ending with species i (1=MMA / 2=MA)	[-]
p	pressure	[bar]
R_p	rate of polymerization	[mol/l s]
r_1, r_2	reactivity ratios for MMA, MA	[-]
r_t	termination radius	[m]
R	organic substituent	
Re	Reynolds number	[-]
ΔS	reaction entropy	[J/mol K]
T	temperature	[K]
T_g	glass transition temperature	[°C]
U	surface specific heat transfer coefficient	[W/m^2 K]
u_z	flow velocity in z-direction	[m/s]
Wf	weight fraction (in GPC distribution analysis)	[-]

w	weight fraction	[-]
X	conversion	[-]
X_c	fitting parameter in the Fenouillot model	[-]
α	parameter for the pressure dependence in US	[m/s bar]
α, β	fitting parameters in the Fleury model	[-]
β	heating rate	[K/min]
ε	volume contraction coefficient	[-]
ε	porosity of the reactor tubes	[-]
κ	compressibility	[1/Pa]
λ	concentration of chain radicals	[mol/l]
λ_l	heat conductivity	[W/m K]
η, η_0	viscosity, zero shear viscosity	[Pa s]
ϕ	volume fraction	[-]
γ'	shear rate	[1/s]
γ	k_{tc}/k_{td}	[-]
$\theta(T)$	fitting function in the CCS gel effect model	
ρ	density	[kg/mol]
$\tau(T)$	fitting function in the gel effect model derived in this work	
τ	residence time	[s]

Abbreviations

AIBN	2, 2'-Azobis(2-methylpropionitrile)
amu	atomic mass unit (in MS analysis)
BPO	Di-benzoyl peroxide
BA	Butyl acrylate
BMA	Butyl methacrylate
BuAc	Butyl acetate
CTA	Chain transfer agent
1,2-DCB	1,2-Dichlorobenzene

DSC	Differential scanning calorimetry
DTBP	Di-tert.butyl peroxide
EB	Ethyl benzene
GPC	Gel permeation chromatography
HS-GC	Head space gas chromatography
MA	Methyl acrylate
MMA	Methyl methacrylate
MMA-OO	MMA polyperoxide
MS	Mass spectroscopy
NMR	Nuclear Magnetic Resonance spectroscopy
PMMA	Poly (methyl methacrylate)
PS	Poly (styrene)
PMMAP	MMA polyperoxide
SEC^3	Size Exclusion Chromatography with triple detection
TBPEH	Tert.butyl-peroxy-2-ethylhexanoat
TBPIN	Tert.butyl-peroxy-3,5,5-trimethylhexanoat
TGA	Thermogravimetry
THF	Tetrahydrofuran
US	Ultrasound
UV	UV-Vis Photospectrometry

Indices

m	monomer
s	solvent
p	polymer
obs	apparant value (for rate constants)

Bibliography

[1]   K.T. Nguyen, *"Mélangeur statique comme réacteur tubulaire de polymérisation"*, Ph.D. thesis: Département de Chimie, no., **EPFL** (Lausanne), 1982.

[2]   T. Meyer, *"Etude à l'aide d'une méthode chimique de la ségragation lors d'une polymérisation dans un réacteur tubulaire à recyclage"*, Ph.D. thesis: Département de chimie, no. 810, **EPFL** (Lausanne), 1989.

[3]   S. Belkhiria, *"Copolymérisations en masse de styrène et d'anhydride maléique dans un réacteur tubulaire à recyclage: Etude cinétique, stabilité de réacteur et qualité des produits"*, Ph.D. thesis: Département de chimie, no. 1258, **EPFL** (Lausanne), 1994.

[4]   L. Cavin, *"Polymérisation radicalaire du styrène initiée par un initiateur bifonctionnel dans un réacteur tubulaire à recyclage"*, Ph.D. thesis: Département de chimie, no. 2083, **EPFL** (Lausanne), 2000.

[5]   P.-A. Fleury, *"Polymérisation du méthacrylate de méthyle à haute température"*, Ph.D. thesis: Département de Chimie Thesis no.1986, no., **École Polytechnique Fédérale de Lausanne** (Lausanne), 1993.

[6]   T. Zeilmann, *"Continuous Methylmethacrylate Polymerization Process - Reaction and Devolatilization"*, Ph.D. thesis: Institute of Chemical and Biological Process Science, no. 2554, **EPFL** (Lausanne), 2002.

[7]   L. Cavin, T. Meyer, and A. Renken, *"On-line conversion monitoring through ultrasound velocity measurements in bulk styrene polymerization in a recycle reactor - Part I: Experimental validation"*, **Polymer Reaction Engineering**, 8(3): p. 201-223, **2000**.

[8]   L. Cavin, A. Renken, and T. Meyer, *"On-line conversion monitoring through ultrasound velocity measurements in bulk styrene polymerization in a recycle reactor - Part II: Mathematical Model"*, **Polymer Reaction Engineering**, 8(3): p. 225-240, **2000**.

[9]   P. Nising, *"Optimization of the Polymerization of PMMA in a Sulzer Pilot Plant"*, Ph.D. thesis: Lehrstuhl für Technische Chemie I, no., **Friedrich-Alexander-Universität** (Erlangen), 2001.

[10]   K. Albrecht, *Polymethacrylat - Ein vielseitiger Kunststoff als Granulat und Halbzeug*, in *Roehm GmbH*. 2001: Darmstadt.

[11]   R. Vieweg and F. Esser, *Polymethylmethacrylate*. **1975**. Carl Hauser Verlag. München.

[12]   C.J. Simon, *Plastics Business Data and Charts*, www.vke.de.

[13]   W.A. Pryor and L.D. Lasswell, *Advances in Free Radical Chemistry*. **1975**. Academic Press. N.Y.

[14]   M. Stickler and G. Meyerhoff, *"Die thermische Polymerisation von Methylmethacrylat, 1 Polymerisation in Substanz"*, **Makromolekulare Chemie**, 179: p. 2739-2745, **1978**.

[15]   M. Stickler and G. Meyerhoff, *"Die thermische Polymerisation von Methylmethacrylat, 2 Bildung des ungesättigten Dimeren"*, **Makromolekulare Chemie**, 181(1): p. 131-147, **1980**.

[16]   E. Brand, M. Stickler, and G. Meyerhoff, *"Die thermische Polymerisation von Methyl-methacrylat, 3 Verhalten des ungesättigten Dimeren bei der Polymerisation"*, **Makromolekulare Chemie**, 181: p. 913-921, **1980**.

[17]   J. Lingnau, M. Stickler, and G. Meyerhoff, *"The spontaneous Polymerization of Methyl-Methacrylate: IV Formation of cyclic dimers and linear trimers"*, **European Polymer Journal**, 16: p. 789-791, **1980**.

[18]   M. Stickler and G. Meyerhoff, *"The Spontaneous Thermal Polymerization of Methyl-Methacrylate: 5. Experimental-Study and Computer Simulation of the High Conversion Reaction at 130°C"*, **Polymer**, 22(7): p. 928-933, **1981**.

[19]   J. Lingnau and G. Meyerhoff, *"The Spontaneous Polymerization of Methyl-Methacrylate: VI. Polymerization in Solution - Participation of Transfer Agents in the Initiation Reaction"*, **Polymer**, 24(11): p. 1473-1478, **1983**.

[20]   F.R. Mayo and A.A. Miller, *"The Oxidation of Unsaturated Compounds. VIII. The Oxidation of Methacrylic Esters"*, **1957**.

[21]   C.E. Barnes, R.M. Elofson, and G.D. Jones, *"Role of Oxygen in Vinyl Polymerization. II. Isolation and Structure of the Peroxides of Vinyl Compounds"*, **Journal of the American Chemical Society**, 72: p. 210-215, **1950**.

[22]   R.S. Lehrle and A. Shortland, *"A Study of the Purification of Methyl Methacrylate suggests that the "Thermal" Polymerisation of this Monomer is initiated by Adventitious Peroxides"*, **European Polymer Journal**, 24(5): p. 425-429, **1987**.

[23]   S. Schulze and H. Vogel, *"Aspects of the safe storage of acrylic monomers: Kinetics of the oxygen consumption"*, **Chemical Engineering & Technology**, 21(10): p. 829-837, **1998**.

[24]   G.L. Batch and C.W. Macosko, *"Oxygen Inhibition in Differential Scanning Calorimetry of Free- Radical Polymerization"*, **Thermochimica Acta**, 166: p. 185-198, **1990**.

[25]   T. Mukundan and K. Kishore, *"Structure and Pyrolysis of Poly(methyl methacrylate peroxide): A Thermochemical Approach"*, **Macromolecules**, 20: p. 2382-2385, **1986**.

[26] K. Ganesh, S. Paramasivam, and K. Kishore, *"Determination of end groups in poly(methylmethacrylate peroxide) by fast atom bombardment mass spectrometry and IR spectroscopy"*, **Polymer Bulletin**, 37(6): p. 785-790, **1996**.

[27] G.V. Schulz and G. Henrici, *"Kinetik Der Polymerisationsreaktionen .22. Reaktionskinetik Der Polymerisationshemmung Durch Molekularen Sauerstoff (Versuche Mit Methylmethacrylat)"*, **Makromolekulare Chemie**, 18-9(MAR): p. 437-454, **1956**.

[28] K. Subramanian, *"Formation, degradation, and applications of polyperoxides"*, **Journal of Macromolecular Science-Polymer Reviews**, C43(3): p. 323-383, **2003**.

[29] K.S. Murthy, K. Kishore, and V.K. Mohan, *"Vinyl Monomer Based Polyperoxides as Potential Initiators for Radical Polymerization - an Exploratory Investigation with Poly(Alpha-Methylstyrene Peroxide)"*, **Macromolecules**, 27(24): p. 7109-7114, **1994**.

[30] K. Kishore, V. Gayathri, and K. Ravindran, *"Formation and Degradation of Polymeric Peroxides"*, **Journal of Macromolecular Science and Chemistry**, A16(8): p. 1359-1383, **1981**.

[31] R. Kerber, *"Kinetische Untersuchungen zur Bildung polymerer Peroxyde des Methylmethacrylates. I."* **Die makromolekulare Chemie**, 40(25): p. 25-38, **1960**.

[32] C. Vila, R. Moreno, M. Perez, E. Abuin, and E. Lissi, *"Methyl Methacrylate Polymerization in the Presence of Oxygen"*, **Anales Asoc. Quím. Argentina**, 61: p. 197-203, **1973**.

[33] C.D. Wagner, R.H. Smith, and E.D. Peters, *"Determination of Organic Peroxides - Evaluation of a Modified Iodometric Method"*, **Analytical Chemistry**, 19(12): p. 976, **1947**.

[34] K. Nozaki, *"Iodometric Method of Analysis for Organic Peroxides"*, **Industrial and Engineering Chemistry-Analytical Edition**, 18(9): p. 583-583, **1946**.

[35] T. Scherzer and H. Langguth, *"Temperature Dependence of the oxygen solubility in Acrylates and its Effect on the induction period in UV photopolymerization"*, **Macromolecular Chemistry and Physics**, 206: p. 240-245, **2005**.

[36] P. Nising, T. Meyer, R. Carloff, and M. Wicker, *"Thermal Initiation of MMA in High Temperature Radical Polymerizations"*, **Macromolecular Materials and Engineering**, 290: p. 311-318, **2005**.

[37] G. Sivalingam, P. De, R. Karthik, and G. Madras, *"Thermal degradation kinetics of vinyl polyperoxide copolymers"*, **Polymer Degradation and Stability**, 84(1): p. 173-179, **2004**.

[38] C.H. Bamford and P.R. Morris, *"The Oxidative Polymerization of Methyl Methacrylate"*, **Die makromolekulare Chemie**, 87: p. 73-89, **1965**.

[39] Personal communication, N. Deusch, 2003.

[40] G. Odian, *Principles of Polymerization*. **1991**. New York [etc.].

[41] PerkinElmer, *Pyris Software online help - Scanning Kinetics theory,*

[42] F. Fenouillot, J. Terrisse, and T. Rimlinger, *"Thermal polymerization of methyl methacrylate at high temperature"*, **International Polymer Processing**, 13(2): p. 154-161, **1998**.

[43]   P. Nising, T. Zeilmann, and T. Meyer, *"On the Degradation and Stabilization of Poly(Methyl Methacrylate) in a Continuous Process"*, **Chem. Eng. Technol.**, 26(5): p. 599-604, **2003**.

[44]   NIST, *NIST Chemistry WebBook*, http://webbook.nist.gov.

[45]   P. Xia, H. Cheng, and D. Yan, *"Free-radical polymerization of methyl methacrylate initiated by thiol alone"*, **Journal of Applied Polymer Science**, 45(4): p. 579-582, **1992**.

[46]   C.J. Albisetti, D.C. England, M.J. Hogsed, and R.M. Joyce, *"Dimers of Methacrylic Comounds"*, **Journal of the American Chemical Society**, 78: p. 472-475, **1956**.

[47]   I.E.H. Brandrup J., *Polymer Handbook*. **1989**. J. Wiley & Sons.

[48]   R. Battino, *Oxygen and Ozone - Solubility Data Series*. **1981**. Pergamon Press. Oxford.

[49]   E. Trommsdorff, H. Kohle, and P. Lagally, *"Zur Polymerisation Des Methacrylsauremethylesters"*, **Makromolekulare Chemie-Macromolecular Chemistry and Physics**, 1(3): p. 169-198, **1948**.

[50]   A. Echte, *Handbuch der Technischen Polymerchemie*. **1993**. VCH Verlagsgesellschaft. Weinheim.

[51]   N. Tefera, G. Weickert, and K.R. Westerterp, *"Modeling of free radical polymerization up to high conversion .1. A method for the selection of models by simultaneous parameter estimation"*, **Journal of Applied Polymer Science**, 63(12): p. 1649-1661, **1997**.

[52]   J.S. Vrentas, *"Review of the applications of free volume theory for diffusion in polymers"*, **Polym Rev.**, 15(136-138), **1981**.

[53]   J.S. Vrentas and J.L. Duda, *"Diffusion in polymer solvent systems. 1. Reexamination of the free volume theory"*, **Journal of Polymer Science: Polymer Physics Edition**, 15: p. 403-416, **1977**.

[54]   J.S. Vrentas and J.L. Duda, *"Diffusion in polymer solvent systems. 2. Predictive theory for the dependence of diffision coefficients on temp. , conc. and molecular weight"*, **Journal of Polymer Science: Polymer Physics Edition**, 15: p. 417-439, **1977**.

[55]   J.S. Vrentas and J.L. Duda, *"Molecular diffusion in polymer solutions"*, **AIChE Journal**, 25(1): p. 1-21, **1979**.

[56]   S. Hoppe and A. Renken, *"Modelling of the free radical polymerisation of methylmethacrylate up to high temperature"*, **Polymer Reaction Engineering**, 6(1): p. 1-+, **1998**.

[57]   S.K. Soh and D.C. Sundberg, *"Diffusion-Controlled Vinyl Polymerization .2. Limitations on the Gel Effect"*, **Journal of Polymer Science Part a-Polymer Chemistry**, 20(5): p. 1315-1329, **1982**.

[58]   W.Y. Chiu, G.M. Carratt, and D.S. Soong, *"A Computer Model for the Gel Effect in Free-Radical Polymerization"*, **Macromolecules**, 16((3)): p. 348-357, **1983**.

[59]   N. Friis and A.E. Hamielec, *"Gel-Effect in Emulsion Polymerization of Vinyl Monomers"*, **Acs Symposium Series**, (24): p. 82-91, **1976**.

[60]   M. Buback, *"Free-Radical Polymerization up to High Conversion - a General Kinetic Treatment"*, **Makromolekulare Chemie-Macromolecular Chemistry and Physics**, 191(7): p. 1575-1587, **1990**.

[61]   F.L. Marten and A.E. Hamielec, **American Chemical Society Symposium Series**, 104: p. 43, **1979**.

[62]   Personal communication, R. Carloff,

[63]   B.M. Louie, G.M. Carratt, and D.S. Soong, *"Modeling the Free-Radical Solution and Bulk-Polymerization of Methyl-Methacrylate"*, **Journal of Applied Polymer Science**, 30(10): p. 3985-4012, **1985**.

[64]   D. Achilias and C. Kiparissides, *"Modeling of Diffusion-Controlled Free-Radical Polymerization Reactions"*, **Journal of Applied Polymer Science**, 35: p. 1303-1323, **1988**.

[65]   P. Nising and T. Meyer, *"Modeling of the High-Temperature Polymerization of Methyl Methacrylate. 1. Review of Existing Models for the Description of the Gel Effect"*, **Ind. Eng. Chem. Res.**, 43(23): p. 7220-7226, **2004**.

[66]   F. Fenouillot, J. Terrisse, and T. Rimlinger, *"Polymerization of methyl methacrylate at high temperature with 1-butanethiol as chain transfer agent"*, **Journal of Applied Polymer Science**, 72(12): p. 1589-1599, **1999**.

[67]   N. Tefera, G. Weickert, and K.R. Westerterp, *"Modeling of free radical polymerization up to high conversion .2. Development of a mathematical model"*, **Journal of Applied Polymer Science**, 63(12): p. 1663-1680, **1997**.

[68]   G.C. Berry, *"The Viscosity of Polymer-Diluent Mixtures"*, **Journal of Physical Chemistry**, 70: p. 1194-1198, **1965**.

[69]   F. Bueche, *"Viscosity, Self-Diffusion, and Allied Effects in Solid Polymers"*, **Journal of Chemical Physics**, 20(12): p. 1959-1964, **1952**.

[70]   D. Panke, *"Polymerization of Methyl-Methacrylate up to High Degrees of Conversion - Model-Calculations Considering the Presence of a Prepolymer"*, **Makromolekulare Chemie-Rapid Communications**, 7(4): p. 171-174, **1986**.

[71]   F.L. Marten and A.E. Hamielec, *"High-Conversion Diffusion-Controlled Polymerization of Styrene .1"*, **Journal of Applied Polymer Science**, 27(2): p. 489-505, **1982**.

[72]   M. Fernandez-Garcia, M.M.C. Lopez-Gonzales, L.M. Barrales-Rienda, E.L. Madruga, and C. Arias, *"Effect of Copolymer Composition and Conversion on the Glass Transition of Methyl Acrylate - Methyl Methacrylate Copolymers"*, **Journal of Polymer Science Part B-Polymer Physics**, 32: p. 1191-1203, **1994**.

[73]   K. TAKASHI and M. MASAHIKO, *Process for production of methacrylate polymers*. 1998, SUMITOMO CHEMICAL CO.

[74]   T. Meyer, *"Etude à l'aide d'une methode chimique de la ségrégation lors d'une polymérisation dans un réacteur tubulaire à recyclage"*, Ph.D. thesis: Département de Chimie, Thesis No. 810, no., **EPFL** (Lausanne), 1989.

[75]   P. Nising, T. Zeilmann, T. Meyer, *"On the degradation and stabilization of PMMA in a continuous process"*, **Proceedings ISCRE 17, HongKong**, **2002**.

[76] N.K. Tien, E. Flaschel, and A. Renken, *"Bulk-Polymerization of Styrene in a Static Mixer"*, **Chemical Engineering Communications**, 36(1-6): p. 251-267, **1985**.

[77] A. Heierle, *"Statische Mischer - Wärmetauscher"*, **Chemie-Anlagen + verfahren**, 7, **1994**.

[78] J.-E. Juvet, *"Etude de la ségrégation thermique dans un échangeur de chaleur tubulaire"*, Ph.D. thesis: Département de chimie, Thesis No. 791, no., **EPFL** (Lausanne), 1989.

[79] K.T. Nguyen, F. Streiff, E. Flaschel, and A. Renken, *"Motionless mixers for the design of tubular polymerization reactors"*, **Chemical Engineering & Technology**, 13(1): p. 214-220, **1990**.

[80] Sulzer, *"Mixing and Reaction Processes"*, **Sulzer Chemtech Sales Brochure**, MRT0655, **1992**.

[81] N.P. Stuber, *"Studies of continuous methylmethacrylate polymerization in a twin-screw extruder"*, Ph.D. thesis: Thesis (Ph.D.), no. 000125258, **University of Minnesota** 1986.

[82] N.P. Stuber and M. Tirrell, *"Continuous polymerization studies in a twin-screw extruder"*, **Polymer Process Engineering**, 3(1-2): p. 71-83, **1985**.

[83] J.J. Zacca and W.H. Ray, *"Modeling of the Liquid-Phase Polymerization of Olefins in Loop Reactors"*, **Chemical Engineering Science**, 48(22): p. 3743-3765, **1993**.

[84] W.-D. Hergeth, *On-Line Monitoring of Chemical Reactions*,

[85] T. Zeilmann and T. Meyer, *"Inline Conversion Monitoring in MMA High Solid Content Polymerization Process"*, **Chimia**, 55(3): p. 249-250, **2001**.

[86] F. Dinger, *"Polymerisationsüberwachung mit Ultraschall"*, **Chemie Technik**, 28(3): p. 30-34, **1999**.

[87] S.L. Oswal, *"Speed of Sound, Isentropic Compressibility, Viscosity, and Excess Volume of Binary Mixtures. 1. Alkanenitriles with Alkyl Acetates"*, **Journal of Chemical Engineering Data**, 40: p. 840-844, **1995**.

[88] S.L. Oswal, O. Oswal, P.S. Modi, J.P. Dave, and R.L. Gardas, *"Acoustic, volumetric, compressibility and refractivity properties and Flory's reduction parameters of some homologous series of alkyl alkanoates from 298.15 to 333.15K"*, **Thermochimica Acta**, 410: p. 1-14, **2004**.

[89] M. Pancholy and S.S. Mathur, *"Adiabatic Compressibility and Ultrasonic Velocity in Esters"*, **Journal of the Physical Society of Japan**, 18(3): p. 449-451, **1963**.

[90] T. Kelen and F. Tüdös, *"Analysis of the Linear Methods for Determining Copolymerization Reactivity Ratios. I. A New Improved Linear Graphic Method"*, **Journal of Macromolecular Science and Chemistry**, A9(1): p. 1-27, **1975**.

[91] H.-G. Elias, *An Introduction to Polymer Science*. **1997**. VCH Verlagsgesellschaft. Weinheim.

[92]   N. Grassie, B.J.D. Torrance, J.D. Fortune, and J.D. Gemmel, *"Reactivity Ratios for the Copolymerization of Acrylates and Methacrylates by Nuclear Magnetic Resonance Spectroscopy"*, **Polymer**, 6(12): p. 653-658, **1965**.

[93]   C. Arias, M.M.C. López-González, M. Fernández-García, J.M. Barrales-Rienda, and E.L. Madruga, *"Free-radical copolymerization of methyl acrylate with methyl methacrylate in benzene solution"*, **Polymer**, 34(8): p. 1786-1789, **1993**.

[94]   M.-J. Park, S.-M. Ahn, and H.-K. Rhee, *"Kinetic Parameter Estimation for the MMA/MA Copolymerization System"*, **Journal of Applied Polymer Science**, 78: p. 2554-2564, **2000**.

[95]   A. Nagy, T. Földes-Berezsnich, and F. Tüdös, *"Kinetics of Radical Polymerization - Investigation of the polymerization of Methyl Acrylate in Solution by the Rotating Sector Method"*, **European Polymer Journal**, 20(1): p. 25-29, **1984**.

[96]   R.A. Hutchinson, D.A. Paquet, and J.H. McMinn, *"Determination of Free-Radical Chain-Transfer Rate Coefficients by Pulsed-Laser Polymerization"*, **Macromolecules**, 28(16): p. 5655-5663, **1995**.

[97]   J.L. De la Fuente and E.L. Madruga, *"Homopolymerization of methyl methacrylate and styrene: Determination of the chain-transfer constant from the mayo equation and the number distribution for n-dodecanethiol"*, **Journal of Polymer Science Part a-Polymer Chemistry**, 38(1): p. 170-178, **2000**.

[98]   M. Fontanille and Y. Gnanou, *Chimie et Physico-chimie des polymères*. **2002**. Dunod. Paris.

[99]   T. Kashiwagi, T. Hirata, and J.E. Brown, *"Thermal and Oxidative-Degradation of Poly(Methyl Methacrylate) - Molecular-Weight"*, **Macromolecules**, 18(2): p. 131-138, **1985**.

[100]   E. Weast, *Handbook of Chemistry and Physics*. **1983**. CRC Press.

[101]   K. Smolders and J. Baeyens, *"Thermal degradation of PMMA in fluidised beds"*, **Waste Management**, 24(8): p. 849-857, **2004**.

[102]   A. Rudin, *The Elements of Polymer Science and Engineering*. **1998**. Academic Press. San Diego.

[103]   S. Beuermann, M. Buback, and M. Gadermann, *"Depropagation in methacrylate polymerizations"*, **Dechema monogr.**, 138: p. 461-465, **2004**.

[104]   N. Grassie and H.W. Melville, *"Degradation of poly (methyl methacrylate) C: The mechanism of the thermal degradation of poly (methyl methacrylate)"*, **Discussions of the Faraday Society**, 2: p. 378-383, **1947**.

[105]   T. Hirata, T. Kashiwagi, and J.E. Brown, *"Thermal and Oxidative-Degradation of Poly(Methyl Methacrylate) - Weight-Loss"*, **Macromolecules**, 18(7): p. 1410-1418, **1985**.

[106]   B.J. Holland and J.N. Hay, *"The kinetics and mechanisms of the thermal degradation of poly(methyl methacrylate) studied by thermal analysis-Fourier transform infrared spectroscopy"*, **Polymer**, 42(11): p. 4825-4835, **2001**.

[107] K.A. Holland and I.D. Rae, *"Thermal Degradation of a compound which models the head-to-head linkage in Poly(methyl methacrylate)"*, **Australian Journal of Chemistry**, 40(4): p. 687-692, **1987**.

[108] Y.H. Hu and C.Y. Chen, *"The effect of end groups on the thermal degradation of poly(methyl methacrylate)"*, **Polymer Degradation and Stability**, 82(1): p. 81-88, **2003**.

[109] T. Kashiwagi, A. Inaba, J.E. Brown, K. Hatada, T. Kitayama, and E. Masuda, *"Effects of Weak Linkages on the Thermal and Oxidative- Degradation of Poly(Methyl Methacrylates)"*, **Macromolecules**, 19(8): p. 2160-2168, **1986**.

[110] G. Madras, J.M. Smith, and B.J. McCoy, *"Degradation of poly(methyl methacrylate) in solution"*, **Industrial & Engineering Chemistry Research**, 35(6): p. 1795-1800, **1996**.

[111] L.E. Manring, *"Thermal-Degradation of Saturated Poly(Methyl Methacrylate)"*, **Macromolecules**, 21(2): p. 528-530, **1988**.

[112] L.E. Manring, *"Thermal-Degradation of Poly(Methyl Methacrylate) .2. Vinyl- Terminated Polymer"*, **Macromolecules**, 22(6): p. 2673-2677, **1989**.

[113] L.E. Manring, *"Thermal-Degradation of Poly(Methyl Methacrylate) .4. Random Side-Group Scission"*, **Macromolecules**, 24(11): p. 3304-3309, **1991**.

[114] L.E. Manring and W.R. Hertler, *"The Thermal-Degradation of Pmma Polymer with Terminal Head-to- Head Linkages"*, **Abstracts of Papers of the American Chemical Society**, 206: p. 19-POLY, **1993**.

[115] L.E. Manring, D.Y. Sogah, and G.M. Cohen, *"Thermal-Degradation of Poly(Methyl Methacrylate) .3. Polymer with Head-to-Head Linkages"*, **Macromolecules**, 22(12): p. 4652-4654, **1989**.

[116] G.R. Morrow and I.D. Rae, *"Thermal-Degradation of Polymers and Polymer Models .4. Thermolysis of a Polymethacrylate Model with an Unsaturated End Group"*, **Australian Journal of Chemistry**, 40(8): p. 1477-1481, **1987**.

[117] J.D. Peterson, S. Vyazovkin, and C.A. Wight, *"Kinetic Study of Stabilizing Effect of Oxygen on Thermal Degredation of Poly(methyl methacrylate)"*, **Journal of Physical Chemistry B**, 103: p. 8087-8092, **1999**.

[118] H.H.G. Jellinek, *Aspects of Degradation and Stabilization of Polymers*. **1978**. Elsevier. Amsterdam.

[119] *Wikipedia Online Encyclopedia*, http://en.wikipedia.org/wiki/Gel_permeation_chromatography.

[120] Viscotek, *Instruction Manual TDA300 SEC3 System*. 2000.

[121] F. Sasse, *"Chemisches Recycling von Acrylgläsern"*, Ph.D. thesis: Lehrstuhl für Technische Chemie I, no., **Friedrich-Alexander-Universität** (Erlangen-Nürnberg), 1998.

[122] L. Gou, C.N. Coretsopoulos, and A.B. Scranton, *"Measurement of the Dissolved Oxygen Concentration in Acrlyate Monomers with a Novel Photochemical Method"*, **Journal of Polymer Science Part A - Polymer Chemistry**, 42: p. 1285-1292, **2004**.

[123]   M. Wulkow, *"The simulation of molecular weight distributions in polyreaction kinetics by discrete Galerkin methods"*, **Macromolecular Theory and Simulations**, 5(3): p. 393-416, **1996**.

[124]   S. Beuermann, M. Buback, T.P. Davis, R.G. Gilbert, R.A. Hutchinson, O.F. Olaj, G.T. Russell, J. Schweer, and A.M.v. Herk, *"Critically evaluated rate coefficients for free-radical polymerizations - Propagation rate coefficients for methyl methacrylate"*, **Macromolecular Chemistry and Physics**, 198: p. 1545-1560, **1997**.

[125]   P.J. Skrdla, *"Thermal decomposition of tert-butyl peroxide in a gas chromatographic reactor: A comparison of kinetic approaches"*, **International Journal of Chemical Kinetics**, 36(7): p. 386-393, **2004**.

[126]   *Crossfire Beilstein Database*,

[127]   N.V. Sastry and M.K. Valand, *"Volumetric behaviour of acrylic esters (methyl-, ethyl-, and butyl acrylate) + 1-Alcohol at 298.15K and 308.15K"*, **Phys. Chem. Liq.**, 38: p. 61-72, **2000**.

[128]   J. George, N.V. Sastry, S.R. Patel, and M.K. Valand, *"Densities, Viscosities, Speeds of Sound, and Relative Permittivities for Methyl Acrylate + 1-Alcohols (C1-C6) at T=(302.15 and 318.15)K"*, **Journal of Chemical Engineering Data**, 47: p. 262-269, **2002**.

[129]   P. Bahadur and N.V. Sastry, *"Densities, Sound Speeds, Excess Volumes, and Excess Isentropic Compressibilities for Methyl Acrylate + 1-Propanol + Hydrocarbons"*, **International Journal of Thermophysics**, 24(2): p. 447-462, **2003**.

Acknowledgements

Firstly, and most importantly, I want to express my deep gratitude and love to my darling wife, Anna, who not only opened my eyes for so many new things, but also supported and comforted me throughout the past four years in Lausanne, which surely was not always easy. Without the strength and confidence that I received from our partnership, I would not be who and where I am now.

I also owe a debt of gratitude to my parents, Annette and Wolfgang Nising, who since I can remember always provided me with far more than the necessary amount of love, education and moral support and thanks to who I never lacked for anything in my life. At the same time, I want to thank my brother, Carl, for all the fun and the good relationship we've shared so far, as well as my parents-in-law, Angela and Nicola Bozzi, for their sincere and hearty compassion and for having included me so in their family.

My first year in Lausanne was quite a challenge in terms of making friends and bonding with people. Without the warm welcome of my two dear friends Nicolas, who has been trying for five years now to motivate me for all different kinds of sport, and Thomas, my compatriot from the Rhineland who immediately made me feel at home, I would probably not have stayed all that long. Having good friends makes life so much easier and also helps enormously to cope with the difficult moments that occur during almost every thesis. Therefore, I want to thank my

closest friends, who I met here in Lausanne, for all the happy moments and the pleasure we had together during the last years: Elisabeth and Mathias, for the innumerable excursions and evenings spent together; Nadia and Marc, for teaching me the beauty of boating on the lake; Benoît, for his linguistic and moral support; and Massimo, for his patience in teaching me and listening to my Italian. I also thank my dear friend Thorsten, with whom together I went through the major part of my school and university time, for keeping in touch through all these years I've been away from Sankt Augustin.

On the side of EPFL, there are a lot of people that have been directly or indirectly involved in this thesis. Most importantly, I express my sincere gratitude to the mechanicians of the ISIC workshop, in particular Gérard Bovard and Jean-Claude Rapit, for their constant help in constructing, maintaining and dismantling the pilot plant. Without them, their knowledge and permanent availability, I would not have been able to carry out this thesis. Another big thank you goes to my numerous diploma students, who not only did a lot of measurements for me but also contributed to the social life in our group: Khaled, Séverine, Nathanael, and especially Valéry and Felix, with who I shared not only working hours but also lots of happy moments as friends. I also want to mention our secretary, Madame Anken, and her various apprentices at this point, who took care of a lot of organizational matters throughout this thesis, for which I want to thank all of them very dearly. During most of my time at EPFL, I shared the office with Ivan Pantchev, who always had some good advice or joke for me and who I could always rely on, which I am very thankful for.

This thesis was made possible with the full financial and scientific support of Röhm in Germany. On their side, I want to express my deep gratitude to Dr. Rüdiger Carloff, Dr. Michael Wicker and Dr. Klaus Albrecht for the trust they put in me and the time they spent for the many discussions and meetings we had during the last four years. In particular, I thank Rüdiger Carloff for the scientific guidance he provided me with throughout this project.

The person who enabled me to do my diploma work and PhD here at EPFL is my supervisor, MER Dr. Thierry Meyer. I want to thank Thierry for the leeway he gave to me and for the confidence he had in me during the last 5 years. Moreover, I am very thankful for the opportunity

to participate in the many international conferences we went together, which is far from being common for PhD students.

Lots of thanks go to the members of the examining board, Prof. Pla, Prof. Klok and Dr. Carloff for their appreciation of my work and the positive feedback I got from their side.

Finally, I want to thank the following people for their help, company and sometimes also moral support: my colleagues Charalampos Mantelis, Patrick Farquet, Petra Prechtl, Pascal Tribolet, Frédéric Lavanchy, Marina Ruta, Alain Fankhauser, Edy Casali and Martin Grasemann; our dutch exchange professor, Maartje Kemmere, for her advice and moral support; the people from the electronic workshop, Gabriel Roch and Olivier Noverraz, for their help with the electric installations in the pilot plant; Peter Péchy for the NMR support; the people from Sulzer Chemtech, in particular Albert Breiter and Claude Passaplan, for their technical support and for organizing spare parts; Sandrine Olivier and Philippe Lievens from Viscotek for their GPC support; and finally Mr. Cottier and the Lausanne firebrigade for coming to EPFL on a sunny sunday afternoon for a false alarm that I triggered with one of my experiments.

Curriculum vitae

Axel Philip NISING

Chemin du Noirmont 15   Age: 30
CH – 1004 Lausanne   Citizenship: German

Married
E-mail: philip@nising.de

Summary

- PhD in Chemical Engineering with specialization in Polymer Reaction Engineering
- *Summa cum Laude* Diploma in Chemical Engineering at the University of Erlangen-Nürnberg, Germany.
- Strong background in polymer science and analytics: pilot plant technology, free-radical polymerizations, GPC, Headspace-GC, TGA-MS, Reaction Calorimetry and Reaction Simulation: Predici®
- German mother tongue, fluent in English, French and Italian.

Current Position

2002 - 2005	**PhD student** at ETH Lausanne, Polymer Reaction Engineering Group (GPM)
	"High-Temperature Polymerization of MMA in a continuous pilot plant process"
	- Conception and Construction of a Pilot Plant for the MMA polymerization at high temperature
	- Realization of an inline conversion measurement by ultrasound
	- Process simulation with PREDICI® and ASPEN PLUS® software packages
	- Excellent knowledge in analytical techniques (GPC, GC, DSC, TGA-MS, UV)
	- Project organization in cooperation with industry
	- Oral and written presentations within international conferences
	- Several scientific publications in international journals, one book chapter
	- Responsible of five diploma works and two interns
	- Teaching and tutoring of students (lectures, exercises and practical work)
	- Network Administrator

Education

2001	**Diploma thesis** at ETH Lausanne, Polymer Reaction Engineering
	"Optimization of the Polymerization of MMA in a Sulzer Pilot Plant"
1996-2000	**Diploma** (*summa cum laude*) **in Chemical Engineering** (Dipl.-Ing. Univ.) at the University of Erlangen-Nürnberg
1986 - 1995	**Abitur** (A-levels)
	Albert-Einstein-Gymnasium, Sankt Augustin (D)

Military service

| 1995 - 1996 | **Military service (compulsory)** in the German Army (Bundeswehr) (10 months)
First-aid man in the medical corps |

Internships

1999 & 2000	**Endress & Hauser Flowtec AG, Reinach (CH)** Internship (2 months) – Marketing and Documentation
1997	**Bayer AG, Leverkusen (D)** Internship (1 month) – Process and Plant Design
1995	**Bayer AG, Leverkusen (D)** Internship (2 months) – Aromatics Production Plant

Languages

German: mother tongue
English: fluent (oral / written)
French: fluent (oral / written)
Italian: fluent oral / good written

Computer Skills

Simulation software Aspen Plus$^{®}$ and Predici$^{®}$
Network and group administrator (GPM) at ETH Lausanne
Excellent knowledge in all important desktop and office applications

Social activities

Student member of the *Studying Committee Chemical Engineering* at the University of Erlangen (2 years)
Foundation and chair of the Students Association *Chemical Engineering* at the University of Erlangen

References

MER Dr. Thierry Meyer
ISIC-GPM, Station 6
EPFL
1015 Lausanne, Switzerland
Tel.: +41 21 693 3614
Email: thierry.meyer@epfl.ch

Dr. Thomas Zeilmann
Ciba Specialty Chemicals AG
Process Development
CE6.23, WMO-369
1870 Monthey, Switzerland
Tel.: +41 24 474 4975
Email: thomas.zeilmann@cibasc.com

Publications

8. **Nising P.** and Meyer Th., *Kunststoffe* (Book Chapter), Wiley VCH, Weinheim, Germany, 2006

7. **Nising P.** and Meyer Th., *Apparate zur Herstellung, Aufbereitung und Konfektionierung von Kunststoffen* (Book Chapter), Winnacker-Küchler Encyclopedia, Wiley VCH, Weinheim, Germany, 2005

6. **P. Nising,** Th. Meyer, R. Carloff, M. Wicker, *Thermal Initiation of MMA in High Temperature Radical Polymerizations*, Macromol. Mater. Eng., 290, 311, 2005

5. **Nising, Ph.** and Meyer Th., *High Temperature MMA polymerization*, Dechema Monograph, 138, 511, 2004.

4. **Philip Nising** and Thierry Meyer, *Modelling of the High Temperature Polymerization of Methyl Methacrylate*, Ind. Eng. Chem. Res., 43(23), 7220-7226, 2004.

3. S. Fortini, F. Lavanchy, **P. Nising**, Th. Meyer, *A new tool for the study of polymerization under supercritical conditions - preliminary results*, Macromolecular Symposia (2004), 206(Polymer Reaction Engineering V), 79-92.

2. **P. Nising**, T. Zeilmann, Th. Meyer, *On the degradation and stabilization of Poly (methyl methacrylate) in a continuous process*, Chemical Engineering & Technology (2003), 26(5), 599-604.

1. Zeilmann, T., **P. Nising**, Th. Meyer, *Thermal stabilization and devolatilization of PMMA in a continuous polymerization pilot loop reactor*, Dechema Monograph., Vol. 137, 481-486, 2001.

Contribution to Conferences

6. **P. Nising**, Th. Meyer, *Continuous high-temperature polymerization of MMA at pilot scale* (Oral Presentation), AIChE Annual Meeting 2005, Cincinnati, 30 October - 4 November 2005.

5. **P. Nising**, Th. Meyer, *Continuous high-temperature polymerization of methyl methacrylate* (Poster Presentation), 7th World Congress of Chemical Engineering, Glasgow, 10-14 July 2005.

4. **P. Nising**, Th. Meyer, *High Temperature Polymerization of MMA* (Poster Presentation), 8th International Workshop on Polymer Reaction Engineering, Hamburg, 3-6 October 2004.

3. **P. Nising**, Th. Meyer, *Modeling of the high temperature polymerization of poly (methyl Methacrylate): I. Review of existing models for the description of the Gel Effect* (Poster Presentation), Polymer Reaction Engineering: Modeling, Optimization and Control, Lyon, France, 30 November -3 December 2003.

2. **P. Nising**, T. Zeilmann and Th. Meyer, *On the degradation and stabilization of poly(methyl methacrylate) in a continuous process* (Oral Presentation), 17th Int. Symposium on Chemical Reaction Engineering, Hong-Kong, 25-28 August 2002.

1. T. Zeilmann, **A.P. Nising**, Th. Meyer, *Thermal stabilization and devolatilization of PMMA in a continuous polymerization pilot loop reactor* (Poster Presentation), 7th International congress on polymer reaction engineering, Hamburg, 8-10 October 2001.